UNIVERSITY OF SOUTHAMPTON

Faculty of Engineering and Physical Sciences
School of Engineering

Space Debris Modelling in the New Space Era

How changes in the use of the space environment will impact the space debris environment and how it is modelled

by

Samuel Diserens

MPhys

ORCiD: 0000-0001-5521-2041

A thesis for the degree of
Doctor of Philosophy

March 2022

University of Southampton

Abstract

Faculty of Engineering and Physical Sciences
School of Engineering

Doctor of Philosophy

Space Debris Modelling in the New Space Era

by Samuel Diserens

Over the last two decades the rise of NewSpace has led to a transition away from traditional space operations altering the characteristics of the spacecraft population. An analysis of the physical and orbital characteristics of spacecraft from 1957 to 2020 identified trends consistent with the increase in NewSpace spacecraft. A divergence was discovered between the physical characteristics of spacecraft in Low Earth Orbit (smaller, lower mass) and those in Geosynchronous Orbit (larger, higher mass). A shift was also found towards greater spatial organisation in orbit with spacecraft becoming clustered into similar orbits and less uniformly distributed. Both trends have the potential to invalidate the assumptions made in debris model components.

An implementation of the NASA Standard Breakup Model was created to investigate the impact of the changing physical characteristics of spacecraft and upper stages on breakup modelling. Validating the model against recent observed breakup events indicated an over-estimation of large debris released and an under-estimation of the number of small debris. A collision tool-set using the Cube and Orbit Trace collision algorithms was developed to study the consequences of increased spatial organisation. Collision probabilities were generated and compared to SOCRATES reports (https://celestrak.com/SOCRATES/) for specific populations of spacecraft and debris. Collision probabilities calculated using the models were reduced relative to the SOCRATES probabilities for scenarios with greater clustering of objects.

The model implementations were combined to perform 25 year simulations of a NewSpace constellation comparing the use of the original models against collision and fragmentation models adjusted to account for NewSpace. The results showed that the reaction of the environment to breakups was sensitive to updates made to component models. In scenarios with an initial collision event the adjusted models led to a 250% increase in the final debris population and a 1564% increase in the cumulative collision probabilities of the constellation. These results suggested that current models underestimate the risk associated with NewSpace leading to the conclusion that modifications to account for NewSpace will be a crucial part of the next generation of space debris models. These models will be essential to ensure that appropriate measures are taken to control debris growth and mitigate the risk to future operations.

To Emma

Thank you for always encouraging me.
Your love, support and patience made this possible.

Contents

List of Figures

List of Tables

Declaration of Authorship

I declare that this thesis and the work presented in it is my own and has been generated by me as the result of my own original research.

I confirm that:

1. This work was done wholly or mainly while in candidature for a research degree at this University;
2. Where any part of this thesis has previously been submitted for a degree or any other qualification at this University or any other institution, this has been clearly stated;
3. Where I have consulted the published work of others, this is always clearly attributed;
4. Where I have quoted from the work of others, the source is always given. With the exception of such quotations, this thesis is entirely my own work;
5. I have acknowledged all main sources of help;
6. Where the thesis is based on work done by myself jointly with others, I have made clear exactly what was done by others and what I have contributed myself;
7. Parts of this work have been published as:
   Samuel Diserens, Hugh G. Lewis, and Jörg Fliege. NewSpace and its implications for space debris models. *Journal of Space Safety Engineering*, jul 2020b. ISSN 24688967. . URL https://linkinghub.elsevier.com/retrieve/pii/S2468896720300914
   Samuel Diserens, Hugh G. Lewis, and Joerg Fliege. Assessing collision algorithms for the newspace era. *Journal of Space Safety Engineering*, jul 2020a. ISSN 24688967.

Signed:..... Date:.....

Acknowledgements

I would like to express my gratitude to my supervisory team, Professor Hugh Lewis and Profession Jörg Fliege, for their guidance and support. I have been very lucky to be able to benefit from their wealth of knowledge, experience and connections. They have always been generous with their time and unfailingly compassionate throughout the difficulties of the COVID-19 pandemic.

This work was supported by the University of Southampton and the EPSRC Centre for Doctoral Training in Next Generation Computational Modelling (NGCM) and funded through the EPSRC grant EP/L015382/1. My thanks go to the CDT directors and all of the support staff both within the CDT and across the university for all of the hard work that goes in to supporting postgraduate research.

I would also like to extend my thanks to the Chief Engineer's Team at the UK Space agency for the opportunity to represent the UK Space Agency at the Inter-Agency Space Debris Coordination Committee (IADC) over the last 3 years. Particular thanks go to Toby Harris who, in his role as Head of Orbital Systems, provided invaluable opportunities to engage in knowledge-sharing with him and his team.

Additional thanks are due to Dr Tim Flohrer and the team at the ESA Space Debris Office for their support and for providing access to their spacecraft database (DISCOS) and to the MASTER 2018 reference populations via the IADC. Thanks also go to Dr T.S. Kelso, who maintains the CelesTrak website and kindly provided insight into the SOCRATES collision prediction service as well as a copy of the historic database of objects' physical radii used in the probability calculations.

I would also like to acknowledge the use of the SGP4 propagator code, provided courtesy of Dr David Vallado, as well as the distlink C++ library published by Dr Roman V. Baluev for the computation of the Minimal Orbital Intersection Distance (MOID).

Acronyms

ADEPT	Aerospace Debris Environment Projection Tool.
ADR	Active Debris Removal.
ASAT	Anti-Satellite Weapon.
ASI	Agenzia Spaziale Italiana.
CART	Classification and Regression Trees.
CASCADE	Computational Adaptive Strategy to Control Accurately the Debris Environment.
CFRP	Carbon fibre reinforced polymer.
CNES	Centre National d'Etudes Spatiales.
CNSA	China National Space Administration.
CSSI	Center for Space Standards & Innovation.
CUDA	Compute Unified Device Architecture.
DAMAGE	Debris Analysis and Monitoring Architecture to the Geosynchronous Environment.
DELTA	Debris Environment Long Term Analysis.
DISCOS	Database and Information System Characterising Objects in Space.
DLR	German Aerospace Center.
DMSP-F13	Defense Meteorological Satellite Program Flight 13.
DRAMA	Debris Risk Assessment and Mitigation Analysis.
ESA	the European Space Agency.
ESOC	European Space Operations Centre.
FADE	Fast Debris Evolution Model.
FAST	Fragmentation Algorithms for Satellite Targets.
FREG	Fragmentation Event Generator.
GEO	Geosynchronous Earth Orbit.
GNSS	Global Navigation Satellite Systems.

GPU	Graphics Processing Unit.
GTO	Geostationary Transfer Orbit.
HAPS	Hydrazine Auxiliary Propulsion System.
IADC	Inter-Agency Space Debris Coordination Committee.
IADC WG2	Inter-Agency Space Debris Coordination Committee's Working Group 2.
ICBM	Inter-Continental Ballistic Missiles.
IDES	Integrated Debris Evolution Suite.
ISRO	Indian Space Research Organisation.
ISS	International Space Station.
JAXA	Japan Aerospace Exploration Agency.
JSON	JavaScript Object Notation.
KSCPROP	Kustaanheimo and Stiefel Canonical Propagation model.
LEGEND	LEO-to-GEO Environment Debris model.
LEO	Low Earth Orbit.
LEODEEM	Low Earth Orbit Debris Environment Evolutionary Model.
LUCA	Long Term Utility for Collision Analysis.
MASTER	Meteoroid and Space Debris Terrestrial Environment Reference.
MEDEE	Modelling the Evolution of Debris on Earth's Environment.
MEO	Medium Earth Orbit.
MLI	Multi-Layer Insulation.
MOID	Minimum Orbit Intersection Distance.
NASA	National Aeronautics and Space Administration.
NEO	Near Earth Orbit.
NEODEEM	Near Earth Orbit Debris Environment Evolutionary Model.
NRLMSISE-00	The Naval Research Lab's Mass Spectrometer and Incoherent Scatter Radar Exosphere - 2000.
ORDEM	Orbital Debris Engineering Model.
PCC	Pearson Correlation Coefficient.
PIB	"Particles-In-a-Box".
PSLV	Polar Satellite Launch Vehicle.

RAAN	Right Ascension of Ascending Node.
RCS	Radar Cross Section.
SDEEM	Space Debris Environment Engineering Model.
SDM	Space Debris Mitigation long-term analysis program.
SDPA	Space Debris Prediction and Analysis.
SDPA-E	Space Debris Prediction and Analysis - Engineering.
SIMPLE	Stochastic IMPressionistic Low Earth.
SOCIT	Satellite Orbital debris Characterization Impact Test.
SOCRATES	Satellite Orbital Conjunction Reports Assessing Threatening Encounters in Space.
SOLEM	Space Objects Long-term Evolution Model.
SSN	Space Surveillance Network.
SST	Space Surveillance and Tracking.
STAT	STochastic Analog Tool.
TLE	Two-Line Element set.
USSF	United States Space Force.
VLEO	Very Low Earth Orbit.

Chapter 1

Introduction

> Our two greatest problems are gravity and paperwork. We can lick gravity, but sometimes the paperwork is overwhelming.
>
> Wernher von Braun

1.1 Background

NewSpace, the 'New Space Age' and the 'New Space Race' are terms which have become increasingly common in recent years and are indicative of the changing activity and changing attitudes towards space technology and the space environment. Now more than 60 years old, the space industry has long been monopolised by national agencies and large government contractors. The NewSpace movement encapsulates wide ranging changes, often associated with the rise of the private investment, innovation and attempts to disrupt the status-quo.

The beginning of the movement dates back to the 1980s and the increasing of commercial activity known as 'Alt.Space'. However, it is only in the last 20 years, following the 'dot-com' boom of the 1990s, that significant growth has been seen. Bryce Space and Technology (2018) report a greater than twelve-fold increase in the average number of space investors per year since the year 2000.

The private companies receiving this investment are working to pioneer a wide range of novel and disruptive ideas. This includes new technologies like reusable rockets (such as SpaceX's Falcon 9) or cheap miniaturised satellites (CubeSats). In addition to technological advancements, there are also new mission types being introduced including active removal of space debris, the on-orbit servicing and refuelling of active satellites, and the operation of 'mega-constellations' consisting of thousands of mid-sized satellites aiming to provide global satellite broadband coverage.

These developments are resulting in diversification of the spacecraft population. More spacecraft are being launched by a greater number of operators, into different orbits, falling at the extremes of the normal ranges of both mass and size, and with potentially different goals and modes of operation. The result of this is that there are no precedents for many of the ongoing behaviours and, as a consequence, spacecraft behaviour is becoming less predictable in the absence of relevant experience.

With the changes brought about by NewSpace come new risks to the safety and sustainability of the space environment including changes to the future evolution of the space debris population. This work attempts to explore some of the implications of the NewSpace era when it comes to modelling and understanding the risk posed by space debris in Near Earth Orbit (NEO).

1.1.1 Space Debris & Modelling

Pollution of the space environment is an increasingly relevant issue as the population of debris objects accumulating around the Earth continues to grow. The issue of space debris is well acknowledged, with hundreds of thousands of objects currently threatening the safe use of the space environment by both crewed and un-crewed spacecraft. Much like the ongoing climate emergency this is a problem which is accelerating and one which potentially becomes more dangerous and harder to reverse the longer it continues. However, the current understanding of how this debris environment will evolve in the future is uncertain.

Debris models have been developed to investigate the response of the environment to different actions and behaviours based on the current understanding of the processes involved. The results of these models are then used to inform decisions made about space activities, including national and international licensing, regulation, and policy as well as spacecraft design and operation. However, appropriate data which could be used to develop and validate these models is in short supply. As a result many of the current debris models share common component models of the underlying processes and so rely on the same set of assumptions about the spacecraft and debris populations.

In recent years, these challenges have been further complicated by the rise of NewSpace and the resulting changes in both the construction of spacecraft and the missions flown. Existing debris models are currently being used to assess the impact on the debris environment of NewSpace changes, such as small satellites (also known as small-sats) and large constellations. Several of the key components of these models are 20 years old, pre-dating the majority of NewSpace development. Given this age and the priority being given to modelling NewSpace it is important to understand what impact NewSpace might have on the models themselves. The development of this understanding provides novel insight into the suitability and limitations of

current models for studying NewSpace problems and hence how useful their results are for informing future decision making.

1.2 Project Overview

This project aimed to investigate the impact of NewSpace on the future modelling of the space debris environment. In light of the changes which have occurred across the space industry and the spacecraft population, it was considered that NewSpace may affect not just the outputs of the models, but also the choice of assumptions, parametrisations and simplifications made in the models. As a result successfully modelling the impact of NewSpace might require next generational debris models consisting of updated or entirely new approaches to the problem.

The project commenced with an in depth analysis of changes being observed in the design and operation of spacecraft in order to define and quantify what the term 'NewSpace' incorporates. This was followed by a rigorous investigation into the different components that make up the current generation of debris models to understand both their underlying assumptions and how they relate to the changes observed with NewSpace. This led into a study of individual performance of these components across a range of scenarios representing the transition from the traditional space environment to one dominated by NewSpace.

The results of the research into both NewSpace and component models were then used to design a series of simulations of a prospective NewSpace population, consisting of a large constellation and a background population of spacecraft and debris. This experiment looked at how potential changes to the underlying models would alter the results of studies of the future evolution of the debris environment.

Hypotheses

Three key hypotheses were identified:

1. NewSpace is associated with measurable changes in the physical and orbital characteristics of the spacecraft population.
2. NewSpace changes fall outside the scope of current assumptions, reducing the accuracy of the existing component models of debris processes.
3. Updates to models to incorporate the effect of NewSpace will change the current understanding of the future evolution of the debris environment.

This work aimed to test the validity of these three hypotheses and identify how future debris models might need to be updated as well as exploring the potential

consequences for the future of space debris modelling and the space debris environment.

1.2.1 Significance and Contribution

By studying the nature of the NewSpace changes and the impact they have on the performance of component models this work contributes to an understanding of the limitations of the current generation of models. This provides novel insights into which components of debris models are most in need of new development or refinement. Some aspects of this work have been published in Diserens et al. (2020b) and Diserens et al. (2020a).

Using these insights the effect of updates to models on the results of simulations of the debris environment has been quantified. These new results can be used to provide direction for the development of the next generation of space debris models and improve comprehension of the true impact of NewSpace on the space debris environment.

The outcomes of this work help with the assessment of NewSpace trends conducted using current generation debris models. By evaluating the limitations of the models and the biases introduced when studying NewSpace identified errors introduced by current models. A quantification of these errors undermine the conclusions drawn from previous studies leading to the inference that poor and inadequate policies and regulations are being formed based on these results. The wider impact of the findings of this work is to contextualise current results, showing that models adapted to NewSpace changes are required and will provide the ability for better decisions to be made regarding future policy and licensing decisions.

1.2.2 Project Structure & Objectives

Figure 1.1 describes the objectives of the different stages of this work, along with their interdependencies. The work-flow was divided into four different streams corresponding to a review of the background literature and the testing of each of the three hypotheses. The different chapters of this thesis are divided across these streams as follows:

- Chapter 2 - The first stream, a review of the background of the problem, based on existing literature and the current state of the art.
- Chapter 3 - The second stream, describes the objectives related to testing the first hypothesis, an assessment of the nature of NewSpace.

- Chapter 4 - The third stream, relating to the objectives for the validation of component debris models and the testing of the second hypothesis with respect to component fragmentation models.
- Chapter 5 - The third stream, relating to the objectives for the validation of component debris models and the testing of the second hypothesis with respect to component collision models.
- Chapter 6 - The fourth stream, deals with objectives around the testing of the third hypotheses and integrated simulations of the debris environment.

The final chapters of the thesis consist of a discussion of the results and their significance for the future of the debris environment and the use of debris models, and a summary of the conclusions of this work. Appendices A, B and C detail the verification processes for the fragmentation model, collision algorithms, and orbital propagator respectively.

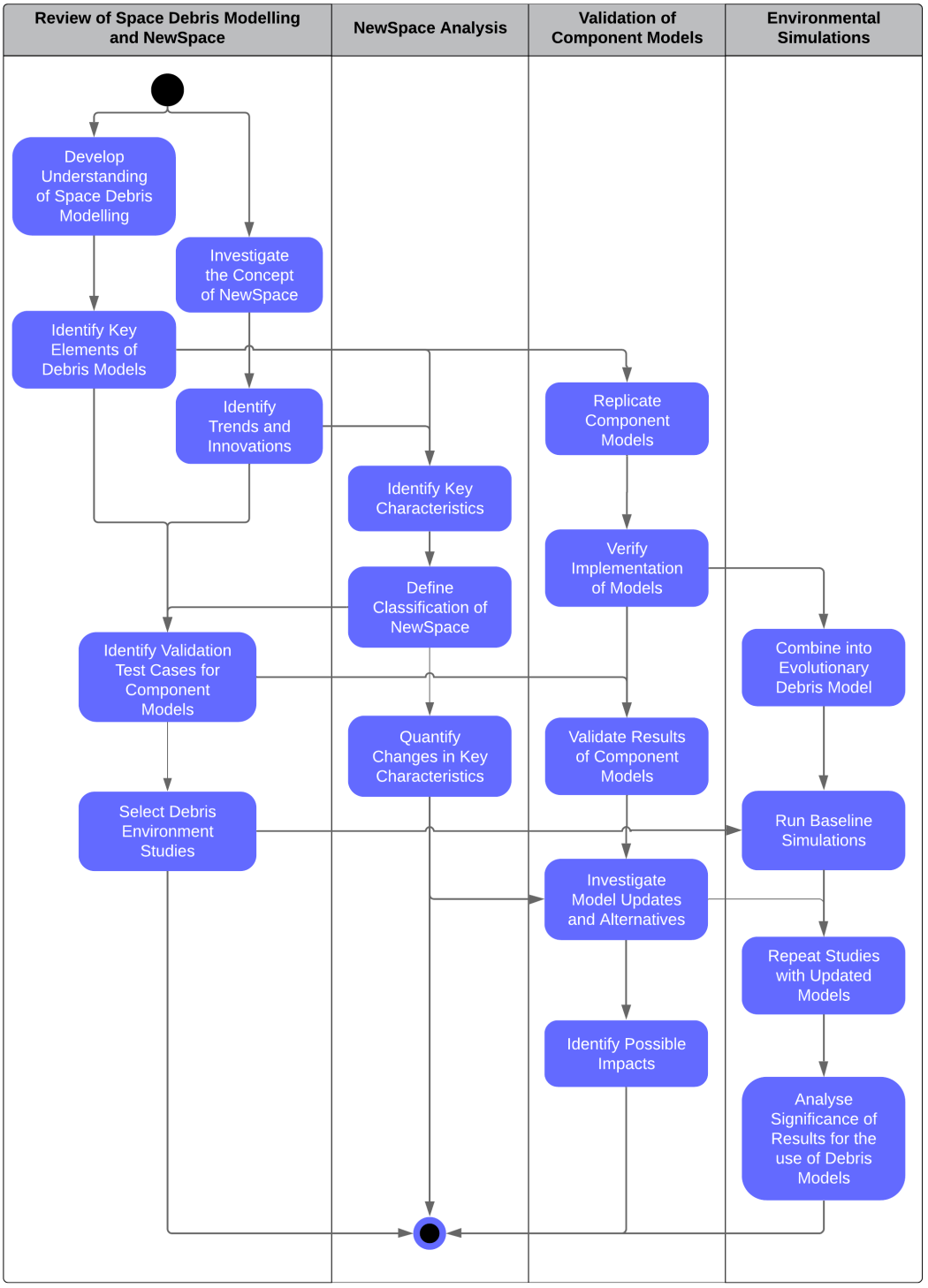

FIGURE 1.1: Flow of project objectives through different work streams

1.2.3 Software Development

As part of this work a suite of software tools was written to facilitate the testing of several existing models (see Chapters 4 and 5) and to run simulations of the evolution of the debris environment (see Chapter 6). The tools consist of a central framework, with the capability to run simulations with a selection of different, configurable component models, as well as a number of sub-programs which allowed the testing and verification of individual component models independently.

The software was written for use on the Windows 10 operating system in Microsoft Visual Studio 17 using the C++ programming language and Nvidia Corporation's Compute Unified Device Architecture (CUDA) for the integration of parallel computation on local Graphics Processing Unit (GPU)s. Code was compiled using a combination of the inbuilt Microsoft C/C++ compiler (MSVC) and the Nvidia CUDA Compiler (NVCC). To support reproducibility of the results, all source code has been made available at https://github.com/SDiserens/Debris-Models. Configuration and scenario files were written using the JavaScript Object Notation (JSON) format to provide inputs to configure each simulation in addition to command line interfaces. The outputs of each run are then logged in date-stamped CSV files.

The simulations conducted in this investigation were all run on the following hardware:

- **Processor**: Intel® Core™ i7-6700 Processor 3.40 GHz
  - Cores: 4; Threads: 8; cached memory: 8 MB
- **Installed RAM**: 32.0 GB
- **GPU**: NVIDIA GeForce GTX 1080
  - 2560 CUDA cores; 320GB/s memory bandwidth; 8GB internal memory

Random Number Generation

One area for concern in the software was the choice of a random number generator. It was thought that the pseudo random number generator used in the computational models may not provide a suitably uniform distribution. There are known issues with 'Linear Congruential Generators', including the default 'rand' function in the c++ standard library, due to their low periodicity.

To avoid these issues a 64-bit 'Mersenne Twister' generator was used (mt19937_64) with has a period of $2^{19937} - 1$ (Harase, 2014). This generator was then seeded using the count of seconds elapsed since epoch on the system clock.

Chapter 2

Literature Review: Space Debris Modelling and NewSpace

> All models are wrong, but some models are useful.
>
> George E. P. Box

2.1 Reviewing the Problem Case

To investigate the impact of NewSpace on the ability of current models to provide insight into the debris environment, and so explore the three core hypotheses of this work, it was first necessary to understand the context of the problem. The first half of this chapter explores the current state of the space debris environment, beginning with the broader background of the debris environment and the risks posed by debris. It then moves on to examine the different ways in which space debris is modelled to identify the key processes involved.

The chapter next looks at how the space debris problem might change in the future. First, by discussing the different ways in which attempts are being made to control the growth of space debris and reduce the risks posed by space debris. Next it addresses how the use of space is changing and what this means for the future of individual spacecraft and the overall environment. By examining these different elements in turn this chapter aims to provide the context for the investigations which follow.

2.2 Background on Space Debris

As of February 2020, the ESA estimated that there were approximately 2,300 functioning spacecraft out of more than 5,500 in orbit (ESA, 2020a). The other 60%, now largely uncontrolled and useless, existed only as debris littering the region around the Earth. The oldest tracked piece of space debris is the Vanguard 1 satellite (Space-Track, 2018) which has been in orbit for more than 60 years. Launched on the 17th March 1958, Vanguard 1 was the 4th artificial satellite to orbit the Earth and since loss of contact in 1964 has remained in orbit in an uncontrolled state. With a perigee of 654 km it is expected to be another 180 years before the combined forces of solar radiation pressure and atmospheric drag will cause its orbit to decay enough for it to re-enter the Earth's atmosphere (NASA, 2018).

Spacecraft and debris objects come in a range of different sizes, posing different levels of threat to active spacecraft. Table 2.1 shows one system for classification of spacecraft by mass.

TABLE 2.1: Satellite classifications (Konecny, 2004).

Satellite	femto	pico	nano	micro	mini	medium	large
Mass	< 0.1 kg	$0.1 - 1$ kg	$1 - 10$ kg	$10 - 100$ kg	$100 - 500$ kg	$500 - 1,000$ kg	$> 1,000$ kg

Objects are tracked using a network of ground based optical and radar telescopes with the main source being the United States Space Surveillance Network (SSN). Limitations on the resolution of tracking systems historically resulted in reliable tracking being possible only for objects with sizes greater than approximately $0.05 - 0.10$ m for objects in LEO and around $0.30 - 1.00$ m for objects in geostationary orbits (ESA, 2018b). In March 2020 the United States Space Force (USSF) completed acceptance testing of the first stage of the next generation Space Fence radar (Lockheed Martin, 2021). The introduction of this system is expected to extend resolution of debris objects down into the $0.02 - 0.05$ m range, greatly increasing the number of trackable objects. Additionally, there are several organisations providing commercial Space Surveillance and Tracking (SST) services, including LeoLabs who provide radar-based LEO tracking; and ExoAnalytic who provide optical tracking of GEO spacecraft.

Certain ground-based radars, such as the Haystack observatory, can detect objects as small as 1 cm in size. However, generally, the presence of smaller debris must be inferred from the amount of larger objects or by using on-board detectors and studying impacts on returned hardware. In February 2020, there were estimated to be roughly 34,000 space debris objects with a diameter greater than 10 cm, with a further 900,000 objects greater than 1 cm and more than 128,000,000 above a millimetre across (ESA, 2020a).

A key source of these smaller debris objects, accounting for more than half of the total debris population (Anz-Meador et al., 2018), is the fragmentation of larger objects and spacecraft either as a spontaneous breakup or due to a collision. According to ESA Safety & Security (2021) more than 550 fragmentation events have occurred since 1961. Table 2.2 lists several of the largest recorded breakup events and their assessed causes.

TABLE 2.2: A Table showing the top 10 breakup events as of 4th January 2016 (Credit: (Anz-Meador, 2016)).

Rank	International Designator		Common Name	Year of Breakup	Altitude of Breakup	Catalogued Debris	Debris in Orbit	Assessed Cause of Breakup
1	1999	25	Fengyun-1C	2007	850	3428	2880	intentional collision
2	1993	36	Cosmos 2251	2009	790	1668	1141	accidental collision
3	1994	29	STEP-2 RB[1]	1996	625	754	84	accidental explosion
4	1997	51	Iridium 33	2009	790	628	364	accidental collision
5	2006	26	Cosmos 2421	2008	410	509	0	unknown
6	1986	19	SPOT-1 RB	1986	805	498	32	accidental explosion
7	1965	82	OV2-1 / LCS 2 RB	1965	740	473	33	accidental explosion
8	1999	57	CBERS 1 / SACI 1 RB	2000	740	431	210	accidental explosion
9	1970	25	Nimbus 4 RB	1970	1075	376	235	accidental explosion
10	2001	49	TES RB	2001	670	372	80	accidental explosion

While the majority of historical fragmentation events are recorded as being due to explosions or of unknown cause, the small number of major collisions have had a disproportionate impact on the debris environment. The severity of any collision occurring between two orbiting objects depends on their relative kinetic energy. With an average collision velocity in LEO of 9.7 km/s (Rossi and Farinella, 1992) the transfer of energy can be in the hundreds of Giga-Joules. As a result these collisions result in the catastrophic breakup of the objects involved, potentially into many thousands of smaller fragments. Many of these fragments retain enough mass to be dangerous, increasing the risk to other spacecraft.

As such, the biggest risk is of high speed collisions between the many intact but defunct medium and large size spacecraft with masses in the hundreds and thousands of kilograms where the initial impact is compounded by the greater number of secondary debris fragments which are generated. The breakups of just three spacecraft due to collisions (Fengyun-1C in 2007 and Iridium-33 and Cosmos-2251 in 2009) were identified as the source of over 30% of all debris in orbit in 2018 (Anz-Meador et al., 2018). Thankfully, collisions of this magnitude have so far remained relatively infrequent.

2.2.1 History of the Space Activity

The presence of artificial objects in the space environment is relatively new. It is only a little over 60 years ago since, on the 4th October 1957, Sputnik-1 became the first

[1] *Rocket Body*

artificial Earth satellite. This achievement marked the commencement of 'The Space Race', with more and more spacecraft being launched as the cold war between the USA and the USSR drove competition to prove superiority in space. Within the following six months the USSR and the USA launched three more spacecraft: Sputnik-2, Explorer-1 and Vanguard-1.

The first spacecraft were launched atop modified Inter-Continental Ballistic Missiles (ICBM)s and were unabashed statements of the ability to deploy nuclear weapons across the world. However, the following 10 years saw extensive development, moving away from these military origins and beginning the development of dedicated launch vehicles and much more advanced spacecraft. Following the success of the Apollo lunar program in the late 60s and early 70s - as well as the failed Soviet lunar program - the crewed space race began to wind down, culminating in the 1975 orbital rendezvous and docking of an American Apollo and Soviet Soyuz spacecraft. Over this period the space industry grew significantly as new technologies and uses of the space environment were developed. By the end of the space race over one hundred uncrewed spacecraft were being launched every year for a variety of purposes including civil, defence and commercial missions (ESA Space Debris Office, 2020).

Figure 2.1 shows the variation in launch rate over the 62 years from 1957 to 2019 including how the ratio of crewed to uncrewed missions has fluctuated. Through the 1970s and 1980s there was a rapid initial growth in launch rates peaking at over 120 launches per year (Kyle, 2021). However, following the dissolution of the USSR and the end of the cold war in the late 1980s and early 1990s there was a noticeable decrease in the number of launches from that peak. The launch rate has since begun to slowly climb back up as more launch operators have emerged, representing both

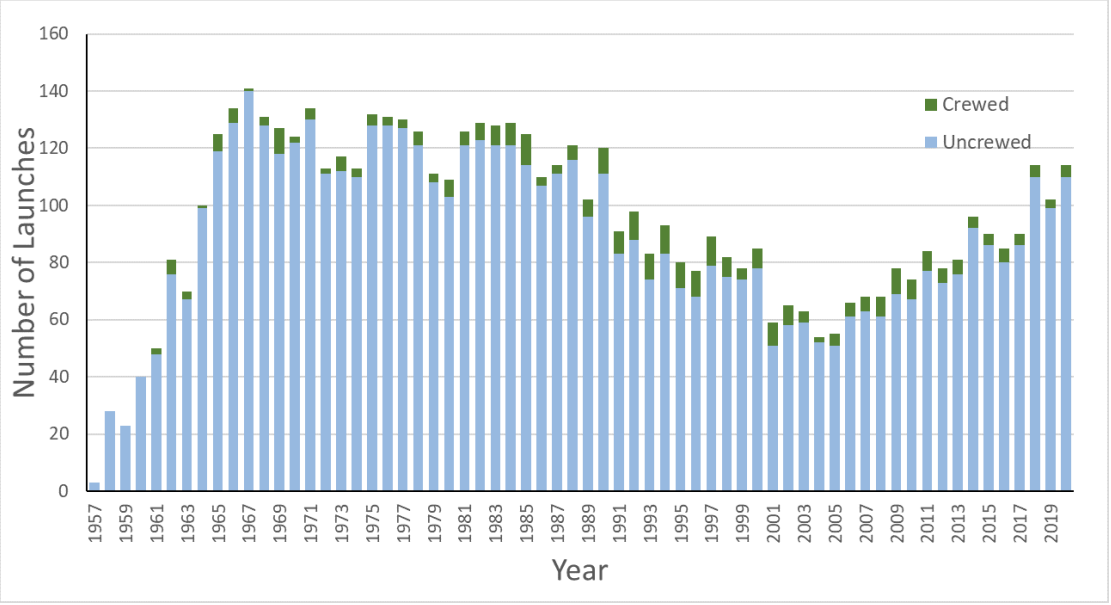

FIGURE 2.1: Global launch rates per year for crewed and uncrewed missions (Source data: Kyle (2021))

national agencies and private companies. This is indicative of the change in the driving force behind the space sector from largely government controlled towards a more commercial focus. The introduction of regular launches for the deployment and replenishment of large constellations, such as Starlink, is likely to cause an increase in the number of launches going forwards (SpaceX, 2018).

Although it has not yet returned to the peak of over 130 launches per year seen in the late 1960s the rate of launches has increased in recent years. The total number of satellites being launched into orbit has grown considerably, by count if not by mass, with an average of around 400 objects per year between 2017 and 2019 (ESA Space Debris Office, 2020). Advancing technology and changing requirements have allowed the average size of satellites to decrease meaning that more spacecraft can now be put into orbit on fewer launches. At the end of November 2018, the total number of active satellites in orbit had reached a record high of 1,957 (Union of Concerned Scientists, 2019) and in the two years that followed the count increased by a further 50% to 2,787 by August 2020 (Union of Concerned Scientists, 2020) and may now have passed the 3,000 mark.

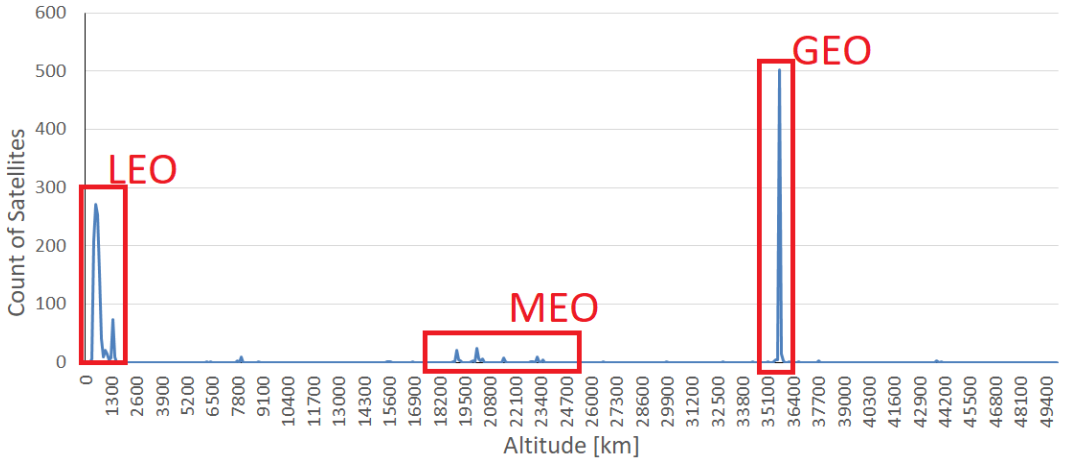

(A) Total altitude distribution of satellites

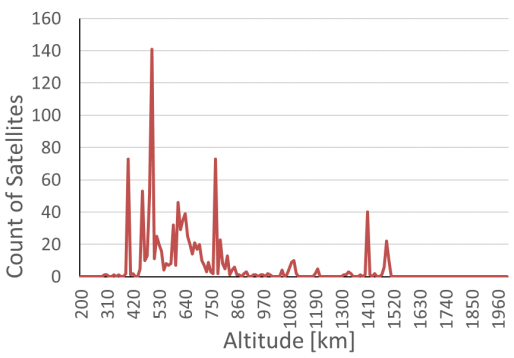

(B) Altitude distribution of LEO satellites

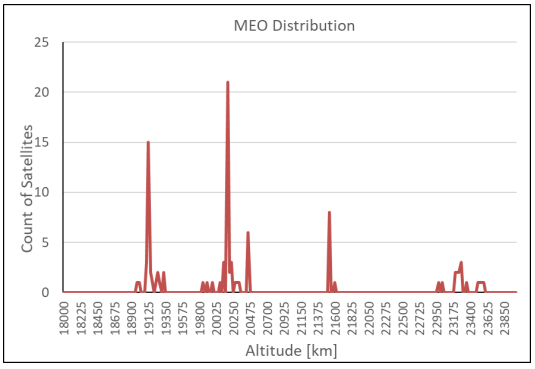

(C) Altitude distribution of MEO satellites

FIGURE 2.2: A set of graphs showing the distribution of satellites by mean altitude (Source data: Union of Concerned Scientists (2017))

The orbits in which these spacecraft operate vary substantially, ranging from altitudes as low as 300 km to geosynchronous satellites around 35,786 km and scientific missions in elliptical orbits at even higher altitudes. However, while this describes a vast volume of space compared to that occupied by the spacecraft themselves, the distribution of these orbits is far from uniform. Of the satellites recorded by Union of Concerned Scientists (2017), 62% operate in the LEO region, with altitudes of less than 2,000 km, and a further 31% at GEO orbits close to around 35,786 km.

Figure 2.2 shows the overall distribution of these satellites, with specific focuses on the distributions within the LEO region and where spacecraft are concentrated in the Medium Earth Orbit (MEO) region, including Global Navigation Satellite Systems (GNSS) satellites in semi-synchronous orbits. It can be seen that even within these regions satellites are clustered into relatively narrow altitude bands and so are more likely to encounter one another than they would be if more evenly distributed.

2.2.2 Space Debris Risks

The presence of artificial space debris threatens the safe operation of spacecraft in Earth orbit. While the probability of collision is low for any specific encounter between two objects the potential severity of a collision and the increasing rate of encounters (as the population grows) means that collision constitutes a considerable risk to spacecraft missions. As the number of debris objects exceeds the number of active spacecraft by several orders of magnitude the most probable collisions are between two debris objects. However there is a significant probability of a collision between a piece of debris and an active spacecraft where a collision could result in loss of the spacecraft or compromise the mission goals. For example, the catastrophic collision in 2009 between the Iridium-33 communications satellite and the defunct Cosmos-2251 satellite which resulted in the destruction of both spacecraft (Pardini and Anselmo, 2009).

The greatest severity threat is to human space flight, which has potentially fatal consequences, although the relative probability of an event is low due to the comparatively small number of spacecraft. This risk is dominated by the International Space Station (ISS) with its large cross-sectional area and long duration mission. Visible damage due to space debris has been observed on crewed spacecraft including the cratering of the ISS cupola window and the pitting visible on returned space shuttles which can be seen in Figure 2.3.

Debris-debris impacts can have long term implications for the near Earth environment as each collision can result in the release of many secondary debris objects which, while smaller, still pose a substantial hazard. Events involving medium or large spacecraft, such as the collision of the Iridium-33 and Cosmos-2251 satellites and the Chinese Anti-Satellite Weapon (ASAT) test in 2007, can generate hundreds or

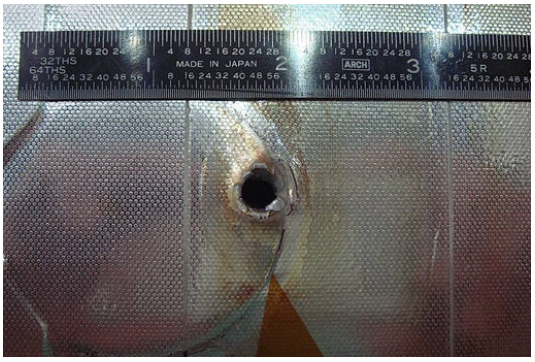

(A) Entry hole in the Space Shuttle Endeavour's radiator panel (Source: (Lear et al., 2008)).

(B) Chip in the window of the ISS cupola (Source: (ESA, 2016)).

FIGURE 2.3: Pictures of damage done to spacecraft by the impact of space debris.

thousands of individual fragments of trackable size. The breakup of Fengyun-1C in 2007 generated 3,430 catalogued fragments with the energy of the collision distributing fragments across a range of intersecting orbits. By 2017 only 600 of the fragments had decayed and 30% were expected to still be in orbit by 2035 (Pardini and Anselmo, 2009; Braun et al., 2017).

In addition to the probability of collision, there is a small but present risk to people and property from debris re-entering Earth's atmosphere (Bouslog et al., 1994; Park et al., 2018). Historically certain materials and components have survived to impact the surface and cause some property damage. While the majority of spacecraft will burn up in the upper atmosphere (Klinkrad, 2006), breakup is poorly understood and there is a greater risk involved for (a relatively few) massive objects and some specific well shielded components with high heat tolerances, such as magnetic torque cores (Pardini and Anselmo, 2019; Kärräng et al., 2019; Park et al., 2021).

2.2.3 The Consequences of Space Debris

There are a number of impacts associated with managing and mitigating the threats posed by space debris. There is, for example, a commitment to tracking debris objects in order to understand the changing environment and to identify potential collisions. Some satellites also carry additional propellant to allow them to perform collision avoidance manoeuvres to prevent collisions with tracked debris objects (Sánchez-Ortiz et al., 2015). However, performing this manoeuvre temporarily removes the spacecraft from the target orbit, causing a break in service. Additionally, the available fuel supply is limited and each use decreases the operational life of the spacecraft. As such, decisions must be made about what risk is acceptable and what should trigger a manoeuvre.

In addition, it has become necessary for spacecraft and space missions to be specifically designed to attempt to mitigate the potential damage caused by small scale (1 mm diameter) debris and so limit the severity of collisions. Measures taken to reduce the severity include the introduction of debris shielding and the arrangement of critical sub-systems within the spacecraft such that it is more likely to survive an impact from small debris (National Research Council, 1995; Schäfer et al., 2005; Stokes and Swinerd, 2005; Zheng and YanGang, 2017).

The result is that there is the risk of a growing economic cost associated with the presence of space debris which increases in proportion to the threat it poses (Adilov et al., 2015; Macauley, 2015). The combination of the increased collision probability along with this cost, including corresponding increases in insurance premiums (Swiss Re, 2011; Wiedemann et al., 2013), raises barriers to the future use of space. In order to prevent certain orbital regions being rendered inaccessible due to prohibitive levels of expense or operational risk, efforts are made to understand and control space debris risks. Some of the different models and mitigation measures involved are explored below.

2.3 Modelling Space Debris

To develop a better understanding of space debris, mathematical models are used to understand or predict the behaviour of the space debris population. There are different approaches which can be taken to this modelling depending on the required outputs of the model. For instance, when investigating the population as a whole it is possible to use a simple systems model. These models provide generic insights, such as the scale of the change a behaviour has on metrics like the rate of growth of the debris population. This allows the outputs of these models to be used to inform decisions and policies around the future use of space.

In contrast, some investigations require the assessment of the impact of individual space missions and architectures. In these cases a more complex evolutionary model is necessary to represent the differences between individual objects within the model. This additional complexity of these models allows more specific details of a future population to be addressed, such as the impact of removing specific objects from the population. However, there are significant uncertainties in the characteristics of the environment, which leads to considerable variation between different models and different simulation runs. As a result these models are not suitable for predicting specific events, such as when collisions will occur, or where debris will be located.

2.3.1 The Debris Environment as a Dynamical System

The changing space debris population can be considered as a dynamical system and described by a differential equation relating the rate of change of the population size to different factors and the population size. The key processes are the introduction of new objects to the environment (e.g. launches), the removal of objects (e.g. decay), and the interaction between objects (e.g. collisions).

$$\frac{dN}{dt} = A - BN + CN^2 \tag{2.1}$$

As such, the differential equation can be formed using a quadratic function as in Equation 2.1. In this equation A, B and C are coefficients which might describe, respectively, the rate of launch, the rate of decay and the rate of collision. Equations like this form the basis for a class of models known as differential or "Particles-In-a-Box" (PIB) models which are explored in more detail later in this section.

The balance of the different processes will determine the future evolution of the environment. Using Equation 2.1 as an example, if the CN^2 term dominates then the population will undergo exponential growth while if the $-BN$ term dominates exponential decline might be seen. However, if population growth ($A + CN^2$) is equal to population removal ($-BN$) then a state of dynamic equilibrium would be reached. In order to understand how NewSpace might impact these coefficients and hence the rate of change of the debris population it is important to understand the mechanics behind the key processes and how they might be changed by NewSpace.

Debris Sources

The key to understanding the rates at which new debris objects are added to this system is to understand how these objects are created and what can be classified as space debris. The current debris population is made up of objects from a diverse range of sources including:

- Satellites which have reached their end-of-life or which are otherwise no longer operational.
- Rocket stages which remain in orbit having delivered their payload.
- Fragments of spacecraft released during breakup events, such as explosions or collisions.
- Mission related debris, such as explosive bolts released by staging rockets, adaptor rings, and payload shrouds.
- Condensed droplets of coolant from nuclear reactors (E.g. a sodium potassium alloy - NaK).

- Condensed droplets of aluminium oxide released by solid rocket motors.
- Flecks of paint which break free of spacecraft as the ultra-violet light causes it to decay.
- Sections of Multi-Layer Insulation (MLI) which has been shed from the outside of satellites.
- The natural micro-meteoroid population of rock and ice particles.

The number and mass of debris of different types can be compared to determine their relative importance and identify the key sources. Figures 2.4 & 2.5 illustrate the breakdown of trackable objects[2] by type for the count and mass respectively of known orbital objects in orbit over time. These figures show how both the mass and number of objects in orbit has grown over time.

The launch of new spacecraft is a significant source both in terms of the number of objects and, particularly, the accumulation of mass in orbit, of which it is the only significant contributor. As a process this is dependent upon how spacecraft design, launch rate and launch capability change over time which are in turn driven by the level of demand and technological development.

Looking at the rate of growth in the orbital population there has been a clear increase since 2006, and in particular two noticeable rapid increases in the number of payload fragments in 2007 and 2009. These jumps correspond to the known events of the destruction of Fengyun-1C and the collision of Iridium-33 and Cosmos-2251. This suggests that, at least historically, the breakup of objects and in particular the collision of large objects is one of the key processes to be considered.

[2]some of the object types mentioned do not feature as the debris is too small to be reliably tracked.

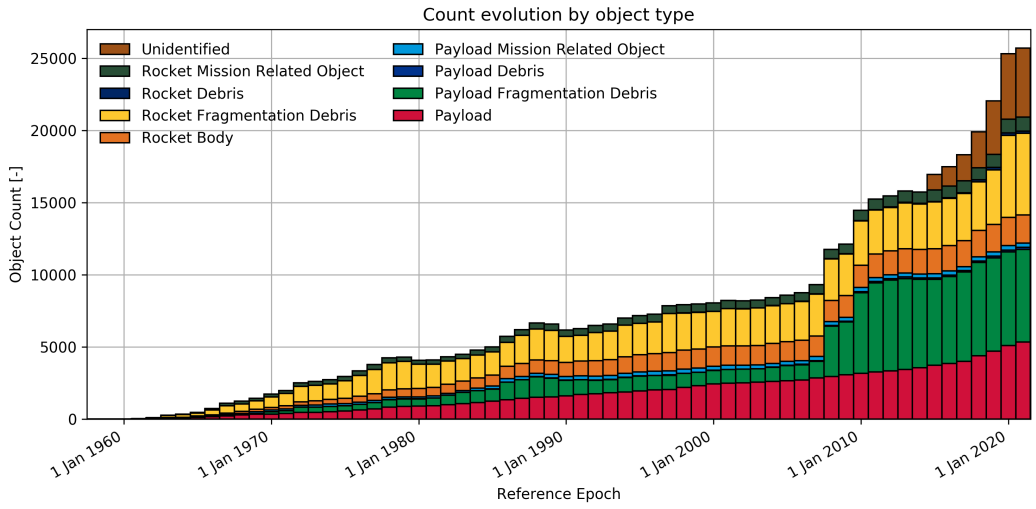

FIGURE 2.4: Breakdown of number of objects in orbit by type: ESA Space Debris User Portal (ESA, 2020b)

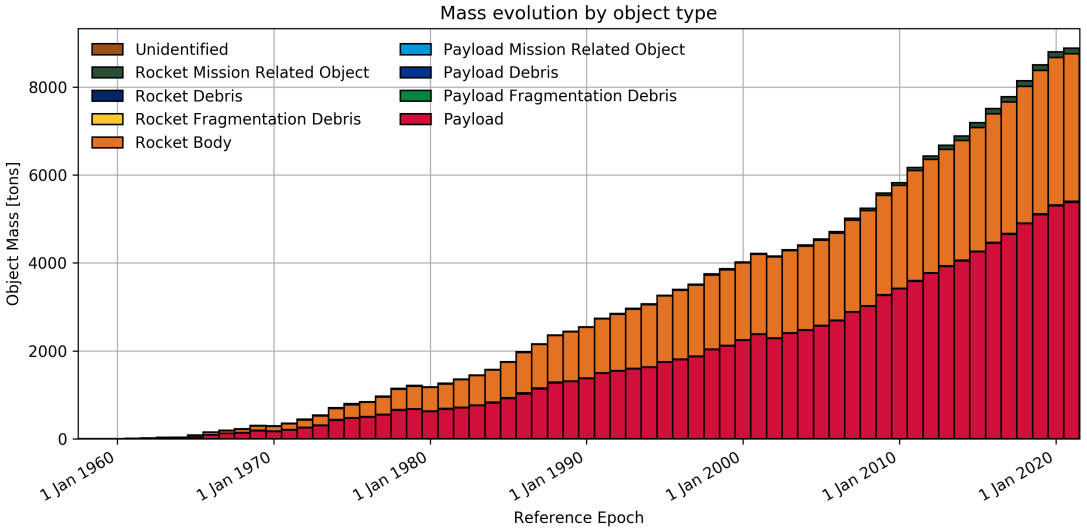

FIGURE 2.5: Breakdown of mass of objects in orbit by type: ESA Space Debris User Portal (ESA, 2020b)

As well as collisions, spacecraft fragmentation due to on-board explosions has historically been a major contributor of new debris objects. Spontaneous breakup can occur due to the release of stored energy from, for example, overloaded batteries or ruptured pressurised tanks. Of the 242 satellites believed to have broken up since 1957, accidental collisions between objects only account for 2.5% of events compared to the number of propulsion-based explosions (44.2% of events) (Anz-Meador et al., 2018). However, while the absolute number of accidental collisions is small they account for a much greater proportion of catalogued debris (11.6%). This suggests that the collision events, when they occur, are far more significant to the overall evolution of the debris environment.

Dynamics of Changing Orbits

The motion of an object in orbit is often described using a set of orbital elements which describe the shape and orientation of the orbit, as well as the position of the satellite along the orbit. Most often used are the 6 so called 'Keplerian elements' named after Johannes Kepler (1571-1630). The elements consist of the semi-major axis, a, the eccentricity, e, the inclination, i, the right ascension of the ascending node, Ω the argument of perigee, ω, and the true anomaly, v. These describe, respectively, the size of the orbit, the shape of the orbit, the angle of the orbital plane relative to the equatorial plane, the rotation of the orbital plane relative to the central body, the orientation of the orbit within the orbital plane, and the position of the object along the orbit.

In the idealised scenario an object exists in a perfect stable 'Kepler' orbit around a spherical planet, of uniform density, with no atmosphere, and with no external bodies to exert their influence. However, this is far from the reality experienced by an object

orbiting the Earth. Instead, an object orbiting the Earth is subject to a multitude of perturbing forces which combine to change the shape, size and orientation of the orbit over time. The most significant perturbations experienced by objects in Earth orbit are:

- **Geopotential perturbations**, due to the asymmetrical distribution of mass about the Earth's centre (Klinkrad, 2006, Annex A)
- **Aerodynamic drag**, due to the passage of the object through the upper levels of the Earth's atmosphere (King-Hele, 1987)
- **Lunisolar perturbations**, due to gravitational influence of third bodies, dominated by the Sun and the Moon (Roy, 1988, chap. 10)
- **Solar Radiation Pressure**, due to the momentum transfer from electromagnetic radiation (Hughes, 1977)

The different effects of these forces can be broken down into categories. As explained by King-Hele (1987, chap. 1), their effect on each of the orbital elements can be separated between those which are periodic and those which are secular (or continuously increasing) as well as by their scale. Table 2.3 shows how the three main perturbations described above affect the different orbital elements.

TABLE 2.3: Showing the effect of each of the three main perturbations on the different orbital elements (King-Hele, 1987).

	Secular		**Periodic**	
	Large	**Small**	**Moderate**	**Small**
Geopotential	Ω, ω		e	i, Ω, ω
Aerodynamic	a, e	i		Ω, ω
Lunisolar				a, e, i, Ω, ω

The dominant perturbing force changes between the different orbital regions. At low altitude in LEO atmospheric drag dominates, however this decreases exponentially with increasing altitude as the residual atmospheric density decreases and above 600 km solar radiation pressure is dominant. In GEO the major perturbing forces are solar radiation pressure as well as geopotential and lunisolar gravity.

Atmospheric drag, in particular, is significant for the evolution of the debris environment. As objects move through space they encounter particles forming the upper reaches of the atmosphere. The impact of these particles on the objects cause them to be accelerated downwards into ever lower orbits until they reach an atmospheric density high enough to prevent them from remaining in orbit and they undergo re-entry (King-Hele, 1987; Vallado and Finkleman, 2014).

As a result of the gradient in the atmospheric density the drag force is stronger for lower objects than higher ones. For elliptical orbits the asymmetric application of the drag force causes apogee to fall faster than perigee resulting in decreasing eccentricity.

This force differential means that for two otherwise identical objects separated in altitude the separation should only grow over time.

However, the key factor is the area to mass ratio of the objects. While the drag force applied is dependent on the air-relative cross sectional area of the objects acceleration is proportional to the area-to-mass ratio. As such objects with a higher area to mass ratio will experience orbital decay faster than those with a low area to mass ratio for the same drag coefficient. This results in atmospheric drag being a major source of population mixing in LEO.

The impact of solar radiation pressure has a similar dependency on the area to mass ratio, causing greater eccentricity changes in objects with high area to mass ratios. This results in solar radiation pressure being the major driver of population mixing in the MEO and GEO regions.

Debris Sinks

It is also important to understand the processes by which debris is removed from the environment. These processes include re-entry into the Earth's atmosphere, departure from Earth orbit, and the destruction of debris objects. Of these processes the most significant to the debris environment is the re-entry of objects, either due to controlled entry from the manoeuvring of the spacecraft or due to the cumulative effect of atmospheric drag causing the altitude of the object to decrease until increasing atmospheric density prevents it from being able to complete a full orbit (normally at altitudes of around 120 km). Re-entering objects normally breakup due to the aerodynamic forces at altitudes in the range of $75 - 85$ km (Ziniu et al., 2011).

Some debris objects will be destroyed by collisions or explosions, however this number is small compared to the overall size of the debris population with events occurring at a rate of only four or five a year (Anz-Meador et al., 2018).

2.3.2 Current Debris Models

A range of different models exist for modelling space debris based on several different approaches, each with their own advantages and disadvantages depending on their design and the type of problem they were created to solve. These different models can be broadly categorised as being one of the following:

- engineering models;
- differential (or Particle-in-a-Box) models; or
- evolutionary models

The different implementations have distinct requirements in terms of prior knowledge and computational resource. Which model is most appropriate can be assessed based on the objectives of the study being conducted and the time and resource available.

Engineering models

Table 2.4 introduces several different engineering models, also known as debris flux or debris environment models. These models exist to assess the flux of debris particles that would be experienced by a specific spacecraft and mission (Klinkrad et al., 1995, 1997; Sdunnus et al., 2004; Baojun et al., 2015). The aim of this is to attempt to represent the possible experiential debris environment for a particular satellite over its life time and so determine what risk it faces from space debris.

TABLE 2.4: Engineering debris models (Klinkrad et al., 1997; Sdunnus et al., 2004; Baojun et al., 2015).

Model	Organisation	Country	Released
Meteoroid and Space Debris Terrestrial Environment Reference (MASTER)	ESA	Europe	2009
Orbital Debris Engineering Model (ORDEM)	NASA	USA	2014
Space Debris Environment Engineering Model (SDEEM)	CNSA	China	2015
Space Debris Prediction and Analysis - Engineering (SDPA-E)	ROSCOSMOS	Russia	2017

These models contain reference debris populations at set epochs. This provides a baseline for the number and characteristics of debris objects in different orbits and so allows for comparison studies to be done with multiple models from the same starting point.

To prevent these models from being too computationally expensive the motion of the majority of the spacecraft and debris populations are precomputed. This allows the modelling of a very large debris population including debris sizes down to the scale of $1\mu m$ (Sdunnus et al., 2004). As a result these models include little variability in the evolution of the environment and so are used to run simulations over relatively short time periods, up to a maximum of around 25-50 years depending on the model(Krisko et al., 2015). However, this allows the direct integration of the motion of the primary spacecraft over much shorter time steps

Differential models

A selection of differential debris models has been shown in Table 2.5. The purpose of differential, or analytical, models is to provide fast, non computationally expensive, methods of simulating the long-term future of the debris environment (Kessler and Cour-palais, 1978; Kessler, 1981; Talent, 1992; Kessler and Anz-Meador, 2001; Lewis et al., 2009). This is achieved by modelling the dynamical system as a whole by using differential equations to model the rate of change of the population. This often

involves the discretisation of space into different regions and quantifying the rates at which objects are added or removed from the environment through different processes.

TABLE 2.5: Differential debris models (Talent, 1992; Rossi et al., 1995; Kessler and Anz-Meador, 2001; Ananthasayanam et al., 2006; Lewis et al., 2009; White and Lewis, 2014a).

Model Acronym	Organisation	Country	Released
Talent - (PIB)	Lockheed Engineering and Sciences	USA	1992
STochastic Analog Tool (STAT)	CNUCE/CNR	Italy	1995
Kessler	NASA	USA	2001
Stochastic IMPressionistic Low Earth (SIMPLE)	Indian Institute of Science	India	2006
Fast Debris Evolution Model (FADE)	University of Southampton	United Kingdom	2009
Computational Adaptive Strategy to Control Accurately the Debris Environment (CASCADE)	University of Southampton	UK	2014

These models enable the population of the debris environment to be estimated at any future time by the integration of the differential equation using simple numerical methods. The advantage of this method is that it reduces the number of calculations required, allowing long term simulations to be conducted with little computational expense. However, a compromise of this is that, by looking at population characteristics, the impact of more complex behaviours and interactions are harder to capture.

Simulations done using these models are used to investigate the potential behaviour of the space debris population over long time scales. The majority of these models are used for research into the future of the overall debris environment.

Evolutionary models

Evolutionary models simulate the movements and interactions of entire populations of objects in orbit, as opposed to engineering models where a primary object (or system of objects) is simulated within a predetermined environment. By contrast to differential models, this is achieved by modelling the behaviour of the individual objects that make up the overall system in order to observe how they interact in the evolution of the environment (Lewis et al., 2001; Liou et al., 2004; Dolado-Perez et al., 2013; Virgili, 2016; Radtke et al., 2017b). This requires numerical methods to propagate the objects forwards through time, taking into account perturbing forces such as the atmospheric drag and solar radiation pressure, adding to the computational complexity involved in simulating a large debris population.

Evolutionary models, such as those listed in Table 2.6, have become the main tool for researching the future of the debris environment and are developed and maintained by a variety of organisations, including national space agencies, universities and private companies. By simulating individual objects it is possible to focus on the impact of behaviours such as specific mission types or mitigation measures, enabling different investigations to those conducted using simpler differential models.

TABLE 2.6: Evolutionary debris models(Source: (Klinkrad, 2006; Beck, 2013; Rossi et al., 2013)).

Model	Organisation	Nation	Published
(EVOLVE)	(NASA)	(USA)	(1991)
Long Term Utility for Collision Analysis (LUCA)	TU Braunschweig / DLR	Germany	1998
Space Debris Mitigation long-term analysis program (SDM)	ASI	Italy	1998
Space Debris Prediction and Analysis (SDPA)	ROSCOSMOS	Russia	2000
Debris Environment Long Term Analysis (DELTA)	ESA	Europe	2002
Debris Analysis and Monitoring Architecture to the Geosynchronous Environment (DAMAGE)	University of Southampton	UK	2004
LEO-to-GEO Environment Debris model (LEGEND)	NASA	USA	2004
Near Earth Orbit Debris Environment Evolutionary Model (NEODEEM)	Kyushu University / JAXA	Japan	2009
Aerospace Debris Environment Projection Tool (ADEPT)	Aerospace Corporation	USA	2009
Modelling the Evolution of Debris on Earth's Environment (MEDEE)	CNES	France	2012
Space Objects Long-term Evolution Model (SOLEM)	CNSA	China	2019
Integrated Debris Evolution Suite (IDES)	QinetiQ	UK	Unknown
Kustaanheimo and Stiefel Canonical Propagation model (KSCPROP)	ISRO	India	Unknown

Due to the uncertainties inherent in attempting to model these complex interactions many of the component models are probabilistic, with stochastic elements representing the uncertainties. As such it is necessary to conduct multiple Monte Carlo runs of each simulation. This has the advantage of generating a probability distribution across the different potential outcomes but has the disadvantage of requiring a significant amount of computational resource in order to complete the necessary runs in a short enough time frame.

One of the problems with this type of model is that many of the different implementations make use of the same base models of the underlying processes. This is due to the complexity of the processes involved as well as the scarcity of data. A result of this is that any systemic errors or mistaken assumptions in these base component models will appear in the output of multiple evolutionary models. As such, care must be taken to avoid interpreting consistency between these models as being an accurate representation of the future debris population when only two or three distinct approaches are being used.

Use of evolutionary models allows the simulation of the debris environment over a relatively long period, often in the 100 to 200 year range. This allows the models to be used to investigate the long term impacts of changes in the way space is used, for example different levels of mitigation, the introduction of ADR, or NewSpace activities (Liou and Johnson, 2009; Liou, 2011; Lewis et al., 2012; White and Lewis, 2014b; Lewis et al., 2017b).

2.3.3 Core Elements of Debris Models

To model the space debris environment there are a number of key processes discussed above which must be understood and replicated within the model. The core of this modelling is normally focussed on the underlying processes which determine the

physical behaviour of objects within the debris environment. Debris models are built around component models of the following physical processes:

- Fragmentation of objects into debris clouds.
- Predicting collisions between pairs of objects.
- Propagation of the position and orbital parameters through time.

Simulating Fragmentation and Breakup

As discussed a key source of debris is the fragmentation of spacecraft or debris objects either due to collisions or explosions. Fragmentation models are a key element to modelling the debris environment. These models generate an approximation of how debris objects are expected to disintegrate, with the mass and momentum of the parent object(s) distributed across an expanding cloud of debris fragments.

One widely used model for simulating breakups is the NASA Standard Breakup Model developed in 1998 with the intention of implementing a refined fragmentation model based on available observational and experimental data (Reynolds et al., 1998; Johnson et al., 2001). However, this model is now over 20 years old and relies on assumptions based on observations of historic spacecraft. As a result, it was hypothesised that some of the behaviours described by this model have changed due to developing technologies.

For example, the choice of construction material may affect the likelihood of a catastrophic breakup. Modern spacecraft, which utilize lightweight composite materials, such as carbon fibre, might have significantly different thresholds due to differences in the speed of sound and speed of propagation of shock-waves. There are also outstanding questions on how the use of novel construction methods such as additive manufacturing (3D printing) will impact this value. As a result the fragmentations of these modern spacecraft might differ significantly from those predicted by the model producing a very different distribution of fragments.

Predicting Object Collisions

Collisions, leading to the catastrophic fragmentation of spacecraft, have been shown to be one of the major sources of space debris. An important part of modelling the evolution of the debris environment is understanding which objects might be involved in collisions, and when and where these events could occur. Collision algorithms exist within debris models to try and answer this question, normally by evolving the environment over discrete time-steps and deciding whether or not a pair of objects will have collided within each step.

As these collisions can only occur between objects whose orbits pass close to one another a large factor in these algorithms is identifying objects which can approach to within a certain distance. In reality this distance must be less than the combined size of the two objects. However, a larger distance is often used within the models to attempt to account for the uncertainty in the exact orbits and positions of the objects.

This can be a very computationally expensive process due to the large number of debris objects being modelled. If potential collisions are examined between each distinct pair of objects then the number of operations required for N objects is:

$$\frac{N(N-1)}{2} \tag{2.2}$$

For a millimetre size debris population of the order 10^8 this gives in the realm of 10^{16} combinations. The purpose of most collision algorithms is to provide a set of rules for filtering the total number of pairs of objects which need to be examined in order to reduce this load. These pre-filters normally operate by defining which pairs have the potential to collide before determining whether or not they do collide.

Collision algorithms operate in one of two ways, deterministically or probabilistically. For deterministic models the decision is a binary decision, a collision either occurs or it does not. This requires knowing the position and path of travel of both objects in a pair to determine if they both occupy the same place at the same time any point in the simulation (Hoots and Roehrich, 1980a; Woodburn et al., 2009). However, a truly deterministic simulation would also require knowledge of the size, shape, attitude and rotational motion of both objects in order to determine whether they ever come into contact.

Probabilistic models, such as the Cube approach (Liou et al., 2003), focus on defining the collision probability of a pair of objects over a period of time (Öpik, 1951; Wetherill, 1967; Kessler, 1981; Liou, 2006; Matney, 2017). In most cases this has the advantage of requiring only the shape, size and orientation of the orbits of the two objects without any knowledge of their position on that orbit. A decision on whether a collision has or has not taken place can then be made by comparing a randomly generated value against the collision probability.

However, it was hypothesised that new developments, such as mass-launch events and the introduction of large constellations, are resulting in changes to the spatial structure of regions of the orbital environment. These changes raise questions about whether these assumptions remain applicable across all regions.

Propagating Orbital Motion

It is the modelling of perturbations that complicates the development of an orbital propagator. Traditionally propagators have fallen into one of three categories: analytical, numerical or semi-analytical; depending on how these perturbations are included. These different approaches each come with different strengths and weaknesses. The choice of propagator for a debris model is a balance between the computational power available, the speed required, and the accuracy required.

The first set of methods, known as analytical techniques or general perturbation methods, involve the analytic integration of the equations of motion of the orbiting object. The use of series expansions allows perturbing forces to be included in an analytic solution which is valid for all initial conditions as an explicit function of time (Brouwer, 1959b; Lyddane, 1963; Deprit and Rom, 1970; Hoots and France, 1987). This has the advantage of allowing the state vectors at any time, t, to be found using only one evaluation. However, there are distinct disadvantages to this method that prevent it from being used to generate accurate solutions. This is mainly due to the complexity of the expansions of the perturbing forces, which make it prohibitive to consider more than low-order approximations.

Numerical, or special perturbation, methods involve the numerical integration of the equations of motion of the objects. As described by Roy (1988, chap. 7), the effects of each of the perturbing forces over a small time step can be computed from the equations of motion and the known starting positions and velocities to find the new state vectors. These values can then be used as the starting values for the next step. Methods such as these (Deprit, 1975; Long et al., 1989; Peláez et al., 2007) allow for the numerical integration of perturbing forces even for scenarios where the analytical solutions are excessively complicated. However, as a result the methods require short integration steps in order for the forces to be accurately approximated. This leads to a computationally expensive process and, while modern computing power allows these to be handled relatively easily, it becomes an inefficient process for handling the propagation of large populations over a long simulation period. As such these methods are normally only used for engineering models where a greater accuracy is required over shorter time periods.

Semi-analytical methods involve the combination of general and special perturbations in an attempt to utilise the strengths of both approaches (Liu and Alford, 1980; Métris and Exertier, 1995; Valk et al., 2009). In general, these methods use analytical techniques to simplify the equations of motion before applying numerical integration to the result. This allows longer integration steps to be used, making for a more computationally efficient scheme, while including the effect of each of the perturbing forces. This results in somewhat reduced accuracy compared to numerical methods, but can allow for efficiencies approaching that of analytical methods.

A fourth approach has been proposed using empirical models to help forecast the orbital state by creating and training statistical models using a known set of data points. Some work has already been undertaken in this area by San-Juan et al. (2016); San-Martin et al. (2016) and Pérez et al. (2013) who have developed a method coined as 'Hybrid Perturbation'. An analytical propagator is used and the results from this are then improved by the inclusion of an error term generated using statistical time series models or computational intelligence. These models were generated using the deviations of the analytical solution from a high order Runge-Kutta numerical solution.

In contrast to the fragmentation and collision components a wide variety of propagators, including many bespoke systems, are used by different debris models. These include semi-analytical propagators, such as the STELA propagator used by Centre National d'Etudes Spatiales (CNES)'s MEDEE (Fraysse et al., 2012; Dolado-Perez et al., 2013), and analytical propagators, such as that used by Low Earth Orbit Debris Environment Evolutionary Model (LEODEEM) (Hanada, 2013) and ESA's FLORA propagator . Based on this variety, as well as the much greater amount of available data, this element of debris modelling is expected to be much more robust in the face of the changes associated with NewSpace.

2.3.4 Supplementary Elements of Debris Modelling

In addition to the core physical components described above, supplementary models are required to describe external influences such as changing environmental conditions and human interactions with the environment. Many of these elements are inherently unpredictable and the focus of entire fields of study. The complexity makes it difficult to include models more sophisticated than stochastic time-series models with random walks between expected upper and lower bounds. To avoid significant increase in the overall computational load these variables are often simulated once, to generate a time series of values. These results are then used in each subsequent simulation.

Environmental factors include physical changes such as variations in the Earth's atmosphere or solar activity. Variations in these factors can significantly alter the orbital perturbations experienced by objects resulting in changes to their orbits and expected lifetimes. In order to simulate the true long-term evolution of the debris environment propagators must include these variations which requires them to be captured within the model.

The human impact on the space environment is a significant one. Attempts to simulate how the environment will evolve must attempt to predict the rate at which new spacecraft will be added to the environment as well as what the human response will be to a growing space debris population. For example, what level of mitigation

will be applied with what success rate? Will ADR be implemented, and if so to what level and how much cooperation will be shown? Many current studies are interested in simulating the future debris environment for specific levels of ADR and mitigation in order to discover what impact the actions of humanity can have upon the existing environment (Liou and Johnson, 2009; Liou et al., 2010; Lewis et al., 2012; White and Lewis, 2014a).

Launch Traffic

Historically the most significant factor to the debris population is changing launch rates. An analysis of the annual launch rate over the previous 60 years shows that this can be highly variable (Kyle, 2021). When this is combined with the record number of satellites being released from recent launches, it can be seen that this is a non-trivial problem.

While predictions can be made about expected launch rates it is impossible to forecast what will actually happen, particularly beyond the short-term future. One approach is to use a recurring cycle of historical launches, for example a repeated eight year cycle of launch traffic (Rossi et al., 2013) using an assumed operational lifetime of 8 years and like for like replacement. This is intended to provide some variability in the introduction of new objects to debris models while providing a common base to allow for comparison of results between different models.

However, the problem with this approach is that it assumes a steady state for launches and spacecraft type which has been demonstrably false in recent years. As can be seen in Figure 2.1 the launch rate has been steadily increasing over the last decade and this is currently being further increased by the mass launch of constellations such as Starlink.

The repeated launch cycle is particularly ill equipped to handle these rapidly changing launch rates and types where only a small portion of the cycle reflects current trends. This results in a launch traffic which is not representative of either the historic population or the new population. For this reason, among others, these models of the debris environment are not attempts to predict, or forecast, the future state of the environment. Instead they are tools to understand the response of hypothetical environments to different behaviours.

Atmospheric models

Atmospheric drag is a key perturbing force causing the orbital decay of objects in LEO which makes it a significant factor in debris modelling. As the atmosphere is rotating with the Earth, the direction of the force applied on the object by the atmosphere

depends on the direction of travel of the object relative to the rotation. However, the major component of the force will be in the opposite the direction of motion of the object and can be described by the following equation (Curtis, 2014):

$$\overrightarrow{p} = -\frac{1}{2}\rho|v_{rel}|(\frac{C_D A}{m})\overrightarrow{v_{rel}} \tag{2.3}$$

where ρ is the atmospheric density, v_{rel} is the velocity of the object relative to the atmosphere, C_D is the drag coefficient, A is the cross-sectional area of the object, and m is the mass of the spacecraft.

However, the depth and density of the atmosphere fluctuates with time and location above the planet (Knipp et al., 2005; Vallado and Finkleman, 2014). This is due to a number of factors including the additional radius of the equatorial bulge pushing the atmosphere higher; regional, seasonal heating causing the atmosphere to expand and contract as it warms and cools; and the effect of solar activity on the temperature of the atmosphere as a whole.

Each of these factors must be taken into account to successfully model the effect of the atmosphere on orbiting objects. In addition to these localised and periodic fluctuations long term trends must also be considered, for example how the impact of pollution on the atmosphere changes its upper reaches, both from the changes to the chemical make-up of the atmosphere and from phenomenon such as global warming (Laštovička et al., 2006; Laštovička, 2009).

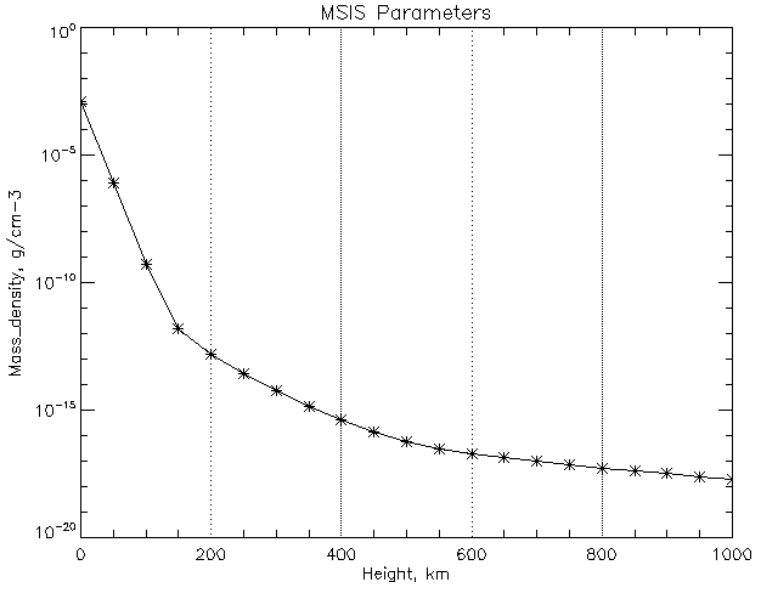

FIGURE 2.6: Atmospheric density for increasing altitudes using the NRLMSISE-00 model (Source: NASA Community Coordinated Modeling Center (CCMC, 2021))

Modelling of the changing atmospheric density is an entire research topic in its own right (Brown et al., 2019). As a result pre-computed reference models of the atmosphere are normally included within orbital propagators, one such commonly used model is the The Naval Research Lab's Mass Spectrometer and Incoherent

Scatter Radar Exosphere - 2000 (NRLMSISE-00) model (Picone et al., 2002) used within the STELA (Fraysse et al., 2012) and FLORA (Schaus et al., 2019) propagators among others. Figure 2.6 illustrates how the atmospheric density predicted by the NRLMSISE-00 model decreases logarithmically with increasing altitude in LEO.

Solar cycles

Another significant physical factor in this process is the level of solar activity. First observed by Samuel Heinrich Schwabe in 1843 (Arlt, 2011), the Sun has periodic variation in sunspot activity over the course of an 11 year cycle. It was later found that the full magnetic cycle of the Sun has a 22 year period, consisting of two non-identical Schwabe cycles (Owens et al., 2015). Beyond this, solar activity varies over longer time-scales, resulting in periods such as the 'Maunder Minimum' of low activity between 1645-1715. The sun is currently in a period of relatively high activity and has been since the early 1900s.

These solar cycles impact the behaviour of space debris due to resultant changes in atmospheric density (which varies with the total incident radiation and level of ultraviolet irradiance). During the high point in a cycle the increased radiation heats the upper atmosphere causing it to expand as the average kinetic energy of the individual molecules increases. The increase in temperature can result in order-of-magnitude increases in the atmospheric density compared to solar minimum (Walterscheid, 1989) with consequent decreases in the orbital lifetime of objects as the drag force increases (see Equation 2.3).

As with atmospheric density the modelling of the projected solar activity is a complex topic worthy of dedicated research (Charbonneau, 2020). Consequently simulations of the debris environment often use simple models such as ESA's SOLMAG to generate a series of randomly generated solar cycles based on historic data on solar activity of the 10.7 cm solar radio flux (Liou, 2006; White and Lewis, 2014a; Virgili, 2016; Radtke et al., 2017c).

Mitigation and Remediation

As well as additions to the debris environment due to human behaviour attempts to minimise or remove debris must be considered. Increases in the number of spacecraft operators has wider ranging impacts beyond the number of objects introduced to the environment. One particular area where this may introduce variability, is the case of mitigation where the increasing number of operators and licensing states makes it harder to predict and monitor behaviour.

Often the impact of different approaches to mitigation and remediation is what is being investigated using the models. For example, the response of the environment to

a range of levels of adherence to mitigation (e.g. 80, 90, 100% disposal rates) and a range of rates of ADR (e.g. 0, 1, 5, 10 objects per year) (Lewis et al., 2012; White and Lewis, 2014a,b). When studying the impact of other factors, such as large constellations, the standard practice is to assume a fixed level of adherence to mitigation standards (Virgili, 2016; Radtke et al., 2017a; Lewis et al., 2017b). This approach is taken in order to study the trends resulting from specific behaviours within a representative scenario rather than as an attempt to predict the eventual state of the debris environment.

2.4 The Future of Space Debris

Drag due to the upper atmosphere will cause the orbits of lower altitude debris objects to decay and eventually re-enter the Earth's atmosphere. However as shown in Equation 2.3, the drag force acting on an orbiting object is proportional to the atmospheric density which, as demonstrated in Figure 2.6, decreases exponentially with increasing altitude (Jastrow and Pearse, 1957; Knipp et al., 2005; Vallado and Finkleman, 2014).

The result, which can be seen in Figure 2.7, is that the debris population at altitudes above 800 km will remain in orbit for hundreds or even thousands of years, posing a continued risk to operational spacecraft. For objects in MEO and above, such as the GNSS and GEO satellites, the effect of atmospheric drag is negligible and objects will remain in orbit indefinitely unless their orbits are actively changed by performing a manoeuvre.

In addition to the rate of decay of historic debris objects, the future debris environment will depend on the rate at which new debris is generated. This rate will be a function of a number of factors, including the frequency of debris generating events (such as breakups) and the average number of new debris objects released per event. These factors will be sensitive to changes to the space industry. For example, an increase in the number of spacecraft being launched may result in a higher frequency of breakups, increasing debris growth. Conversely, improvements to technology and quality assurance might result in fewer breakups and so lower debris growth. Alternatively, a reduction in the average mass of spacecraft may reduce debris growth as the breakup of a smaller, lighter spacecraft must produce either fewer fragments or less massive fragments than a spacecraft with a greater initial mass.

According to the 15th edition of NASA's 'History of On-Orbit Satellite Fragmentations' (Anz-Meador et al., 2018) debris generation has historically been dominated by fragmentation of spacecraft; accounting for 65% of growth in the tracked object catalogue since 2008 and 53% of the total catalogue. However, ongoing efforts to reduce explosions and increased collision probabilities means that

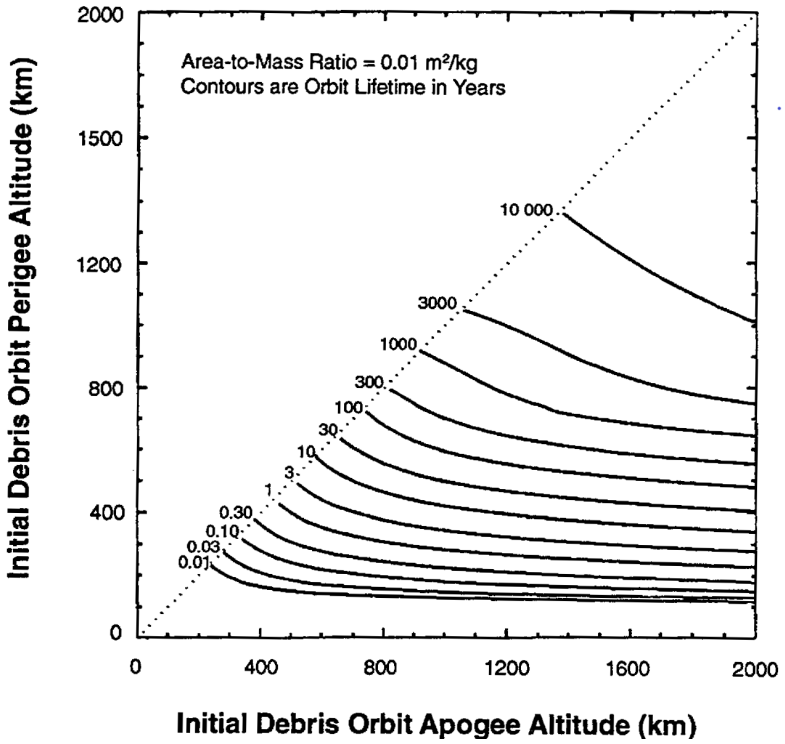

FIGURE 2.7: Orbital lifetimes for different altitudes (Source: NASA Space Safety Guidelines (Nasa, 2019))

explosions may be less important to the future environment and ongoing debris growth may be driven by collisions between objects.

2.4.1 Space Debris Policy (Mitigation)

In response to the recognised risks to space sustainability posed by the growth of the space debris population many space agencies and national regulatory bodies have developed specific policies relating to the mitigation of space debris. Several have dedicated space debris research programs, such as ESA's Space Debris Office (ESA, 2021) and NASA's Orbital Debris Program Office (ODPO, 2021). These policies include criteria around debris release, mission plans and spacecraft designs, which operators must meet in order to be issued a license.

In the pursuit of this goal there is a level of coordination and collaboration between space agencies. At present the majority of space debris policy is focussed on the idea of mitigation, pre-emptive steps aimed at minimising the generation of space debris as much as possible. However, opportunities for remediation through the removal of existing debris objects are also being explored. This section will go on to explore each of these areas.

Mitigation Measures

In 2002 the United Nations Office for Outer Space Affairs published a set of mitigation guidelines (with revisions published in 2007) recommended by the Inter-Agency Space Debris Coordination Committee (IADC) (UNCOPUOS, 2010). These outlined best practice for limiting the growth of space debris in orbit. The guidelines were focussed around the following key mitigation measures:

1. Limit debris released during normal operations.
2. Minimise the potential for breakups during operational phases.
3. Minimise the potential for post mission breakups resulting from stored energy.
4. Limit the probability of accidental collision in orbit.
5. Avoidance of intentional destruction and other harmful activities.
6. Limit the long-term presence of spacecraft and launch vehicle orbital stages in the low Earth orbit region after the end of their mission.
7. Limit the long-term interference of spacecraft and launch vehicle orbital stages with the geosynchronous region after the end of their mission.

These guidelines are aimed at reducing the rate at which orbital debris is added to the space environment and where possible removing objects from congested orbits at end of life. Two protected regions are defined from which all spacecraft should be removed at end of mission. The regions are: all LEO orbits up to $2,000$ km; and the GEO region ± 200 km for inclinations up to 15°. For the LEO region spacecraft should be re-orbited outside of the region, or placed in an orbit where they will re-enter the atmosphere as soon as possible and within a maximum of 25 years. For GEO, satellites should be placed into a graveyard orbit at least 235 km above GEO with eccentricity ≤ 0.003 with additional allowance for decay due to solar radiation pressure.

The Inter-Agency Space Debris Coordination Committee

The IADC was founded in 1993 as an inter-governmental forum for the coordination of worldwide activities in the field of space debris. The organisation is made up of 13 member space agencies from around the world and consists of a steering group and working groups focussing on: Measurements, Environment and Database, Protection, and Mitigation; and has the following stated purpose (IADC, 2016):

> "To exchange information on space debris research activities between member agencies, to facilitate opportunities for cooperation in space debris research, to review the progress of ongoing cooperative activities and to identify debris mitigation options."

However, as a political body, the success of the IADC requires a level of consensus between different nations which can often be difficult to achieve. As a result it can sometimes be slow to react to the changing space industry. For example when responding to proposals of large broadband constellations in LEO. While a statement on large constellations was issued in 2017 (Group, 2017) recommendations within the most recent revision to the IADC Space Debris Mitigation Guidelines (Group and 4, 2020) remain vague, so far being limited to:

> "For specific operations such as large constellations, a shorter residual orbital lifetime and/or a higher probability of success may be necessary. Retrieval is also a disposal option."

Meanwhile hundreds of constellation spacecraft are already in orbit and thousands more have been licensed by national regulators based on the existing guidelines.

Measuring the Impact of Mitigation

The published space debris guidelines have formed the basis of the space debris policies adopted by a number of space agencies, including ESA and NASA (ESA, 2015; NASA, 2017). However, while the mitigation measures themselves might be effective, success will depend on the level of compliance with the policies and guidelines. The benefit to the environment will be limited if the guidelines are not widely implemented by the space community and, alone, are unlikely to be sufficient to prevent the growth of the debris population.

While operators are required to meet many of these guidelines in their mission plans this is not a guarantee that the implementation will be successful. Spacecraft may suffer failures before they reach end of life and so are unable to undertake passivation or re-orbiting manoeuvres. For example, of the 95 satellites launched for the first Iridium constellation 30 failed and 25 remain on-orbit in an uncontrolled state (Sladen, 2020). The exploration of the impact of mitigation, in particular from varying levels of post mission disposal, has become a common theme to research being performed by the debris modelling community (Lewis et al., 2012; Rossi et al., 2013; Dolado-Perez et al., 2015; Bastida Virgili et al., 2016a; Lewis et al., 2017b).

Some effort has been made to assess the level of adherence to the guidelines. Frey and Lemmens (2017) conducted an investigation into the perceived adherence over the 15 year period since their publication. The results of this study suggested that 53.3% of LEO payloads reaching end of life between 2006 and 2015 were compliant with the 25 year requirement, of which 49.9% were already in naturally compliant orbits. It should be noted that the determination of which spacecraft are compliant is subject to the assumptions in the propagator used to predict re-entry time and to the assumptions used to determine the end-of-life. These values are potentially sensitive

to small changes in the base assumptions and no detail was provided on the errors for these values or their method of calculation.

In section 6 of the latest Annual Space Environment Report released by ESA Space Debris Office (2020) an overview of the latest estimates of compliance is provided across multiple figures. Figure 2.8 shows the relative percentages of spacecraft reaching end of life in each year which are expected to comply with the mitigation guidelines for clearing the LEO protected region. These results indicate that spacecraft are increasingly compliant with the mitigation guidelines, with more successful post mission disposal operations and fewer making no attempt to clear the region.

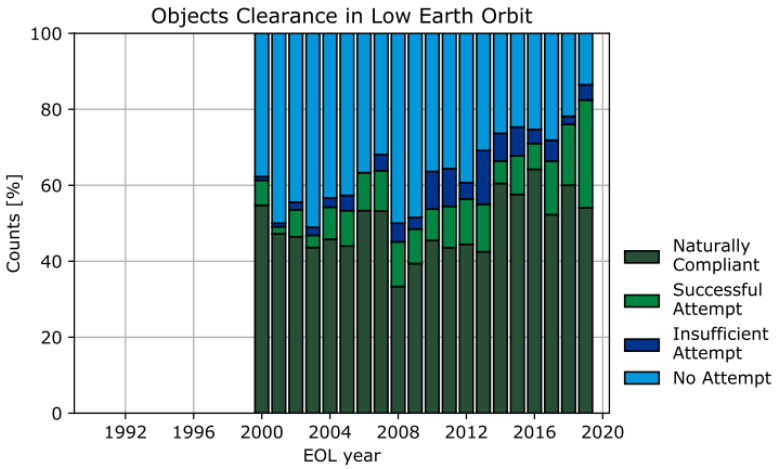

FIGURE 2.8: Rate of clearance from protected LEO region across all objects (Source: ESA's Annual Space Environment Report (ESA Space Debris Office, 2020))

In addition, an investigation was undertaken to evaluate the robustness of the calculation of compliance shares. Figure 2.9 shows the evolution of the compliance share of payloads including the 10, 50, and 90% quantiles of the calculated share across a minimum of 500 Monte Carlo runs, varying the ballistic coefficients and the predictions of solar and geomagnetic activity (ESA Space Debris Office, 2020). The grouping of these quantiles indicates that error on the calculated compliance is approximately $\pm 2\%$.

It has now been 19 years since these mitigation measures were first proposed but questions still remain about exactly how effective these measures are and whether they are sufficient to control the growth of the debris population. It is worth considering however, that when combining the average life-time of spacecraft with the time taken for the guidelines to have been included in the design, construction and licensing process; some of the effects of these mitigation guidelines may be yet to be seen.

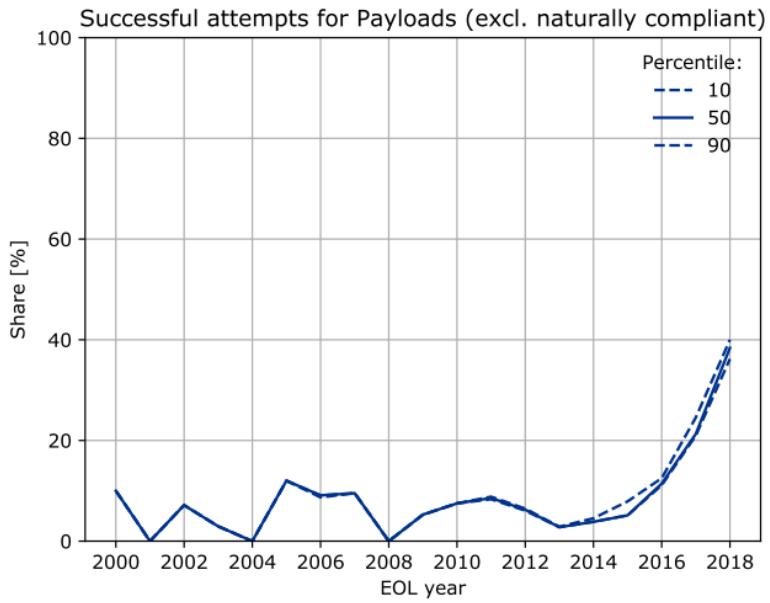

FIGURE 2.9: Share of LEO payloads compliant with space debris guidelines for End-of-Life (Source: ESA's Annual Space Environment Report (ESA Space Debris Office, 2020))

2.4.2 Active Debris Removal

One approach which has been discussed for managing the debris problem is ADR. The core aim of ADR is to control or reverse growth in the debris population by removing from orbit those debris objects which are estimated to be the greatest threat to the environment. Normally this is understood as targeting either large defunct satellites or rocket bodies with long decay periods which have significant mass and show the greatest chance of undergoing a breakup event, whether being a known explosion risk or having a high collision probability (White and Lewis, 2014a; Anselmo and Pardini, 2017; Seong et al., 2017; McKnight et al., 2021).

While the idea of missions to capture spacecraft was first discussed in the early 1980s, at the time the idea was deemed not to be feasible (Reynolds et al., 1983). Further speculation continued in the 1990s, including proposals to use lasers to ablate a target and lower its perigee to speed up the decay process (Eichler and Bade, 1990; Schall, 1991; Monroe, 1993; Eichler and Bade, 1993; Campbell and Taylor, 1998). However, it is only in recent years, following the accidental collision of Iridium-33 and Cosmos 2251, that the topic has really generated interest. This can be seen in Figure 2.10 which shows the substantial increase in the number of published papers discussing debris removal.

There are currently several concepts in advanced stages and some early on-orbit testing has taken place, including technologies tested by the University of Surrey's RemoveDEBRIS mission (Kramer, 2018) which has demonstrated the use of both nets and harpoons to capture example debris objects. Some companies, such as the start-up Astroscale, are attempting to capitalise on this perceived niche market by providing

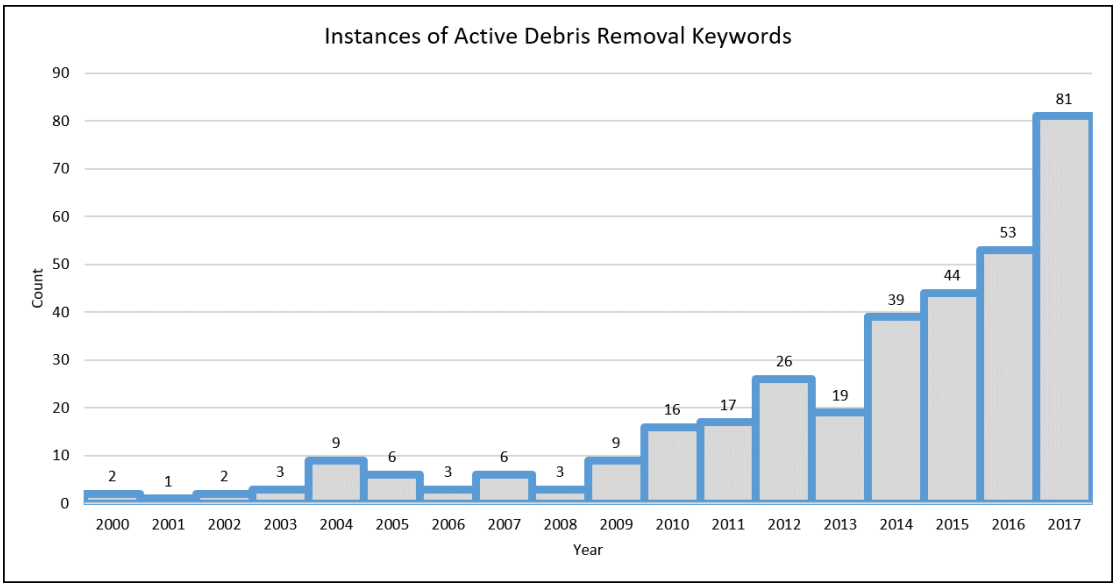

FIGURE 2.10: Showing the number of instances of ADR keywords in journal articles on Web of Science.

ADR as a service to other operators. At present, most plans focus on defunct spacecraft with specific design elements to allow docking and de-orbiting. For this approach to be widely usable it would require the majority of all spacecraft to be fitted with common attachment points in order to allow the small percentage of failures to be removed from orbit. It seems unlikely that this will see widespread adoption without being driven from the top down by policy or insurance requirements.

While ADR might now be considered technically feasible there are still outstanding challenges to prove the concept useful in the larger orbital environment. There are high costs associated with the implementation of any debris removal scheme, including the price of developing the technology, for what may be relatively low gain. Rendezvous missions include a risk of failure should the spacecraft itself fail or be involved a collision, the result of which would be no gain or, in a worst case scenario, a contribution to the debris environment. While the use of laser ablation is an attractive option it poses its own problems, particularly around the political and legal ramifications, with the potential to accidentally damage other satellites and the fear of weaponisation (Weeden, 2011; Bowen, 2014).

Not least of the challenges surrounding ADR is the legal considerations around removal of objects. This is a complicated question with a lack of a clear, legally binding definition of space debris and the potential to violate another nation's sovereign jurisdiction or ownership (Weeden, 2011; Su, 2016). Without a solid international agreement on this subject, operators are likely to restrict themselves to removing only objects which can be definitively proved to be under their jurisdiction.

One of the biggest issues which remains to be solved is the question of how to identify which objects to remove. Any organisation considering underwriting the costs of

systematic debris removal would want to be assured that doing so was in their own best interest. The outstanding question of whether removing any particular object will have any long-term benefit to the environment is one of the focusses of current debris modelling activity.

In a recent study eleven different approaches to this question were compared and each used to generate a list of the top 50 objects threatening space sustainability (McKnight et al., 2021). These lists were then combined to form a composite list of the top 50 statistically-most-concerning derelict objects in LEO. Of particular note is that that top 20 objects in this new list were all SL-16 rocket bodies with masses of 9,000 kg. These objects are considered among the highest risk due to a combination of the probability of collision (they occupy congested high inclination orbits at altitude of around 800 km) and the severity of any potential breakup (the high mass suggests a large number of resultant fragments). However, this high mass makes these more expensive and challenging targets for ADR due to the higher amount of fuel required to place the derelicts into disposal orbits. As a result it may prove more cost effective to remove multiple smaller but less concerning spacecraft to achieve the same reduction in threat to the sustainability of the environment.

2.5 A Changing Approach to Spaceflight

The last 20 years have have been a period of growth and change in the space sector. One prominent feature of this period is the competition between private companies, such as Rocket Lab, Blue Origin and SpaceX, dubbed the 'billionaire space race' (Lafranco, 2015; The Week, 2016). This competition is reducing launch prices for both national and commercial operators, and is further helped by the development of reusable launch technologies to save on costs (Blackmore, 2016). One impact of this has been to improve accessibility to space for smaller organisations such as academic institutions and start-ups leading to an era of 'NewSpace' based around new ideas, new technologies and new actors in both the spacecraft and launch sectors.

The graphs in Figures 2.11 and 2.12 show how the segmentation of the space industry has changed historically. Since 1980 the space industry has become much more commercially focussed with the proportion of commercial spacecraft rising from 4.6% of the launch population in the 1980s to 55.6% in the last decade. A corresponding increase has been seen in the proportion of spacecraft owned by academic institutions from 1.9% to 18.0%. Meanwhile, there has been an undeniable drop in the proportion of military satellites since the end of the cold war, from 76.5% to only 10.5% of launched spacecraft. While the total number of launches in the civil and military categories has remained consistently around 700 per decade, there has been a 213% increase in the total number of launched spacecraft from the 1980s to the 2010s. Of this

increase, 208% is accounted for by increased numbers of commercial and academic spacecraft, from 34 to 1292 and 5 to 253 respectively.

This change in the use of space has been accompanied by changes in the priorities driving the development of spacecraft and their missions. While national and regional programs still face some of the same pressures, the growing private sector is far more concerned with 'cost-benefit considerations' (Paikowsky, 2017). The competitive nature of the commercial ecosystem (and the often restrictive budgets of academic institutions) has become a major force for on-going development, fuelling innovation and providing a niche for start-up companies attempting to disrupt the status-quo.

With the advent of NewSpace further changes and technology developments are likely. As the most cost effective approach is generally to obtain the greatest functionality for the lowest cost, it is these drivers that are resulting in the changes being seen in spacecraft design, such as the increase in smaller, lighter satellites (Konecny, 2004; Virgili and Krag, 2015; Radtke et al., 2017c), novel methods like additive manufacturing (Orbex, 2019), along with mass production and the development of commercial off the shelf components.

Many of these new ventures may not survive to maturity and so it is very difficult to know how long the current rate of change will continue or what the future of the space industry will look like (Denis et al., 2020). However, it is expected that these changes will have implications for the future of the space debris environment and are already introducing new challenges for managing the environment, including the increase in the number of space systems, number of spacecraft operators and the rate of launches (Muelhaupt et al., 2019). The challenges of large satellite constellations and changing spacecraft design are explored in more detail below and this thesis will go on to study their impact on space debris modelling.

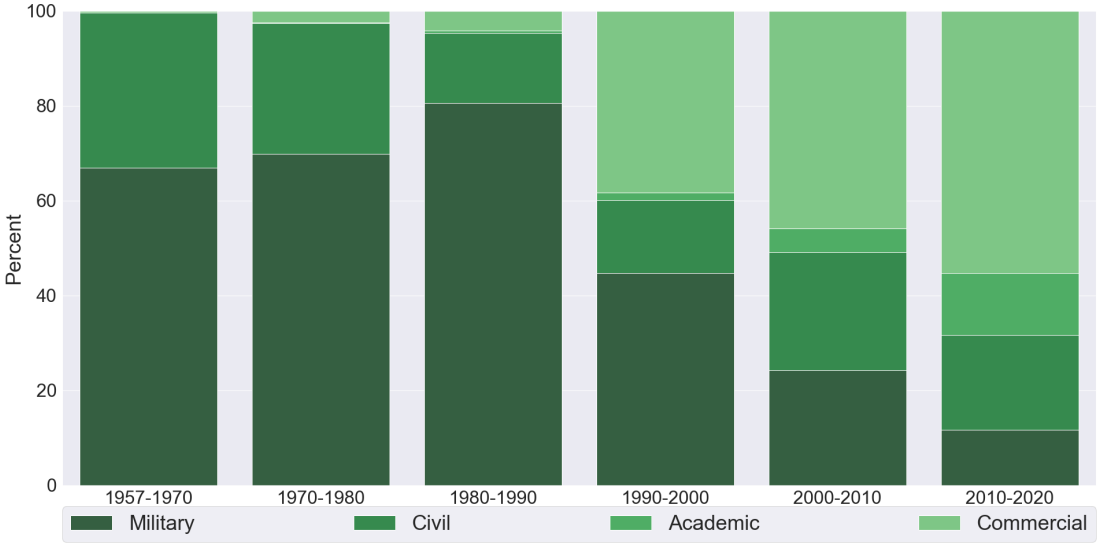

FIGURE 2.11: Graphs showing the distribution of LEO spacecraft by operator type over different decades.

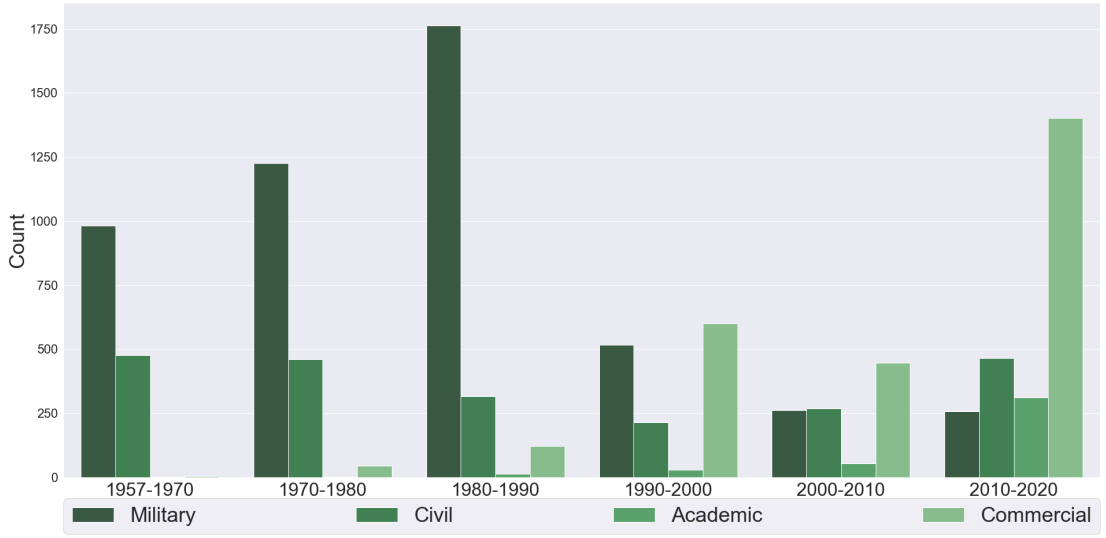

FIGURE 2.12: Graphs showing the distribution of LEO spacecraft by operator type over different decades.

2.5.1 Space Use in the Future

These changes in the distribution of spacecraft by operator are accompanied by an ongoing shift in the way in which space is used. Over the last 20 years there has been a substantial diversification of mission types, deployment methods and operations. Current indications are that these changes will represent an increasing proportion of future space activity. This has resulted in a need to understand the impact of these developments on the future of the space debris environment.

The novel deployment methods which have provided affordable deployment for small spacecraft include the Nano-racks CubeSat deployer on the ISS and the mass-deployment of spacecraft from single launches. Examples of this include PSLV-C37 which deployed 104 spacecraft in 2017 (Purna Sudhakar, 2018), SSO-A SmallSat Express which launched 64 spacecraft in 2018 (Spaceflight Industries, 2019), and SpaceX's Transporter-1 rideshare mission which carried 143 spacecraft into orbit in 2021 (Foust, 2021). These mass deployments often result in large numbers of spacecraft being deployed into very similar orbits without any ability to manoeuvre to avoid collisions with each other or debris.

New mission types are being explored as companies seek out new markets such as on-orbit servicing, end-of-life management and ADR (Bryce Space and Technology, 2018). For example, the Singapore based company Astroscale, launched a technology demonstrator mission (ELSA-d) in March 2021. The US defence firm Northop Grumman achieved a proof of the concept with the successful docking of Mission Extension Vehicle-1 (MEV-1) with Intelsat 901 (IS-901) in February 2020(O'Callaghan, 2020) providing IS-901 with additional manoeuvring capability and extending its operational life.

Morgan Stanley (2018) predicted that the largest area of market growth will be the provision of satellite broadband. While there are some companies such as Telesat and Viasat with GEO constellations there is an on-going competition to provide high bandwidth, low latency, broadband using LEO satellites. The frontrunners in this are the large constellations being deployed by SpaceX and OneWeb.

Large Constellations

In recent years the prospect of these large, next-generation constellations consisting of thousands of spacecraft, sometimes dubbed 'mega-constellations', has been a major area of research for engineers focused on the sustainability of the space debris environment (Peterson et al., 2016; Bastida Virgili et al., 2016a,b; Lewis et al., 2017a,b; Radtke et al., 2017a; Vavrin et al., 2019b). While OneWeb and SpaceX's Starlink constellations have begun deployment, there are a several other planned constellations in various stages of development several of which are listed in Table 2.7.

TABLE 2.7: Planned large constellations (SpaceX, 2018; Schneiderman, 2019).

Constellation	Altitude	Planned Spacecraft	Currently Launched
Starlink - Phase 1 proposed	540 km	1,584	0
	550 km	1,584	1740
	560 km	336	0
	560 km	172	0
	570 km	720	0
OneWeb	1,200 km	720	288
	8,500 km	1,280	0
Project Kuiper	590 km	784	0
	610 km	1,296	0
	630 km	1,156	0
Telesat - Lightspeed	1,015 km	78	0
	1,325 km	220	0
Starlink - Phase 2	335.9 km	2,493	0
	340.8 km	2,478	0
	345.6 km	2,547	0
OneWeb - Phase 2	1,200 km	6,372	0
CASC Hongyan	1,100 km	300+	1
Kepler	575 km	140	2
Planet Labs - Flock/Dove	475 km	150	150
Spire - Lemur	400 – 500 km	150	133
Swarm	150 – 550 km	150	45

It remains to be seen whether many of these constellations will come to fruition, particularly in light of the uncertainty caused by the COVID-19 pandemic. However, even the current deployment levels (mainly from SpaceX) are significant when comparing to the previous active spacecraft population of only 2,000 (Union of Concerned Scientists, 2017). As a result, due to sheer numbers, constellation spacecraft are likely to be a significant source of debris within the future environment unless

mitigation measures for these systems are more successful than historic attempts have been. Even a small number of failures in orbit for one of the higher altitude constellations has the potential to significantly impact the debris risk for hundreds of years in the event of a worst case scenario, due to the increased orbital lifetime in these regions. In the constellation simulations performed by Bastida Virgili et al. (2016b) the number of objects larger than 10 cm in LEO after 200 years was four times greater for a constellation with 60% post mission disposal than for a baseline no-constellation case.

The deployment of constellations is already causing an increase in the number of spacecraft conjunctions which must be considered to determine when avoidance manoeuvres are required. By the last week of January 2021 Starlink spacecraft accounted for 31.2% of all predicted conjunctions under 5 km (Lewis, 2021) with only 1,000 out of a planned 4,408 spacecraft deployed. One particularly high profile example is the predicted conjunction of ESA's Aeolus satellite with Starlink-44 on Monday 2nd September 2019 (ESA, 2019). In this instance the ESA team decided it was necessary to perform a collision avoidance manoeuvre early on the Monday as collision probability reached around 1 in 1000.

2.5.2 Future Spacecraft

Alongside these changes in the use of space have come changes in the design and construction of spacecraft. Novel uses of composite materials such as honeycomb panels, have already allowed for the development of lighter spacecraft structures (Bianchi et al., 2010; Kamalieva and Charkviani, 2017; Gdoutos et al.). Advances in additive manufacturing, particularly using novel metal alloys and the ability to create more complex lattice structures, continue to enable improvements in the weight, performance and affordability of spacecraft structures (Walker et al., 2019; Mohd Yusuf et al., 2019; Blakey-Milner et al., 2021; Dumitrescu et al., 2021).

Additionally, improvements in the efficiency of solar cells have made them the de-facto choice for spacecraft power-supply for Earth-orbiting missions. In order to meet the power requirements of the mission deployable solar arrays are often used to expand the area available for energy collection. While this design provides an advantage in terms of power budget it also increases the cross sectional area of the spacecraft, resulting in a larger target for debris impacts.

Additional components such as drag sails increase the area to mass ratio of spacecraft in order to accelerate the rate of decay due to atmospheric drag, shortening residual lifetime after end of mission. However, while this approach reduces the time the spacecraft spends in orbit it may not reduce the cumulative collision risk across the residual lifetime of the spacecraft (Colombo et al., 2017). Increasing the cross sectional area of the spacecraft also increases the volume of space swept by the spacecraft causing a greater exposure to debris impact per orbit. As a result the lifetime collision

probability of the spacecraft is unchanged, although as debris impacts on a drag sail are likely to be less destructive than a collision with the spacecraft bus the consequences of collision may be less severe.

One trend which has gained particular focus among the space debris community is the growing popularity of cheap, effectively disposable, small satellites which have allowed many more organisations to put a spacecraft into orbit at the cost of reduced operational capabilities in terms of attitude control and orbital manoeuvrability (Lewis et al., 2014; Virgili and Krag, 2015; Radtke et al., 2017d).

The most common example of these small spacecraft is the CubeSat, a design which allows for the easy, standardised construction of spacecraft using low cost off the shelf components. The design is based on multiples of a $10 \times 10 \times 10$ cm unit cube with a mass of up to 1.33 kg (Lee et al., 2014). These are generally deployed as secondary payloads or launched from the ISS using systems such as the NanoRacks CubeSat Deployer (NRCSD) which can automatically deploy CubeSats up to six units (6U) in length and two in width. While these spacecraft are often launched into Very Low Earth Orbit (VLEO), with altitudes below 450 km and relatively short orbital lifetimes of around 6 months or less, they often lack any manoeuvring capability which would allow them to avoid a collision.

The trend to smaller spacecraft has provided a market for small launch vehicles which can provide launch options which are cheaper than the historic launch market while being more customisable than ride-share agreements. Rockets operating in this niche include RocketLab's Electron and Virgin Orbit's air-launched LauncherOne as well the under-development Orbex Prime. They typically have launch masses of under 25 tonnes, compared to hundreds of tonnes for traditional vehicles, and have payload capacity in the range of 100-500 kg (Wekerle et al., 2017; Pelton and Madry, 2019).

2.6 Summary

This literature review explored the state of the art of understanding space debris and the historical and future risks it poses, primarily to the safe operation of spacecraft. Three key types of debris models were identified, and evolutionary models in particular were highlighted as being relevant to understanding the future of space debris. The most important components of these evolutionary models were determined to be the individual models predicting the collision between objects and describing spacecraft fragmentation. It was however, noted that many of the most prominent evolutionary models were built on a common set of underlying models of these components. An impact of this is that the limitations of these models are less obvious due to the consequences becoming systemic throughout on-going research.

Concurrently, it was identified that the future of space debris is likely to be different from historical norms. In particular the rise of "NewSpace" has led to ongoing changes in the use of space, with a much greater commercial presence across both the launch and operation of spacecraft. New spacecraft and mission types mean that the future spacecraft population is likely to be much more diverse than in the past. The interaction of these population level changes with the assumptions made in debris model components could compromise the utility of such models for understanding the future environment.

Chapter 3

Modelling in the NewSpace Era

> We're going to make it happen. As God is my bloody witness, I'm hell-bent on making it work.
>
> Elon Musk

3.1 The State of Debris Modelling

When looking at modelling for the NewSpace era it is important to understand what questions are being asked before determining if the models can provide suitable answers. While NewSpace may impact the future evolution of the debris population many of the questions being asked remain fundamentally the same. For individual spacecraft and space systems there is the question of "what risk does debris pose to safe operation?", and of "what is the potential contribution to the debris hazard?". Looking at the environment as a whole the question remains "how sustainable is the debris environment?". However what has changed is the nature of the spacecraft and space systems and there is an ongoing need to understand the risks they might pose and what the consequences, both intended and unintended, might be for the environment.

Figure 2.4 showed how the number of objects in orbit has grown over the last 63 years. Models of the debris environment are used to study the debris population and how the environment might evolve in the future. In their formative work on space debris Kessler and Cour-palais (1978) concluded that collisions between objects in orbit could drive an exponential increase in debris flux even if no new objects were launched. Further work (Kessler, 1991; Kessler and Anz-Meador, 2001) aimed to identify the critical spatial densities for different regions above which the rate of fragment production would exceed the rate of decay due to atmospheric drag. As of 2001, the

LEO regions between 600 km and 1,000 km were thought to be unstable, and in particular the region from 800 km to 970 km was believed to have already reached this critical density with the potential for uncontrollable runaway growth in the debris population (Kessler and Anz-Meador, 2001; Anselmo, 2001).

The aim of much of the research conducted using debris models is to understand the impact of different activities, including possible methods of controlling the growth of the debris population by limiting this exponential growth. However, in order to do this it is necessary to understand how these processes and the way in which they are represented in models are impacted by the on-going changes in the space industry.

This chapter looks to understand and quantify the nature of the changes introduced by NewSpace and so investigate the first hypothesis of this work, that "NewSpace is associated with measurable changes in the physical and orbital characteristics of the spacecraft population".

3.1.1 Current Research

A review of recent publications identifies several key topics on which research has been centred. One topic of particular interest regarding the changing use of space was the growing use of small satellites, such as CubeSats (Lewis et al., 2014; Virgili and Krag, 2015; Peterson et al., 2016; Radtke et al., 2017d). There was considerable concern about how the stability of the debris environment might be altered as cost reductions allowed more spacecraft to be launched, while potentially reducing reliability, and at the same time size reductions resulted in more limited manoeuvring and tracking capabilities.

Over the last 5 years this concern has been focussed specifically on the need to study the impact of proposed large constellations of small satellite and the potential addition of thousands of new spacecraft in LEO (Bastida Virgili et al., 2016a; Radtke et al., 2017a; Lewis et al., 2017b; Le May et al., 2018; Anselmo and Pardini, 2019; Vavrin et al., 2019a,c; Pardini and Anselmo, 2020).

In addition, the study of methods of controlling the debris population has seen significant attention. This has included studies of the response of the environment to different debris mitigation strategies (Lewis et al., 2012; Rossi et al., 2018; Kawamoto et al., 2018; Letizia et al., 2019; Jenkin et al., 2019) as well research into the effectiveness of the introduction of different rates of ADR (Liou and Johnson, 2009; Liou, 2011; White and Lewis, 2014a; Anselmo and Pardini, 2017; Seong et al., 2017; Kawamoto et al., 2019).

As discussed in Chapter 2, different types of debris model fill different niches when it comes to investigating the debris environment. Each serves a purpose depending on the time frame being investigated and whether the investigator is interested in looking

at the evolution of the overall environment or the experience of a particular object. In the case of recent research a substantial focus has been on understanding how specific behaviours impact the long term sustainability of the space environment. As such evolutionary models were primarily used to conduct this research.

3.1.2 Key Characteristics for Modelling Debris

Having identified the components of evolutionary debris models as a primary area of focus (and specifically the core physical models which describe fragmentation, collision and propagation), it is possible to identify a set of key debris and space vehicle characteristics which should be examined.

A range of physical characteristics, including the mass, size and cross-section of objects, are important for fragmentation, collision and propagation models. Object mass determines the maximum cumulative mass available for fragments generated in a breakup as well as the kinetic energy of any collision event. The size of the fragmenting objects provides an initial limit on maximum fragment size (although this is complicated as structures can fold and unfold under stress, resulting in objects with a greater size than the original object) while cross-sectional area determines both the probability of collision and the magnitude of the major perturbing forces of atmospheric drag and solar radiation pressure. For propagation in particular, the relationship between the mass and cross section, i.e. the area-to-mass ratio, is important in understanding how perturbations will affect the orbit and the acceleration due to perturbations.

In addition, there are a number of orbital characteristics which are also important within the modelling of these processes. In particular, the orbital elements of semi-major axis and eccentricity (which describe the size and shape of the objects orbit) are important for determining where orbits might overlap. The remaining elements which describe the orientation of the orbit (the inclination, right ascension and argument of perigee) are subject to substantial rates of change resulting from geo-potential perturbations. As a result, the rates of change of these elements are of interest as this determines how the orientations of orbits change relative to one another and hence how frequently objects may be able to encounter one another. The rates of change of the right ascension and argument of perigee respectively can be calculated for each object using the following equations:

$$\Delta\Omega = \frac{-3\pi J_2 R_E^2 cos(i)}{2a^2(1-e^2)^2} \quad radians/orbit \tag{3.1}$$

$$\Delta\omega = \frac{3\pi J_2 R_E^2}{2a^2(1-e^2)^2}(2 - \frac{5}{2}sin^2(i)) \quad radians/orbit \tag{3.2}$$

where R_E is the equatorial radius of the Earth and $J_2 = 1.08262668 \times 10^{-3}$ is the second zonal harmonic of the geopotential, which is a first order perturbation caused by the oblateness of the Earth.

One final set of characteristics which is worth considering are those of space vehicle explosions, as explosions are a major contributor to the debris population. The rate at which debris fragments are produced by explosions depends upon the rate at which explosions occur as well as the size and mass of the objects exploding. An increase in the rate of explosions, for example due to there being more objects in orbit, might suggest a greater rate of fragment production. However if the objects which are most likely to explode are smaller in size and mass than historic breakups then this might result in fewer fragments being released.

To explore the impact of NewSpace on existing debris models the nature of the changes in these characteristics of spacecraft, space systems and the environment as a whole must first be understood. This understanding provides insights into where errors might arise in the current models and what changes might be necessary to accurately model NewSpace scenarios.

3.2 Classifying NewSpace Spacecraft

In order to quantify the impact of NewSpace on debris modelling it is important to specify what is meant by the label NewSpace when applied to spacecraft and space systems. In particular, if and how can NewSpace be distinguished from traditional spacecraft design and operation. In an attempt to clarify what NewSpace is, HobbySpace, identified the following list of primary philosophies (Kerolle, 2015):

1. Focus on cost reductions,
2. An assurance that the low costs will pay off,
3. Ensuring incremental development,
4. Foray into commercial markets with high-consumer rates,
5. Primary emphasis on optimising operations,
6. At the heart of it all, innovation.

However, this list only provided a qualitative description of NewSpace. To properly understand the impact of NewSpace a quantitative, rigorous and definitive definition was required based on the changing characteristics of spacecraft.

3.2.1 Building a NewSpace Decision Tree

Decision trees were investigated as a potential classifier for distinguishing between NewSpace and Traditional (or TradSpace) spacecraft - a TradSpace spacecraft was considered to be any object which was not NewSpace. The Classification and Regression Trees (CART) algorithm (Breiman et al., 1984) was used to train a classifier using a sample set of manually classified objects. Classification trees are constructed by the successive branching of the dataset until a defined criterion is met. For each node split points are chosen by examining split points across the range of values for all input variables and evaluating them using a cost function. This creates a tree with a series of end points, known as leaf nodes.

Of the cost functions commonly used for the CART algorithm the Gini impurity was chosen for this work but alternative functions such as information gain or entropy should produce similar results for a simple two class classifier (Breiman, 1996). The Gini impurity is a measure of the probability that a randomly chosen object would be incorrectly labelled by the split, which has a value between 0 and 0.5. This allows the impurity of the leaf nodes generated by the split to be calculated as:

$$G(k) = \sum_{i=1}^{J} P_i(1 - P_i) \tag{3.3}$$

Where $G(k)$ is the impurity of node k, J is the number of classes, and P_i is the probability of a classification i across the training dataset.

In the case of a binary choice of classifications where $P_1 = 1 - P_2$ this simplifies to become:

$$G(k) = P_1(1 - P_1) + P_2(1 - P_2) = 2P_1P_2 = 1 - (P_1^2 + P_2^2) \tag{3.4}$$

The Gini impurity of the potential split can then be calculated by weighting the impurity of the two branches according the proportion of each class of object allocated to each branch:

$$G_{weighted} = \frac{N_{left}}{N_{parent}}(2P_{left,1}P_{left,2}) + \frac{N_{right}}{N_{parent}}(2P_{right,1}P_{right,2}) \tag{3.5}$$

Where N_{left} and N_{right} are the number of objects classified into each branch.

Using the CART algorithm the dataset is split at the point with the lowest impurity. Each generated sub-node is then split recursively until a stopping criterion is met, e.g. a leaf with an impurity of zero, or the node meets a pre-defined level for depth (i.e. number of branches), minimum impurity or leaf size (i.e. number of objects in the leaf).

It was determined that distinct decision trees were required for classifying NewSpace and TradSpace for each of payload spacecraft and upper stages. Subsets of 2044

payload spacecraft and 883 upper stages were manually classified by the author as being either TradSpace or NewSpace. The data was then randomly split into a training set (70%) which would be used to create the decision tree, and a testing set (30%) for evaluating the accuracy of the classifier.

The initial manual classification was largely qualitative and prioritised the labelling of acknowledged NewSpace spacecraft and upper stages, such as the Starlink and Flock constellations and RocketLab's Electron upper stages. Meanwhile the TradSpace examples were chosen from among historic civil and military space vehicles, including the older Cosmos models and the Delta II and Centaur upper stages. As a result of the manual classification step, the generated decision tree may have inherited some level of unconscious bias from the human classifier and will be of limited accuracy for vehicles whose characteristics diverge significantly from those of the pre-classified data-set. However, in the absence of an existing definition of NewSpace the classifier provided useful quantification and internal consistency in what was considered NewSpace.

The variables used in the training of the decision trees for spacecraft and upper-stages were the mass, area-to-mass ratio, orbital region (between VLEO, LEO, MEO and GEO), eccentricity, inclination, and count of objects on the same launch. To reduce the risk of over-fitting the model orbital region was used rather than the semi-major axis resulting in a switch to discrete categories rather than a continuous range. The reason average cross section and semi-major axis were not included was due to the information already being captured by the area-to-mass ratio and orbital region variables respectively. Manual tuning of the hyper-parameters of the model resulted in the selection of stopping conditions for the decision tree of a maximum depth of three nodes, a minimum number of samples per leaf of ten, and a minimum decrease in impurity of 0.01. These conditions constrained the total complexity of the decision tree to prevent over-fitting to the training data.

Figure 3.1 describes the decision tree produced for upper stages. This tree is very simple, a single split on object mass at 550 kg is sufficient to generate two pure leaves. This then achieved 100% accuracy against the test set. The decision tree was then applied to the full data-set. Figure 3.2 shows the changing proportion of each category over the history of the space age.

Interestingly, when using this classifier the largest proportion of NewSpace spacecraft are identified in the 1950s and 1960s, where $40 - 60\%$ of the upper stages launched are classified as NewSpace. The results indicate that what is being classified NewSpace by this decision tree is actually more similar to historical spacecraft than modern rocket bodies. However, this classifier is designating based on mass alone with no knowledge of the technology involved which may be an artefact of the examples chosen for the manual classification step.

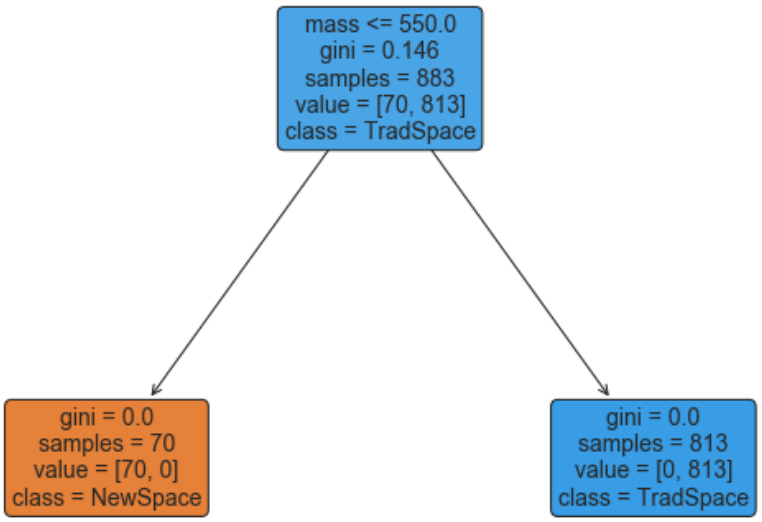

FIGURE 3.1: Decision tree for upper stages.

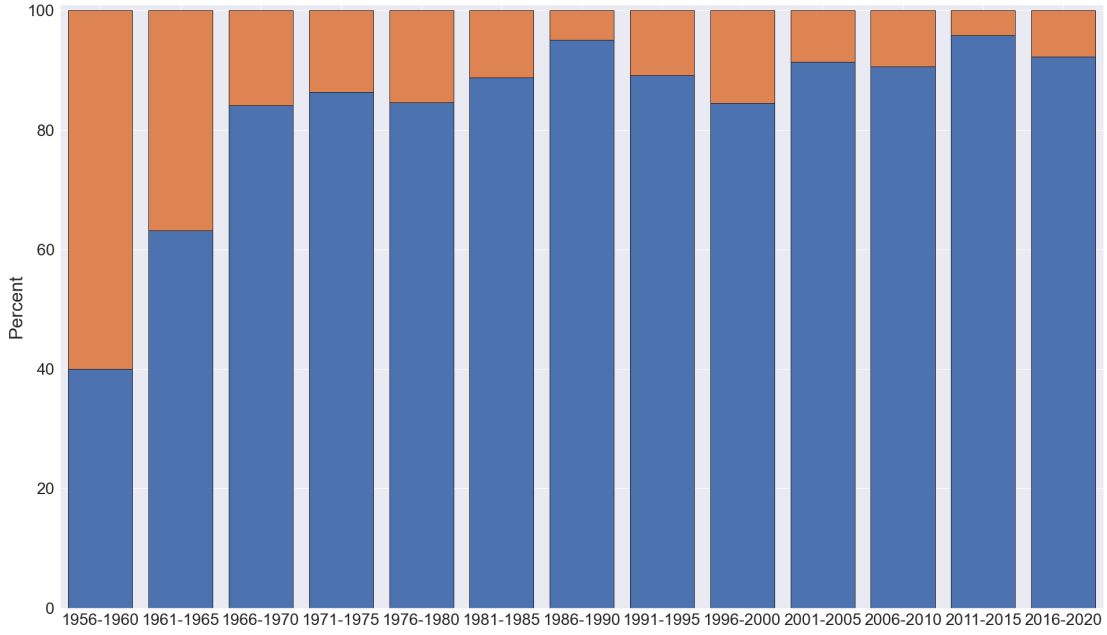

FIGURE 3.2: Distribution of NewSpace (orange - upper) vs TradSpace (blue - lower) over time for upper stages using a decision tree classifier.

This result does not necessarily indicate that the classifier is wrong, but that the historic spacecraft launched at this time, which were more experimental in nature and had more limitations on their mass, have similarities with what was considered as NewSpace for current upper stages during the manual classification step. In contrast, in recent years this proportion has been much lower, remaining consistently around 10% for the last 50 years. This suggests that either NewSpace upper stages have not yet had a noticeable impact on the population in orbit or the definition of NewSpace upper stages adopted by this classifier is not quite correct.

The corresponding decision tree for payloads, shown in Figure 3.3, is more complex.

In this scenario two key branches are identified corresponding with the different physical versus orbital characteristics of NewSpace. In one branch NewSpace is determined based on the number of objects per launch, while in the other it is determined by the physical characteristics of the spacecraft. The classifier identifies as NewSpace objects with a high number of objects per launch (> 9), or a low mass (< 22.30 kg), or a higher mass and a high area-to-mass ratio ($>0.015\ m^2/kg$).

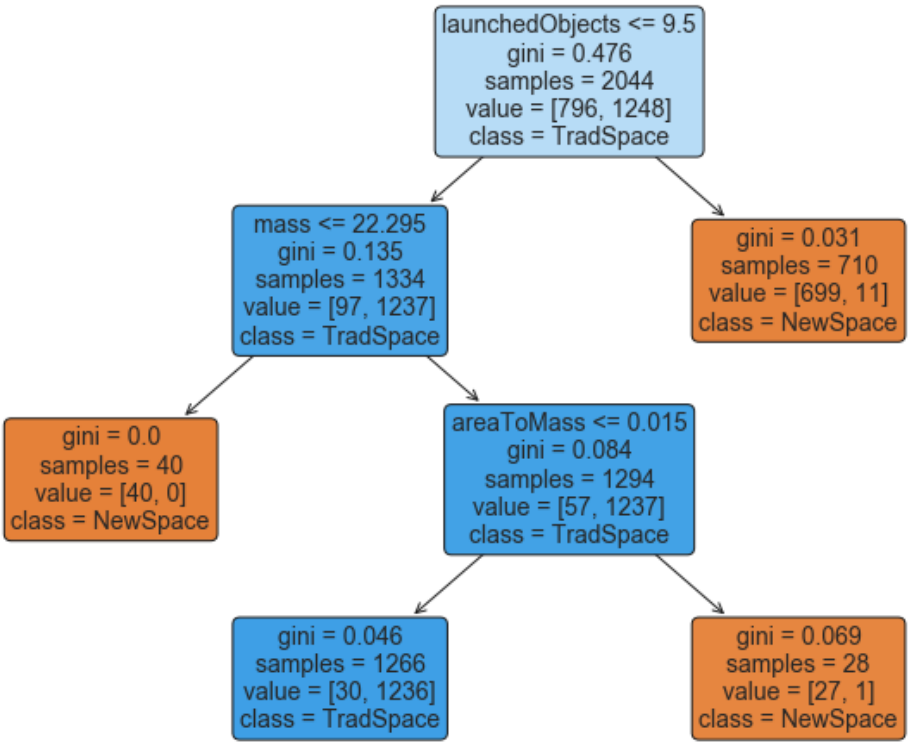

FIGURE 3.3: Decision tree for payloads.

Looking at the distribution of the objects between NewSpace and TradSpace (the value split [NewSpace, TradSpace]) in each of the leaf nodes in Figure 3.3 it can be seen that this classifier does not achieve a perfect classification of the training set. However, the classifier achieved an accuracy of 97.7% when measured against the testing dataset alone and 97.95% against the combined testing and training sets.

Figure 3.4 shows how the split between NewSpace and TradSpace changes over time when this classifier is applied to the entire data-set. The proportion of launched objects identified by this classifier as being NewSpace increases from 1970 onwards. Particularly large increases are visible since 2010, with more than 70% of spacecraft launched in the period 2016-2020 being classified as NewSpace. This increase suggests that there has been substantial change in the characteristics of spacecraft since 2010. These changes are investigated further in section 3.3.

What can also be seen in Figure 3.4 is that, as with upper stages, a noticeable proportion of spacecraft launched in the 1950s and 1960s are classified as NewSpace. One similarity between the spacecraft of this period and NewSpace is the greater

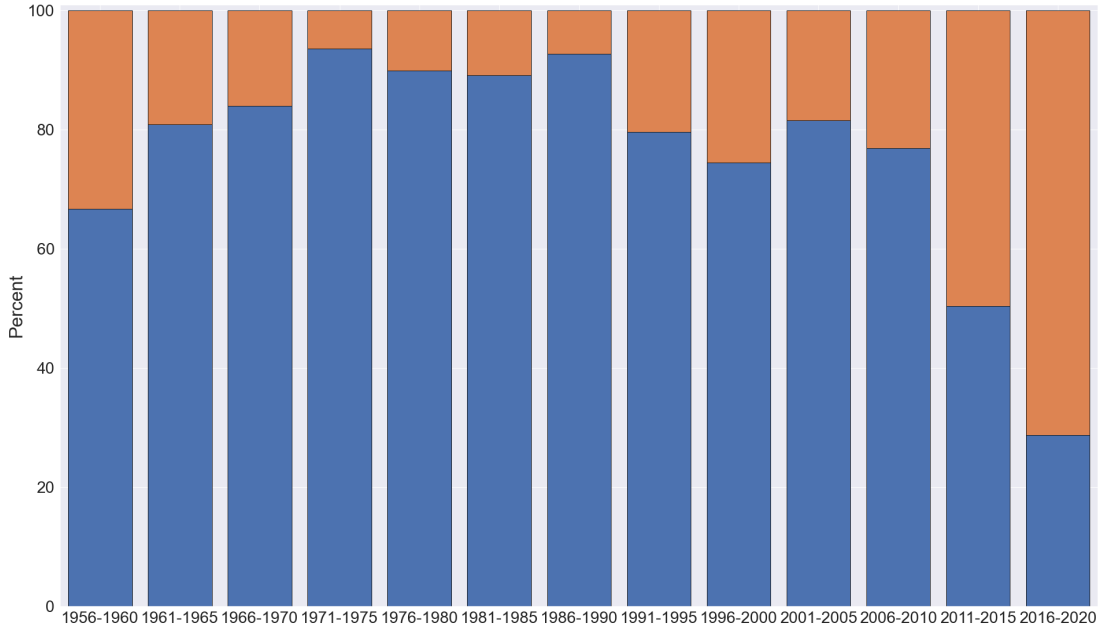

FIGURE 3.4: Distribution of NewSpace (orange - upper) vs TradSpace (blue - lower) over time for payloads using a decision tree classifier.

limitations (technological or budgetary) and their often experimental nature. These commonalities between NewSpace trends and historic spacecraft raises an important point for consideration, whether the observed trends can be expected to continue, or whether they will reverse as NewSpace technologies reach maturity. However, it is also possible that the model is not accurately classifying spacecraft, either due to the chosen characteristics being insufficient to properly distinguish between NewSpace and TradSpace or due to errors introduced during the manual classification step.

3.2.2 Generating a Random Forest

One of the limits of the decision tree approach is that it can only provide a binary output without much understanding of the uncertainty of the classification. By quantifying the uncertainty of the classification it was possible to gain a better understanding of whether there is a clear distinction between NewSpace and TradSpace, or if they exist as extremes on a continuum.

The random forest ensemble method was explored as an alternative (Breiman, 2001). In this method many classification trees are generated for a dataset. Each of these trees is trained using a randomly selected sample of the input dataset and by choosing between a random subset of the input variables at each node. A class is then chosen for an object based on which class has the most 'votes' across all of the trees in the forest.

A random forest classifier of 100 trees was generated for the payload spacecraft dataset using the same stopping criteria as the decision tree above. This achieved a small increase in accuracy across the combined dataset to 98.29%.

As before the distribution of NewSpace versus TradSpace was examined for spacecraft launched in different periods. Figure 3.5 showing the results can be compared against Figure 3.4 for the single decision tree. The random forest classifier is less likely to classify historic spacecraft as NewSpace, but still captures the expected increase since 2000 and particularly since 2010.

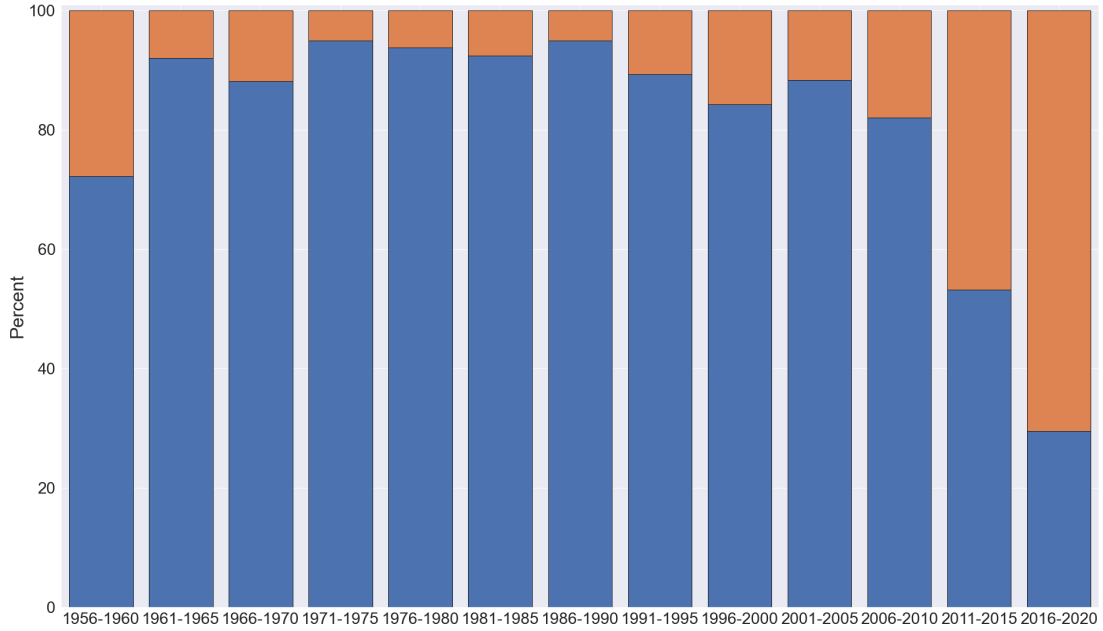

FIGURE 3.5: Distribution of NewSpace (orange - upper) vs TradSpace (blue - lower) over time for payloads using a random forest classifier.

The advantage of this classification method is that it provides a quantification of the confidence of the classification based on the probability of a certain classification being achieved across the entire forest. This can be interpreted as a measure of how closely the spacecraft corresponds to what is NewSpace, or "how NewSpace" the spacecraft is.

Figure 3.6 shows how the probability of a spacecraft being classified as NewSpace has changed over the decades. Spacecraft launched between 1957 and 1990 have a low probability of being classified as NewSpace while in the 2010s the most likely outcome is a NewSpace classification. In the 1990s and 2000s the number of spacecraft classified as NewSpace by the ensemble (probability $> 50\%$) is still low, however, there is an increase in the number of spacecraft with a $20 - 50\%$ probability. This is consistent with expectations and the trends seen above. It also supports the idea of NewSpace as a continuum with fuzzy boundaries, rather than an entirely distinct category of spacecraft.

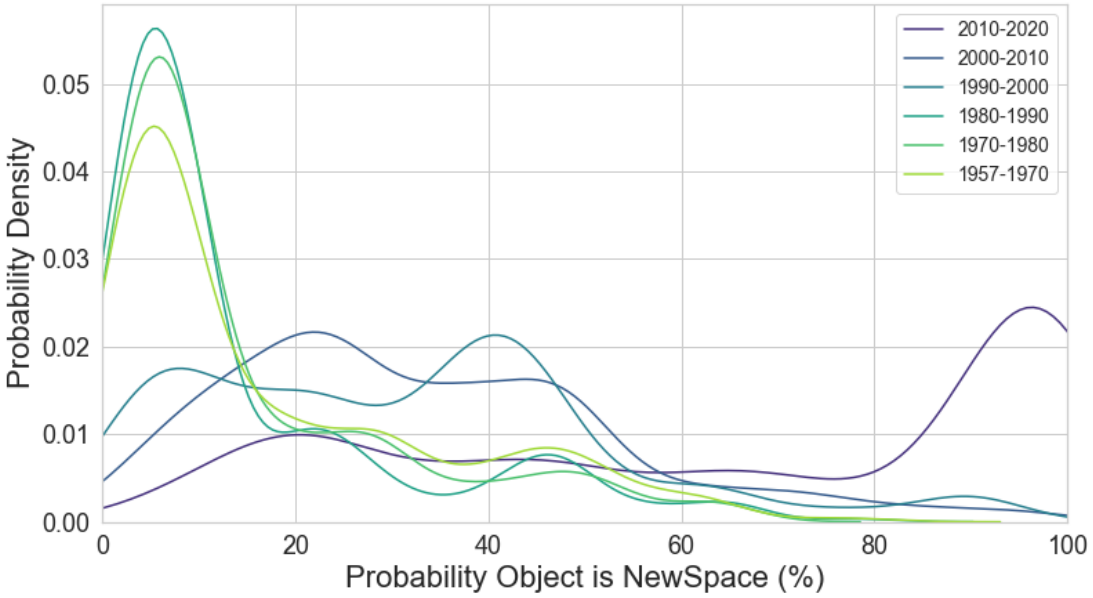

FIGURE 3.6: Distribution of confidence of classification as NewSpace for payloads using a random forest classifier.

3.3 Studying NewSpace Trends

To quantify the changes that are occurring within the spacecraft population, analysis was conducted into the variation of the key characteristics identified for spacecraft launched between October 1957 and March 2020. This work was enabled by data provided by ESA from the DISCOS database (ESA, 2018a).

A total of 15,917 records, classified as either 'Rocket Body' or 'Payload', were found in the database. This dataset was then filtered to remove records which were incomplete[1] and those associated with crewed space-flight, including space stations, resupply missions and crewed missions such as the Space Shuttle flights. This resulted in a dataset of 11,998 spacecraft ranging from the Soviet Sputnik (8K71PS) Blok-A, launched on 4th October 1957 to the Chinese XJS F launched on 19th February 2020.

3.3.1 Analysing Physical Trends

Three key physical characteristics, the mass, cross-sectional area and area-to-mass ratio were examined for each of the payload spacecraft and rocket-bodies for the LEO and GEO regions. Figures 3.7 to 3.9 show how the distributions of these characteristics have changed through the decades across the history of space-flight.

Looking first at the distributions of spacecraft mass, shown in Figure 3.7, there has been an exponential trend of decreasing average mass for payload spacecraft in the

[1] Incomplete records are likely to include a disproportionate number of military spacecraft where characteristics were classified.

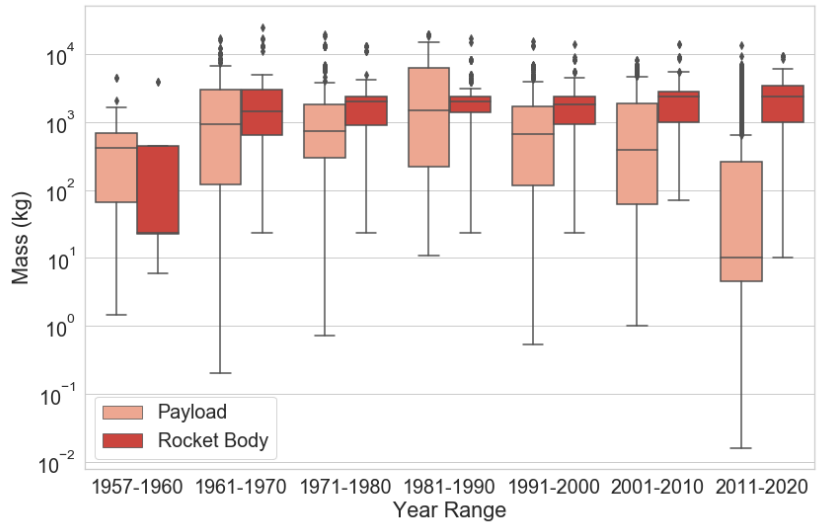

(A)

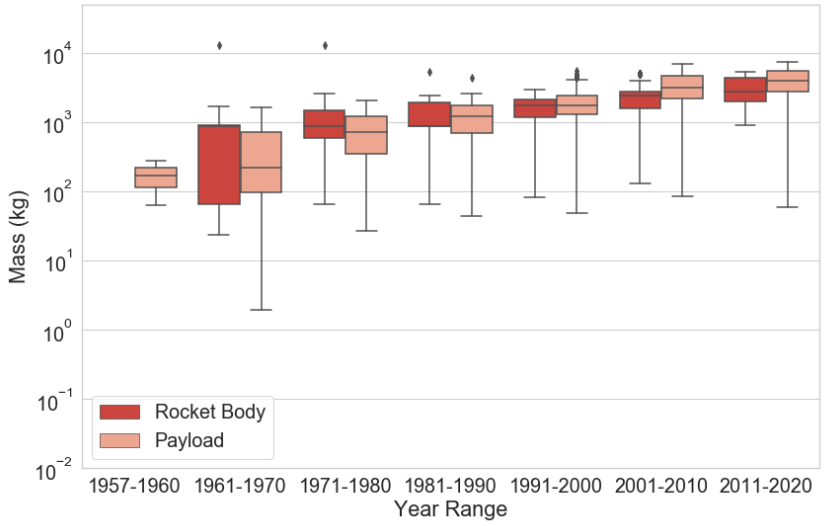

(B)

FIGURE 3.7: Boxplots of the variation in mass over time for (A) LEO and (B) GEO spacecraft.

LEO region. This has been particularly substantial over the last 10 years. Average spacecraft mass dropped from around 1500 kg in the 1980s to $\sim$ 400 kg in the 2000s and then to $\sim$ 10 kg in the last decade. Across these periods the average mass of rocket bodies has remained consistently around 2000 kg which is in keeping with the lack of change in the proportion of NewSpace rocket stages seen in Figure 3.2.

Analysis of the mass of spacecraft in the GEO region, in contrast, shows an exponential increase in the average mass of payload spacecraft, from around 1000 kg in the 1980s to over 3000 kg in the 2000s and around 4000 kg in the 2010s. This increase was accompanied by an analogous trend in the mass of GEO rocket bodies which is likely to have resulted in the accumulation over time of a substantial amount of mass in Geostationary Transfer Orbit (GTO).

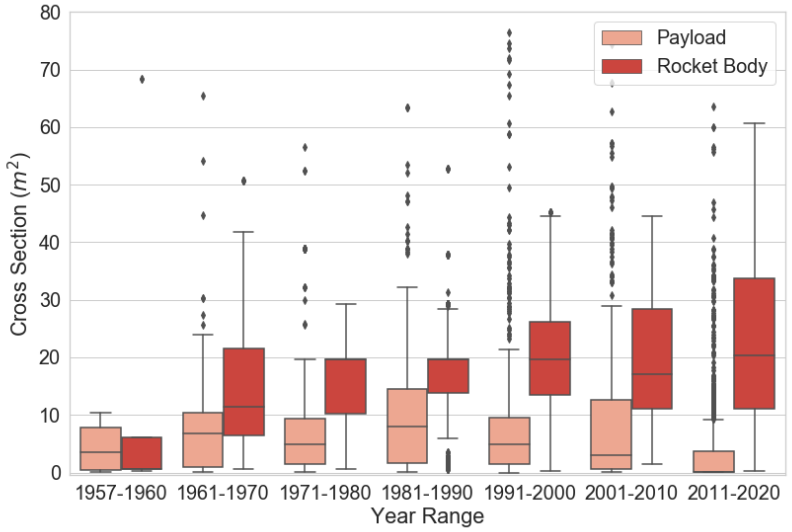

(A)

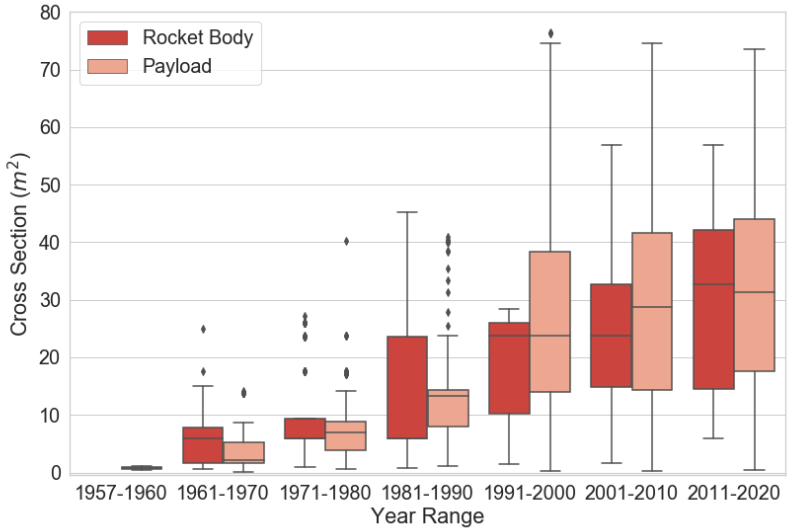

(B)

FIGURE 3.8: Boxplots of the variation in cross-sectional area over time for for (A) LEO and (B) GEO spacecraft.

A comparative study of the distributions of the cross-sectional area of spacecraft, visible in Figure 3.8, shows similar trends to those observed for the mass. Within the LEO region the size of payload spacecraft has been decreasing since 1980, from an average of $\sim 8\ m^2$, to 3 m^2 in the 2000s. Post 2010 there is an abrupt decrease down to an average of 0.1 m^2 which correlates with the decreases seen in the mass graph. This is likely to have been caused by the increase in the use of the CubeSats in the same period. The figure suggests that while the average cross section of rocket bodies has remained at around 20 m^2 throughout this period there has been greater variation in size in recent years, and a larger maximum cross section.

Looking at the data for the GEO region, illustrated in Figure 3.8 (b), it can be seen that the cross-sectional area for both rocket bodies and payload spacecraft has increased

steadily over the decades. This correlates with the observed trends in the mass. A study of the cross section over shorter time periods indicates a large increase in the average cross-sectional area, from $\sim 18\ m^2$ to $\sim 30\ m^2$ occurred in the mid-1990s. This may be due to the increasing prevalence and size of deployable solar arrays as power demands have increased.

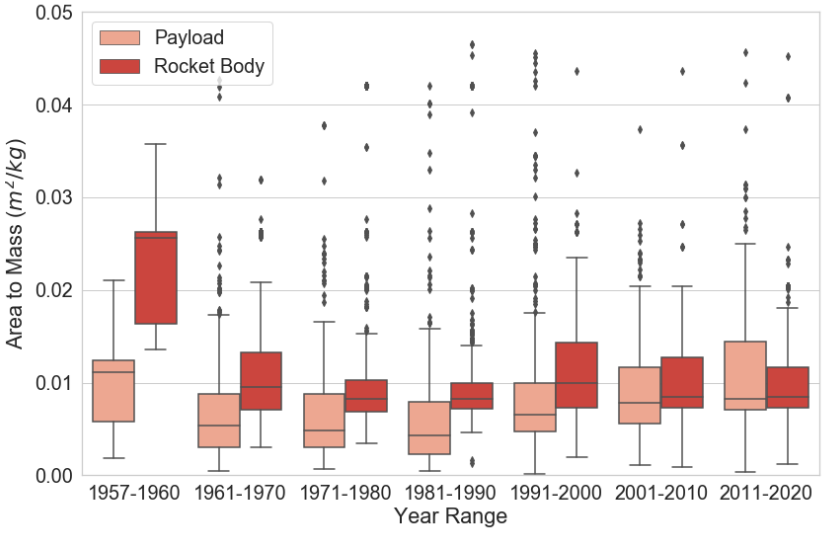

(A)

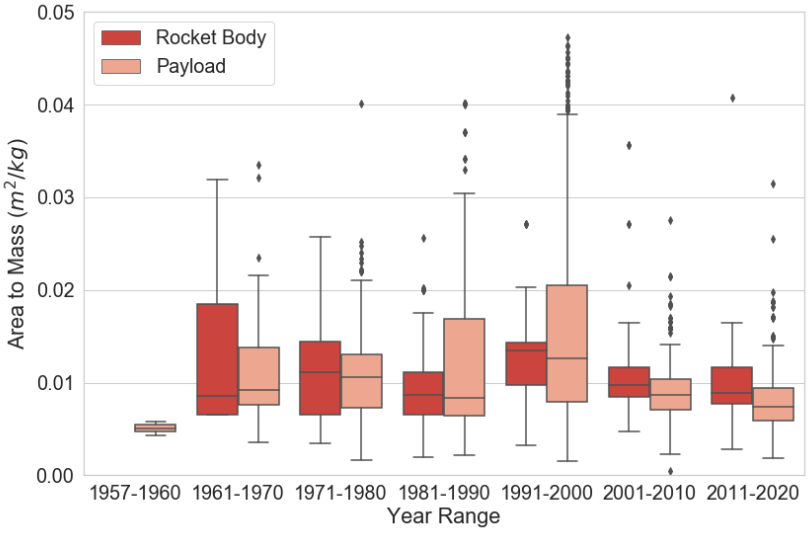

(B)

FIGURE 3.9: Boxplots of the variation in area-to-mass ratio over time for (A) LEO and (B) GEO spacecraft.

Figure 3.9 shows how the combined trends in mass and cross section are reflected in the area-to-mass ratio of spacecraft. The average area-to-mass ratio for rocket bodies in both the LEO and GEO regions has remained consistently between 0.008 and 0.01 m^2/kg, with the exception of a common peak in the 1990s. The consistency indicates that, while there have been some observed increases in size, there have not been significant changes in design and choice of materials for rocket bodies. Again this is congruent with the results of the decision tree in Figure 3.2.

However, for LEO payload spacecraft increasing trends are apparent for both the average value and the variance. The average area-to-mass ratio appears to have increased linearly from around 0.004 m^2/kg in the 1980s to 0.008 m^2/kg in the 2010s. This is consistent with the trends observed in both the mass and cross-section towards smaller spacecraft (mainly CubeSats) - a decrease in volume with a constant density leads to a reduced area-to-mass ratio due to the relationship between volume and area. Another cause for this trend might be an increase in the use of light weight composite materials and an increase in the scale of the deployable structures relative to the main spacecraft bus in order to meet rising payload demands. This is congruent with the selection of a high area-to-mass ratio as a decision metric for identifying NewSpace observed for the decision trees above.

In contrast the area-to-mass ratios of GEO spacecraft appear to have increased from 0.008 m^2/kg in the 1980s to an average of 0.012 m^2/kg in the 1990s, but then decreased back to 0.008 m^2/kg after 2000. At the same time the variance in the area-to-mass ratios has greatly reduced, suggesting a regression towards a common design for GEO spacecraft.

These changes in the characteristics of spacecraft, and the divergence between the LEO and GEO regimes, may cause significant differences in how the future space debris population evolves, in its entirety as well as specifically in each of these regimes. These trends are indicative of the characteristics of spacecraft launched in the future, however, new technologies may result in further changes to these characteristics. The use of electric propulsion, for example, could lead to a reduction in the mass of future GEO spacecraft (Lev et al., 2017).

3.3.2 Analysing Orbital Trends

An analysis was also conducted into the changes in the orbital characteristics of spacecraft and of the population as a whole. It was hypothesised that modern operational concepts, such as large constellations and launch practices, might result in spacecraft being more tightly grouped in similar orbits resulting in increased collision risk. A major consideration in this was the number of spacecraft being released from a single launch. Figure 3.10 illustrates the changes which have been seen in the median and variance of this metric.

It is clear that there has been an increase in the number of launches releasing multiple spacecraft. A particular step change can be identified in the final column, for the years 2016-2020. A smaller increase in the previous column, for 2011-2015 suggests that the change started to occur at some point in this period. This corresponds with changes noticed earlier in the size and mass of the spacecraft population related to the rising popularity of small satellites and CubeSats. Over the last 4 years the median number of spacecraft released per launch has increased to over 20, with the top 75% of

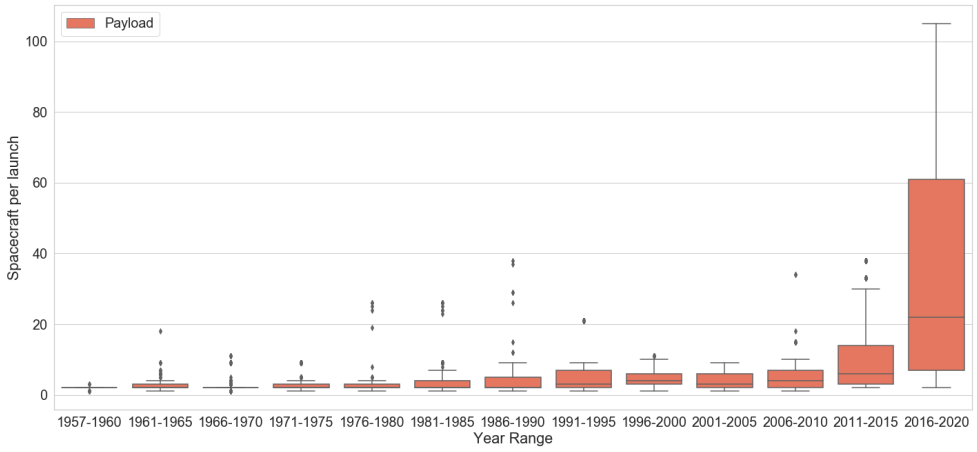

FIGURE 3.10: Showing growth in the median number (and increasing variance) of spacecraft released per launch over time.

launches releasing more spacecraft than the median number released per launch for the next greatest, between 2011 and 2015.

Figure 3.11 shows the distribution in semi-major axis-Inclination phase space of the LEO spacecraft launched in each decade. Some clustering of these orbital elements is immediately visible, with the majority of spacecraft clustered within specific inclination bands. In recent years there has been a particular concentration within sun synchronous orbits ($90 - 100°$ inclination range), polar orbits ($80 - 90°$ range), and a growing presence at around $50°$ inclination. This last is likely to be a result of the number of spacecraft released from the ISS which operates at an inclination of $51.6°$.

The increase in the number of spacecraft per launch shown in Figure 3.10 and the clustering of orbits visible in Figure 3.11 is indicative of increasing organisation within the orbital environment with spacecraft becoming concentrated into specific orbital regions. In order to quantify this change in the spatial structure, a metric was calculated for the population density of the semi-major axis vs inclination phase-space using the same grid as Figure 3.11. The metric used was the sum of the squared deviations from the mean, SSDM:

$$SSDM = \sum_{i}^{N}((x_i - \overline{x})^2) \tag{3.6}$$

Where x_i is the number of objects in the ith cell of the grid and $\overline{x}$ is the mean number of objects per cell.

Figure 3.12 shows the evolution of this value when calculated across a rolling 5 year window for LEO spacecraft launches. While the result is noisy there appears, on aggregate, to have been an increasing trend from 1960 to 2014. Since 2014 there has been a dramatic increase, correlating with the change seen in in Figure 3.10. This corresponds with the observed changes in launch operations, including the massed

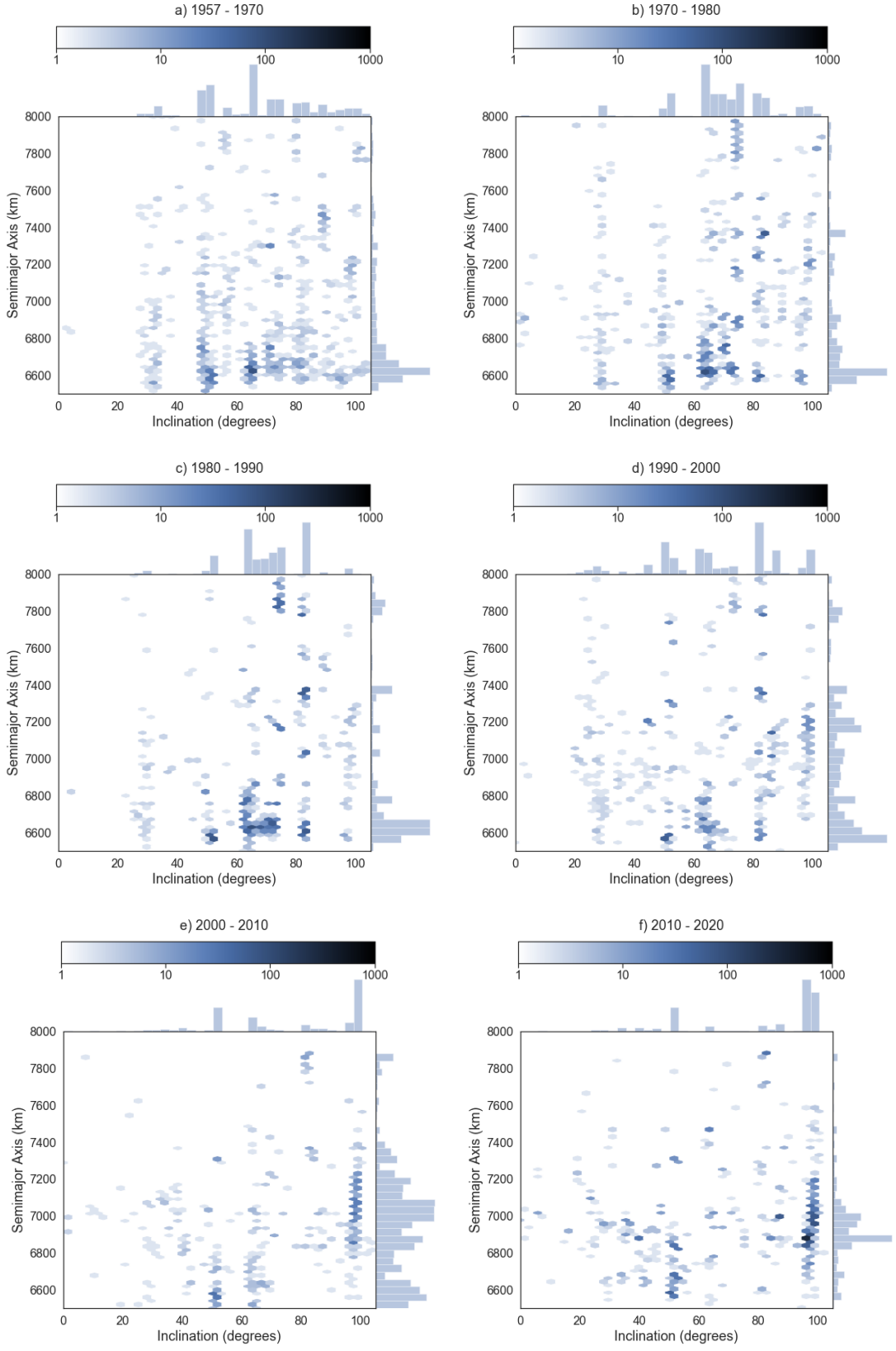

FIGURE 3.11: Heatmaps showing the number distribution of LEO spacecraft orbits by inclination and semi-major axis.

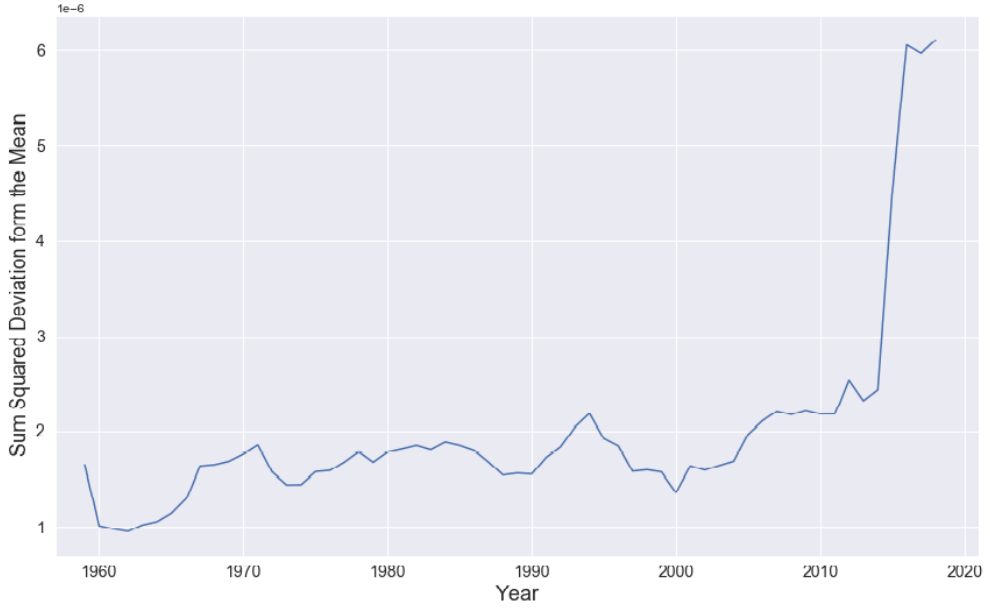

FIGURE 3.12: Showing the sum-squared-deviation from the mean for semi-major axis-inclination phase space for spacecraft launched in a rolling 5-year window.

spacecraft launches of PSLV-C37 and SSO-A SmallSat Express as well as the initial Starlink deployments.

These results highlight that the rise of NewSpace has been accompanied by corresponding changes in the orbital characteristics of spacecraft resulting in increased spatial structure. While this impact is diluted by the large number of residual spacecraft in orbit it is likely to be more pronounced when studying the behaviour of specific space systems, such as constellations. As a result, the reliability of current collision algorithms, which were developed based on the historically more disordered environment, may be compromised when assessing these systems.

3.3.3 Analysing Explosion Trends

Debris generation has historically been dominated by fragmentation events. According to the 15th edition of NASA's 'History of On-Orbit Satellite Fragmentations' (Anz-Meador et al., 2018) breakup fragments account for 65% of growth in the tracked object catalogue since 2008 and 53% of the total debris catalogue. The historic explosions in this report were analysed to understand the rate and nature of spontaneous spacecraft breakups and explosions.

Figure 3.13 shows how the distribution of explosion events by type has changed over successive 4 year periods. The events have been divided into propulsion based explosions (the most prevalent cause historically), other explosions (including battery based and deliberate self destructs) and the events where the causes are still unknown. There was a peak in the proportion of known propulsion based explosions in the

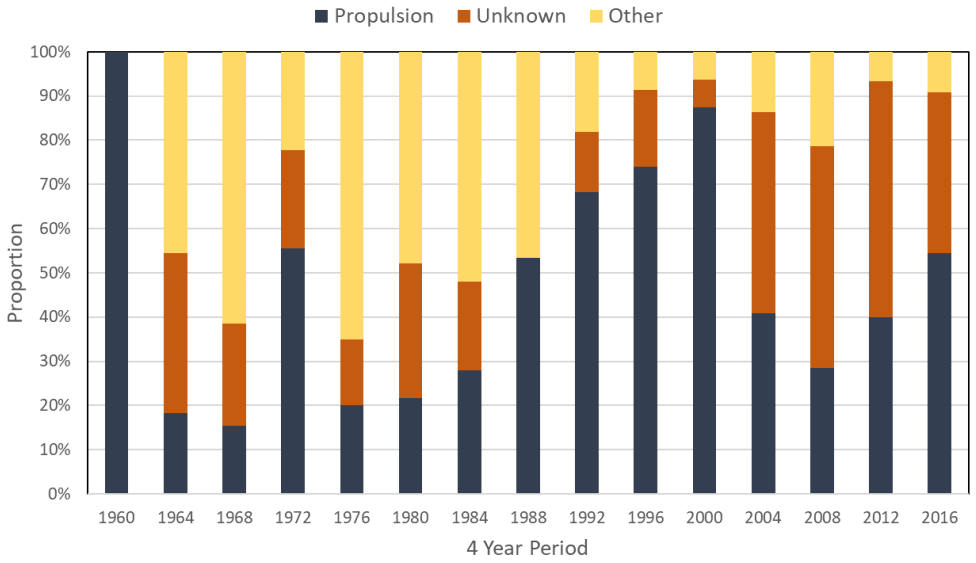

FIGURE 3.13: Showing the changing breakdown of explosion events by cause.

1990s. This can be attributed to a decrease in the number of deliberate self-destructions which had been more common during the Cold War.

Since 2000 there appears to have been a decrease in the proportion of events which were propulsion related. This may be related to the mitigation measures which were introduced to avoid the release of debris, including developments in spacecraft design and procedures such as passivation at end-of-life, which were implemented to reduce the probability of explosion for individual spacecraft. One side-effect of this is expected to be that propulsion based explosions may become less prevalent in the future. However, due to the large number of events with unknown causes it is impossible to definitively comment on whether this has changed.

Figures 3.14 and 3.15 show the cumulative number of fragmentation events and tracked fragments respectively over time. This analysis indicates that the rate at which fragmentations have occurred has remained consistent at about 4-5 breakups per year since 2000 despite the growth seen in the number of spacecraft on orbit (see Figure 2.4). This suggests that mitigation efforts have been somewhat successful at reducing the probability of a spacecraft experiencing a debris producing event.

There also appears to be a linear trend in the number of fragments observed as being produced by these events, which shows that the average severity of the events taking place has remained constant. This implies that mitigation, while reducing the probability of an event, does not change the severity of the events which do occur.

What can also be seen from these figures is that, despite there being fewer upper stages than payloads in orbit, these rocket bodies currently represent a greater proportion of the explosions occurring. A single rocket design, the Ullage motor of the Russian Blok DM-2 upper stages used on Proton-M rockets, accounts for 49 out of 125

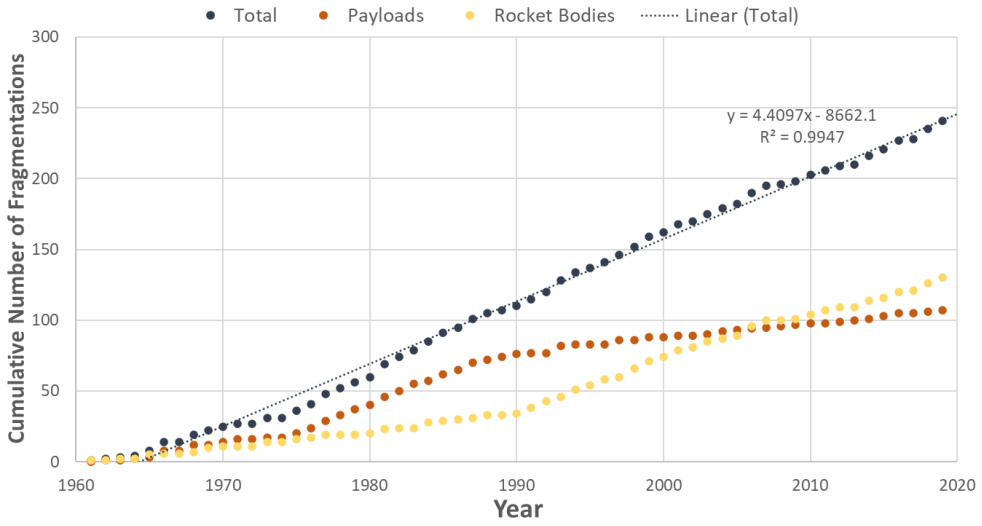

FIGURE 3.14: Showing the cumulative number of explosion events against year for rocket bodies, payloads and all objects.

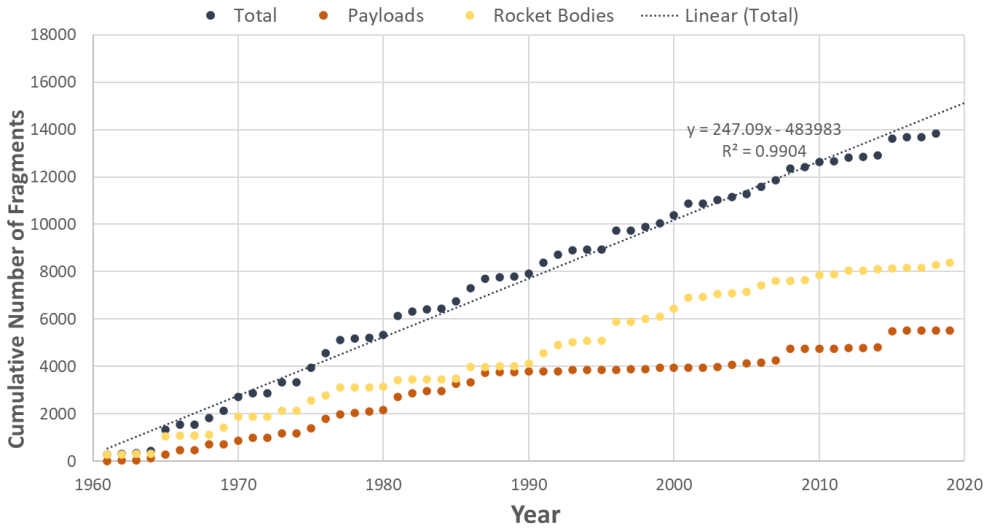

FIGURE 3.15: Showing the cumulative number of fragments released against year for rocket bodies, payloads and all objects.

rocket body fragmentations identified. While many of these rocket motors remain in orbit their use was phased out in 2012 in favour of the newer Blok DM-03 motor. It remains to be seen whether this will reduce the number of explosions.

In order to understand how the probability of explosion for a spacecraft might have changed the number of events was compared to the number of intact spacecraft in orbit (based on the launch and decay dates listed in DISCOS). Figure 3.16 shows the change in the fragmentation-to-population ratio per year for the upper stage, payload, and total spacecraft populations. Trend-lines have been added to show the moving average of these values across a 10 year window.

These results show that there has been an overall decreasing trend in the probability of

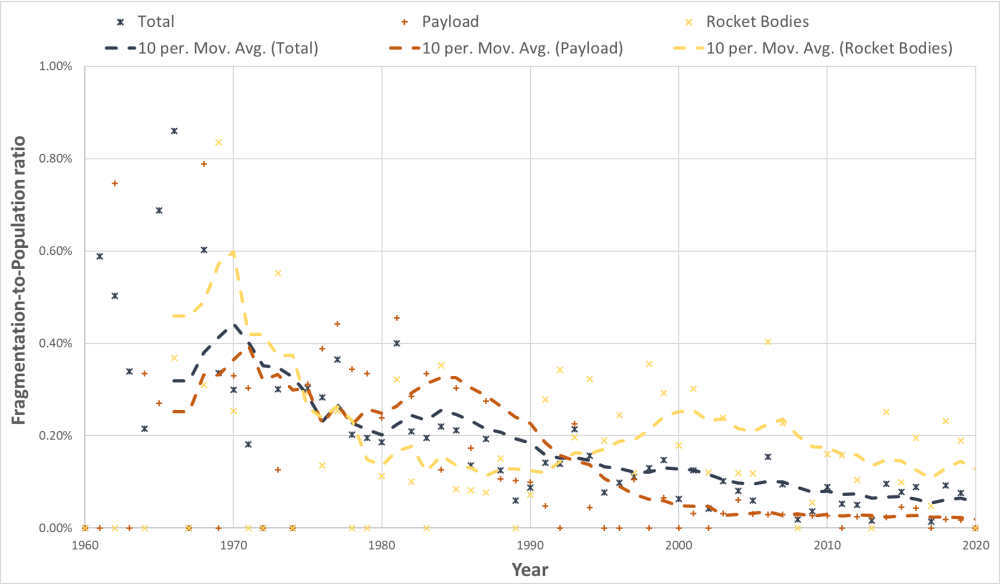

FIGURE 3.16: Showing the number of fragmentation events relative to the number of intact objects in orbit across rocket bodies, payloads and all objects.

an individual spacecraft exploding. This is particularly noticeable for payload spacecraft where the percentage of the population which might explode in one year has fallen from around 0.3% in the mid 1980s to around 0.05% since 2005. The change is less significant for the rocket body population with an increase between 1980 and 2000 followed by a decrease since 2000 from ∼0.25% to ∼0.15%.

Taken together these results show small but consistent changes in explosions which might indicate improvements such as in end of life procedures and in the design, manufacturing and quality assurance of spacecraft are reducing the risk of explosion. The timing of these changes correlates with the rise of NewSpace and the introduction of different mitigation measures. However, this trend could also be an artefact of the diversification of the spacecraft population. The large number of CubeSats launched, for example, could be biasing the results as they have increased the number of spacecraft, but as short-lived low energy systems they are unlikely to have been involved in any fragmentation events.

An alternative consideration is that this trend also coincided with an increase in the rate at which spacecraft were launched leading to a greater number of intact objects but with a lower average age. Explosions often occur many years after an object is launched and so a lower proportion of older objects could also lead to the observed decrease in the number of fragmentation events relative to the size of the population. As a result it is difficult to draw any strong conclusions with respect to the impact of NewSpace.

These trends indicate that explosions are likely to remain a significant source of new debris objects as the rate of explosions is remaining constant. However, the decreasing probability of explosion for individual spacecraft suggests that collisions may soon

pose a greater risk than explosions, particularly if the growth in the total population leads to an increase in collision frequency.

3.4 A Summary of the Implications of NewSpace

It was hypothesised that the rise of the NewSpace, associated with growth of the commercial segment from 4.7% in the 1980s to 54.9% since 2010 and an increasing diversity of launch vehicles and spacecraft operators, has led to substantial changes in the spacecraft population. The behaviour of fragmentations and the probability of collisions were identified as being sensitive to variability in several key characteristics which may be changing as part of this process.

The trends in different characteristics, orbital and physical as well as in explosions of space vehicles, were analysed to determine the extent of these changes and their potential impact on debris modelling. Divergent trends between physical characteristics of the LEO and GEO regions, including the mass and area-to-mass ratio, indicate that there has been an increasing diversification of spacecraft and is suggestive of greater flexibility in spacecraft design. As a result, the idea of an 'average spacecraft' which applies for both older and recently launched spacecraft across the LEO and GEO regions is increasingly unrealistic. The implication of this variability is that spacecraft fragmentations are also likely to have much more variability in the future and that the average fragmentation will vary significantly from region to region.

Over this period it was also observed that there has been an increase in the number of spacecraft being released by a single launcher, with a substantial increase in the average number released per launch seen for the last five years. These changes, among other practices, imply an increased spatial structure, rather than a more random distribution in orbit. This was supported by a study of the inclination to semi-major axis phase, with an analysis of the distribution of launched objects in phase space showing an increase in the population density of orbital clusters relative to the background distribution.

A study of the probability of spontaneous spacecraft breakups suggests that the probability of an individual object experiencing an event is decreasing even though events in general are becoming no less common. Combined with increasing spacecraft numbers this will likely result in collision events becoming the dominant source of debris generation in the future.

These results confirm the presence of ongoing changes in the spacecraft population, identifying both long term trends in spacecraft characteristics and more recent substantial shifts. This validates the accuracy of the first hypothesis of this work, that

NewSpace represents a substantial change in overall characteristics of the spacecraft population.

3.4.1 Expectations for the Future

The assumption is made that observed trends will continue for the near term future, in particular those related to the orbital characteristics. In addition to currently observed changes, the future development of the environment is expected to include the introduction of novel concepts and mission types such as ADR and multiple large satellite constellations. These large constellations, such as Starlink which is currently being deployed and others described in Table 2.7, involve hundreds or thousands of satellites being placed into a small number of highly structured orbital shells. The impact of this will be to drastically increase the spatial organisation of these regions and the population as a whole due to the numbers of constellation spacecraft relative to the number of non-constellation spacecraft.

With regard to the physical characteristics of spacecraft the availability of small satellites and new small launchers suggests that the current trends in size will persist. However there are practical considerations on the minimum size of spacecraft which suggests that there will be a limit to any further decreases in the mass and cross-section of LEO spacecraft. Additional details on spacecraft, including characteristics beyond those discussed, is expected to be important to enable future models to distinguish between traditional and NewSpace spacecraft. One potential requirement is information on the composition of spacecraft given the changes being seen in manufacturing methods and advanced material types for both core spacecraft components and debris shielding (Orbex, 2019; Olivieri et al., 2020).

3.4.2 Questioning Current Models

Having shown the presence of NewSpace changes within the spacecraft population it was important to understand the impact of these changes on the future debris environment. However, before this could be done an understanding was required of how the debris models themselves are impacted by these changes. This would help to determine the validity of these models and whether they are appropriate for modelling a NewSpace environment. The analysis of NewSpace changes highlighted several areas for further investigation, in particular the processes which govern fragmentations and collision probability which are explored in Chapters 4 and 5 respectively.

More work was required in order to quantify the impact of these changes on current debris models. This leads to the investigation of the second hypothesis of this work, that “NewSpace changes fall outside of the scope of current assumptions, reducing the

accuracy of the existing component models of debris processes". Subsequent chapters detail the investigation into the impact of NewSpace on the component models of fragmentations and collisions.

Chapter 4

Fragmentation Modelling

> When you're getting ready to launch into space, you're sitting on a big explosion waiting to happen.
>
> Sally Ride

4.1 A Review of Fragmentation Modelling

In previous chapters the process of fragmentation was identified as one of the most important areas for consideration when looking at the evolution of the debris environment. Breakups are a major source of new debris and collisions in particular are expected to become the dominant source of future debris objects (Kessler and Cour-palais, 1978; Kessler and Anz-Meador, 2001). Fragmentation models are important for not only identifying how many new objects are added to the environment, but also for describing the key characteristics of the generated fragments, such as their size, mass and delta-V relative to the parent body.

When modelling the fragmentation of spacecraft, the most common approach within the debris modelling community (Beck, 2013) is to use the EVOLVE 4.0 NASA Standard Breakup Model (Reynolds et al., 1998; Johnson et al., 2001). Since its original publication, this model has become the commonly used tool for fragmentation modelling. Different implementations of the model are used in ESA's DELTA model, the University of Southampton's DAMAGE model, Indian Space Research Organisation (ISRO)'s KSCPROP model) and Japan Aerospace Exploration Agency (JAXA)'s LEODEEM as well as NASA's EVOLVE and LEGEND models.

The most notable exception to this is the Aerospace Corporation's ADEPT model which makes use of an in house tool known as IMPACT (Jenkin et al., 2015; Sorge and

Mains, 2016). Unfortunately, being privately owned and operated, this tool is not readily available for comparison and comparatively little information has been published on the internal mechanisms of the model.

Prior to the introduction of the EVOLVE 4.0 version of the NASA Standard Breakup Model a wider range of fragmentation models were in use. This included a breakup model developed for ESA by the Battelle Institute and the University of Braunschweig (Klinkrad et al., 1995) and Kaman Sciences Corporation's Fragmentation Algorithms for Satellite Targets (FAST) model, as well as earlier versions of EVOLVE and IMPACT. The influence of the NASA Standard Breakup Model on the results of simulations of the debris environment was noted in Beck's report on debris modelling (Beck, 2013). In Beck's report a review of published simulation results by year, for the population of objects greater than 10 cm in size, identified an increase in predicted population following the introduction of the NASA Standard Breakup Model.

4.1.1 Sources of Fragmentation Data

In order to understand and develop models such as NASA's Standard Breakup Model experiments were undertaken to investigate the behaviour of fragmenting spacecraft, including:

- P-78 Solwind ASAT test (1985) (Jackson et al., 2000)
- European Space Operations Centre (ESOC) tank explosion ground tests (1992) (Klinkrad et al., 1995).
- Satellite Orbital debris Characterization Impact Test (SOCIT) hypervelocity collision ground test series (1992) (Ausay et al., 2017).

The SOCIT series was conducted in 1992 by NASA and the United States Department of Defense. The purpose was to generate data which could be used to develop models of the breakup of satellites in orbit. These experiments involved the recreation of hyper-velocity impacts by using a light gas-gun to fire an aluminium sphere at simulacra of satellites, including a flight ready Navy transit satellite bus (Ausay et al., 2017). These achieved a maximum collision velocity of 6.1 km/s.

The data collected from these hyper-velocity tests suggested that there existed a threshold above which the collision would result in the complete and catastrophic breakup of both objects (McKnight et al., 1995). This threshold was found to be a function of the ratio of the energy of the collision to the mass of the target. Analysis of the data indicated a value for this threshold of between 35 and 45 J/g. Most subsequent work has assumed the nominal value of 40 J/g for the threshold between catastrophic and non-catastrophic collisions. This catastrophic breakup appears to

occur when the shock-waves from the impact propagate faster than the speed of sound in the material; in the case of the SOCIT experiments primarily aluminium and plastic (Krisko et al., 2008).

Ideally the relative orientation of the colliding objects would be considered when determining whether a collision is catastrophic or non-catastrophic. For example, a collision with an appendage, such as a solar panel, is unlikely to result in the breakup of the entire spacecraft. It is more likely that the appendage itself will fragment but break away from the main body before significant energy from the collision can be passed to the parent body. Additionally, some empirical understanding of breakups can be gained by looking at the fragments produced from historic fragmentations such as those listed in Table 2.2.

Tracking Capabilities

Unfortunately the ability to derive insights from the observation of fragmentations is limited by the lack of capability when it comes to tracking fragments below a certain size using radar. Return signal strength decreases with decreasing Radar Cross Section (RCS) of a debris object. However, in addition to this, Rayleigh scattering further degrades signal strength for objects below a certain size (dependent on the wavelength used). This means that the resolution of the radar installations used to track debris is limited by the operating wavelength and the sensitivity of the radar (i.e. the signal-to-noise ratio).

The result is that the current tracking performed by the US SSN, which maintains the Space-Track database, is limited to objects approximately 10 cm in size or larger for LEO based on the UHF and VHF radars currently in use (Walsh, 2011). For debris objects in higher orbits, such as the GEO ring, tracking is achieved using optical telescopes. The resolution of the telescopes currently used for this task limits the size of tracked debris to 1 m or larger for GEO objects.

Collision Data Sources

Since the development of the NASA breakup model a number of additional tests and observed breakups have taken place which might provide more information on the behaviour of breakups:

- Fengyun-1C ASAT Test (2007) (Pardini and Anselmo, 2009; Braun et al., 2017).
- Ground based micro-satellite impact tests (2007 by Kyushu University and NASA (Hanada et al., 2009))
- 'Operation Burnt Frost': An American ASAT test against USA-193 (2008) (Kaur, 2014).

- Iridium-33/Cosmos-2251 collision - Accidental (2009) (Office, 2009)
- DebrisSat and DebrisLV hypervelocity collision ground test series (2014) (Polk and Roebuck, 2015)

Of these additional sources of data the DebriSat experiment is expected to be of particular use for fragmentation modelling. Two areas which have been the particular focus of research are the variations in the shape and material composition of the debris fragments produced (Hanada et al., 2009; Hanada and Liou, 2011; Lan et al., 2014). The initial results of this research suggest some of the ways in which future models may differ, including distinguishing fragments with different shapes, e.g. plates or needles/rods, and using multi-modal distributions when assigning area-to-mass ratios to help include the effect of different material densities.

DebrisSat

The DebriSat program was created in order to answer some of the outstanding questions on fragmentation. In collaboration with the United States Air Force in 2014 NASA, the Aerospace Corporation, and the University of Florida conducted a new series of hyper-velocity impact tests (Polk and Roebuck, 2015; Ausay et al., 2017; Cowardin et al., 2017). The goal of DebriSat was to provide data to update NASA's existing breakup model by investigating the collisional breakup of a spacecraft of modern design, and identifying and analysing the resultant fragments aiming to account for over 90% of the spacecraft's original mass.

A two-stage light gas gun was used to propel a ∼500 g hollow aluminium cylinder at speeds of up to 7 km/s into a target. For this series of tests three different targets were used. First a 5 times scale multishock shield was tested, to study whipple shields for protection against small space debris and then two mock space vehicles were tested. These consisted of DebrisLV, a 17.6 kg structure similar in design to many of the rocket upper stages in LEO, and DebriSat, a 56 kg model satellite constructed using the same techniques, materials, sub-systems and components as a modern LEO satellite and including one deployable solar panel (Cowardin et al., 2017).

This test configuration allowed the replication of collisions with energy-to-mass ratios well in excess of the catastrophic collision threshold. For the DebriSat test case a velocity of 6.8 km/s was achieved for a projectile weighing 570 g giving an energy-to-mass ratio for the collision of 235 J/g (Ausay et al., 2017).

At this point in time the process of cataloguing and analysing the fragments generated is still ongoing. No published updates have yet been made to debris models based on this investigation. However, it is expected that the results will stimulate significant changes to the existing model as the experiment is much more representative of expected collisions than the SOCIT series, with much more refined techniques used to

analyse the generated fragments, including 3D scanning to enhance characterization measurements.

4.2 The NASA Standard Breakup Model

The current version of NASA's Standard Breakup Model was developed in 1998 for the Evolve 4.0 evolutionary debris model with the intention of implementing a refined fragmentation model based on available observational data in addition to the experimental data generated by experiments such as the SOCIT test series and the ESOC tank explosion tests. Variations on this model have since been incorporated into a range of evolutionary debris models. Some of these implementations have included a number of refinements to the original model. The Fragmentation Event Generator (FREG) employed by ESA (Andrișan et al., 2017), for example, implements several refinements including:

- Creation of two differentiated clouds in the event of a collision, allowing each fragment to be associated with a parent body.
- Assigning delta velocities to the fragments as vectors rather than scalars, to include a directional element.
- Inclusion of conservation of kinetic energy by scaling fragment velocities.

It is noted that while many of the implementations include refinements and additions to NASA's original model the underlying assumptions remain the same as when it was first created, 20 years ago, without any significant update using more recent data.

4.2.1 The Workings of the Model

The NASA Standard Breakup Model generates a population of fragments to represent the on-orbit breakup of an object by drawing from distributions for each of size, area-to-mass ratio and velocity. Three specific modes are identified for fragmentations: catastrophic collisions, non-catastrophic collisions and explosions, with different behaviour attributed to each.

Fragment Generation

The key variable in this model is characteristic length (L_C) of the fragments, which is then used to define the distributions from which each of the other characteristics are generated. The characteristic length is based on the diameter estimated for an object with a given RCS value by the NASA size estimation model (Reynolds et al., 1998).

When characterising the size of an object the RCS value used is an average across multiple measurements to account for shape and orientation.

In terms of the physical dimensions of the object this length is defined as the average of the longest three orthogonal dimensions of the object:

$$L_C = (A + B + C)/3 \tag{4.1}$$

Where A is the longest dimension of the object, B is the longest dimension normal to A, and C is the longest dimension normal to both A and B.

The simplest example is a sphere, where the characteristic length is the sphere diameter, and is also the version of the object with the largest volume:

$$V_{sp} = \frac{4}{3}\pi r^3 = \frac{\pi}{6}L_C^3 \tag{4.2}$$

In the model, the number of fragments generated by a particular fragmentation event is governed by a power law describing the cumulative number of fragments, $N(L_C)$, greater than or equal to a characteristic length. The coefficients and exponents of the equation vary depending on the event mode being modelled:

$$N(L_C) = \begin{cases} 6\,S\,L_C^{-1.6}(\frac{1}{m^{-1.6}}), & \text{if Explosion.} \\ 0.1\,M_e^{0.75}\,L_C^{-1.71}(\frac{1}{kg^{0.75}m^{-1.71}}), & \text{if Collision.} \end{cases} \tag{4.3}$$

Where the explosion scaling factor, S, is 1 for upper stages in the $600 - 1000$ kg mass. The literature indicates that this scaling factor varies between 0.1 and 1 dependent on the type of spacecraft but little information is available on specific scaling factors for specific cases.

For collision scenarios the expected ejecta mass, M_e, of a collision is dependent on whether the event is categorised as catastrophic or non-catastrophic.

$$M_e = \begin{cases} M_{target} + M_{projectile}, & \text{if Catastrophic.} \\ M_{projectile}\,(\frac{v_{relative}}{1000})^2, & \text{if Non-catastrophic.} \end{cases} \tag{4.4}$$

Where $v_{relative}$ is the velocity of the projectile relative to the target in m/s.

The determining factor on whether a collision event should be modelled as being a catastrophic or non-catastrophic collisions is the energy-to-mass ratio of the event. The threshold for this in the NASA Standard Breakup Model is set at 40 J/g of target mass, based on the results of the SOCIT test series (Ausay et al., 2017). This results in an upper limit to the ejected mass that the model generates in non-catastrophic collision scenarios. Using the threshold value of 40 J/g of target mass it is possible to calculate that the maximum ejected mass of a non-catastrophic collision is 8% of the target mass.

Dependent Characteristics

Fragment mass is generated from an area-to-mass ratio distribution which is a function of the characteristic length. The area-to-mass distributions are differentiated into two defined size regimes: 11 cm and greater, and 8 cm and smaller, as well as an intermediate region between the two. Using these area-to-mass ratios the mass of the object can be derived by calculating the cross sectional area of the fragment from its characteristic length:

$$A_X = \begin{cases} 0.540424\, L_C^2, & \text{where } L_C < 0.00167\, m. \\ 0.556945\, L_C^{2.0047077} \left(\frac{m^2}{m^{2.0047077}}\right), & \text{where } L_C \geq 0.00167\, m. \end{cases} \tag{4.5}$$

And then calculating the mass as:

$$M = \frac{A_X}{(A/M)} \tag{4.6}$$

The area-to-mass distributions used in this model were generated using a range of observational and experimental results. For the larger regime ($L_C \geq 11$ cm) area-to-mass ratio is modelled based on the observed atmospheric decay rates for real collision and explosion fragments (Johnson et al., 2001). This results in a bi-modal normal distribution in log space, with the parameters varying according to characteristic length. The parameters for the small regime ($L_C \leq 8$ cm) were derived using data from ground based hypervelocity impact tests due to tracking limitations. This resulted in a common normal distribution in log space being used for all scenarios. A bridging function is used to calculate area-to-mass within the intermediate region based on the parameters of the regimes for larger and smaller characteristic lengths.

A delta-velocity relative to the parent object is assigned to each of the generated fragments by randomly sampling from a normal distribution. The distribution was derived from observational data of the relationship between ejecta velocity and ejecta area-to-mass ratios for the breakups of upper stages. While velocity is a vector quantity, the original model makes no accounting of the direction of travel of generated fragments. The values generated are merely scalar quantities of speed. Later integrations of this model into three dimensional evolutionary models have attempted to introduce this by generating a uniform distribution of velocity directions for each fragment.

Conservation of Mass, Momentum and Energy

One issue noted when implementing this model is that the total mass generated across all of the fragments is often less than the combined initial mass of the object or

objects. Clarifications published in NASA's Orbital Debris Quarterly News (Krisko, 2011) revisited the model with new details on how conservation of mass is implemented within the model.

The steps described above are followed to create fragments from 1 mm to 1 m in size and the mass of these objects is totalled. To conserve the initial mass across the generated objects, some large fragments with size greater than or equal to one metre are generated and the remaining mass is distributed between these fragments.

The number of fragments generated in this largest size regime, N_{Large}, is dependent upon the breakup mode being modelled:

$$\begin{cases} 2 \leq N_{Large} \leq 8, & \text{if Explosion.} \\ N_{Large} = 1, & \text{if Non-catastrophic.} \\ 2 < N_{Large} & \text{if Catastrophic}^1. \end{cases} \tag{4.7}$$

Where the single massive fragment generated in the non-catastrophic case is intended to represent a cratered target mass.

No specific provision is made within the original model to handle conservation of either momentum or energy. It may be that this was not considered necessary, or practical, considering the non-directional nature of the velocities generated.

4.2.2 Assumptions and Limitations of the Model

Spacecraft fragmentations are complex to model as the behaviour is the result of a number of different processes. As an empirical model the NASA Standard Breakup Model provides an alternative means converting from a set of input parameters about the fragmenting object or objects into a set of output parameters describing the fragments produced based on observations of historic breakups. This relies upon a number of simplifying assumptions which allow them to generate approximate results while allowing for some uncertainty in the exact parameters. However, this introduces certain limitations on the use of the model, particularly with regard to the fidelity of results when these assumptions start to break down.

The amount of data available for the development of the NASA Standard Breakup Model was limited, particularly for collisions. Consequently the model may be biased towards the breakup of a specific class of objects, such as large historic spacecraft. The resultant fragments predicted would not necessarily be representative of the number and size of fragments produced by the broader population which now consists of many smaller spacecraft. For example, the explosion mode of the breakup model

[1] The literature states that 'several' fragments should be generated. In practice this has been implemented by generating a series of successively larger fragments until all mass is accounted for.

operates on the assumption of spacecraft in the $600 - 1,000$ kg range, which is consistent with only a small proportion of the overall population.

One of the main assumptions made in the NASA Standard Breakup Model is that the collisions modelled are body-to-body, with the full mass of both being involved. For most catastrophic collisions it is expected that the entire body of the spacecraft will breakup due to the propagation of shock-waves throughout the body of the spacecraft. However, this does not take into account spacecraft consisting of multiple connected structures, such as the presence of appendages, for example gravity gradient booms or deployed solar panels. It is likely that in these situations the incoming object will either hit the body of the spacecraft and not the appendages or will hit the appendages but not the body. In these situations the shock of the impact would cause connection between the structures to fail, potentially preventing the shock-wave from propagating throughout the entire object and so avoiding a complete fragmentation.

In such an event, where only a sub-section of the spacecraft is impacted, it can be expected that only the affected appendage would fragment with the remaining mass being left as large intact objects. This gives rise to the idea of 'involved' mass which fragments as a result of the collision and 'non-involved' mass which does not. Some subsequent models have attempted to include this concept (Vallado and Oltrogge, 2017).

A second assumption made is the energy threshold between catastrophic and non-catastrophic collisions. A value of 40 J/g is used for all collisions in the model, however, the experimental values for the catastrophic threshold ranged from between 35 J/g and 45 J/g (McKnight et al., 1995). The results generated by the model for collisions in this energy range will be sensitive to the value chosen for this threshold. The ratio of the number of fragments for a catastrophic collision, $N_{Catastrophic}$, to the number of fragments for a non-catastrophic collision, $N_{Non-catastrophic}$ can be calculated to fall within a range of values:

$$\frac{N_{Catastrophic}}{N_{Non-catastrophic}} = \frac{0.1\, M_{e_{Cat}}^{0.75}\, L_C^{-1.71}}{0.1\, M_{e_{Non-cat}}^{0.75}\, L_C^{-1.71}} = \left(\frac{M_{e_{Cat}}}{M_{e_{Non-cat}}}\right)^{0.75} \tag{4.8}$$

Substituting Equation 4.4 into Equation 4.8 and introducing the kinetic energy $KE = \frac{1}{2} M_{projectile} V^2$ allows the equation to be simplified, substituting in the energy-to-mass ratio by converting from kilograms into grams:

$$E/M = \frac{KE}{1000 \times M_{Target}} \tag{4.9}$$

Combining and simplifying of Equations 4.8 and 4.9 using the stated value of 40 J/g for the energy-to-mass ratio gives the upper and lower limits of the ratio to be:

$$\frac{N_{Catastrophic}}{N_{Non-catastrophic}} = \begin{cases} (25)^{0.75} = 11.18, & \text{as } M_{Projectile} \to M_{Target}. \\ (12.5)^{0.75} = 6.65, & \text{as } M_{Projectile} \to 0. \end{cases} \tag{4.10}$$

Consequently a discontinuity in the predicted number of fragments exists around the catastrophic energy threshold. Significantly more fragments are generated by the model for a catastrophic collision when compared to a non-catastrophic collision when the energy-to-mass ratio is close to 40 J/g. Hence, for otherwise identical collisions, with velocities differing by a small value, the model will produce noticeably different results.

Additionally, the literature describing the model does not provide a definition of the bridging function used to interpolate between the area-to-mass distribution of small fragments ($L_C < 8$ cm) and that of the large fragments ($L_C > 11$ cm) which has the potential to cause discrepancies between implementations. The large and small distributions were fitted to different datasets (Reynolds et al., 1998); the fragments observed for on-orbit breakups were used to define for the larger distribution, but the smaller distribution was based on the results of the SOCIT tests. The limitation of this is that, as these tests were ground based, the resulting fragmentation may not be an accurate representation of an orbital breakup. A known limitation of the model exists for the assignment of area-to-mass ratios for small fragments ($L_C < 8$ cm) which is currently assigned by sampling from a single normal distribution. However, analysis of the small fragments produced by ground based experiments (Hanada et al., 2009; Hanada and Liou, 2011; Lan et al., 2014) indicates that a bi-normal distribution is more appropriate with separate peaks corresponding to low and high density materials. This becomes increasingly relevant with the growth in the use of lighter materials such as carbon fibre relative to the use of heavier materials such as aerospace grade aluminium.

The velocity change of the fragments relative to the velocity of the parent body is an important characteristic for environmental evolution. The delta velocity will change the orbits of the fragments relative to the original parent object. As a result some of the fragments will experience different levels of drag due to differences in the apogee and perigee of their orbits and this can have a significant impact on the orbital lifetime of the fragments. The directionality of the velocity perturbations are only modelled in a simple fashion within implementations of the NASA Standard Breakup Model, for example using a uniform distribution to spread the delta-velocities out equally. However, research into the relative velocities of fragments resulting from observed high velocity collision events suggest that there is a greater dependence on the geometry of the collision (Tan et al., 2013; Sorge and Mains, 2016). Analysis of the velocity perturbations of the Iridium-33 - Cosmos-2251 collision conducted by Tan

et al. (2013) indicated that the largest fragments of both spacecraft received retrograde and downward velocity perturbations. The effect of this would be to reduce the residual orbital lifetime of the largest fragments. If this behaviour is general across high velocity collision events then it suggests that the current iterations of the breakup model might, on average, over-predict the lifetime of large debris fragments, inflating the perceived risk of secondary collisions.

4.2.3 Implementation

For the purposes of this investigation an implementation of the NASA Standard Breakup Model was created based on the descriptions in Reynolds et al. (1998); Johnson et al. (2001); Krisko (2011). The model was implemented such that each predicted fragment would be created as a unique object, with its own values for characteristic length, mass and velocity. While being useful for investigating the limits of the model, this had a negative impact on the computational performance when it came to generating the small-sized fragment sizes due to the exponential increase in the number of objects required. In order to control this, a minimum fragment length was included within the model. This was set to 1 mm by default, but can be set manually for each cloud of fragments generated.

At several points during the implementation, decisions had to be made on how to implement steps left ambiguous in the published descriptions. The most significant of these stemmed from the generation of the largest fragments used for conservation of mass. No provision was made within the literature for how to define the maximum fragment size generated by the model. In this implementation the length of the parent object is used as an upper bound for the size of any fragments generated.

Several options were implemented for the bridging function between the larger and smaller area-to-mass regimes to allow investigation of the consequences this has on the outputs of the model. Four different options were identified: (1) to extrapolate the larger regime down to the smaller; (2) to extrapolate the smaller regime up to the larger; (3) to take the mean average of the two regimes; or (4) to interpolate between the two, based on where the value of the characteristic length falls on the interval. For the purposes of this investigation the final option of interpolating between the two regimes was used as this was considered the most realistic in the absence of any physical evidence of a discontinuity.

Volumes were estimated for the different objects to allow an investigation of the density of the generated fragments. Various shapes were considered for this, including that of a thin flake or wafer. However, all fragments were generated as spheres with a diameter equal to their characteristic length. This should have resulted in the highest possible volume for an observed cross-section and so generated objects with the lowest density.

In order to verify this implementation of the NASA Standard Breakup Model a set of specific test cases were replicated and compared against previously published data. Data from two previous studies were chosen for this, which included data on the size, mass and velocity distribution of fragments for both explosions and collisions. The results of this along with further verification work, including analysis of the distributions of the different fragment characteristics against the results of Rossi (2006), can be found in Appendix A at the end of this work.

4.3 The Relevance of NewSpace Trends

The analysis conducted in Chapter 3 showed that there are on-going changes to what can be considered an average spacecraft. Object mass and size were identified as two of the key characteristics which impact the modelling of spacecraft fragmentation. Trends in these physical characteristics of spacecraft showed a divergence in the median size and mass of the spacecraft population, towards lower values in the LEO region and higher values in the GEO region.

As a result, the current spacecraft population has much greater variety in these key characteristics when compared to spacecraft involved in historic breakups which have been used to develop fragmentation models. Existing fragmentation models may not generate accurate estimates of the number and size of fragments produced by the breakup of objects at the extremes of the size/mass range further away from the original assumptions.

In addition, the trends in the area-to-mass ratios of spacecraft are suggestive of changes in material density. This may result in further differences in fragmentation behaviour, including changes in the energy required for a catastrophic breakup. An analysis of on-orbit collisions (Pardini and Anselmo, 2014) showed that, of five events expected to have an energy-to-mass ratio greater than 40 J/g, only the intact-intact collision of the Iridium and Cosmos satellites underwent a catastrophic breakup. One possible reason is that the collisions may have been with an appendage, rather than body-to-body as initially assumed. Another is that a fixed threshold for all spacecraft is an oversimplification. It is worth testing the sensitivity of evolutionary simulations to variations of the threshold value.

4.3.1 Impact on the NASA Standard Breakup Model

Since the release of the NASA Standard Breakup Model 20 years ago there have been significant changes in the space industry. It is hypothesised that these developments have materially changed the behaviour of breakups for at least some of these new spacecraft. It is expected that changes in the size, mass and material type will result in

different numbers of debris fragments being produced, with a different size distribution.

A key assumption identified for the NASA Standard Breakup Model is that the fragment size distribution based on exploding spacecraft in the $600 - 1,000$ kg mass range can be generalised as a common size distribution for all explosion events. The trends in spacecraft mass in Chapter 3 showed a departure from this range which suggests that this assumption may no longer be valid. The characteristics of the spacecraft listed in DISCOS show that only 7.9% of spacecraft and 16.3% of rocket bodies launched since 2010 conform to this assumption, compared to 18.7% and 18.2% respectively between 1990 and 2000.

There was also an observed deviation in spacecraft size between LEO and GEO spacecraft which may result in different errors in the model in different regions. For example an over-prediction of the number of fragments generated by the smaller spacecraft in LEO but an under-prediction in GEO. The altitude at which fragments are generated will have significant impacts on the future environment suggesting a more robust approach may be required.

Expected Impact on the Outputs

Beck's report on debris modelling identified the introduction of the NASA Standard Breakup Model as having a noticeable impact on the results of simulations of the debris environment (Beck, 2013). The comparison in Figure 4.1 of the results included in different published work by year showed an increase in the population of objects greater than 10 cm in size following the introduction of the NASA standard Breakup Model to evolutionary models (followed by a decrease due to decline in traffic rate and the introduction of the CUBE collision model). These results highlighted the sensitivity of evolutionary models to the results of fragmentation models.

Analysis of the current limitations of the NASA Standard Breakup Model identified several potential issues which may impact its suitability for modelling the fragmentation of NewSpace spacecraft. For example, the size distribution of the fragments produced is based on the behaviour of an average breakup irrespective of the type or age of spacecraft. However, novel developments in spacecraft structures and the methods used in their manufacture, as well as the deviation in spacecraft characteristics between the LEO and GEO regions, indicates that this might be an oversimplification. Consequently, the environment might see a significantly different distribution of fragment sizes than currently predicted by simulations. This could, in turn, lead to an error in the predicted number of secondary catastrophic collisions involving the fragments generated or the effectiveness of different mitigation and ADR strategies.

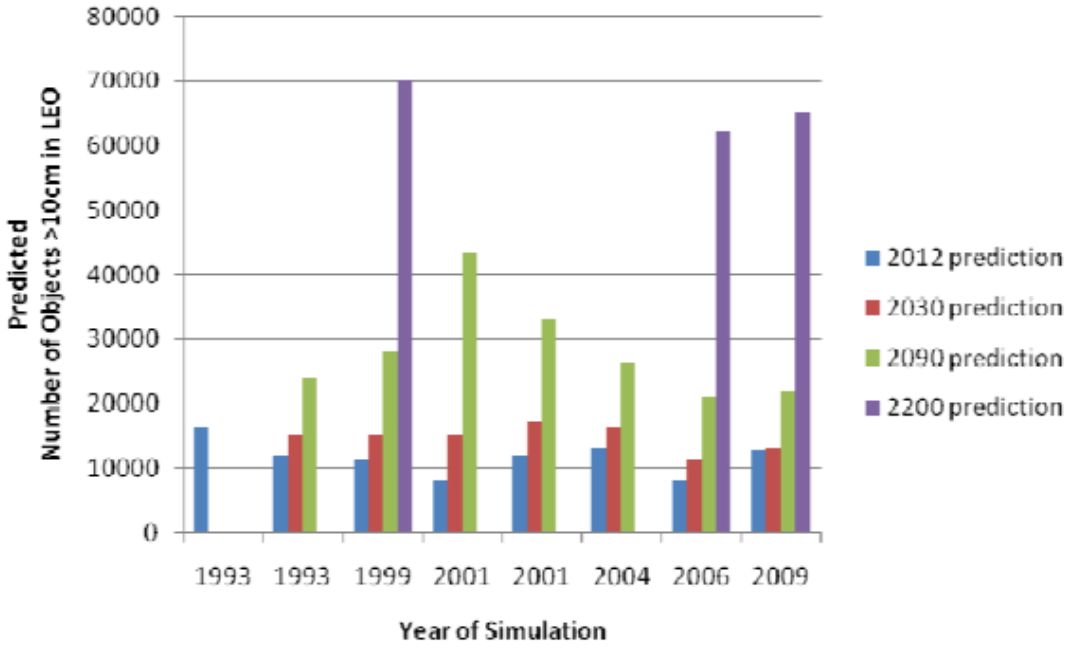

FIGURE 4.1: Graph of model results by year of simulation (Beck, 2013).

4.4 Validating and Testing the NASA Standard Breakup Model

Having implemented and verified a reproduction of the NASA Standard Breakup Model, a series of tests were conducted to study how the known changes of the NewSpace era might impact the use of the model for different scenarios. This validation was conducted by comparing the output of the model against a number of observed on-orbit fragmentation events.

A range of different fragmentation events were selected from three categories: upper-stage explosions; satellite explosions; and catastrophic collisions[2]. The decision was taken to separate the explosion events between payload and upper-stage and investigate each individually to identify differences in breakup behaviour due to the differences in design and the different trends in physical characteristics identified for each in Chapter 3.

Fragmentations were first identified using the ESA's DISCOS (ESA, 2018a). Detailed information on the number and size of fragments for each of the identified events was then extracted from the Space Track catalogue (Space-Track, 2018). Each event was then simulated using the model and the results collated for comparison against the recorded data.

Within the Space Track catalogue fragments are categorised as being either 'Small', 'Medium', or 'Large' using an estimation of their size based on their observed RCS.

[2]At this time no examples have been identified and simulated for non-catastrophic collision events.

These categories are defined as:

$$\begin{cases} A_{RCS} < 0.1\,m^2, & \text{Small} \\ 0.1\,m^2 < A_{RCS} < 1.0\,m^2, & \text{Medium} \\ 1.0\,m^2 < A_{RCS} \quad , & \text{Large} \end{cases} \tag{4.11}$$

The assumption was made that these RCS areas could be treated as cross-sectional areas and substituted into Equation 4.5 to convert from these size categories to values of the characteristic length. This assumption is consistent with how the NASA Standard Breakup Model was originally developed using fragment sizes estimated from RCS values. This conversion results in the following characteristic length ranges:

$$\begin{cases} 0.1\,m < L_c < 0.425\,m, & \text{Small} \\ 0.425\,m < L_c < 1.339\,m, & \text{Medium} \\ 1.339\,m < L_c \quad , & \text{Large} \end{cases} \tag{4.12}$$

where a minimum characteristic length of 0.1 m has been assumed for the small fragments. The minimum length was chosen based on the stated tracking limits of the the SSN which USSTRATCOM uses to populate the Space-Track database. The limit of 10 cm is an approximation of the lower limit, due to the uncertainties which exist in the sensing process.

Using this conversion the cumulative number of fragments with characteristic lengths greater than 0.1 m, 0.425 m and 1.339 m was extracted from the Space Track catalogue for each of the scenarios. Fragmentations were modelled using the implementation of the NASA Standard Breakup Model for each of the selected scenarios and the size distribution of the fragments generated was then compared to the observed results. In addition to this, an analysis was made of the mass assigned to fragments of different sizes for each scenario to investigate the potential densities of the fragments and how the fragments created in the largest regime for conservation of mass compared to the rest of the population.

An analysis of the individual RCS values of the observed fragments would be preferable to improve comparability of the results by allowing comparison against a larger number of data points. However, at present these data are not readily available in the public domain[3].

[3] An attempt was made to access these data by submitting an Orbital Data Request through Space Track to the SSA Partnership and Coalition Engagement (SPACE) Office of the 18th Space Control Squadron. However, numeric RCS is not something usually provided to the general public and after a review of the request by USSPACECOM and their legal section the request was denied (Sharing, 2020)

4.4.1 Upper Stage Explosion Events

The candidate scenarios chosen for modelling the explosion of upper stage rocket bodies were selected from the list of top ten breakup events (Anz-Meador, 2016). This table contains six upper stage breakups. The most recent four of these were selected for this investigation as being the most likely to be representative of modern breakups. The characteristics of these breakup events can be seen below in Table 4.1.

TABLE 4.1: A table of the characteristics of the upper stage explosion events used in validation (Sources: (NASA, 2008; ESA, 2018a; Space-Track, 2018)).

Parent Body	International Designator	Mass(kg)	Maximum Dimension (m)	Number of Fragments		
				Large	Medium	Small
Long March 4 third stage	1999-057C	1000	5	7	64	430
PSLV[4]final stage	2001-049D	900	3	2	30	372
Ariane 1 third stage	1986-019C	1400	10	7	161	499
Pegasus HAPS	1994-029B	97	1	0	72	755

Of these four breakups, two - those of the Chinese Long March 4 third stage and the Indian Polar Satellite Launch Vehicle (PSLV) upper stage - are within the identified normal mass range for the NASA Standard Breakup Model of $600 - 1,000$ kg. Of the remaining two, one (the European Ariane 1 third stage), has a higher mass, at $1,400$ kg, and the other (the US Pegasus Hydrazine Auxiliary Propulsion System (HAPS) manoeuvring stage) considerably less with only 97 kg. As such both should be expected to require scaling to correctly represent the breakup. However, due to lack of information this was not applied in this investigation.

While not a recent launch, the Pegasus upper stage involved an air-launched rocket body with a much lower mass which would have resulted in it being classified as NewSpace by the classifier developed in Chapter 3. Similar small launchers are expected to become more common with the future development of NewSpace, and the mass and launch method of this upper stage is similar, in particular, to Virgin Orbit's LauncherOne which recently conducted it's first successful mission(Clark, 2021).

4.4.2 Satellite Explosion Events

The scenarios selected for the second mode of event, satellite explosions, were chosen based on recent observed satellite breakups. One of these, the breakup of the Russian Cosmos-2421, also features in the list of top ten breakup events (Anz-Meador, 2016). The other two breakup events were of US Earth observation satellites, the NASA operated NOAA-16 and the U.S. Air Force's Defense Meteorological Satellite Program Flight 13 (DMSP-F13) satellite. The cause of the the Cosmos-2421 breakup remains

[4]ISRO's Polar Satellite Launch Vehicle

uncertain but an explosion is assumed due to the number of fragments generated. The two US satellites are believed to have fragmented as a result of battery explosion due to overcharged battery packs (Foust, 2015). As such, these breakups are interesting examples as they provide a counterpoint to the historic propellant tank explosions.

The launch dates of these satellites are comparable with those of the upper stage scenarios discussed above suggesting that the same technologies and manufacturing processes were available. It is expected that differences in observed breakup patterns would be due to other causes such as the differences in spacecraft structures compared to upper stages or the source of energy for the explosion (i.e. battery based as opposed to propellant based). The masses of these spacecraft is more representative of traditional spacecraft than of the NewSpace trends observed. However, batteries as a cause for explosions have the potential to be a more significant proportion of future explosions due to increasing levels of passivation.

TABLE 4.2: A table of the characteristics of the satellite explosion events used in validation (Sources: (ESA, 2018a; Space-Track, 2018)).

Parent Body	International Designator	Mass(kg)	Maximum Dimension (m)	Number of Fragments		
				Large	Medium	Small
NOAA-16	2000-055A	1403	1	1	3	455
DMSP-F13	1995-015A	815.66	3.7	1	1	238
Cosmos-2421	2006-026A	3150	2	1	10	498

It is noted that as these scenarios were chosen from a list of the largest breakup events this may result in the outputs being biased towards more energetic events.

4.4.3 Collision Events

The scenarios chosen for validating collisions were: the intentional destruction of the Chinese Fengyun-1C in 2007 using a kinetic kill vehicle and the unintentional collision of the Russian Cosmos-2251 and American Iridium-33 satellites in 2009. The characteristics used to simulate each of these breakups are summarised in Table 4.3 below.

Each of the values for fragment counts in this table are the cumulative number of fragments of equal or greater size than the lower limit of the category. While the masses of these spacecraft were not consistent with the NewSpace trends identified, these events were the first catastrophic collision events to occur since the development of the model and so provide insight into the performance of the model in a future, collision dominated, environment.

When simulating these events the Iridium-Cosmos collision was treated as two fragmentation events leading to two distinct debris clouds. For this the ejecta mass for

[5]Some uncertainty exists on the exact characteristics of the Fengyun-1C collision as details of the kinetic kill vehicle used remain classified by the Chinese administration.

TABLE 4.3: A table of the characteristics of the fragmentation events used in validation resulting from collisions (Sources: (Office, 2009; ESA, 2018a; Space-Track, 2018)).

Parent Body	Mass(kg)	Projectile Mass(kg)	Relative Velocity(m/s)	Maximum Dimension (m)	Number of Fragments		
					Large	Medium	Small
Cosmos-2251	900	556	11,570	2	1	29	1668
Iridium-33	556	900	11,570	4	1	24	628
Fengyun-1C[5]	850	600	9,000	2	0	34	3408

each fragmentation was taken to be the mass of the original object, such that the total ejecta mass of the collision was equal to that in Equation 4.4.

4.5 Results from the Model

The NASA Standard Breakup Model was used to simulate each of the breakups identified in Tables 4.1-4.3. The outputs of these simulations were then juxtaposed against observational data and compared to identify if there was any systemic deviation from the model outputs. An analysis was then conducted of the deviations with the expected impact of NewSpace identified in Section 4.3 and used to suggest how future models may differ from the current model.

4.5.1 Fragment Size Distribution

The size distribution of the observed fragments compared to those generated by the model was investigated for scenarios of each of the three identified categories. The output of the fragmentation model was compared to the count of observed fragments above the specific threshold sizes and the coefficients of power laws fitted to these threshold points.

Upper Stage Explosion Events

Figure 4.2 shows the comparison between the results of the simulations and observed fragment populations for the different upper stage rocket body explosions described in Table 4.1. Observed fragment counts were plotted at the lower bound of each size bracket with an error bar illustrating the uncertainty in the sizes of the individual fragments which was inherent in the categorisation of potential fragment sizes. This matches the model which predicts total number of fragments greater than a characteristic length.

By fitting a line to the observed data points for each simulation a value was calculated for the exponent of a power law to be compared with the value of -1.6 used in Equation 4.3. An analysis of these results showed a reasonable level of agreement

between the slopes of the simulation and observed results, but with a consistent under-prediction of the absolute number of fragments generated.

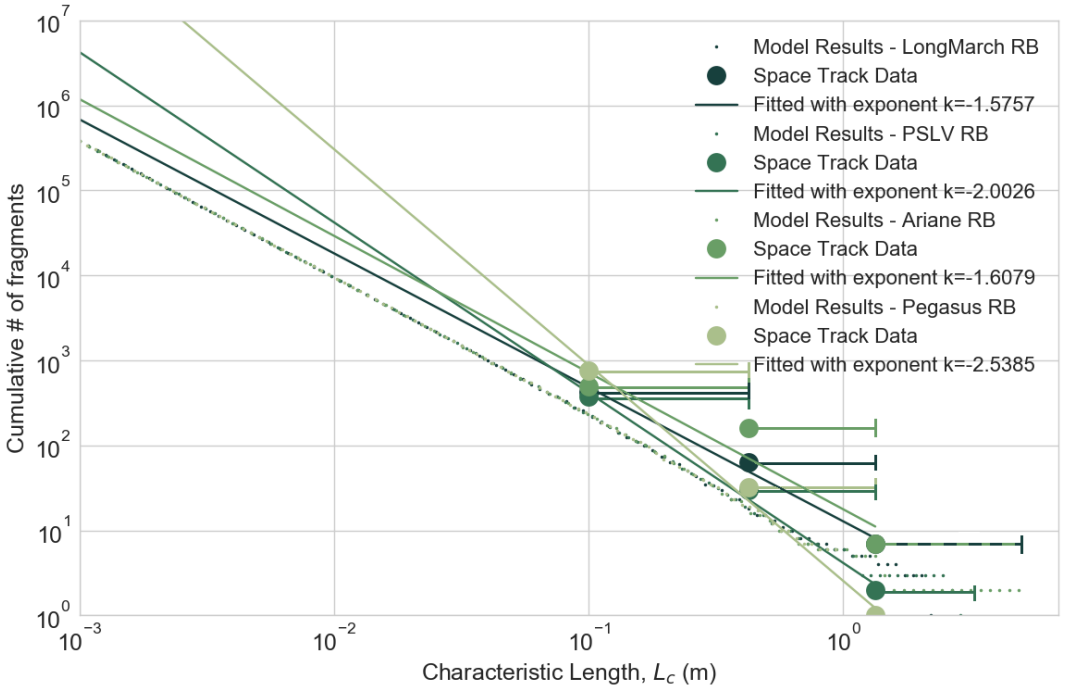

FIGURE 4.2: Graph showing the observed debris fragments created for known rocket body explosions events compared to the fragments generated by the NASA Standard Breakup Model (Diserens et al., 2020b).

The results of this line fitting for the LongMarch and Ariane rocket bodies appear to be consistent with the model, with fitted values of -1.5757 and -1.6079 respectively. The slightly lower mass PSLV rocket body (900 kg as opposed to 1000 kg and 1400 kg) deviated from this value with a fitted exponent of -2.0026. However, the model did not appear to be a good fit for the significantly smaller, 97 kg, Pegasus rocket body and the fitted value deviates noticeably with a value of -2.5385. The results show that the NASA Standard Breakup Model over predicts the number of large fragments produced by the breakup of the small Pegasus upper stage which could be indicative of a systemic error for small upper stage breakups. However, the results for the Pegasus HAPS rocket body will have been impacted by its unique construction which included an outer layer of Carbon fibre reinforced polymer (CFRP). When the rocket body exploded it is likely that these carbon layers will have de-laminated into many thin sheets. As these would be excellent radar reflectors this would result in an artificial increase in the apparent size of the fragments produced.

Applying a scaling factor to these results could correct the number of large fragments predicted but result in an under-prediction of the number of small fragments which indicates that a change in the exponent of Equation 4.3 is required. Figure 4.3 shows the correlation between the fitted values of the exponent and the original mass of the objects. A linearly fitted trendline was a good fit to the data points, with an R^2 value

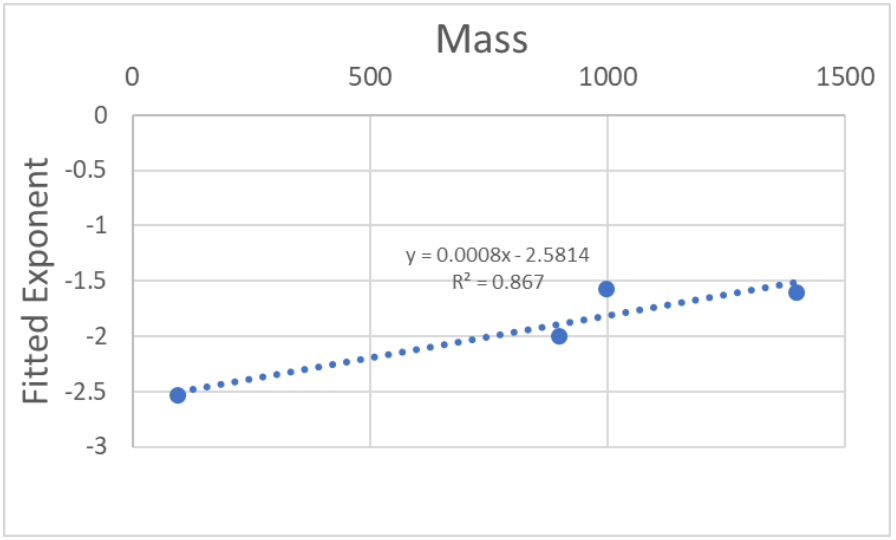

FIGURE 4.3: Graph showing the correlation between fitted exponent and object mass for rocket body explosions events.

of 0.867 and Calculating the the Pearson Correlation Coefficient (PCC) for these results gave a value of 0.931115 indicating a strong correlation[6]. This correlation suggests that there is a relationship between the size distribution of fragments and initial mass of the fragmenting spacecraft which is not accounted for in the current model.

Satellite Explosion Events

The category of satellite explosions is addressed in Figure 4.4 for the different explosions identified in Table 4.2. As with the rocket body explosions, the results of the NASA Standard Breakup Model were plotted against the numbers of observed fragments and a line fit was used to compare against Equation 4.3.

A comparison of the exponent used in the model (-1.6) to the fitted coefficient for the power law supports this analysis with values of -2.4061, -2.1802 and -2.4068 respectively for each of NOAA-16, DMSP-F13 and Cosmos-2421. These fitted trend lines suggest that the model is not a good fit for these breakup events where the fitted values for the exponent indicate that it over-predicted the number of large fragments generated with length greater than 30 cm, and under-predicted the number of small fragments with lengths less than 5 cm.

In contrast to the previous results the relationship between the mass of the spacecraft and the exponent of the fitted line, shown in Figure 4.5, was weaker with an R^2 for the linear fitted trendline of 0.4852 and a PCC of -0.69654. The results do, however, suggest that alternative parameters might be needed when modelling the breakup of satellites. This indicates that while the current breakup model may provide good

[6]Values of the PCC range from $+1$ for the strongest positive correlation to -1 for the strongest negative correlation. Correlations are normally considered to be strong for values of $r > 07$(Overholser and Sowinski, 2008).

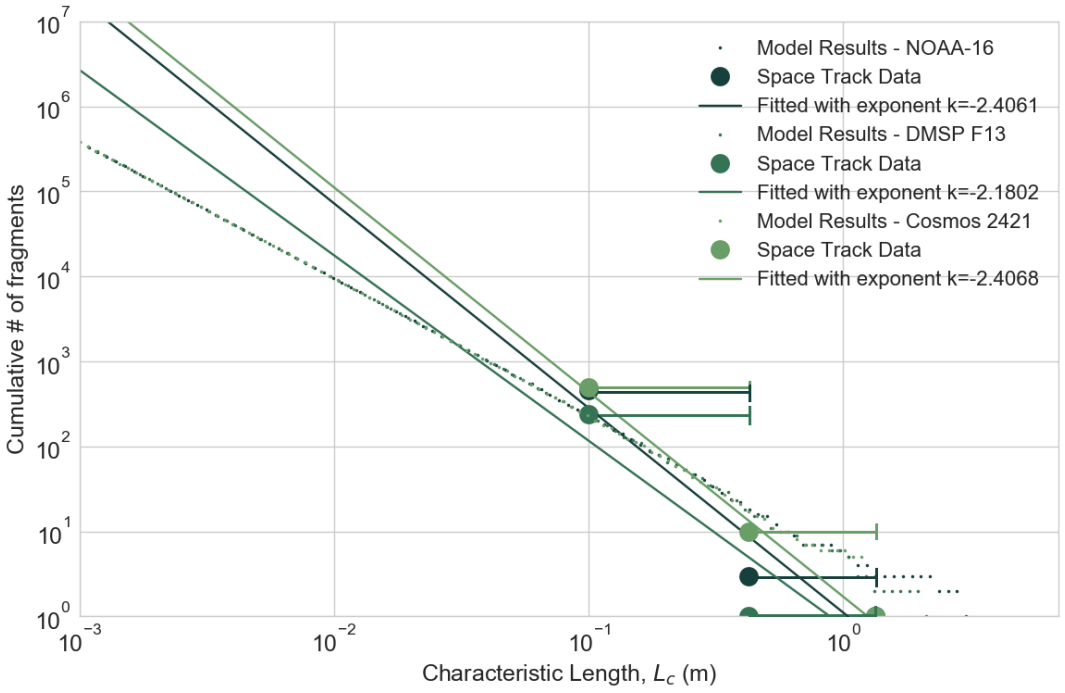

FIGURE 4.4: Graph showing the observed debris fragments created for known satellite explosions events compared to the fragments generated by the NASA Standard Breakup Model (Diserens et al., 2020b).

results for the breakup of large rocket bodies it may currently be less suitable for simulating the breakup of satellites. This may be due to the different characteristics of the objects, including differences in material and structure as well as potentially different sources of energy for the explosion, e.g. battery based as opposed to propellant based.

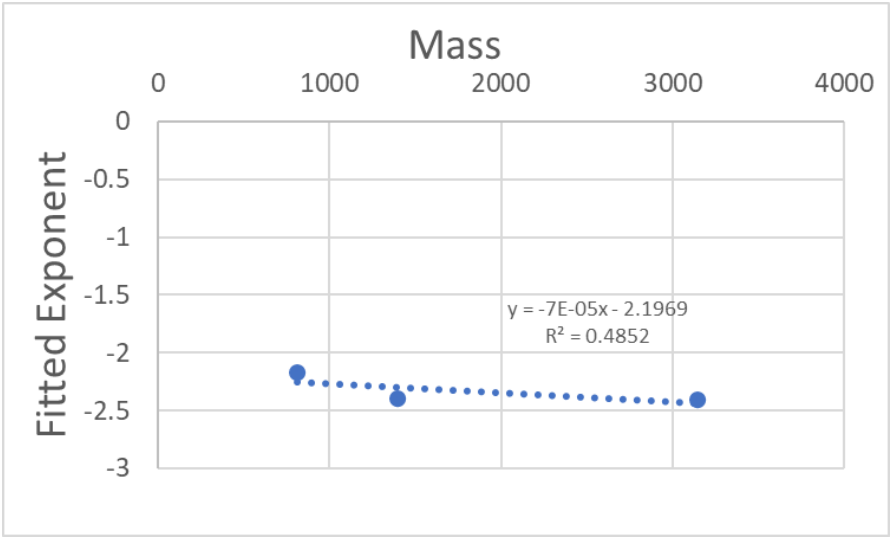

FIGURE 4.5: Graph showing the correlation between fitted exponent and object mass for satellite explosions events.

Collision Events

The results from the final set of test cases, for the breakups of satellites listed in Table 4.3 due to catastrophic collisions, can be seen in Figure 4.6. Across all three cases more fragments are observed than the simulation predicts for the small size band, and fewer for the largest size band. Fitting trend lines to these data points in log-space gives values for the gradients of -2.8572, -2.4736 and -3.1372 respectively for Cosmos-2251, Iridium-33 and Fengyun-1C compared to the value of -1.71 used in the model. The higher than expected values for the exponent are consistent with the results seen for the explosive breakup of satellites.

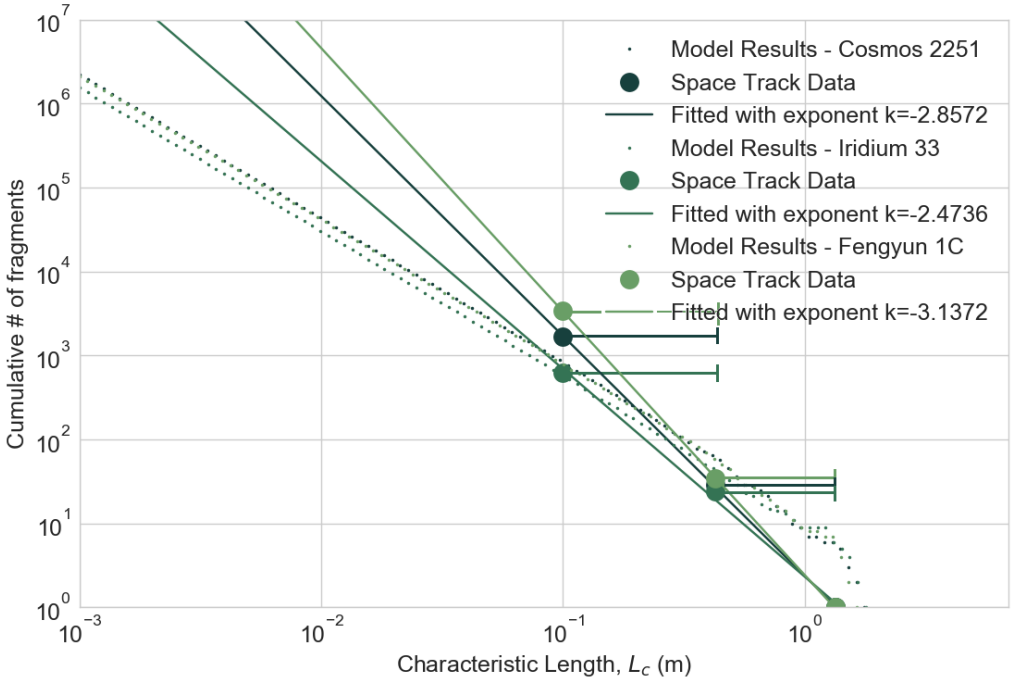

FIGURE 4.6: Graph showing the observed debris fragments created for known collision events compared to the fragments generated by the NASA Standard Breakup Model (Diserens et al., 2020b).

Averaging these three values gives a potential gradient of -2.8227 which, if used in the model, would provide a considerable difference in the size distribution of number of fragments. Using the example of the breakup of a 1,000 kg spacecraft. The model would currently generate 46,773 fragments larger than 1 cm in length. However the averaged value above used as the exponent the model would generate 7,859,591 fragments above 1 cm, a 168-fold increase. This suggests that the current model may be underestimating the number of fragments in the one to ten centimetre range by several orders of magnitude. This has significant impacts for the long term evolution of the debris population.

4.5.2 Mass Assignment

In addition to studying the distribution of fragment sizes, an analysis was also conducted into how the mass of the parent object is distributed across the fragments generated by the model. Figure 4.7 looks at how the distribution of the densities of fragments generated by the model vary with increasing fragment size compared to some examples densities for different materials. These density values are based on the assumption of spherical objects and so reflect the minimum density for the assigned area-to-mass ratio. This may be a reasonable approximation for the smallest objects, however larger objects are likely to have more complex geometries including a mix of materials and some empty space. As a result the densities of the larger objects are expected to be lower than those of the smaller objects and this is reflected in the results in Figure 4.7 for larger characteristic lengths.

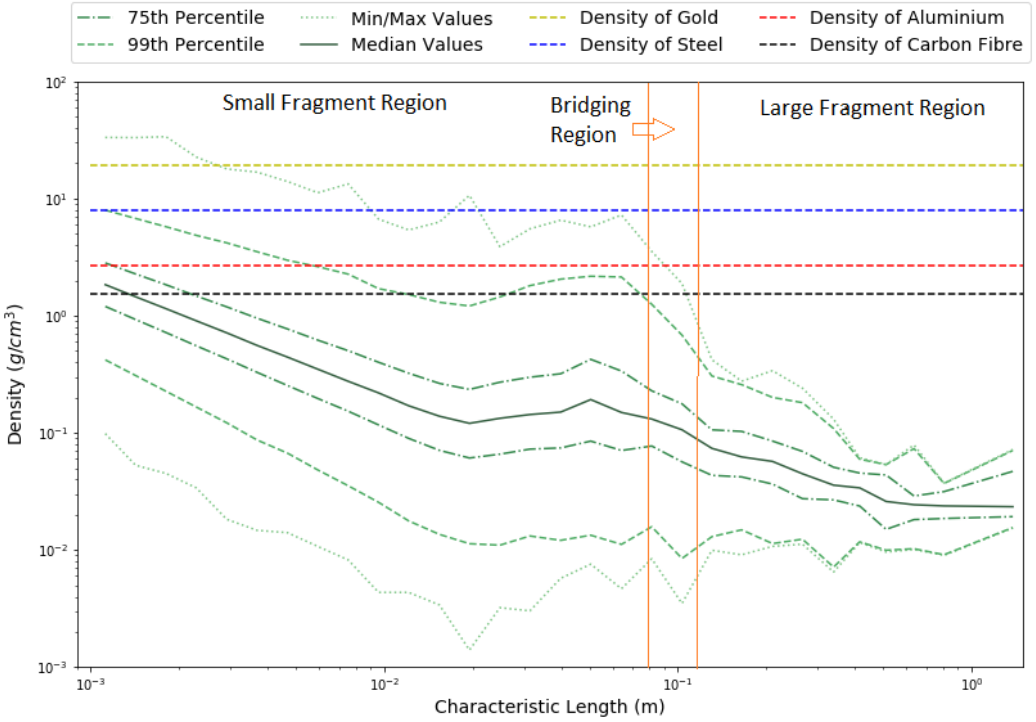

FIGURE 4.7: A graph showing the densities of fragments of different characteristic lengths for a catastrophic collision.

Some of the densities predicted for fragments around 3 mm in diameter and smaller, appeared to be unrealistically high. For spherical fragments the maximum densities were predicted to be as high as $40\,g/cm^3$. For perspective this can be compared to the density of the heaviest naturally occurring element, Osmium, which is $22.59\,g/cm^3$. This suggests that these fragments are too massive and that mass should potentially be limited when generating fragments across the small size regime. This might increase the mass that would need to be included in larger fragments for conservation of mass.

4.5.3 Comparison to Expectations

Analysis of the algorithm used in the NASA Standard Breakup Model identified several sections of the model which might not be robust to the changes in the spacecraft population including those brought about by NewSpace such as the increase in the diversity of the physical characteristics. In particular, the trend towards smaller, lighter spacecraft in LEO and larger, more massive, spacecraft in GEO (as well as changes in area-to-mass ratios) are indicative of changes in spacecraft design and manufacturing. The hypothesis was that the changes observed in the distributions of physical characteristics might result in differences in the distribution of fragments by size and the concentration of mass in different sized fragments, which would not be adequately captured by the model.

The results generated in this investigation provide some evidence in support of this hypothesis. Comparing against data on the observed breakup of rocket-bodies there appeared to be a good fit for the fragments generated by the explosion of large rocket bodies above the traditional $1,000$ kg. However, the fit became noticeably worse for objects with lower masses. This implies that any substantial change in what can be considered an average upper stage will result in changes to the average distribution of fragments for an explosion and so require updates to the model.

When simulating the explosions of satellites, the model again appears to consistently over-estimate the number of large fragments generated by the breakup. Differences in the gradient of fitted power laws to the model were greatest for the most recently launched spacecraft. These results support the theory that changes to the design and construction of spacecraft will have had a considerable impact on the fragments resulting from a breakup. If this theory is correct, then changes will be required to future models to take it into account. Further work, without the limits on the available data, might be able to provide more definitive evidence and investigate if the results are consistent for a greater number of scenarios.

Of particular interest was the performance of the model for simulating collisions, which are expected to be the major source of new debris in the future environment. Comparisons of the observed numbers of fragments for three collision events against the results generated by the model suggested an under-estimation in the numbers of small fragments with characteristic lengths less than 10 cm and showed an over-estimation in the number of fragments with lengths greater than 1 m. The consistent deviation across all three scenarios suggests that the current collision fragmentation model, and the historical and ground based breakups it is based on, is not representative of recent or future collision breakups.

Due to the limited amount and precision of the available observational data and as a result the small number of cases which could be considered it was not possible to make a definitive assessment of the accuracy of the NASA Standard Breakup Model,

either in general or in the specific case of NewSpace. However, the results indicate that, for the cases investigated, the output of the model deviated from observational data for spacecraft with characteristics different to traditional assumptions. This supports the second hypothesis of the project, that ”NewSpace changes fall outside of the scope of current assumptions, reducing the accuracy of the existing component models of debris processes”.

Based on the lines fitted to the observed fragment numbers it appears that significantly more small fragments could be produced with characteristic lengths below 10 cm than predicted by the model for collisions and spacecraft explosions. However, observational data on the number of small debris fragments produced is severely limited resulting in some uncertainty in the numbers. As a result it is not possible to conclusively state whether the fitted power laws can be extended beyond this point. However, the limitations on fragment tracking mean that the uncertainty is likely to be greater for the smallest size category, resulting in it being likely that there are more un-tracked fragments at the smaller end of the scale than for the larger. The consequence of this would be to exaggerate the deviation between predicted and observed fragments and so, on balance, the uncertainty in the fragment sizes does not alter the conclusions formed.

The implications of this are that while the NASA Standard Breakup Model remains a useful tool for modelling fragmentations (as the results suggest that the model provides a good representation of the breakup of traditional spacecraft) some modifications or extensions to the original model would enable it to better handle the changes seen with NewSpace. Based on the results produced, and the identified changes in physical characteristics, a greater dependence on the mass and area-to-mass ratio are indicated when generating fragment distributions.

4.6 Impact on the Evolution of the Space Debris Environment

The previous section has investigated the validity of the second hypothesis when applied specifically to models of object fragmentation. Simulations conducted using an implementation of the NASA Standard Breakup Model highlighted issues which may impact the simulation of the future debris environment. The simulations of the breakup of large upper stages, which have traditionally been the dominant source of new fragments, showed good agreement with observed results for the size distribution of fragments. However, the analysis of the NewSpace environment conducted in Chapter 3, indicate that a wider range of events, including battery based explosions and, in particular, collisions, will be important for the future debris environment.

Based on the results of this investigation it was concluded that the current model provides a good approximation of the average breakup of historic spacecraft.

However, the model is not well suited to describing the outcome of a specific breakup event, particularly when the characteristics of the object fall outside the traditional range. This could be problematic when looking to study specifically NewSpace cases, including the impact of NewSpace breakups, for instance the breakups of CubeSats or constellation spacecraft.

The results of the review of published simulation results conducted by Beck (2013) highlight the sensitivity of environmental models to the choice of fragmentation model. One consequence is that current simulations might fail to accurately reflect a real world future environment where collisions become the dominant source of new debris. The results indicate a potential shift towards fewer large fragments and many more small fragments being produced.

While this shift may represent more overall fragments being generated in the initial event it might result in lower debris growth over the long term evolution of the environment. Fewer large fragments will result in fewer high mass collisions and so fewer secondary debris fragments being generated in the future. At the same time smaller objects tend to have a higher area-to-mass ratio and so be shorter lived due to the increased effect of aerodynamic drag.

However, 1 cm objects can still be fatal in the event of a collision and the presence of more and harder to track objects is likely to result in a greater rate of collisions. This would represent a significant impact to the ongoing space safety and also the sustainability of the space debris environment with these collisions disabling even a large spacecraft, resulting in more derelicts and reducing the opportunity to avoid future collisions. The expectation would be of an increased risk to individual spacecraft missions and a higher number of anomalous events and disruption to spacecraft services.

Overall, based on these results, it is expected that NewSpace trends are contributing to changes to the number and size of debris fragments generated by breakup events. This could lead to meaningful differences between the future environment and the results of current models, due to a greater number low mass collisions with less secondary debris generation. With a potential increase in the risk of collisions it becomes even more important to assess the impact of NewSpace trends on the performance of the models used to predict collisions within simulations of the environment. As such further development of fragmentation models is required for them to be used in meaningfully assessing the possible future evolution of the debris environment.

Chapter 5

Predicting Collision Events

> If you wish to avoid foreign collision, you had better abandon the ocean.
>
> Henry Clay

5.1 A Review of Current Collision Algorithms

Collisions between orbiting objects have been identified as one of the major sources of future space debris and the calculation of collision probabilities is one of the key components of debris models. The analysis conducted in Chapter 3 revealed trends associated with the rise of NewSpace each with the potential to change collision rates. In particular, an increase in the spatial structure of spacecraft in orbit was expected to have implications for the performance of current collision algorithms.

A review of the different evolutionary debris models identified variants of two particular collision algorithms as being the most commonly implemented. The first and most widely used is the Cube approach developed by NASA for LEGEND (Liou et al., 2003). A probabilistic method based on the discretisation of space which has also been implemented in DAMAGE (in a modified form), MEDEE, SDM, LUCA and SOLEM (in a modified form) (Lewis et al., 2001; Liou et al., 2004; Rossi et al., 2009; Dolado-Perez et al., 2013; Radtke et al., 2017b; Wang and Liu, 2019). The second commonly used method, known as Orbit Trace, has been implemented in various forms in SDM, LUCA and ADEPT and is a probabilistic method based on identifying the intersections of different orbits (Rossi et al., 2009; Jenkin et al., 2015; Radtke et al., 2017b). An alternate method is implemented in ESA's MASTER and Debris Risk Assessment and Mitigation Analysis (DRAMA) models using the work of Alfriend et al. (1999) where the positional uncertainties of the two objects are treated as

uncorrelated Gaussian distributions to form a common combined covariance matrix (Klinkrad, 2006; Krag et al., 2016).

5.1.1 Sources of Collision Data

When developing models, such as these collision algorithms, a source of truth is required for validation in the form of the expected results for a given scenario. In the case of the empirical fragmentation model in Chapter 4 the model was both developed and validated using observational data about historic breakups. However, for collision algorithms the amount of absolute data is much smaller as relatively few collisions have been observed and so the frequency of collisions must be estimated based on the rate at which objects experience close encounters. As a result mechanistic models have been developed based on the physics of orbital motion to make a prediction of the expected collision rate of a pair of objects and hence the probability of collision in a given time frame.

The lack of available data is problematic when attempting to test the models, as the available observational data on tracked objects does not enable a definitive collision rate or collision probability to be calculated which could be used to validate the output of these models empirically. An alternative approach for this validation is to compare the output of a model against the results of another method, ideally one based on different principles. For example, the probabilistic collision algorithms used in evolutionary debris models could be compared with the shorter-term, more deterministic, models used to report on the risk of collision between current objects. One such set of results which might be used for comparison are those provided by Center for Space Standards & Innovation (CSSI)'s Satellite Orbital Conjunction Reports Assessing Threatening Encounters in Space (SOCRATES) service (Kelso and Alfano, 2006), which provides updates three times per day on the predicted collision risk between tracked objects for the following seven days.

Estimating whether a collision will occur or not requires an understanding of the position and velocity of a pair objects, even if inexact. When comparing with collision prediction models such as SOCRATES it is important to use a comparable set of assumptions about the original state of an object population. A key source of information on the state vectors of different objects in orbit is the Space-Track's 'SatCat database' (Space-Track, 2018) maintained by USSPACECOM. This provides information on the estimated orbital elements of the catalogue of tracked objects in orbit at different times using the Two-Line Element set (TLE) format (Space-Track, 2020).

SOCRATES

The SOCRATES service has been mentioned as a possible source of collision data for comparison with the algorithms used in evolutionary debris models. The service uses the latest published TLEs to provide seven-day reports of forecast conjunction events consisting of the close approaches between any payload spacecraft and all other objects in the tracked catalogue.

The SOCRATES methodology utilises the STK conjunction analysis tool (STK, 2020) with the SGP4 propagator to analyse the expected motion of the tracked population of objects and identify all close approaches with a miss distance of less than 5 km (Kelso, 2020). The minimum distance between the objects is then reported along with a calculated prediction of the collision probability and the time of closest approach. The collision probability reported is calculated using a specific maximum probability method (Alfano, 2004) to avoid under-estimating the true collision risk due to uncertainty in the object position.

The calculation of the maximum collision probability in SOCRATES is based, where possible, on a database of the hard-body radii of historic objects, however when data is not available the model reverts to the STK default of a one metre hard-body radius.

5.2 Investigating the Algorithms

The Orbit Trace and Cube collision algorithms are widely used across the debris modelling community, having been adopted from models of the wider solar system. However, the commonality of approach, combined with the lack of observational data, means that there has been very little opportunity to confirm the validity of these approaches. Additionally, as the Cube approach was originally developed and verified using the results from the Orbit Trace approach, agreement between the two approaches is expected. The two algorithms were investigated to understand how they work and what limitations they have as a result of any assumptions made.

5.2.1 The Cube Approach

As it provides a fast, scalable method for identifying collisions within long-term evolutionary models, the Cube algorithm has become one of the most commonly used approaches for identifying potential collisions in space debris evolutionary models. One of the issues with applying collision algorithms to large populations of objects is the number of pairs which must be checked for possible collisions. The Cube method avoids this by sub-dividing near-Earth space into an array of cubes and identifying which objects are co-located when the positions of every object are sampled at

different points in time. This allows the computation to be reduced from an operation with $O(N^2)$ complexity to one with $O(N)$.

At each time-step the instantaneous positions of every object are calculated. When calculating the collision rate at each step a collision between two objects is only considered possible if the sampled positions of the objects show them to be located within the same cube. Across many samples this provides a Monte-Carlo estimate of the encounter rate of a pair of objects. The overall probability of a collision between a pair of objects is then represented by the probability that they appear within the same cube combined with the probability that they collide when co-located.

The total number of collisions N_{tot} between a pair of objects i and j is estimated by sampling the collision rate, $P_{i,j}$, uniformly across the simulation projection period. Long term perturbations on the orbits are considered as small instantaneous changes, at each time-step, removing the need to integrate the collision rate. This results in the simplification in Equation 5.1 where N_{tot} becomes the integral over all of the time-steps of the collision rate at each step, multiplied by the length of the time-step.

$$N_{tot} = \int_{t_{begin}}^{t_{end}} P_{i,j}(t)dt \; = \; \sum_{s=0}^{s=L} \int_{t_s}^{t_{s+1}} P_{i,j}(t)dt \tag{5.1}$$

The use of a sufficiently short time-step between samples allows the assumption of a constant collision rate across the time-step, resulting in Equation 5.2:

$$N_c = \sum_{s=0}^{s=L} [t_{s+1} - t_s] P_{i,j}(s) \tag{5.2}$$

where $P_{i,j}(s)$ is the collision rate at step s and L is the number of time-steps between t_{begin} and t_{end}. The total collision count is then the sum of the collision rate at each time-step.

The collision rate within a cube is calculated for the conjunction of any pair of co-located objects by applying the kinetic theory of gas on the scale of the cube, as seen in Equation 5.3:

$$P_{i,j} = S_i \, S_j \, V_{rel} \, \sigma \, dU \tag{5.3}$$

where S_i and S_j are the spatial densities in the cube of objects i and j respectively which are equivalent to $\frac{1}{dU}$ the reciprocal of the volume of the cube used. V_{rel} is the relative velocity between the two, $\sigma = \pi(r_i + r_j)^2$ is the collision cross-sectional area and dU is the volume of the cube.

One of the key parameters of the model is the cube size used, which should relate to the short-period perturbations acting on the objects. The original published work on the model identified a cube size of 1% or less of the average semi-major axis of the objects in a system as being be small enough to capture the true collision nature of the

system. For simulations of the space debris environment a cube with side length of 10 km is normally used, roughly 0.15% of the semi-major axis of the lowest objects in LEO.

Within evolutionary debris models the mean anomalies of the objects are sampled from a uniform random distribution to generate a position for each object. This allows the identification of co-located objects and the generation of a set of potential collisions at each time-step of the simulation. The collision rate within a cube is calculated for each pair of co-located objects and used to determine whether a collision occurs by comparing the result to randomly generated number drawn from a uniform distribution.

Assumptions and Limitations

While the Cube method is a fast and scalable method for assessing collision probabilities it relies on certain assumptions. These must be made for practicality when implementing the model but introduce limitations which must be considered.

The predominant limitation arises from sampling through time. As possible collisions are only identified between objects which are co-located at a specific instant in time, the model does not capture all of the possible interactions but only a small sub-set. Consequently, thousands of samples are required to provide a good estimate of the overall collision rate. Rather than representing the true collision probability for every object at every time the model relies on a regression to the mean collision probability across all samples of the objects.

This is an acceptable compromise when the model is used as originally intended, i.e. for large sets of objects over a long simulation period with many samples and averaging the results across a large number of Monte Carlo runs of the simulation. However, when looking at small sub-sets of the population or when using shorter simulation periods a greater number of runs or a greater sampling rate will be required to ensure convergence of the collision probability.

Assumptions are also made about the independence of the motion of different objects. When the instantaneous sample of position is taken at each time-step these positions are normally determined by randomly generating mean anomalies for each object. However, while for the majority of objects the difference in their mean anomalies varies rapidly there are pairs of objects where this is not the case which impacts the validity of this random sampling. For instance, for spacecraft flying in formation (such as constellation satellites) the difference in their mean anomalies will be largely fixed, or vary in a controlled manner to prevent conjunction of the spacecraft. This means that the model can predict collisions which are not possible due to the configurations of the orbits. This is exacerbated by the fact that these objects are often in very similar orbits to one another and so will potentially have a much greater encounter rate.

The calculations of the probability of collision within a cube, which relies on an application of the kinetic theory of gases, is another issue. The assumption is made that each object could be found anywhere within the cube. Within the Cube model this is explained by the uncertainty in the instantaneous positions of any orbiting object due to the variability of the short-term perturbations they experience. However, while these perturbations exist, their magnitude varies between different orbital regions and with the eccentricity and inclination of the orbit. As a result, a cube size which represents the variability in position for one orbit will not necessarily be appropriate for another. Consequently, the accuracy of the model might vary between different altitudes and so cause a bias in where collisions are predicted in simulations of the environment. In particular this may be an issue when modelling constellations as the orbits of many objects may be of the same size and have fixed eccentricities and arguments of perigee and so spacecraft might be located very close together but nevertheless have no opportunities to collide.

An additional complication exists due to the choice of cube-size being used. A smaller cube size reduces the number of instances of co-located objects, meaning a greater number of samples must be taken to accurately represent the collision rate. However, while a larger cube increases the frequency of objects being co-located it also increases the risk of false positives for collisions. For example, where objects can fall within the same cube but are not capable of colliding, such as objects in orbits at different altitudes without any overlap. As a result the selection of cube-size is a compromise between being able to generate enough co-located samples while not exceeding a realistic level of variability in the possible object positions. Further investigation into the impact of varying the cube size on the convergence rate and the resulting collision probability can be found later in this chapter.

Implementation Challenges and Verification

The implementation of the Cube algorithm provided several challenges to reaching the optimal efficiency of $O(N)$. The principle barrier was the efficient identification of objects co-located within the same cube. Each object was assigned a 3-integer identifier (i, j, k) corresponding to the cube occupied by the object at the specified mean anomaly. This created a set of N cube IDs which were passed through a hashing function and placed in an ordered list. This list could then be scanned in $O(N)$ time to identify which objects had the same hashed ID, identifying that they occupied the same cube.

The hashing function implemented, shown in Equation 5.4, was a simple XOR as described in Teschner et al. (2003).

$$hashID(i, j, k) = (i * p1 \bigoplus j * p2 \bigoplus k * p3) \ \boldsymbol{mod}\ n \tag{5.4}$$

Where $p1$, $p2$, $p3$ are the large primes 73856093, 19349663, and 83492791. For the hash table size, n, a value of $1,000,000,000$ was chosen as being sufficiently large to minimise the number of hash clashes. Nevertheless, during testing of the implementation, hash-clashes were identified which caused the algorithm to report false object conjunctions, raising the output collision rates. To resolve this clash an additional check was performed on the un-hashed cube ID for all identified object pairs, to ensure they were located in the same cube.

Further investigation into this field suggests that alternative hashing functions such as Space Filling Curves (SFC) or Density Coordinate based (DECO) hashing may provide a more suitable alternative to this approach by removing the risk of clashes (Buckley et al., 2018). However, due to the relatively low number of co-locations identified at any one step this issue was resolved with a simple test of the un-hashed cube IDs of any duplicates to confirm that they were co-located.

This implementation of the model was then verified by testing against the results reported by Liou et al. (2003) for collisions between a set of Jovian moons and for objects in the asteroid belt. The results generated by this implementation can be seen in Appendix B and showed agreement with published results with errors of 2% and 4.2% for the Jovian moon and asteroid cases respectively. However, billions of samples were required to generate a significant number of conjunctions to allow the generated collision probabilities to converge for individual collision pairs. As a result further, testing was conducted into the rate of convergence for the Cube algorithm.

5.2.2 The Orbit-Trace Algorithm

The Orbit Trace algorithm was originally developed for investigating potential collisions between asteroids and other celestial bodies (Öpik, 1951; Wetherill, 1967; Kessler, 1981; Greenberg, 1982). The Minimum Orbit Intersection Distance (MOID) for the orbits of each pair of objects is calculated and a collision probability is generated based on the proportion of time each object spends in the region around the intersections of the orbits.

In contrast to the Cube method this requires processing for every pair of objects at every time-step. This has the advantage of ensuring that all possible collisions are examined at each step, but results in $O(N^2)$ complexity. To reduce the computational burden pre-filters, similar to those used in the analytical collision approach described by Hoots et al. (1984), can be applied to reduce the number of pairs which must be fully considered. The major example of this is the perigee-apogee filter which identifies orbits which do not overlap, and so cannot collide, using only a few simple operations.

A collision is identified as being possible for a pair of objects where the MOID is less than the combined hard-body radius of the two objects. Historically the collision

probability has been calculated for these cases in a number of different ways. For this investigation, collision probabilities were calculated using the method described by JeongAhn and Malhotra (2017, Equation (13)) for each qualifying close approach point between the two orbits:

$$P_{i,j}(t) = \frac{\pi\tau V_{rel}}{2|\nu_i \times \nu_j|T_{u,i}T_{u,j}} \tag{5.5}$$

where $\tau = (r_i + r_j)$ and r_i and r_j are the hard body radii of the two objects, V_{rel} is their relative velocity as a scalar, ν_i and ν_j are the velocity vectors of the objects, and $T_{u,i}$ and $T_{u,j}$ are their orbital periods.

In the LUCA model developed by the Technical University of Braunschweig (Radtke et al., 2013, 2017b) the Orbit Trace algorithm has been implemented with an additional set of filters which can be used to reduce false positives for synchronised objects, such as those in constellations. These include:

- A coplanar filter which identifies objects where the maximum separation between the orbital planes is less than the combined collision radius of the objects, ρ:

$$\alpha_{limit} = 2 \cdot arcsin(\frac{\tau/2}{\bar{a}}) \tag{5.6}$$

  where α_{limit} is the maximum angle between planes considered to be coplanar, τ is the combined hard-body radius and $\bar{a}$ is the mean semi-major axis, $\frac{a_1 - a_2}{2}$.

- A head-on filter is used to determine if head-on collisions are possible between objects on coplanar orbits. Head on collisions are identified as possible if either:

  - both orbits are (near) circular, i.e. eccentricity is less than ϵ_{limit} where:

$$\epsilon_{limit} = \frac{a + \tau}{a} - 1 = \frac{\tau}{a} \tag{5.7}$$

  - or, both orbits are eccentric but have arguments of perigees within one degree, $\Delta\omega \leq 1^\circ$, where:

$$\Delta\omega = |180 - \omega_1 - \omega_2| \leq 1^\circ \tag{5.8}$$

- If the orbits are not head-on then a synchronisation filter determines if the motions of the two objects are synchronised. This is done by investigating the drift in the relative positions of the two objects, ΔM, over a period of time, δt, where Δn is the difference in the mean motions of the two objects:

$$\Delta M_{year} = |\Delta n| \cdot \delta t \tag{5.9}$$

  If $\Delta M_{year} \geq 360^\circ$ then the objects are not synchronised and collision probability is calculated as normal, but if not then the proximity filter must be applied.

- The proximity filter determines if the objects approach their intersection at the same time:

$$\Delta M_{linear} < d_{max} \tag{5.10}$$

where d_{max} is the maximum possible separation for a collision and:

$$\Delta M_{linear} = \Delta M_{Angle} \cdot \overline{a} \Delta M_{Angle} = |\Delta M_2 - \Delta M_1| \tag{5.11}$$

and where:

$$\Delta M_1 = |M_{1,i} - M_{1,t_0}| \Delta M_2 = |M_{2,i} - M_{2,t_0}| \tag{5.12}$$

The Orbit Trace algorithm, particularly with the addition of the LUCA filters, provides an interesting counter-point for investigation. While it can be used in much the same manner as the Cube approach, allowing them to be easily interchanged, it avoids some of the limitations identified with the Cube approach. Advantages include a robustness to the synchronicity of object's orbits, as well as the consideration of the collision probability of each pair of objects across the intervals between each step. As such it may provide a better means for investigating the probability of NewSpace systems being involved in a collision.

Assumptions and Limitations

While there are advantages to the use of the Orbit Trace algorithm over the Cube approach, these are also additional limitations associated with this method. By directly comparing the orbits of each object with every other, the sampling issues that exist for the Cube method are avoided, but the complexity increases to $O(N^2)$. The application of pre-filters can speed up the algorithm by truncating the processing chain for some objects, but processing is still required for each individual object pair. The impact of this mitigation can be somewhat mitigated by parallelising sections of the algorithm, however the improvement gained in this way is limited by the available hardware.

Consequently the Orbit Trace algorithm scales much more poorly with population size than the Cube method and can be significantly slower for simulations of large population sets. This runtime issue can become a limiting factor for the use of the algorithm, particularly when incorporating the large number of additional objects generated by fragmentation events. Consequently, either a greater runtime must be accepted, increased computational power is required, or compromises must be made regarding the number of objects modelled in the simulation (and hence the minimum size of objects in the model).

The Orbit Trace algorithm, as described above, also makes the assumption that each object is following a perfect Keplerian orbit for the duration of each step. The algorithm identifies a collision only when the described orbits of two objects approach

to within their combined hard-body radius. As a result the model does not produce collision probabilities for close encounters of objects which do not overlap, and so accounts for uncertainty in the position of the object along the track of its orbit but not radially or across track. This contrasts with the cube which, by design, accepts that exact object positions would vary around the base orbit. This assumption might lead the algorithm to fail to identify possible collisions and so underestimate the collision rate.

Implementation Challenges and Verification

When implementing the Orbit Trace algorithm a key consideration was optimisation, so that runtime would remain at a usable level despite the $O(N^2)$ scaling. One of the most computationally expensive steps is the calculation of the MOID between two orbits. Several algorithms were implemented and investigated to determine which would allow the model to run fastest.

The three different MOID algorithms compared were: an implementation of the Newton's method approach described by Hoots et al. (1984, Equations 19-23) for a geometric filter; the C++ code for the 'distlink' implementation (Baluev and Mikryukov, 2018) of the algorithm described by Baluev and Mikryukov (2019) for solving an algebraic 16th order polynomial describing the stationary points of the distance function; and the C++ code for the MOID algorithm from the Project Pluto astronomical software library (Gray, 2018) which uses a similar approach to that described by Hedo et al. (2018).

Of the three options the Newton implementation was originally favoured as faster, however issues were discovered with the ability of the algorithm to converge on local minima for pairs of objects with more eccentric orbits. The consequence was that the code would fail to identify the second of a pair of close approaches (e.g. on the opposing side of the orbit) which fell within the threshold distance for a collision. As a result the 'distlink' solution (modified to return both intersection points of the orbits) was found to be the most suitable for this implementation of Orbit Trace. Some alterations to the original code were required in order to store and return secondary close approach distances in addition to the primary MOID.

To gain additional speed increases large scale parallelism was investigated using the large number of cores on a current generation GPU to run the algorithm for multiple object pairs simultaneously. This was achieved by using the Thrust C++ template library for NVIDIA's CUDA. While this increased the overheads around the algorithm and so resulted in slower run-times for small populations it successfully achieved speed-ups of up to ten times for large population sets (see below section on performance testing).

It was found during the verification process that, due to the requirement for objects to have a minimum separation less than their combined hard-body radius, it was often problematic to generate a statistically significant sample of conjunctions for small populations. A solution to this issue was implemented as proposed by JeongAhn and Malhotra (2015, 2017) where collision probabilities were calculated for all close approaches with a MOID less than an enhanced collision threshold, τ'. The probabilities are then subject to a correction factor $C = (\frac{\tau}{\tau'})^2$ to account for the linear increases seen for both collision probability and number of conjunctions with increasing τ.

As with the implementation of the Cube algorithm this implementation of Orbit-Trace was then verified by testing against the two collision scenarios of Jovian moons and of objects in the asteroid belt. The results generated by this implementation showed strong agreement with published results (Wetherill, 1967; Kessler, 1981; Greenberg, 1982; Bottke and Greenberg, 1993) with average errors of 1.37% and 5.66% for the Jovian moon and asteroid cases respectively. Further details of the process can be found in Appendix B.

5.2.3 Comparison and Testing

Once the implementations of the Cube and Orbit Trace algorithms had been verified the models were used to conduct additional testing to better understand the relative limitations of the models. A key element of this was to test the performance of the two models to asses their utility for different sizes of population. This testing investigated the effect of sampling on the convergence rate of reported collision probabilities, as well as runtime scalability for increasing population size.

The cube size was identified as having the potential to significantly impact the output of the Cube model. As such, an additional investigation was carried out into the sensitivity of the Cube method to the choice of cube size.

Convergence Testing

Initial testing of the Cube Approach during the verification process highlighted that the rate of convergence of the collision rate is slow for individual collision pairs. Figure 5.1 shows the convergence of the average collision rates for the Jovian moons verification scenario (Kessler, 1981; Liou et al., 2003) over 365 billion samples (organised as $1,000,000$ evaluation sets each averaged over $36,500$ samples). After $200,000$ evaluation sets of 36500 days (the first grid-line corresponding to 7.3 billion applications of the algorithm) a variation still exists of up to 5% of the final collision rates.

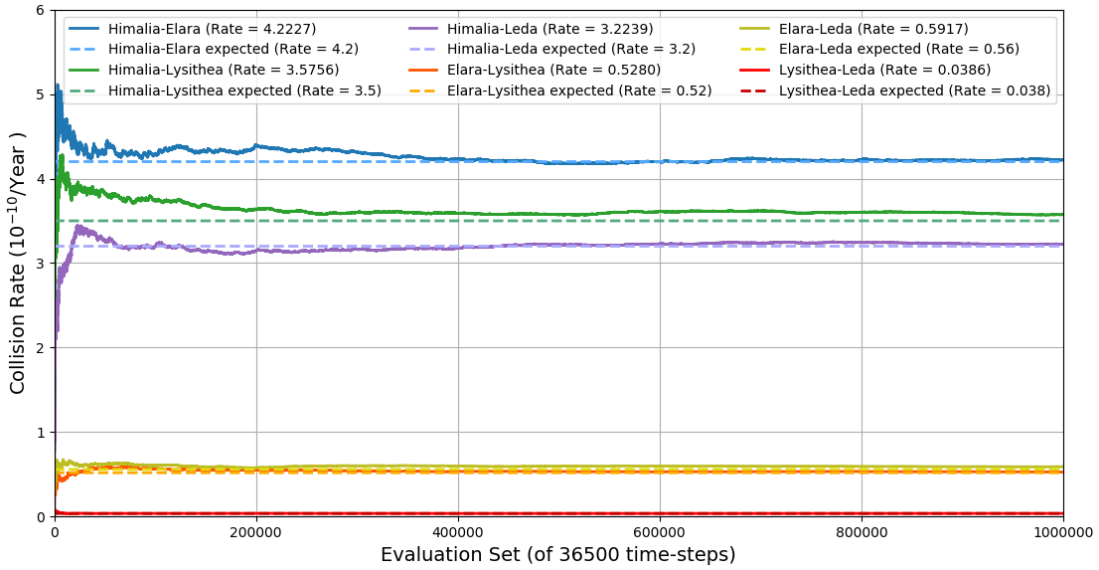

FIGURE 5.1: Convergence over increasing step count for Cube towards the expected Jovian moons collision rates taken from Liou et al. (2003).

In comparison, simulations of the long-term debris environment are often run using 5 day time-steps over a 200 year period. This results in only 14,610 samples per simulation for any specific pair of objects. As such gaining a good estimate of the mean collision rate requires the result to be averaged across hundreds or thousands of Monte Carlo runs of the simulation. Additionally, large changes in the eccentricity and semi-major axis can be expected for many of the objects in Earth orbit due to perturbations, meaning that fewer of the samples relate to any particular combination of orbits.

Figure 5.2 shows a similar plot for the required convergence of the Orbit Trace algorithm with three degrees of freedom (right ascension, argument of perigee and mean anomaly) of the Jovian moons scenario. In contrast to the results for the Cube, a similar level of convergence can be seen after only 200 evaluation sets of 365 days (only 73 thousand applications of the algorithm, i.e. 100,000 fewer samples).

The rates of convergence will be different for debris modelling in Earth orbit where the position of the objects vary with fewer degrees of freedom (random sampling only of the mean anomaly and not of the right ascension and argument of perigee). In particular, Orbit Trace results should not require any convergence as collision rate is independent of any sampling of the mean anomaly.

Taking the cube root of the number of samples required for the Cube method to converge for the Jovian moons ($\sim$1,940) gives a baseline for the expected number of samples required for convergence when sampling with only one degree of freedom rather than three. However, at the normal sampling rate of five days this still equates to 26.5 years, significantly longer than the operational lifetime of most spacecraft and more than enough time for substantial changes in the original orbits of the objects.

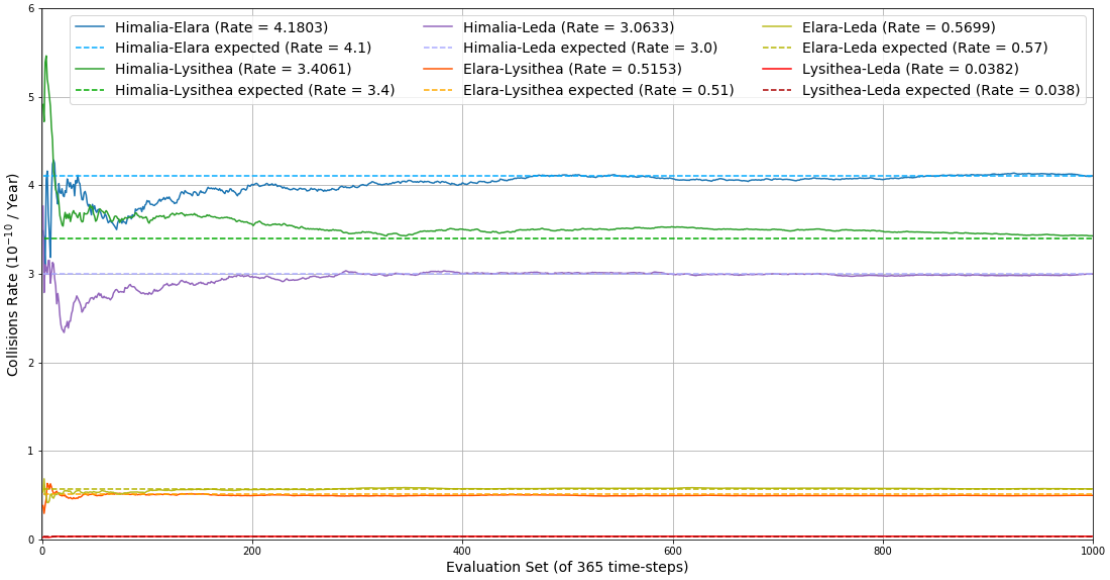

FIGURE 5.2: Convergence over increasing step count for Orbit Trace towards the expected Jovian moons collision rates taken from Liou et al. (2003).

Comparison with the results from the Orbit Trace algorithm indicate that the sampling of mean anomaly might be more significant than that of Right Ascension and Argument of Perigee, increasing the required number of samples by 100,000. This would mean that debris collision rates need to be averaged over a still greater number of time-steps.

This increase in the required number of samples indicates that a large number of Monte Carlo runs or a large population of object pairs are required for robustness in the collision rates produced by the Cube algorithm. The number of samples taken in typical space debris simulations is unlikely to be sufficient to form a good approximation of the probability that any specific object will be involved in a collision without averaging over multiple simulations. However, a sufficiently large object population may provide a good approximation of the environmental collision rate as a whole. Achieving 7.3 billion samples using 5 day time-steps over a 200 years period for example, would require ~499,500 possible collision pairs, which is a population of 1,000 interacting objects.

Performance Testing

To test the expectations around the scaling of the performance of the two models a set of test cases was generated. Expectations were that the Cube method should scale with $O(N)$ and the Orbit Trace with $O(N^2)$. Test cases consisted of a geometrically increasing number of objects, in solar orbits, with randomly generated orbital elements. For each test case the required processing time was recorded for simulations consisting of 10,000 one day time-steps performed using the Cube Approach

algorithm (with a cube size of 4,500,000 km) and the Orbit Trace algorithm (including different attempts at hardware acceleration).

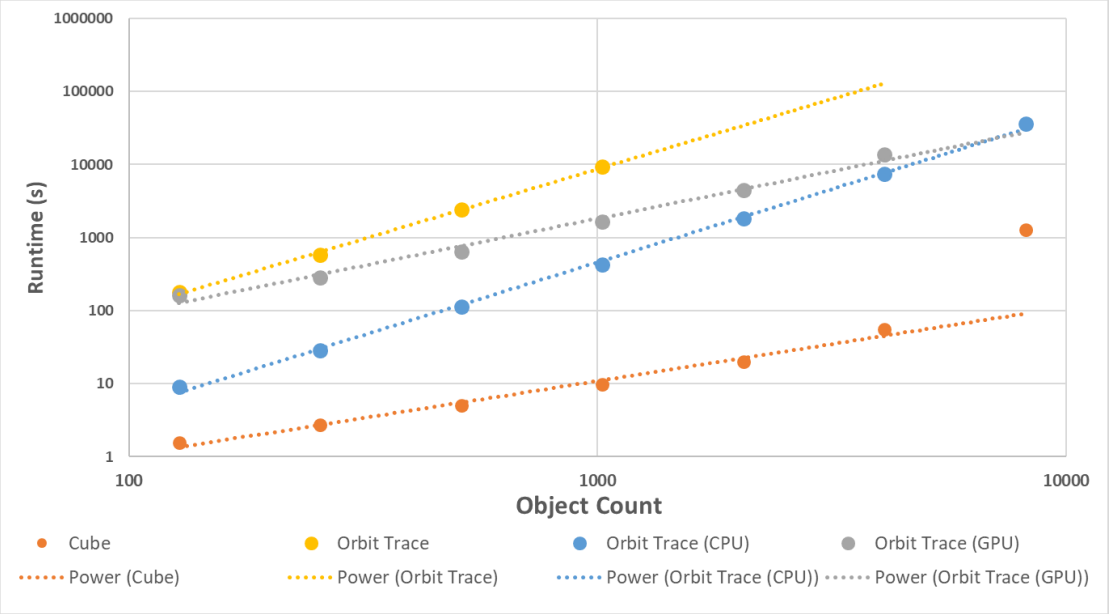

FIGURE 5.3: Graph showing how runtime for different methods scales with object count.

The results of this investigation for populations of 128, 256, 512, 1024, 2048, 4096 and 8192 objects are shown in Figure 5.3. Simulations for the largest population sizes were not run using the non parallelised Orbit Trace algorithm as the scale of the runtime became unmanageable. However, for the lower population sizes a four times increase in runtime was seen with each doubling population size which is consistent with the expected scaling of $O(N^2)$.

For the Cube algorithm the runtime for test cases with lower numbers of objects can be seen to double with each doubling of the number of objects. This fits with the expectation of $O(N)$ scaling and can be seen more clearly in Figure 5.4. However, the runtime for the largest two cases of 4096 and 8192 objects deviate from this trend.

Two hypotheses were formed to explain this discrepancy. One was that this is a computational issue with how the current implementation stores results in dynamically allocated memory. The second was that the calculation time for these larger cases is being dominated by the calculation of collision probabilities for identified conjunctions. While identifying conjunctions is expected to scale with the number of objects, $O(N_{objects})$, calculating the collision probabilities should scale with the number of conjunctions, $O(N_{conjunctions})$. This in turn is proportional to the square of the number of objects: $N_{conjunctions} \propto N_{objects}^2$. For the low number of conjunctions experienced when using the smaller numbers of objects this results in a negligible effect on the runtime. However, as the number of conjunctions grows quadratically with number of objects this could become the major component of the runtime.

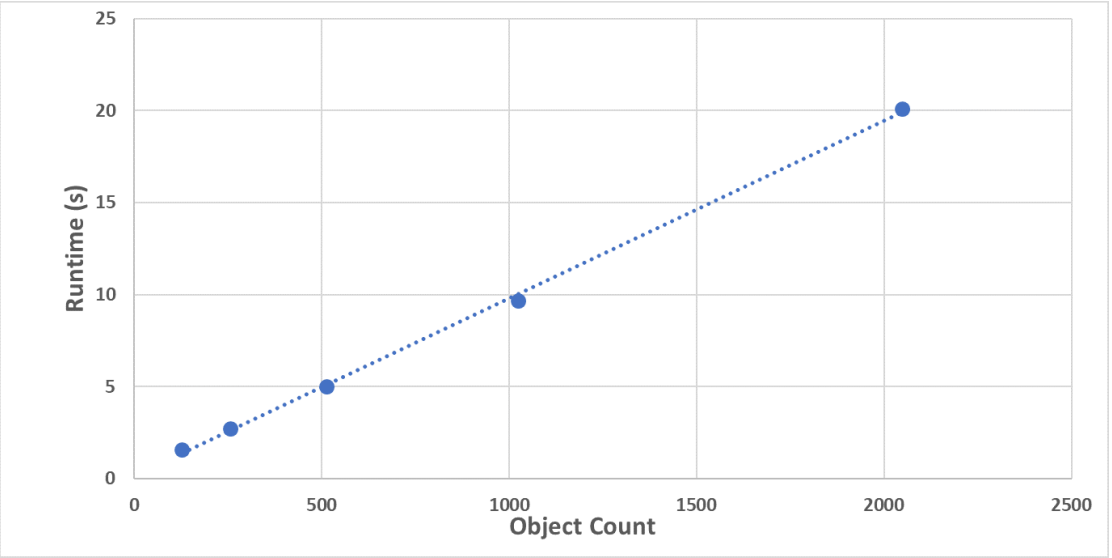

FIGURE 5.4: Graph showing how runtime scales for the Cube method.

For the Orbit Trace implementation a speed increase of around twenty times was achieved through parallelising the code to distribute the different object pairs across all 8 threads of the CPU. $O(N^2)$ scaling was still seen using this configuration, however the decrease in runtime made the algorithm much more usable for higher population sizes. In comparison the alternative of massive parallelism on the GPU did not provide a significant increase in speed when simulating the 128 object population. This is in part due to the added overheads associated with transferring data into and out of graphics memory and in part due to the decreased power of the individual processors on the GPU compared to the CPU. However, due to the large number of individual cores the effective scaling of the runtime when using this method was much better resulting in the runtime approaching that of the CPU configuration for large population sizes.

Unfortunately the limit of available memory on the GPU device was reached when attempting to create the list of object pairs for the simulation of 8192 objects and this prevented further experimentation with higher population sizes to see if the increases would continue. However the existing data points indicate that this would be possible. The results generated using both the CPU and GPU configurations suggest that significant speed increases are possible for the Orbit Trace algorithm, despite the $O(N^2)$ scaling. However, the limitations of current technology mean that for larger population sizes it may be necessary to run the simulations on high-performance computing platforms, which provide greater resource in terms of available memory and processing threads.

Overall the results of the convergence and performance testing indicate that, in terms of usability, the Cube approach is better suited to simulations of large populations, where a greater number of samples are taken, and Orbit Trace algorithm is more

suitable for simulations of specific sub-populations of objects, where fewer object pairs are considered.

Cube Size Testing

To test the importance of the choice of cube size an investigation was conducted into how cube size affected the results of the Jovian moons scenario. Eight different simulations were run with cube sizes corresponding to 0.1%, 0.2%, 0.5%, 1%, 2%, 5%, 10% and 20% of the average semi-major axis of the moons. This gave cube sizes of 115,075 km, 230,150 km, 575,375 km, 1,150,750 km, 2,301,500 km, 5,753,750 km, 11,507,500 km and 23,015,000 km respectively.

The simulations were conducted using the same seed value for the random number generator to ensure that the sampled positions of each moon at each step did not vary between simulations. Figure 5.5 shows how the overall collision rate of the system converged for each of these different cube sizes compared to the expected collision rate taken from Liou et al. (2003).

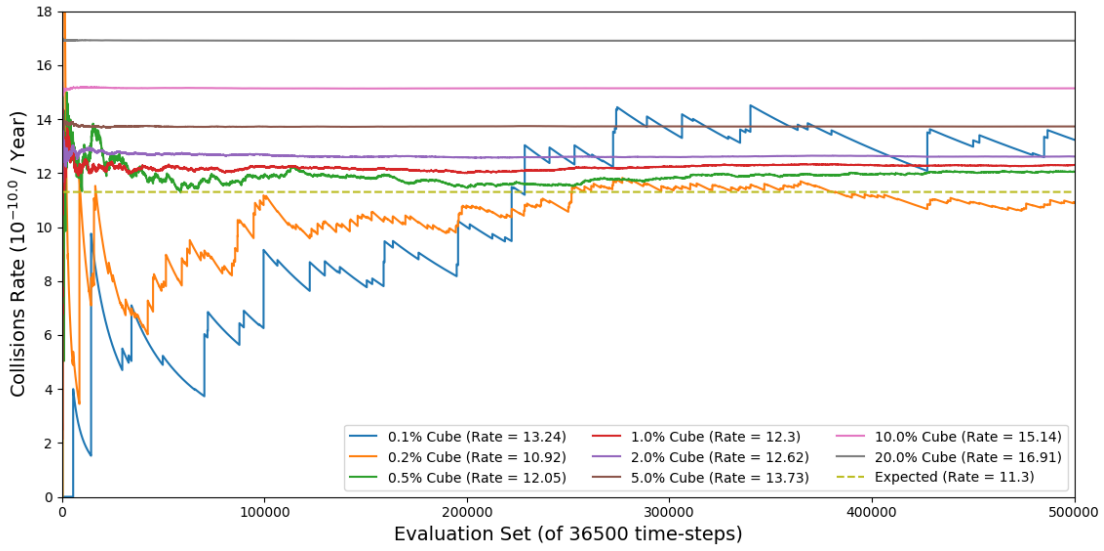

FIGURE 5.5: The convergence over increasing step count of the collision rate for cube sizes representing percentages of the average semi-major axis in a reproduction of the Jovian Moons test case.

Two conclusions can be drawn from these results. Firstly, that the rate of convergence for the collision rate is dependent on the size of cube used, with smaller cubes requiring more steps to converge. Secondly, that the final converged value of the collision rate also varies with cube size with a larger cube size resulting in a higher collision rate. Figure 5.6 shows a quadratic trend fitted to the values of the final collision rate and compared to the expected rate taken from Liou et al. (2003).

The first of these conclusions is expected, as smaller cube sizes result in there being fewer possible opportunities for two objects occupy the same cube and so a reduced

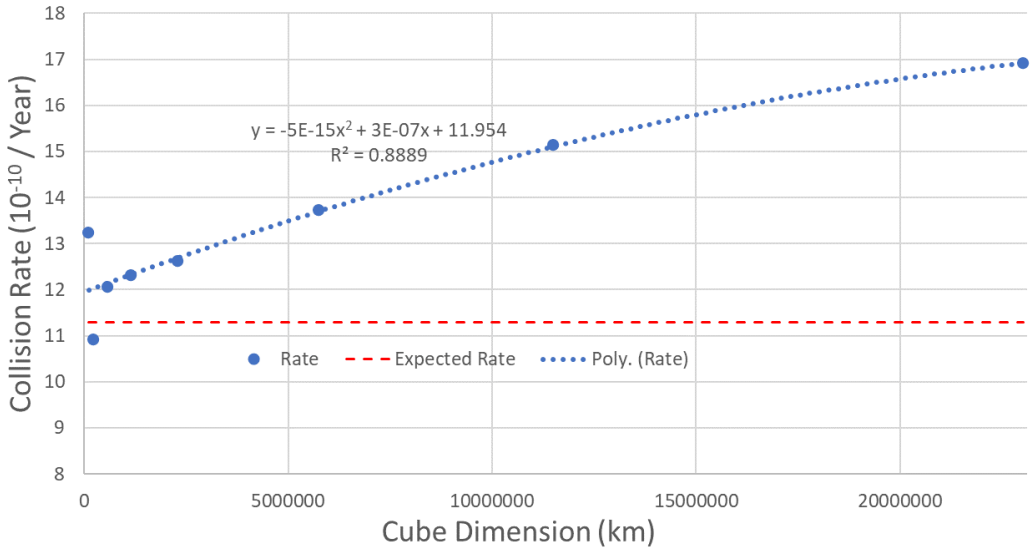

FIGURE 5.6: Relationship between average collision rate and cube size for the Jovian moons scenario.

conjunction frequency. This means that a greater number of samples are required to generate a statistically reliable number of evaluations of the collision probability. The second observation, however, is less intuitive. Simplifying Equation 5.3 for the Cube shows that the collision rate within the cube is inversely proportional to the cube length, L, cubed:

$$P_{i,j} \propto \frac{1}{dU} = \frac{1}{L^3}$$

(given that $s_i = s_j = 1/dU$). As a result, in order for the collision rate to be increasing with the cube size, the probability that the sampled positions of the two objects are both within the same cube, P_{conj}, must be increasing at a greater rate:

$$P_{conj} \propto L^x; \quad \text{where } x > 3$$

The results in Figure 5.6 to the cube size indicate that the resulting relationship is quadratic, which suggests that $x = 5$.

However, in these simulations of the Jovian moons, three of the angular orbital elements (right ascension, argument of perigee, and mean anomaly) are being randomised at every step. Having these three degrees of freedom leads to the position of each object varying in three dimensions within a defined volume. In contrast in simulations of the debris environment only the mean anomaly is randomised. In this case the position of the object will only vary in one dimension along the line of the orbit. Studies performed by Lewis et al. (2019) showed that for simulations of the debris environment the estimates of the collision probability were inversely proportional to the size of the cube for a specific pair of objects and approximately inversely proportional to the square root of the size of the cube for larger systems of objects.

5.3 The Impact of NewSpace Activities

The analysis of NewSpace trends in Chapter 3 identified changes in the operation of spacecraft which result in changes to the characteristics of the orbital environment. A trend towards a clustering of greater numbers of spacecraft sharing similar orbital elements is resulting in a more organised spatial structure. The introduction of large satellite constellations and increases in the number of mass launch events, where many spacecraft are deployed from the same launch vehicle, will exacerbate this effect.

This change reflects the development of a more ordered orbital environment with an increase in the spatial structure of the population and greater correlation between the motions of different objects. One possible consequence is that this could reduce the accuracy of the current collision models for investigating the probability of collisions within these regions. This would be particularly relevant to research into the risks posed by large satellite constellations, which have a highly ordered structure.

5.3.1 Impact on Collision Modelling

The assumptions which underlie both the Orbit Trace and the Cube algorithms appeared to be contraindicated by this change. For both algorithms the assumption is made that the motion of any object is independent relative to the motion of any other object, both when determining the probability of an encounter and when calculating the probability of a collision occurring for a particular encounter.

With regard to the probability of encounter, this can be mitigated in the Orbit Trace algorithm by using the filters described in Equations 5.6 - 5.10. However, for the Cube method this assumption is built in to the randomised sampling of the mean anomaly used to identify encounters. It was hypothesised that this would cause the collision algorithms to identify possible collisions which are not possible physically, resulting in an over-prediction of the encounter rate. This would be particularly noticeable for a population of objects in highly similar orbits. However, in contrast to this, if the sampling rate used in the Cube method is not sufficient then this may result in the algorithm failing to identify any conjunctions between some pairs of objects resulting in an under-prediction of the encounter rate.

The calculation of the collision probability in both algorithms makes use of the kinetic theory of gases to predict rate of collision of objects within a defined region (either a cube, or immediately around the intersection of the orbits). However a key tenet of this theory is the idea of molecular chaos, that the positions and velocities of the particles are uncorrelated. While this has been true on average for the historic environment, it does not hold for the more structured regions of orbital space now being observed.

Historical encounter geometries would have been random, resulting in a uniform distribution on average. However, as many of the objects in these structured environments are in highly similar orbits the conjunctions of an object are more likely to be with an object in these orbits. As a result, a bias is introduced towards encounters with common geometries which would not be represented in the collision algorithms.

Expected Impact on Debris Models

Modelling of the space debris environment has historically suggested that collisions will become the primary driver of population growth within the space debris environment (Kessler and Cour-palais, 1978; Kessler, 1991; Kessler and Anz-Meador, 2001; Anselmo, 2001; Liou, 2006; Rossi et al., 2013). A particular threat is of secondary collisions, due to the increased collision risk following fragmentation from an initial collision. As such any systemic error in the calculation of collision probabilities has the potential to be compounded across the duration of a long term simulation.

The initial analysis of the assumptions present in the collision algorithms indicated that the increased spatial structure being seen as a result of NewSpace would lead the models to over-predict the probability of collisions for these populations. This would lead current debris models to predict accelerated growth in the debris population within these regions. This may result in the exaggeration of the risks posed by these NewSpace systems and introduce unfair bias into the decision making processes for licensing and managing these systems.

5.4 Validating the Algorithms

In order to experimentally test the impact of NewSpace on the collision algorithms, a set of validation tests were conducted using the implemented versions of the Cube and Orbit Trace models. A number of different scenarios, covering examples of both TradSpace and NewSpace, were created (consisting of selected sub-populations of the spacecraft and debris in Earth orbit). Simulations were run using different configurations of the collision models over a fixed period for each scenario. Cumulative collision probabilities were recorded based on identified conjunctions for a set of primary objects within each population.

A common simulation configuration was used to ensure that the results could be compared in a meaningful manner. A duration of 365 days was chosen for the simulation periods, with collision probabilities being calculated at 0.05 day intervals (an effective sampling rate of just over once per orbit for LEO). This equated to $7,300$ samples being taken over the course of each simulation. The number of samples presented a potential issue with the use of the Cube method, as it was expected to be

insufficient to provide a good approximation of the collision rate for individual objects. As a result the sampling rate of the Cube method was artificially inflated by applying the algorithm one hundred times at each step. This meant that the effective time-step ($[t_{s+1} - t_s]$ from Equation 5.2) was only 0.0005 days.

In order to provide a common baseline for comparison between the different scenarios, the results were also compared with the conjunctions predicted by SOCRATES (Kelso and Alfano, 2006) over the same period. While this did not provide an actual 'ground truth' for the collision probability, it did provide a consistent and completely independent method based on regularly updated tracking and a full propagation of the object positions. However, the outputs from this service are maximum collision probabilities and so cannot be compared directly to the output of the Orbit Trace and Cube models. Instead this investigation aimed to compare the differences in the output of the models as a proportion of the SOCRATES maximum collision probability.

Scenarios were developed by selecting a primary population of objects, for example a satellite constellation, and a secondary population based on the conjunctions identified by SOCRATES for the simulation period. This resulted in scenario populations of between $1,000$ and $4,000$ objects being selected. These population sizes were large enough to provide a reasonably large number of conjunctions for each object but small enough to allow the use of Orbit Trace to be practical.

Information on the orbits of the individual objects was obtained from the Space-Track database (Space-Track, 2018). This information was extracted in the form of TLEs chosen from around the start time of each scenario and then used to initialise each object in the simulation.

5.4.1 The SGP4 Propagator

An orbital propagator was required to account for the perturbations influencing the orbits of the objects over the course of the simulation. The SGP4 propagator (Hoots and Roehrich, 1980b; Vallado et al., 2006) was determined to be the best option as it is the same model behind the SOCRATES service and was designed specifically to propagate TLEs.

SGP4 is an analytical propagation model developed for use with near Earth spacecraft and accounts for the most common perturbations experienced in Earth orbit. These include an estimation of gravitational perturbations, based on Brouwer (1959a), and the effect of atmospheric drag, using a power density function as the atmospheric model.

Verification of the SGP4 Integration

As this is a well established model, an existing C++ implementation, created by Vallado et al. (2006), was integrated with the implementation of the Cube and Orbit Trace collision models. Verification testing was conducted in order to test this new integration with average errors of 9.53×10^{-8}% and 1.10×10^{-5}% for the position and velocity respectively compared to the listed values for the test set. The results gave a high level of confidence in its use for this investigation. Full details on the verification can be found in Appendix C.

5.4.2 Simulation Scenarios

The candidate scenarios for collision simulations were chosen to represent a range of examples from different points in the last 15 years. This variation allowed the examination of environments both before and after the watershed moments of the Fengyun-1C ASAT test and the Iridium-33/Cosmos-2251 collision. The first step in generating each scenario was the identification of the primary population of objects which would be the focus of the collision study. The SOCRATES reports were analysed for the year following the simulation start date to identify all conjunctions involving the primary objects. From these conjunctions a larger background population of objects was defined for each scenario.

Depending on the scenario, the primary objects consisted of either a population of disparate spacecraft, representing a TradSpace environment, or a more homogeneous population as is expected in a NewSpace environment. The NewSpace scenarios were chosen to exemplify the spatial structure identified in Chapter 3 and so were based on existing constellations and mass-launch events with obvious well defined primary populations. For the TradSpace scenarios the primary objects were selected from a larger pool of objects. The selection was made by using graph theory to identify networks of groups of objects which experienced multiple conjunctions with one another. Table 5.1 provides an overview of the eight scenarios chosen for this investigation including four older scenarios, based on populations from 2006, and four newer scenarios based on periods from 2015 onwards.

The four older scenarios consist of three TradSpace examples (TS 2006 #1, TS 2006 #2 and TS 2006 Random) and one NewSpace example (Iridium 2006) with each having a start date of 1st January 2006. For the first two scenarios, the primary population was chosen by analysing the SOCRATES data to identify networks of objects with common secondary populations in order to be more comparable to the NewSpace scenarios and to minimise the total object population. The third scenario, TradSpace 2006 Random, was created by randomly selecting a similar sized selection of spacecraft involved in LEO conjunctions. The Iridium 2006 NewSpace scenario was identified as a representative of an older satellite constellation with the spatial structure identified as

TABLE 5.1: Table of identified collision scenarios.

Scenario Type	Scenario	# Primary Objects	Total Objects	Start Date	SOCRATES Conjunctions
TradSpace	TS 2006 #1	48	979	01-01-2006	13616
TradSpace	TS 2006 #2	63	1442	01-01-2006	27565
TradSpace	TS 2006 Random	48	4043	01-01-2006	18036
NewSpace	Iridium 2006	60	1752	01-01-2006	15091
TradSpace	TS 2015	52	2504	01-01-2015	30354
NewSpace	PSLV C37	79	1355	15-02-2017	24833
NewSpace	Iridium Next (Partial)	24	4539	29-06-2017	9553
NewSpace	Iridium Next (Full)	75	4810	01-03-2018	29736

a NewSpace characteristic. The primary objects being 60 of the Iridium spacecraft which SOCRATES identified as having conjunctions in 2006.

The four more recent scenarios consist of only one TradSpace example (TS 2015) and three NewSpace examples (PSLV C37, Iridium Next (Partial) and Iridium Next (Full)). The primary population for TS 2015, as with the 2006 examples, was chosen based on an identified network of objects with common conjunctions for a start date of 1st January 2015.

The start dates for the NewSpace cases were chosen more specifically to fit around launch dates of the spacecraft. The first scenario, PSLV C37, examines a mass launch event, with the primary objects being a sub-set of the 104 spacecraft deployed into a polar sun-synchronous orbit by the Indian PSLV-C37 mission on the 15th February 2017 (Purna Sudhakar, 2018).

The remaining two NewSpace scenarios focus on different stages of the deployment of the next generation 'Iridium Next' constellation. The first, starting on 29th June 2017, focusses on 24 of the initially deployed spacecraft. The second, starting on 1st March 2018, looks at all 75 spacecraft, of which $\sim$50 are in orbit at the start of the simulation and the remainder are launched as the simulation progresses.

Comparing the Scenarios

In Chapter 3 a clustering of objects into similar orbital regions was identified as one of the features resulting from NewSpace trends which may impact the probability of collisions occurring. The orbital characteristics of the populations of each of the eight scenarios were analysed to understand their differences. One approach was to study the distribution of the different rates of change of RAAN, $\dot{\Omega}$, resulting from the J2 gravitational perturbation; a function of the inclination, semi-major axis and eccentricity of an objects orbit (see Equation 3.1).

The differences in the drift rate of RAAN as a result of this perturbation is one of the major causes of mixing within populations in Earth orbit, as the changes in the relative orientations of the orbits enables different objects to experience close approaches. Figures 5.7 and 5.8 show the population distribution of $\dot{\Omega}$ values for the four TradSpace and four NewSpace scenarios respectively.

Some common features were visible in the distributions of $\dot{\Omega}$. Peaks were visible for all scenarios at $\sim$0.02 radians per day and for either or both of -0.04 and -0.01 radians per day. The most prominent of these peaks, at 0.02 rad/day, corresponds to the population of objects in retrograde sun-synchronous orbits. The other peaks correspond to objects in near-polar and other high inclination prograde orbits. The particular prominence of the sun-synchronous peak across all scenarios indicates that these objects are a common source of close approach conjunctions, and hence collision risk, within the orbital environment.

Comparing the distributions for the NewSpace scenarios in Figure 5.8 against those for TradSpace in Figure 5.7, narrower and more prominent peaks were visible for NewSpace than TradSpace. However, an inspection of the start date of the different scenarios revealed that the magnitude of these peaks increased for later scenarios. This correlation between the magnitude of the peaks and scenario start date suggested that the difference is a result of systemic changes in the background population and not an artefact of choosing a NewSpace population in similar orbits. However, the increases

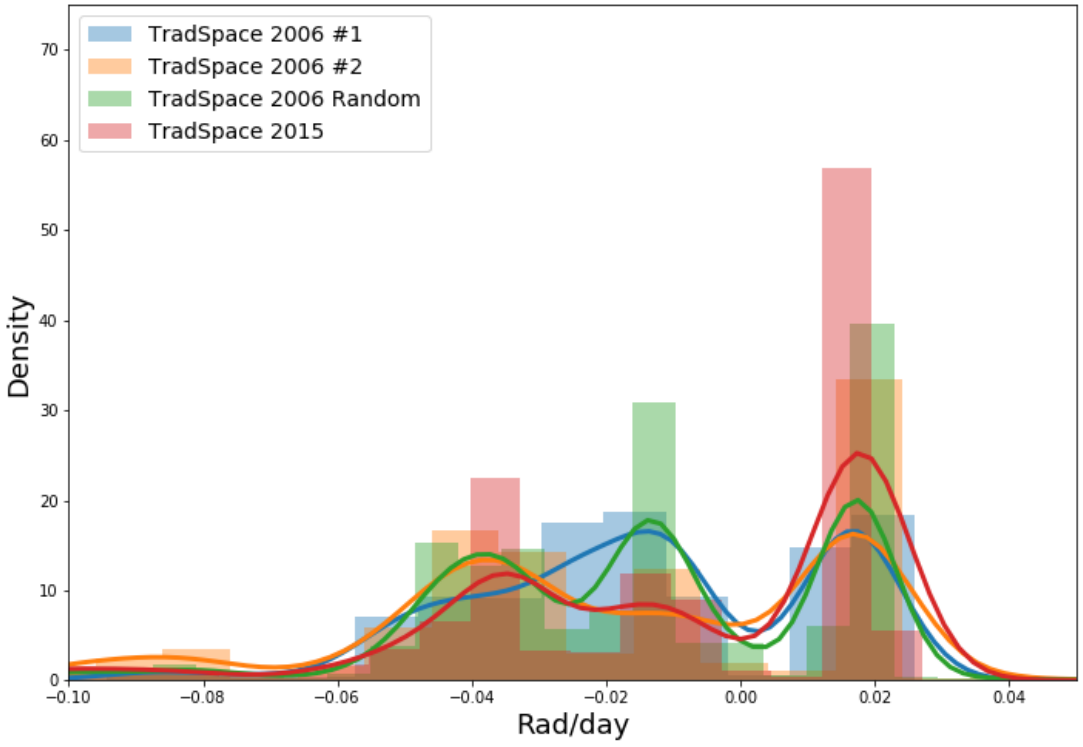

FIGURE 5.7: Barplot with density kernel showing the rate of change in RAAN for all objects in the TradSpace scenarios.

in peak density for the NewSpace scenarios are consistent with the clustering of launched objects into similar orbits identified in the analysis conducted in Chapter 3.

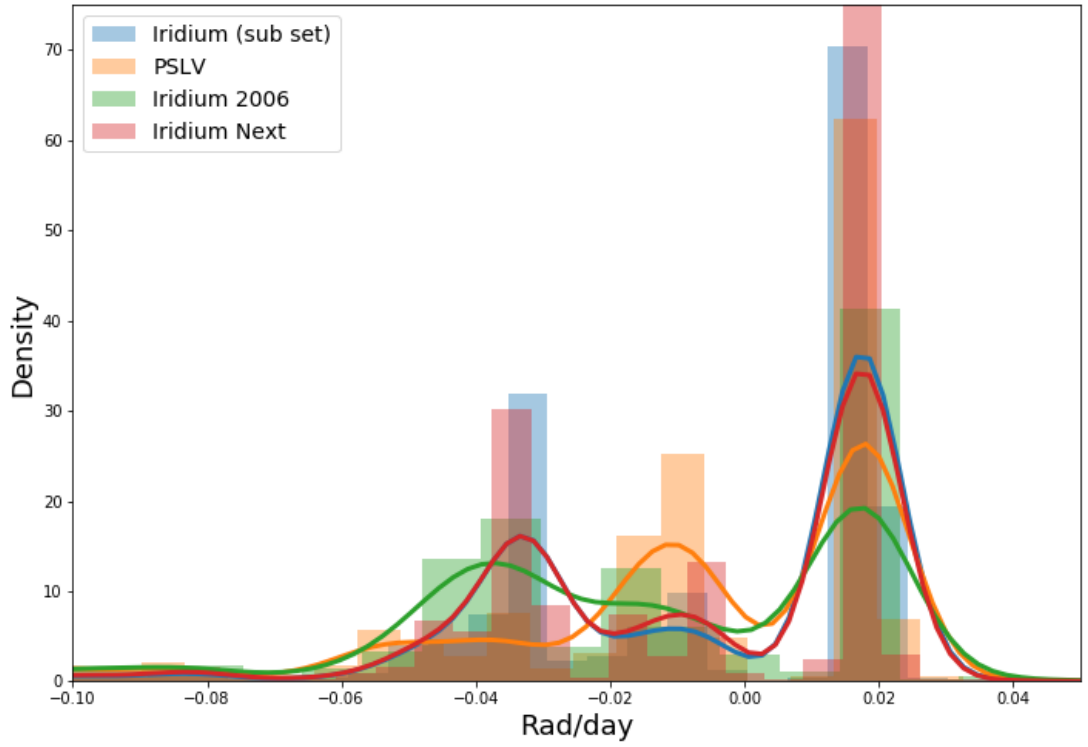

FIGURE 5.8: Barplot with density kernel showing the rate of change in RAAN for all objects in the NewSpace scenarios.

Another measure investigated was the differences in the congestion of regions around the Earth. This helped to understand how structural changes in the object populations may impact the probability of a collision occurring. The spatial density was calculated for different areas in LEO based on a sub-division of the region by altitude and declination into a set of concentric spherical segments.

A ten kilometre banding was used for altitudes up to 2,000 km with a declination banding of 3° creating a 200×30 matrix (distribution by declination is symmetric around the equatorial plane so only 0° to 90° was considered). A spatial distribution was determined separately for each of altitude and declination by calculating the proportion of an orbit spent in each cell and summing across every object in the population. In calculating these proportions the assumption was made that both argument of perigee and RAAN would vary for each object over the course of the simulations. As such the orientation of the objects' orbits was not included in the assessment of the congestion, only the altitude and declination of the objects.

Due to the mechanics of the orbits, objects spend a greater proportion of their time at higher altitudes and declinations. A two dimensional matrix was then created using the matrix product of the two distributions. The resulting matrix of occupation proportion was then converted into a set of spatial densities by dividing each cell by

the volume of the respective segment of the spherical shell. For comparability between scenarios with different population counts, the altitude vs. declination density matrices were normalised to make the sum of each grid equal to one:

$$\phi_{ij} = \frac{\rho_{ij}}{\sum_{ij}^{N} \rho_{ij}} \tag{5.13}$$

where ρ_{ij} is the spatial density in the ith altitude and jth declination cell and ϕ_{ij} is the corresponding normalised density.

Figures 5.9 and 5.10 show polar projections of the resulting spatial density distributions. These show that some of the congested declinations are common across the scenarios. In particular, the bands at $60 - 66^{\circ}$, $78 - 84^{\circ}$ and $87 - 90^{\circ}$ show increased spatial density compared to the background spatial density for every scenario. The increased density is consistent with the inclination banding observed both for the general environment in Chapter 3 and when investigating the rate of

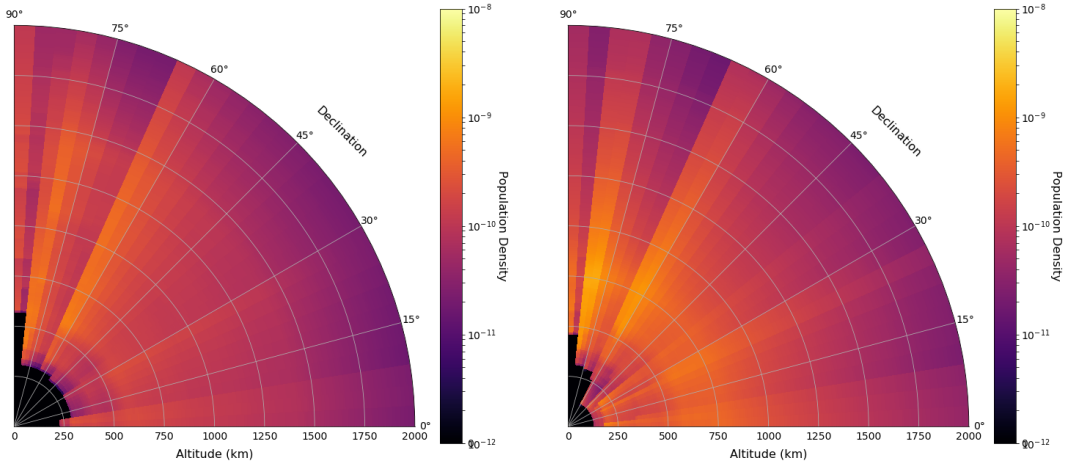

(A) TradSpace 2006 #1

(B) TradSpace 2006 #2

(C) TradSpace 2006 Random

(D) TradSpace 2015

FIGURE 5.9: Heatmaps of the population density of different altitude-declination regions for TradSpace scenarios.

change of RAAN. The consequence is that, for these scenarios, more spacecraft are passing through these regions, increasing the opportunities for a collision.

An increase in peak spatial density relative to the TradSpace scenarios is particularly visible for the PSLV-C37 and Iridium Next (full) NewSpace scenarios. The peak regions of spatial density appear at 750 km altitude and 80° for the three Iridium scenarios which is consistent with the positioning of the constellations at 784 km and 86° inclination. Meanwhile for PSLV-C37, the regions of greatest density are focussed around the 500 km deployment altitude of the spacecraft, but show high congestion regions across a greater range of declinations. This indicates that the background population with which the PSLV-C37 spacecraft experienced conjunctions included more spacecraft in lower inclination orbits which resulted in an increase in the spatial densities at lower declinations.

Studying the TradSpace scenarios the TradSpace 2015 scenario represents a noticeable

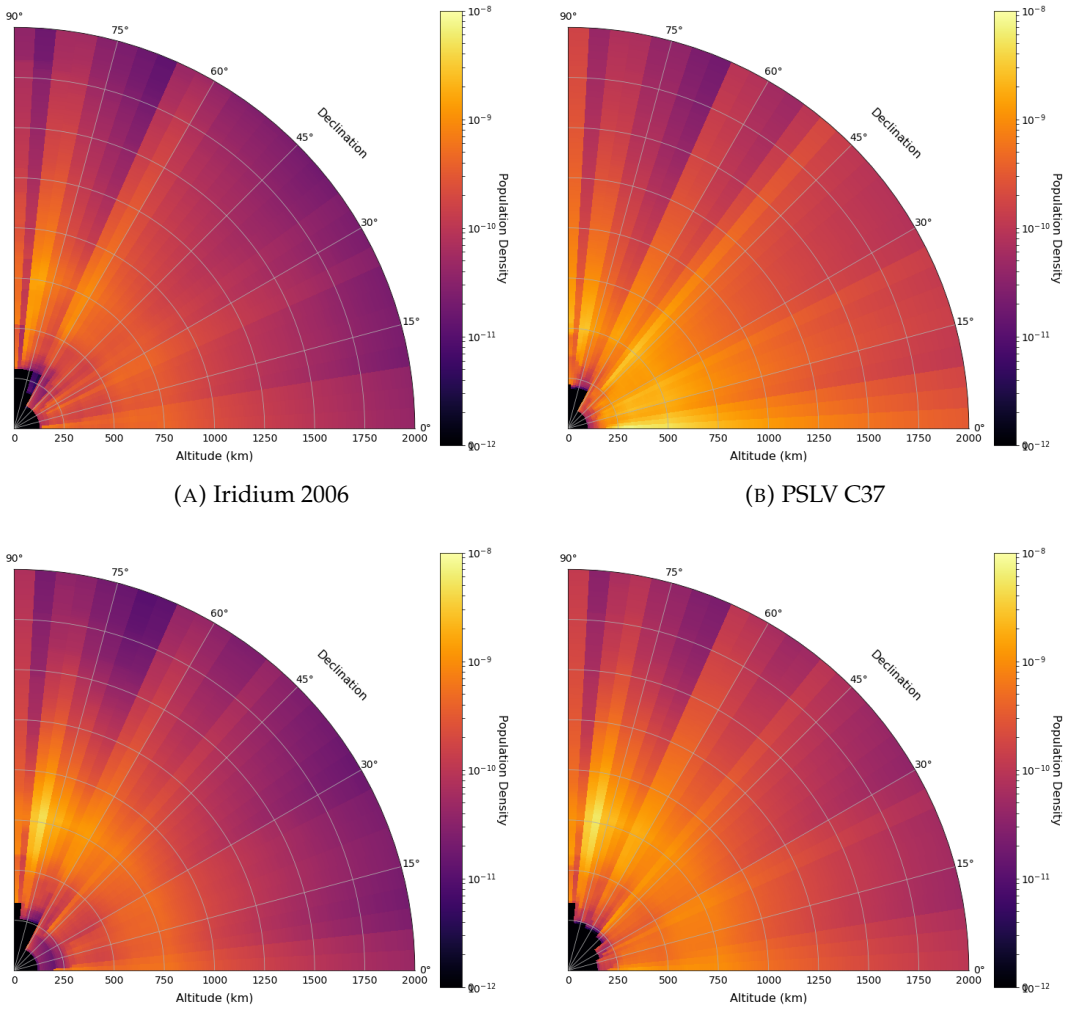

(A) Iridium 2006

(B) PSLV C37

(C) Iridium Next (partial)

(D) Iridium Next (full)

FIGURE 5.10: Heatmaps of the population density of different altitude-declination regions for NewSpace scenarios.

increase in peak spatial density from the 2006 scenarios. As with the results for $\dot{\Omega}$ this is suggestive of systemic changes in the background population. However, in addition to this systemic change, differences between NewSpace and TradSpace can be seen when contrasting the congestion plots for the scenarios. Higher population densities are seen for the most congested regions of the NewSpace plots compared to those for TradSpace. With the density normalisation in place to account for differences in population size this increase in peak population density indicates that there is a meaningful difference between the NewSpace and TradSpace cases which can be used when investigating the results of the collision models.

A single metric for each population, similar to that used for Figure 3.12, was calculated to quantify the extent of the clustering effect observed. The sum of the squared deviations from the mean, SSDM, was used to understand the deviation of the highest spatial densities from the background population:

$$SSDM = \sum_{ij}^{N}((\phi_{ij} - \overline{\phi})^2) \tag{5.14}$$

Where ϕ_{ij} is the normalised density and the mean normalised density per cell $\overline{\phi} = \frac{1}{N}$.

The resulting SSDM values for each scenario can be seen in Figure 5.11. The deviation from the mean was lowest for the TradSpace scenarios and greatest for the NewSpace scenarios, in particular for the Iridium Next (partial) scenario. This provided a clear feature for quantifying the differences between the scenarios when analysing the results.

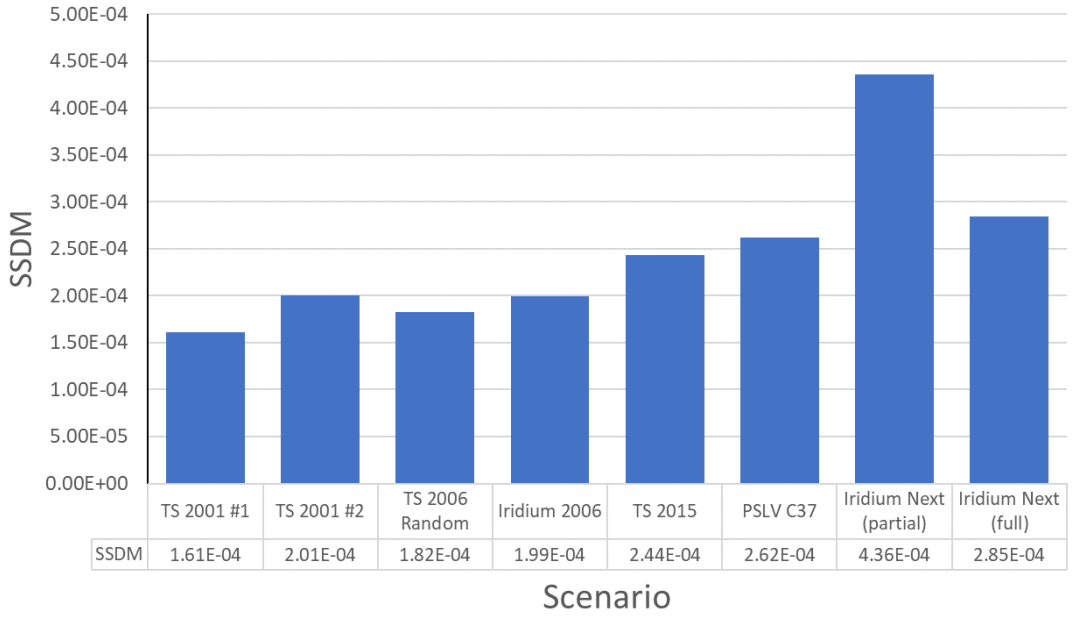

FIGURE 5.11: Sum of the squared deviations (SSDM) for the normalised spatial densities of the different scenarios

5.5 Results from the Model

Each of the eight scenarios were simulated over a 365 day projection period using the Cube and Orbit Trace algorithms, in conjunction with the SGP4 propagator. Collision probabilities were compiled using configurations of the Cube algorithm with cube sizes with side lengths of 2 km, 5 km, 10 km and 20 km and for Orbit Trace with no enhanced collision radius. When using the Cube method a stochastic element is present (due to sampling the mean anomaly) leading to variation in the results. To account for this the cube results were averaged over ten different simulation runs allowing mean results to be calculated. Simulations run using the Orbit Trace method were deterministic within this model and so the results were taken from a single simulation run.

5.5.1 Collision Results

The results were first inspected for each of the different scenarios in isolation. The number of identified conjunctions and the collision probability across the simulation period were evaluated for objects in the primary populations. Overall collision probabilities were then calculated for each object in the primary population and for the primary population as a whole. Cumulative probabilities were calculated from the product of the inverse collision probabilities of each conjunction, i.e. the probability that no collision occurred across the projection period:

$$P_{collision} = 1 - P_{no\,collision} = 1 - \prod_{i=1}^{n}(1 - p_i) \tag{5.15}$$

where p_i is the collision probability of the ith individual conjunction out of a total n relevant conjunctions. The maximum collision probabilities reported by SOCRATES for conjunctions involving primary objects were combined in the same way and used as a baseline to compare the results of the different simulations.

TradSpace Scenarios

The cumulative collision probabilities generated by the different methods and configurations are compared in Figures 5.12 to 5.15 for the primary objects of the four TradSpace scenarios. To enable an easy comparison of the relative differences between the models, the different data are presented on radar plots with a logarithmically scaling radial axis of the collision probability between 1×10^{-6} and 0.1.

Comparing the results of the different scenarios the calculated probabilities were of the same order of magnitude, between 1×10^{-4} and 1×10^{-3}. Across the different cube sizes the calculated results were consistent across the 5 km, 10 km and 20 km

cubes with an average coefficient of variation[1] of 17%. Looking at the results from the Orbit Trace model, the calculated collision probabilities for the individual objects were 29% greater on average than the results from the Cube method, but both are consistently of the same order of magnitude. However, the results for the final cube method configuration, using a 2 km cube size, are not consistent with the larger cubes, being lower on average and having greater variability. This suggests that there may be issues with generating accurate results when using small cube sizes. This discrepancy may have been due to under sampling relative to the increased number of samples required for convergence when using smaller cube sizes (as found in section 5.2.3).

The results of the Cube and Orbit Trace models were compared against the combined SOCRATES maximum collision probabilities for each object. Comparing the different objects relative to one another there was a correlation between SOCRATES and the results of the two models in the relative collision probabilities. However, a consistent order of magnitude bias existed for the SOCRATES results compared to the Cube and Orbit Trace models, on average by five to ten times. This bias was expected due to the

[1]The ratio of the standard deviation to the mean of the collision probabilities.

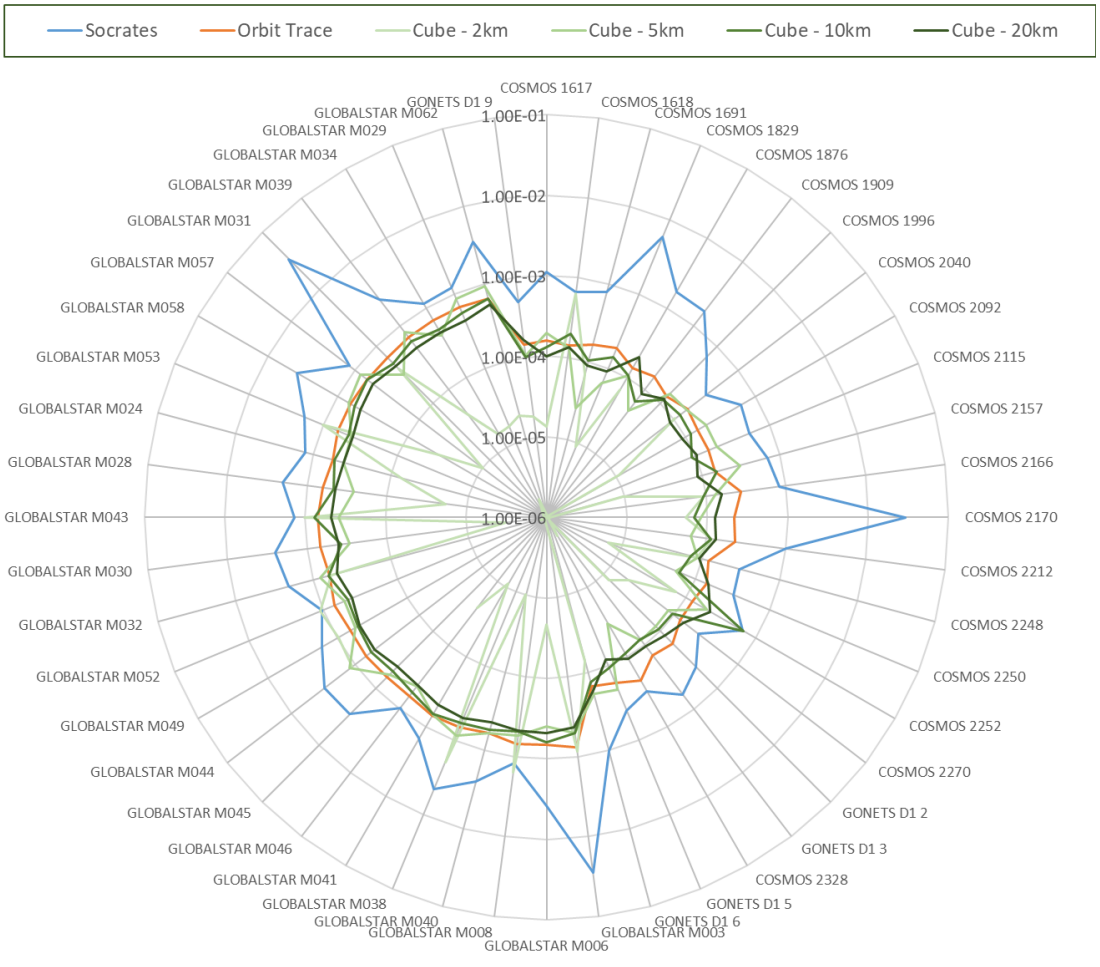

FIGURE 5.12: Collision probabilities from different methods for primary objects in the TS2006 #1 scenario

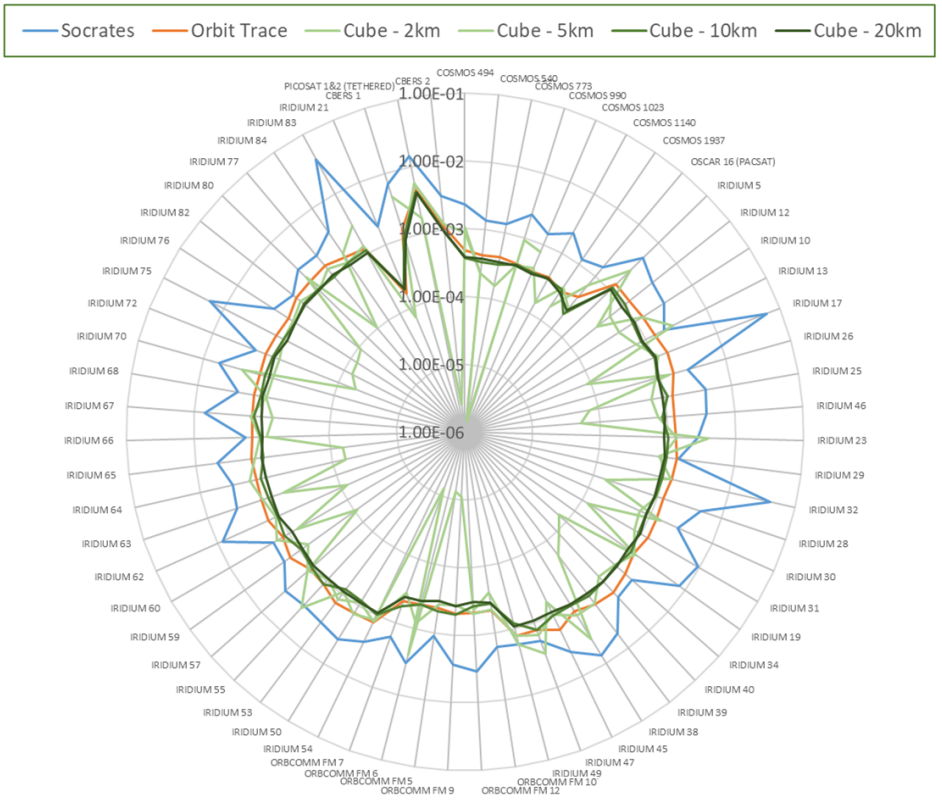

FIGURE 5.13: Collision probabilities from different methods for primary objects in the TS2006 #2 scenario

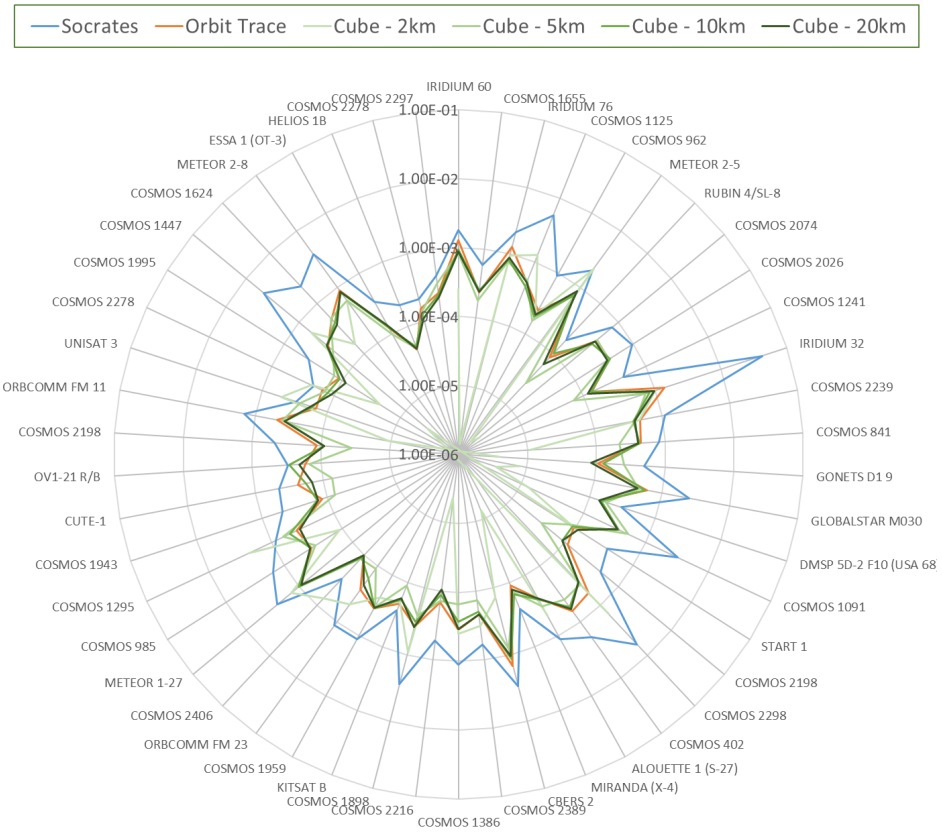

FIGURE 5.14: Collision probabilities from different methods for primary objects in the TS2006 Random scenario

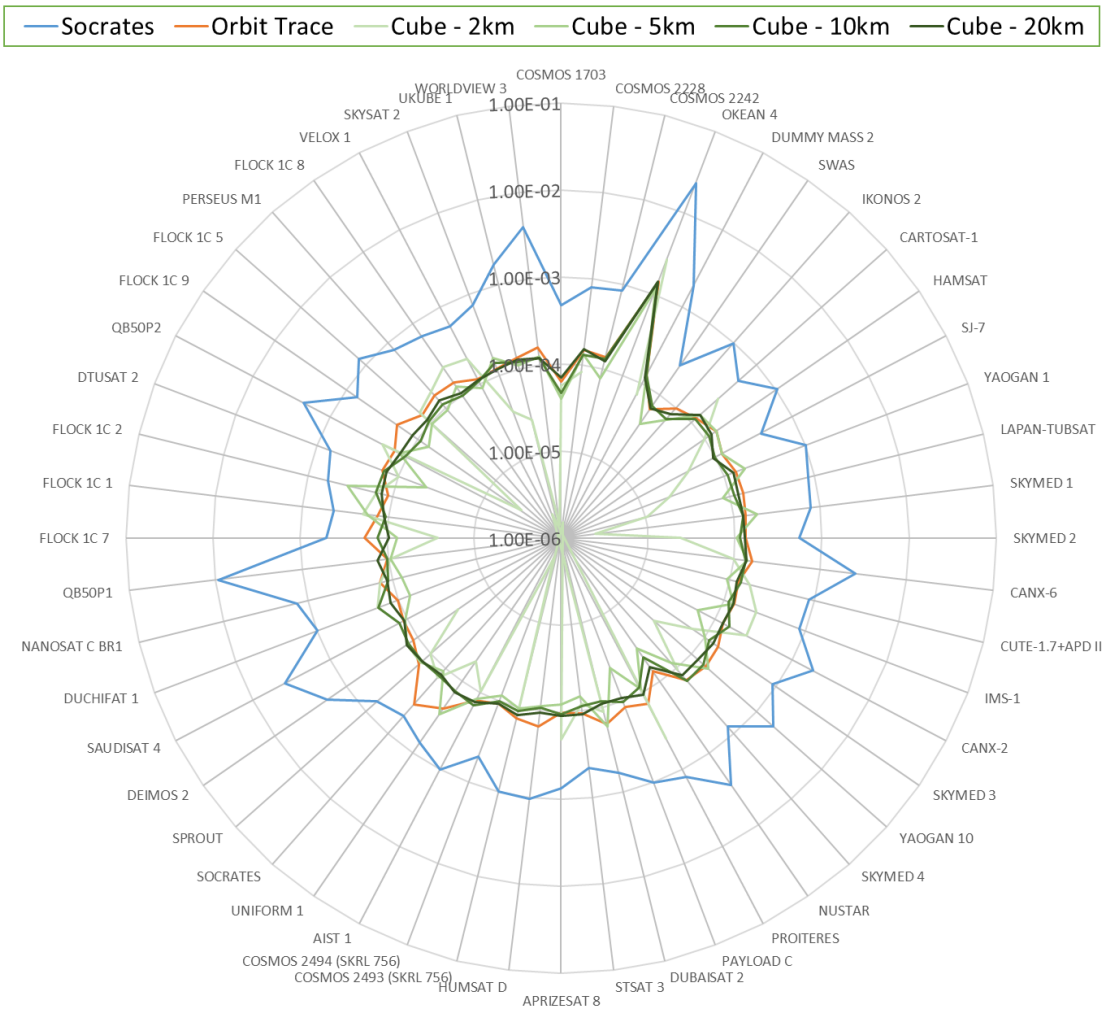

FIGURE 5.15: Collision probabilities from different methods for primary objects in the TS2015 scenario

collision probabilities reported by SOCRATES being the maximum collision probabilities for the conjunction (Alfano, 2004). The correlation was most apparent in the TradSpace case TS2006 Random, for which PCC values of 0.82 for Orbit Trace and an average of 0.76 for the cube showed a strong positive correlation was present (based on a comparison of each of the generated collision probabilities and the SOCRATES probabilities in log-space). The results of the scenario can be seen in Figure 5.14 where the differences in the collision probabilities of the individual spacecraft make the relative changes in each set of results clearer.

However, there were some noticeable peaks in the SOCRATES collision probabilities which appear to be exceptions to this agreement. Notable examples include the results for GlobalStar M031, GlobalStar M003 and Cosmos 2170 in Figure 5.12 for the first TradSpace case, TS2006 #1, as well as Iridium 32, Iridium 17 and Iridium 83 in Figure 5.13 of the second scenario, TS2006 #2. These peaks are the result of specific individual conjunctions with high probabilities which are dominating the cumulative collision probability. The calculation of the maximum collision probability is dependent on the directionality of the close approach displacement, so a conjunction with a very low

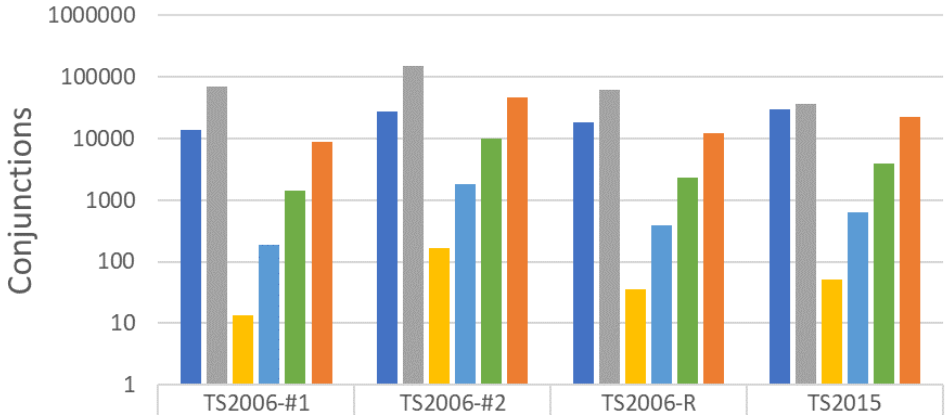

	TS2006-#1	TS2006-#2	TS2006-R	TS2015
Socrates	13616	27565	18036	30354
Orbit Trace	68854	149613	61168	36275
CUBE 2	13.2	164.7	35.5	51.4
CUBE 5	189	1805	383.9	632
CUBE 10	1418.8	9965.3	2274	3953.3
CUBE 20	8826.3	46691.9	12328.7	22566.5

FIGURE 5.16: Comparison of the TradSpace collision simulation conjunctions

miss distance along the major axis of the combined satellite covariance would typically result in a very high collision probability (Kelso and Alfano, 2006). A similar peak is visible for Okean 4 in Figure 5.15 of the final TradSpace scenario, TS2015. However, for this spacecraft corresponding peaks are also visible for the Cube and Orbit Trace results which suggests that this is due to consistently high collision probabilities.

The overall results of the TradSpace scenarios are directly compared in Figure 5.16 and Figure 5.17 using the metrics of number of conjunctions and total primary object collision probability respectively. The overall number of conjunctions predicted by the the 20 km cube size was closest to the number identified by SOCRATES, with an average of 94.2% of the number of conjunctions (ranging from 64.8% to 169.4%. The Orbit Trace generated a greater number of conjunctions, averaging 376.8% of the number of SOCRATES conjunctions. However, for both the Cube and Orbit Trace models the number of conjunctions identified is limited by the number of samples taken across the simulation as, unlike the collision probability, the number of conjunctions per step does not scale with the length of time-step used. As such this metric is not useful as a comparison between SOCRATES and the models, but it does provide insight on whether the sampling rate was sufficiently high that the cumulative collision probability was likely to have converged.

Comparing the number of conjunctions reported by each method highlights how few results were available using the 2 km cube size. This suggests that the greater variability seen for the collision probabilities was due to a much smaller number of conjunction events being identified using the smaller cube size. Across the results for different cube sizes the average coefficient of variation was 5.62%, showing good

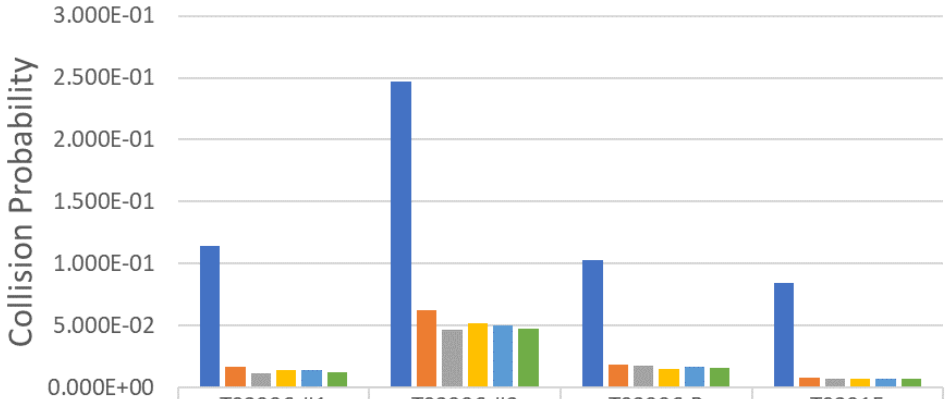

	TS2006-#1	TS2006-#2	TS2006-R	TS2015
Socrates	1.139E-01	2.47E-01	1.02E-01	8.42E-02
Orbit Trace	1.669E-02	6.21E-02	1.87E-02	8.13E-03
CUBE 2	1.188E-02	4.70E-02	1.78E-02	7.53E-03
CUBE 5	1.437E-02	5.22E-02	1.51E-02	6.68E-03
CUBE 10	1.384E-02	4.99E-02	1.63E-02	6.97E-03
CUBE 20	1.217E-02	4.74E-02	1.61E-02	7.14E-03

FIGURE 5.17: Comparison of the TradSpace collision simulation probabilities

agreement and indicating that while choice of cube size affects the number of samples needed, the impact on the overall collision probabilities is small.

The total collision probabilities reported for each scenario confirm the observations made of Figures 5.12 to 5.15. That is, the results of the different cube configurations are self-consistent, with the results of Orbit Trace being consistently higher but of the same order of magnitude. The results from all of the simulations are between four and ten times lower than the SOCRATES maximum collision probabilities.

NewSpace Scenarios

Figures 5.18 to 5.21 compare the different calculated collision probabilities for the four NewSpace scenarios using the same radial plotting style.

For the three more recent scenarios (Figures 5.19, 5.20 and 5.21) the collision probabilities were mostly consistent between the methods (as with the TradSpace scenarios). The probabilities generated by the Orbit Trace algorithm and the different configurations of the Cube method tended to be smaller than for TradSpace, with results between 1×10^{-5} and 1×10^{-4}. The 2 km cube was again the exception and the results using this cube size are much more variable for some of the primary objects, particularly in the partial Iridium Next scenario. This is likely to be due to the same issue with an insufficient number of conjunctions being predicted to gain a good estimate of the overall collision rate. Comparing the NewSpace scenarios against the SOCRATES results, the SOCRATES maximum collision probabilities are again much higher than those estimated by the collision models. However, while for the

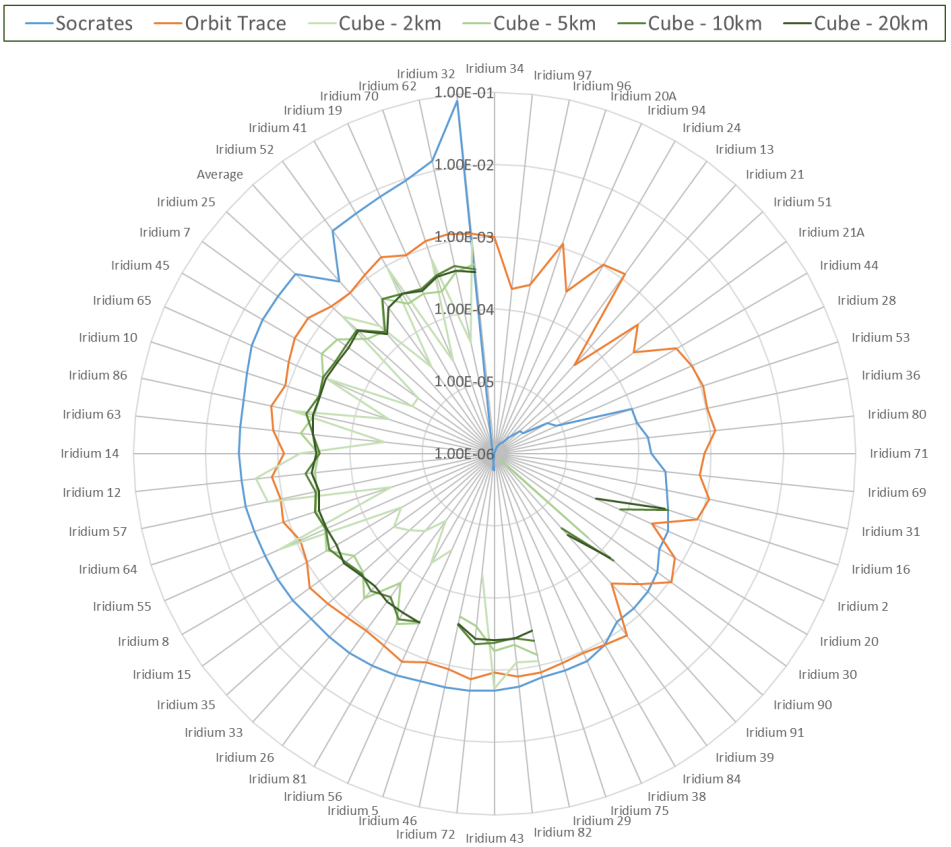

FIGURE 5.18: Collision probabilities from different methods for primary objects in the Iridium 2006 scenario

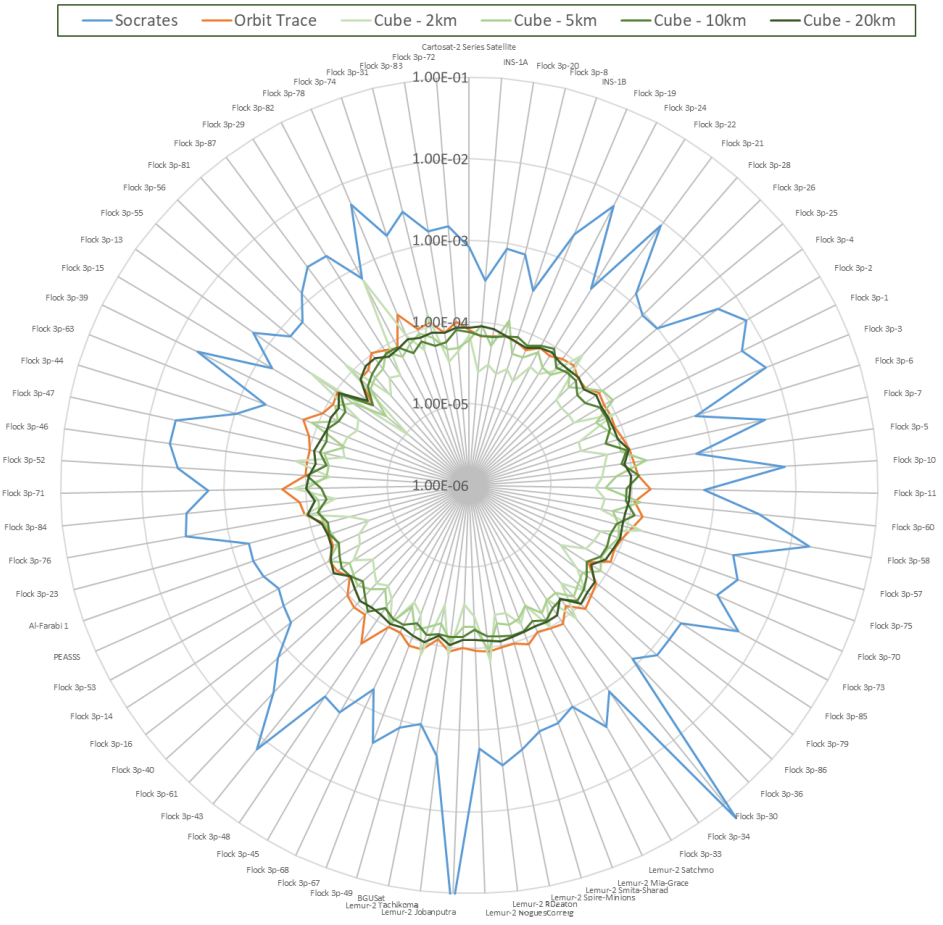

FIGURE 5.19: Collision probabilities from different methods for primary objects in the PSLV-C37 scenario

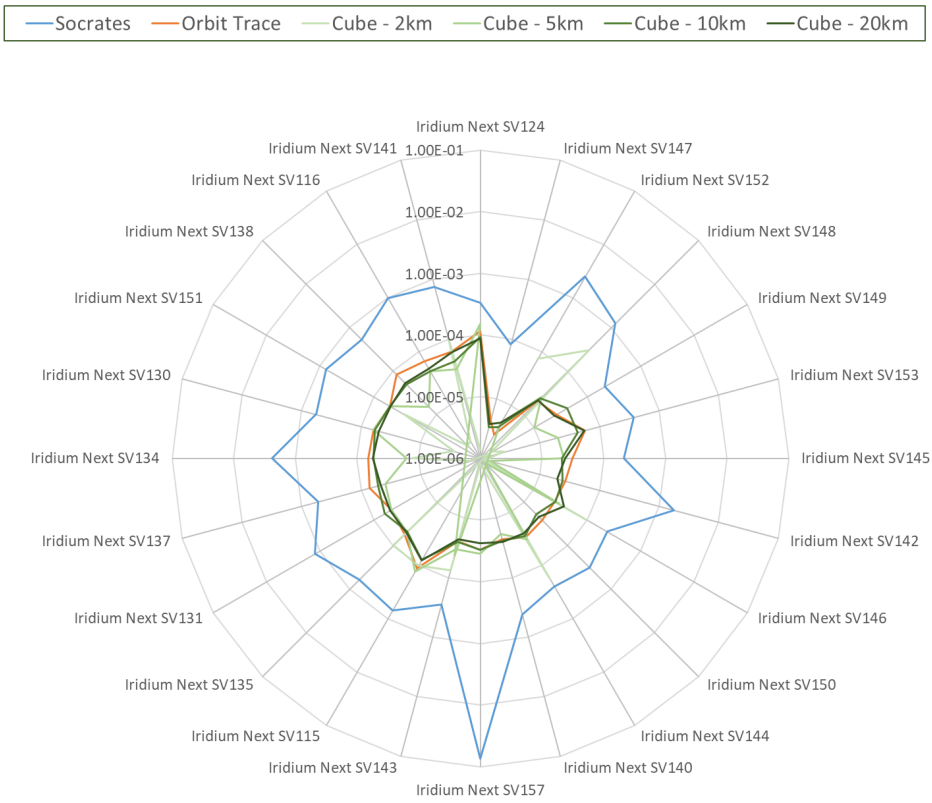

FIGURE 5.20: Collision probabilities from different methods for primary objects in the partial Iridium Next scenario

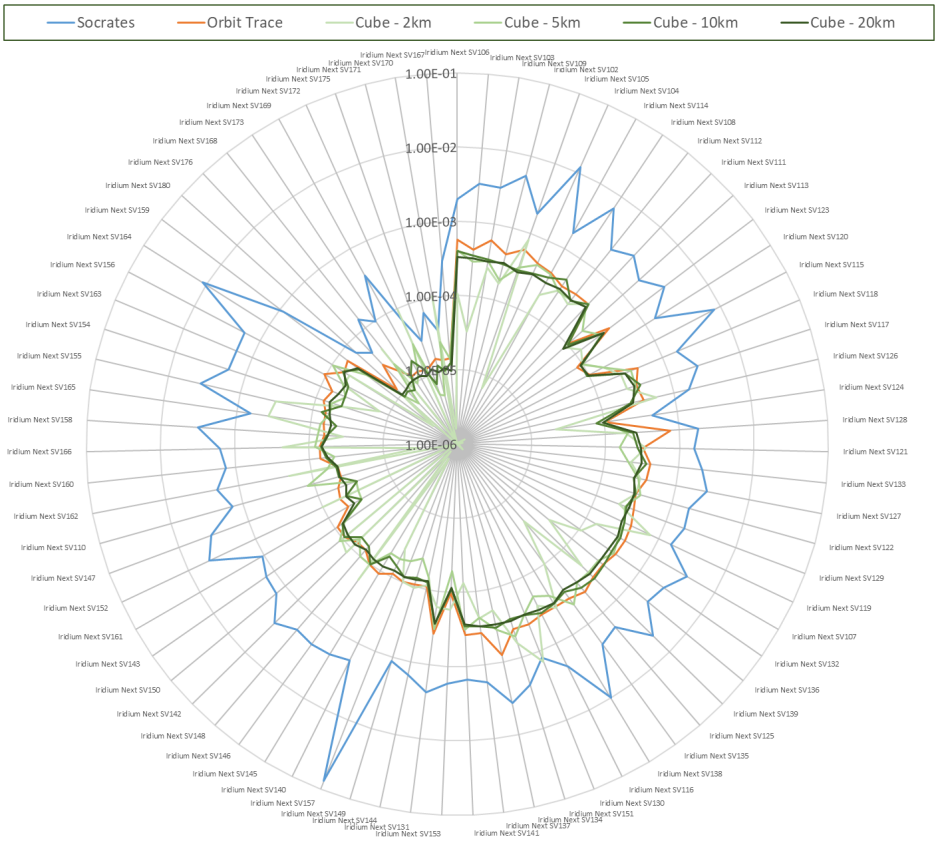

FIGURE 5.21: Collision probabilities from different methods for primary objects in the full Iridium Next scenario

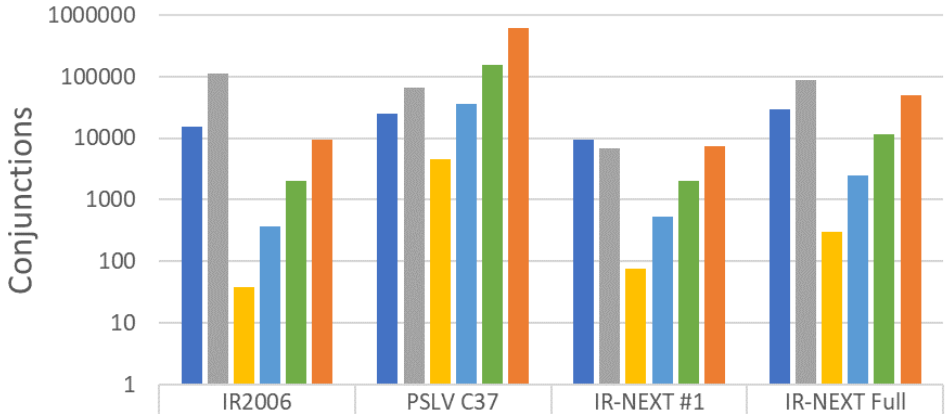

	IR2006	PSLV C37	IR-NEXT #1	IR-NEXT Full
Socrates	15091	24883	9553	29736
Orbit Trace	112747	65863	6735	88714
CUBE 2	37.3	4631.5	75	295.2
CUBE 5	372.8	35418.5	525.5	2493.8
CUBE 10	2045.5	154769	2047.2	11430.2
CUBE 20	9418	624217	7421.5	50261.7

FIGURE 5.22: Comparison of the NewSpace collision simulation conjunctions

TradSpace scenarios this difference was on the order of five to ten times, for the NewSpace scenarios the SOCRATES probabilities were ten to one hundred times greater. This indicated that there was a material difference to using these models for TradSpace cases versus NewSpace cases.

However, in Figure 5.18 (showing the results of the Iridium 2006 scenario) different results were seen. While there was consistency between the collision probabilities predicted by different cube sizes ($\sim 2 \times 10^{-4}$) the probabilities were around 20% the values generated using Orbit Trace ($\sim 1 \times 10^{-3}$). This discrepancy between the models indicated that one of the models was not capable of appropriately dealing with the scenario.

The Cube simulations failed to identify any conjunctions for around half of the primary population in contrast to the Orbit Trace method which generated collision probabilities for all of the primary objects. The results reported for the SOCRATES system for the Iridium 2006 scenario were also variable, with few conjunctions and very low, or no collision probability for some of the objects over the simulation period. To highlight the discrepancy seen for the Iridium 2006 scenario the results in Figure 5.18 were ordered according to the SOCRATES probability. Figure 5.18 shows that the objects which the Cube method did not identify conjunctions were consistent with the objects with low SOCRATES collision probabilities while the Orbit Trace method resulted in collision probabilities in excess of the SOCRATES maximum collision probability. On the balance of the evidence the Orbit Trace method is not capable of capturing the nature of the system present in this scenario and as a result is over estimating the collision probabilities for several of the spacecraft.

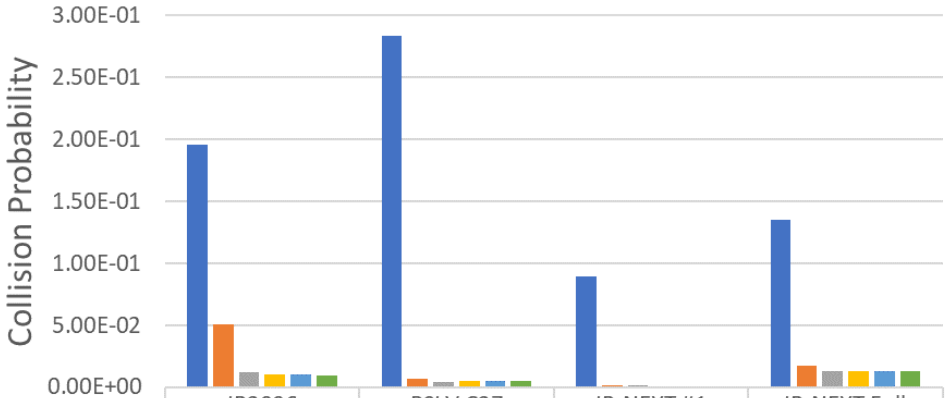

	IR2006	PSLV C37	IR-NEXT #1	IR-NEXT Full
Socrates	1.95E-01	2.84E-01	8.92E-02	1.35E-01
Orbit Trace	5.06E-02	6.34E-03	1.08E-03	1.69E-02
CUBE 2	1.23E-02	4.24E-03	1.07E-03	1.28E-02
CUBE 5	1.03E-02	4.62E-03	8.56E-04	1.29E-02
CUBE 10	1.05E-02	4.79E-03	9.35E-04	1.32E-02
CUBE 20	9.68E-03	5.16E-03	9.30E-04	1.25E-02

FIGURE 5.23: Comparison of the NewSpace collision simulation probabilities

Figures 5.22 and 5.23 show the number of conjunctions and combined collision probabilities respectively for the simulations of the NewSpace scenarios. As before, when using this sampling rate the closest match to SOCRATES in terms of number of conjunctions was the 20 km cube for every scenario except PSLV C37, where the 10 km cube is a better fit. Again the 2 km cube did not identify a sufficient number of conjunctions to provide a robust estimate of the collision probability for any scenario except PSLV C37. However, given the consistency of the collision probabilities calculated with the larger three cube sizes confidence was gained that the choice of cube size is not a major issue in modelling NewSpace, provided that an appropriate sample rate is used to generate a sufficient number of potential conjunctions.

The collision probabilities calculated using the Orbit Trace method were up to 50% greater than those generated by the Cube (with the exception of the Iridium 2006 scenario, where the Orbit Trace results were 469% greater on average). This was consistent with the results seen for the TradSpace scenarios. However, the differential between SOCRATES and the results of the two collision models ranged from a factor of ten to a factor of one hundred. When compared to the differential of five to ten times that was seen for the TradSpace cases this indicates that the collision algorithms are under-estimating the collision probabilities of the NewSpace scenarios. This implies that the impact of the spatial structure on the collision geometries is resulting in collisions being more likely and that this is not being captured in either the Orbit Trace or Cube algorithms. For the Cube algorithm this also suggests that any sampling bias due to the identification of conjunctions where collisions are not physically possible was not a significant factor, contradicting the original expectation.

5.5.2 Investigating Trends in the Results

Having identified a discrepancy between the collision probabilities of the TradSpace and NewSpace scenarios relative to the SOCRATES data, the results of eight scenarios were compared directly to establish the nature of any trends. As the collision probabilities for each of the scenarios was calculated based on the conjunctions of a different number of primary objects it was first necessary to normalise the results.

In Equation 5.15 the cumulative collision probability was calculated as the product of the inverse collision probabilities of each conjunction. As such the normalisation was achieved by taking the geometric mean of the inverse collision probabilities to give the average contribution to the collision probability from a single object:

$$P_{collision-normalised} = 1 - (1 - P_{collision})^{1/n} = 1 - (\prod_{i=1}^{n}(1 - p_i))^{1/n} \tag{5.16}$$

where n is the number of primary objects. Figure 5.24 shows the resulting collision probabilities of the different scenarios for each of SOCRATES, Orbit Trace, and Cube (averaged over the 5 km, 10 km and 20 km configurations).

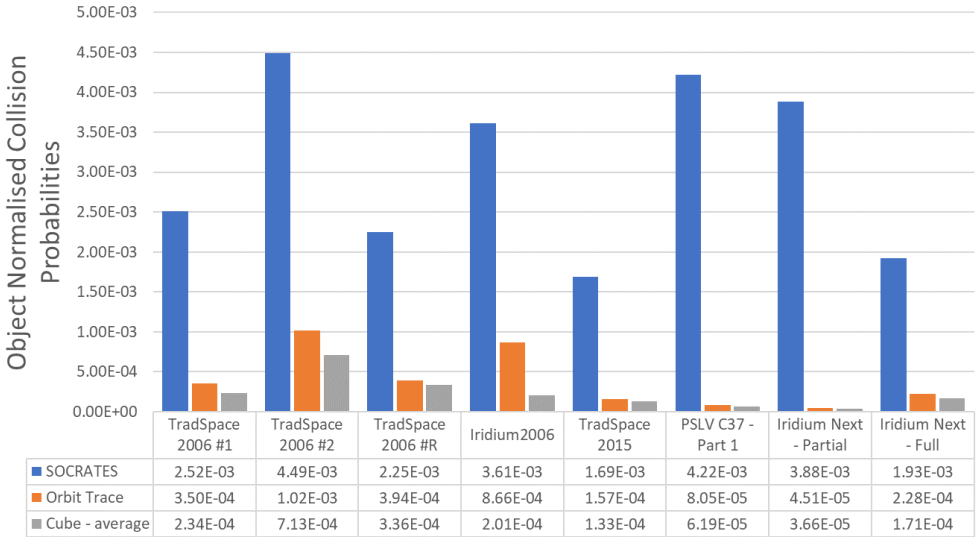

	TradSpace 2006 #1	TradSpace 2006 #2	TradSpace 2006 #R	Iridium2006	TradSpace 2015	PSLV C37 - Part 1	Iridium Next - Partial	Iridium Next - Full
SOCRATES	2.52E-03	4.49E-03	2.25E-03	3.61E-03	1.69E-03	4.22E-03	3.88E-03	1.93E-03
Orbit Trace	3.50E-04	1.02E-03	3.94E-04	8.66E-04	1.57E-04	8.05E-05	4.51E-05	2.28E-04
Cube - average	2.34E-04	7.13E-04	3.36E-04	2.01E-04	1.33E-04	6.19E-05	3.66E-05	1.71E-04

FIGURE 5.24: Collision simulation results normalised by the number of primary objects.

After applying this normalisation to the different collision probabilities there was still a clear differential between the NewSpace and TradSpace scenarios. The average of the collision probabilities for the NewSpace scenarios was 8.93% of the average SOCRATES probability for Orbit Trace and 3.45% for Cube compared to 17.53% and 12.94% respectively for the TradSpace scenarios. As the SOCRATES data is being used to provide a baseline for this investigation it is this relation between the SOCRATES probabilities and the results of the model that is primarily of interest when looking for trends in the data. A new metric was calculated to show the Cube and Orbit Trace results as a proportion of the SOCRATES maximum collision probability.

The different probability proportions are compared in Figure 5.25 alongside the values of the sum squared deviation from the mean (SSDM) previously calculated for each scenario. This allowed the deviation of the model results from SOCRATES to be compared against a measure of the spatial structure.

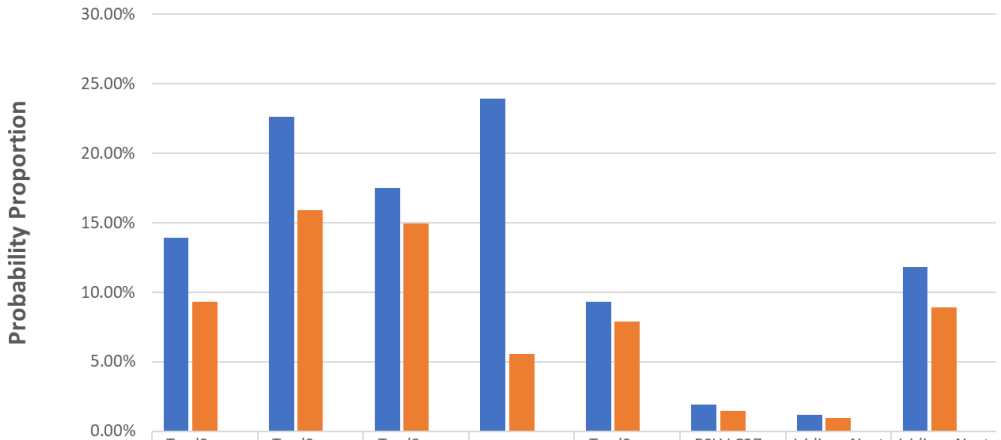

	TradSpace 2006 #1	TradSpace 2006 #2	TradSpace 2006 #R	Iridium2006	TradSpace 2015	PSLV C37 - Part 1	Iridium Next - Partial	Iridium Next - Full
Orbit Trace	13.93%	22.64%	17.52%	23.95%	9.29%	1.91%	1.16%	11.82%
Cube - average	9.31%	15.88%	14.93%	5.56%	7.87%	1.47%	0.94%	8.89%
SSDM	1.608E-04	2.005E-04	1.823E-04	1.992E-04	2.436E-04	2.621E-04	4.363E-04	2.846E-04

FIGURE 5.25: Collision simulation results relative to SOCRATES

Comparing these results it can be seen that the scenario with the highest value SSDM (4.36×10^{-4} for the partial Iridium Next scenario) corresponds to the lowest probability proportions of the SOCRATES maximum collision probability (1.162% and 0.943% for the Orbit Trace and Cube models respectively).

This relationship is further explored in Figure 5.26 which plots the log of the probability proportion against the SSDM. The decision was made to compare the probability proportion in log space based on the expectation that it would approach zero asymptotically as it is not possible for the proportion to pass zero. Fitting linear trend-lines through the data points resulted in R^2 values of 0.606 and 0.670 for the Orbit Trace and Cube results respectively. The key data points in this trend were those of the Iridium Next - partial scenario, to the right of Figure 5.26, which had substantial effect on the relationship.

To investigate the correlation, the PCC was calculated for the results of the collision models against the SSDM. This gave values of $r = -0.818654969$ for the results of Orbit Trace and $r = -0.778462302$ for the averaged results of the Cube configurations. These values show that there exists a strong negative correlation between the SSDM and the log of the probability proportion for the results of both collision models[2].

The relationship indicates that the change in the log of the SOCRATES maximum collision probability is proportional to the level of clustering. This deviation points

[2]Values of the PCC range from $+1$ for the strongest positive correlation to -1 for the strongest negative correlation. Correlations are normally considered to be strong for values of $r > 0.7$(Overholser and Sowinski, 2008).

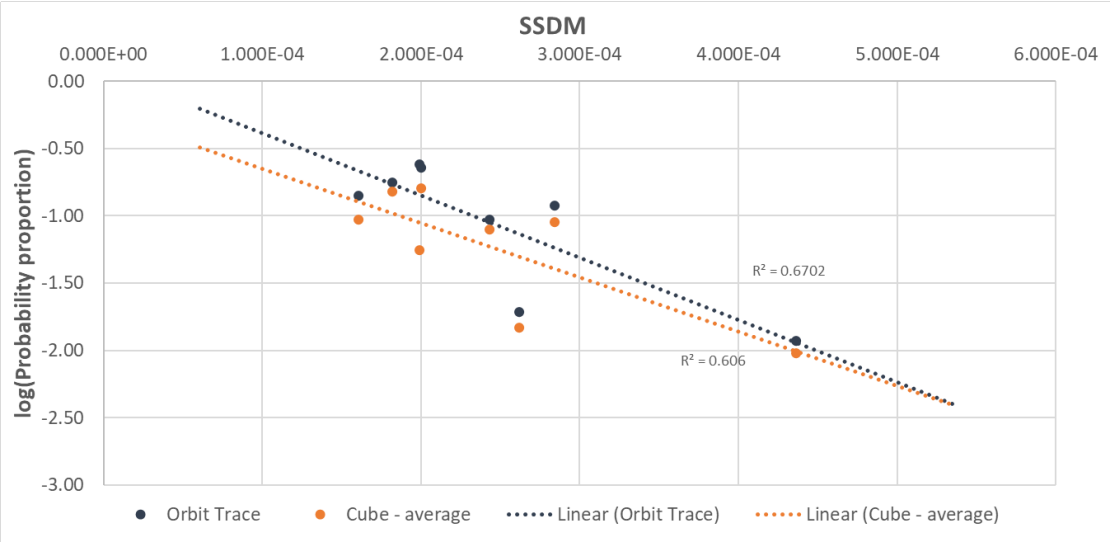

FIGURE 5.26: Trend in collision probability as a proportion relative to SOCRATES as a function of the SSDM of the spatial density.

towards a systemic under-prediction by the Cube and Orbit Trace algorithms for the collision probabilities of objects in orbital configurations with high spatial organisation.

5.5.3 Comparison to Expectations

The investigation into the assumptions of the Orbit Trace and Cube collision algorithms identified several areas as having the potential to impact the accuracy of the results. The initial investigation into the Cube method also identified that the rate of convergence and the overall collision probability of the test case was dependent upon the choice of cube size.

For smaller cubes a greater number of samples was required for convergence and the collision rate decreased proportionally with decreasing cube size. However, a comparison of different approaches for the more restricted case of spacecraft in Earth orbit showed consistency between the total collision probabilities when using each of the Orbit Trace and Cube methods at a level several orders of magnitude below that reported by SOCRATES.

Looking specifically at NewSpace systems there are several issues when applying the Cube algorithm. In particular, when modelling large constellations there are issues with the approach of sampling from the mean anomaly. This randomization of the position is not consistent with the structured relationship of the constellation orbits. It was also hypothesised that the increase in spatial structure resulting from the rise of NewSpace would result in an mis-estimate of the collision probability due to the greater organisation resulting in a bias towards specific collision geometries and invalidating the assumption of molecular chaos utilised in both the Cube and Orbit

Trace models. The results of this investigation showed that, for these scenarios, this mis-estimate manifested as a relative decrease in predicted collision probability (relative to SOCRATES) for scenarios with greater spatial structure.

Making the assumption that the differences in probability proportion are caused by errors which arise when the collision models are applied to the NewSpace scenarios, the interpretation of these results is that the Cube and Orbit Trace models both under-predict the collision probabilities of NewSpace systems. However, some alternative explanations are possible if the assumptions made are incorrect. It is also possible that the probabilities for the TradSpace cases are under-predicted by the models, or that the SOCRATES predictions used as a baseline are over-predicting the collision probabilities of the NewSpace cases.

Nonetheless, this discrepancy has the potential to result in long term impacts on the accuracy of simulations of the debris environment. The existence of this deviation between the results for the NewSpace and TradSpace scenarios is in agreement with the hypothesis that ”NewSpace changes fall outside of the scope of current assumptions, reducing the accuracy of the existing component models of debris processes”.

5.6 The Consequences for Environmental Evolution

In this chapter the second key hypothesis of this work has been tested by examining the results of the Cube and Orbit Trace component collision models for scenarios which exhibit the orbital characteristics of NewSpace space systems. Impact on collision models was considered significant, as a change in which objects are likely to be involved in collisions could substantially alter how many, and at what altitude, fragments are generated. This, in turn, would impact the life-time of the fragments produced and the collision risk they pose to other objects.

An initial study highlighted that a choice between the two models was a balance of competing priorities. The Cube method scales better with increasing population size but requires many samples to provide an accurate estimate of the collision probability of an individual pair of objects, while the Orbit Trace algorithm exhibits poor scaling but a better instantaneous estimate of the collision probability. As such, the Cube algorithm, with its speed benefits over Orbit Trace, will be useful for studying the overall environmental hazard of future debris populations which might experience exponential growth. However, the Orbit Trace model might be a better option if the investigation is focussed on the collision risk being posed by, or to, an individual spacecraft or particular space systems, such as large constellations. As such it was important to understand the impact of NewSpace on both models.

The issues raised by the initial investigation created doubts about the applicability of the results of simulations of the debris environment. Further investigations, using both collision models highlighted a deviation between the TradSpace and NewSpace scenarios. The increased spatial organisation of the NewSpace scenarios was accompanied by a decrease in the magnitude of the collision probability relative to the maximum collision probability predicted by SOCRATES, indicating that the models under-predict the collision probability of NewSpace systems.

If this under-prediction is being made, then simulations of the environment using these models can be expected to predict fewer collisions than would occur in the real world debris environment. The absence of these collisions will likely result in slower predicted growth of the debris population, potentially to an exponential degree due to the absence of secondary collisions which could arise due to the fragments produced. As such, this under-prediction of the collision probability could result in debris modelling research giving a falsely optimistic view of the future environment and greatly under-estimate the risk posed by additional, highly structured, space systems such as planned large constellations.

Chapter 6

Impact on Environmental Evolution

> When we try to pick out anything by itself, we find it hitched to everything else in the universe.
>
> John Muir

6.1 Current Research into the NewSpace Environment

Studies of the impact of NewSpace on the future evolution of the debris environment are being conducted using the current generation of debris models. However, the investigations conducted in Chapters 4 and 5 identified specific limitations related to NewSpace in the underlying components of these debris models. In particular the models used to simulate fragmentations and to identify possible collisions are in need of updating to account for the discrepancies introduced by NewSpace.

It has been hypothesised that "Updates to models to incorporate the effect of NewSpace will change the current understanding of the future evolution of the debris environment". It is plausible that a next generational debris model might lead to substantially different conclusions than are currently being found. This idea is supported by the difference in results following the introduction of the NASA Standard Breakup Model that was identified by Beck (2013).

To understand the impact of updating these component models on the results of simulations, the key foci of current evolutionary debris modelling research must be examined. The current state of debris modelling research was discussed in Chapter 3. The four key areas of current research into debris evolution which were identified were: the impact of different levels of debris mitigation measures; the effectiveness of different rates of ADR; the growing use of small satellites; and the introduction of large LEO constellations.

The studies of large constellations in particular were considered to be susceptible to the changes to models required to account for NewSpace and as one of the most high profile and recent areas of work, was identified as an appropriate focus for this chapter.

6.1.1 Constellation Studies using Existing Models

A considerable number of studies have been conducted to investigate the effects of large constellations on the evolution of the debris environment. These can be broadly divided into two categories, simulations of the debris environment over the long term with a shorter-lived generic constellation, and simulations which focus on the operational risk over the lifetime of a specific constellation.

The longer term simulations were run for projection periods ranging from 100 years (Kawamoto et al., 2018) to 250 years (Lewis et al., 2017b), with most opting for 200 years (Peterson et al., 2016; Virgili, 2016; Bastida Virgili et al., 2016a; Lewis et al., 2017a). Within these simulations constellations were operated for up to 50 years and the focus of the research was on the response of the environment to the introduction and removal of the constellations. This was generally measured by looking at environmental metrics, such as the total number of objects in LEO or the number of catastrophic collisions predicted by the models.

The simulations focussing on the constellations over their operational lifetime investigated the immediate collision risk of the constellations by looking at different metrics of the debris environment, including: the debris flux and collision probabilities experienced by constellation spacecraft (Radtke et al., 2017a); the number of collisions involving failed constellation spacecraft (Le May et al., 2018); and the increase in LEO collision rates due to the constellation (Pardini and Anselmo, 2020). These studies tended to have much shorter projection periods of 10-50 years and simulated constellations using the published details of planned systems such as OneWeb and SpaceX's Starlink.

In general the conclusions of these investigations were that large constellations would result in increased risk and debris population growth across the regions of the space environment in the vicinity of the constellations. The extent of the risk was dependent on the failure rate of the constellation and could be mitigated with an appropriate level of post-mission disposal to reduce residual lifetimes. However, the validity of these results and their assessment of the risk involved is dependent upon whether the debris models used are suitable for answering these questions.

6.2 Adjusting for NewSpace

Having identified that updates to component models are required the purpose of this investigation was to test the sensitivity of simulations of the NewSpace environment to NewSpace updates to the component models. This testing enabled the assessment of the hypothesis that NewSpace updates will impact on the current understanding of the future evolution of the debris environment for NewSpace scenarios. Based on the investigations detailed in Chapters 4 and 5 empirical adjustments were made to the existing component models in order to correct for the errors identified. Due to the limited amount of data available to create and validate the new component models, the adjusted models were prototypes and not optimised for general use. However, they provided a useful tool for investigating specific NewSpace scenarios and gave an indication of the direction and scale of the required updates enabling an exploration of possible impacts.

6.2.1 Fitting Alternative Fragmentation Models

The results of the NASA Standard Breakup Model in Chapter 4 identified that the model did not fit well with the fragment size distribution for observed collisions and satellite explosions. The results of the comparisons made were used to create an adjusted version of the breakup model which would better fit these results. A limitation present when developing this adjusted model was the restriction of fragment size data to the three RCS categories available on Space-Track. This restriction resulted in a risk of over-fitting the model. Future work could look to refine the model using data with greater resolution to avoid this problem.

Using key characteristics for modelling breakups based on the analysis conducted in Chapter 3, updated equations for payload explosions and collisions were formed for the distribution of fragments by characteristic length. These equations were formed empirically using an initial guess followed by an iterative method of adjusting the parameters and testing the goodness of fit of the modelled number of fragments against observed results.

For the explosion of payload spacecraft a comparison was made against observed numbers of different sized fragments from the breakups of NOAA-16, DMSP-F13, and Cosmos-2241. The spacecraft mass was used to scale the total number of fragments (as was already the case for collisions) and normalised to 800 kg based on the mass range for spacecraft of $600 - 1,000$ kg assumed in the original model. In Chapter 4 the magnitude of the fitted exponent for these breakups varied from -2.1802 to -2.4068. As such the magnitude of the exponent applied to the characteristic length in the equation was increased to a base value of -2. Experimentation identified a function of the area-to-mass ratio as providing a suitable further modification to the exponent.

This resulted in a relative prioritisation of smaller fragments over larger ones. The new version of this equation is:

$$N(> L_C) = 0.1\frac{M_{target}}{800} \times L_C^{-2-\frac{0.1}{\sqrt{\sigma}}} \tag{6.1}$$

where σ is the area-to-mass ratio of the spacecraft.

To test the goodness of fit of this equation a reduced chi-squared statistic was calculated for the number of fragments of different sizes in each scenario. As the relationship is a power law the calculation of this statistic was made based on log(N) to equally weight the deviations at different orders of magnitude. These results of this testing (summarised in Table 6.1) were an average value across the scenarios of $\chi^2 = 0.970$ for the adjusted model compared to $\chi^2 = 0.652$ for the original model, demonstrating a better fit to the observed data.

TABLE 6.1: A table of the goodness of fit of the different payload explosion models.

	Parent Body	**Number of Fragments**			**log(N)**			χ^2
		Large	**Medium**	**Small**	**Large**	**Medium**	**Small**	
Observed	NOAA-16	1	3	455	0	0.477	2.658	
	DMSP-F13	1	1	238	0	0	2.377	
	Cosmos-2421	1	10	498	0	1	2.697	
Original Model	NOAA-16	3.757	23.590	238.854	0.574	1.373	2.378	**0.699**
	DMSP-F13	3.757	23.590	238.854	0.574	1.373	2.378	**0.412**
	Cosmos-2421	3.757	23.590	238.854	0.574	1.373	2.378	**0.846**
New Model	NOAA-16	1.070	3.528	231.251	0.0295	0.547	2.364	**0.977**
	DMSP-F13	1.037	2.901	268.649	0.016	0.463	2.429	**0.942**
	Cosmos-2421	1.156	6.896	573.725	0.063	0.839	2.759	**0.991**

In each of the known collision events investigated in Chapter 4 the distribution of observed fragments by size revealed more smaller fragments and fewer larger fragments indicating a more negative exponent for the equation with fitted exponents of -2.8752, -2.4736 and -3.1372. The adaptation was made to use a base value of -2 for the exponent with an additional term based on the characteristics of the collision event. Empirical experimentation with the model identified a possible version of this additional term as the reciprocal of the logarithm of the energy-to-mass ratio of the collision. The fact that this collision characteristic is already used to distinguish between catastrophic and non-catastrophic collisions supports the rationale that it may be important to the fragment size distribution. The resulting adapted equation can be seen in Equation 6.2:

$$N(> L_C) = 0.02\, M_{ejecta}^{0.75} \times L_C^{-2-\frac{4}{log(\psi)}} \tag{6.2}$$

where ψ is the energy-to-mass ratio of the collision and M_{ejecta} is the ejecta mass.

The equation governing the distribution of fragments by size for collisions already incorporated the spacecraft mass. The relationship to the mass was maintained while the leading coefficient was adjusted to scale the total number of fragments produced using the observed distributions of the different events.

TABLE 6.2: A table of the goodness of fit of the different collision fragmentation models.

	Parent Body	Number of Fragments			log(N)			χ^2
		Large	Medium	Small	Large	Medium	Small	
Observed	Cosmos-2251	1	29	1668	0	1.462	3.222	
	Iridium-33	1	24	628	0	1.380	2.798	
	Fengyun-1C	0	34	3408	-1	1.531	3.533	
Original Model	Cosmos-2251	9.962	70.980	842.717	0.998	1.851	2.926	**0.763**
	Iridium-33	6.942	49.461	587.227	0.841	1.694	2.769	**0.794**
	Fengyun-1C	9.544	68.002	807.354	0.980	1.833	2.907	**0.573**
New Model	Cosmos-2251	1.420	38.188	2416.434	0.152	1.582	3.383	**0.988**
	Iridium-33	1.010	25.020	1426.612	0.00464	1.398	3.154	**0.967**
	Fengyun-1C	1.348	37.574	2487.268	0.130	1.575	3.396	**0.874**

The tests of the goodness of fit of this adjusted model (summarised in Table 6.2) resulted in average values across the scenarios of $\chi^2 = 0.943$ for the adjusted model compared to $\chi^2 = 0.710$ for the original model, which indicates an improvement to the fit to the observed data.

Figures 6.1 and 6.2 show the results generated when using the new adaptations of the model to repeat the simulations of the breakups originally shown in Figures 4.4 and 4.6.

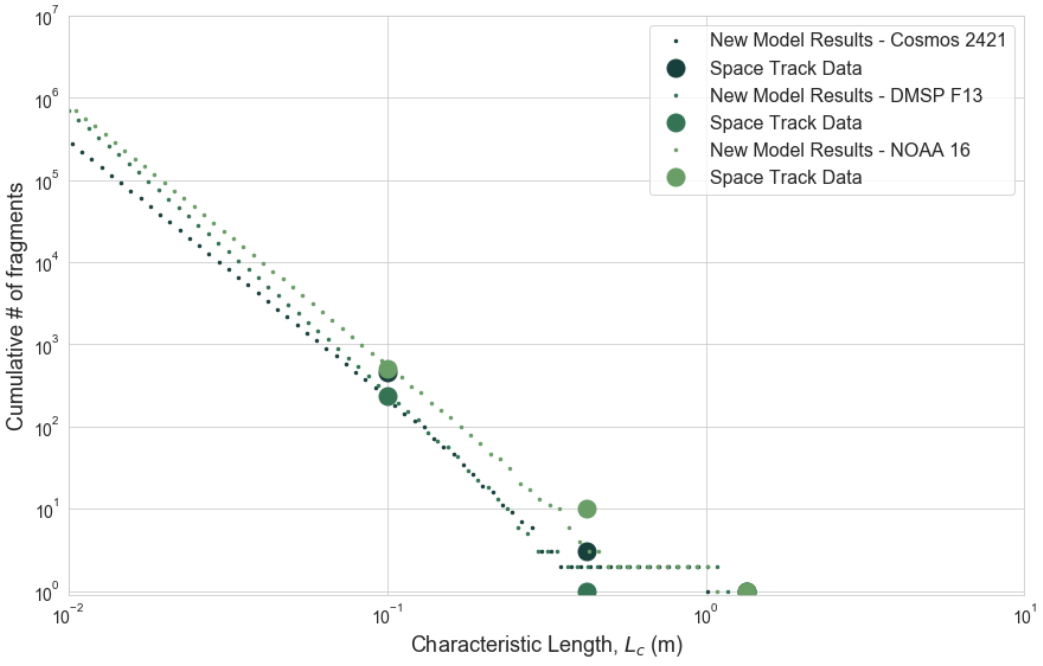

FIGURE 6.1: Comparison of the adjusted fragmentation model against the observed debris fragments for satellite explosions events.

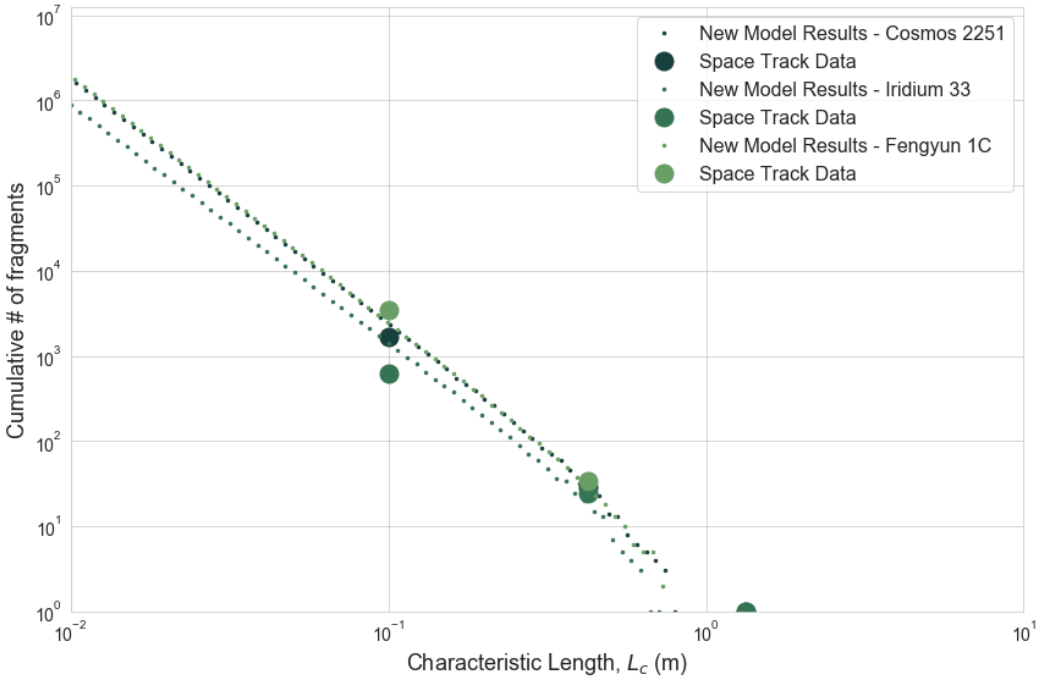

FIGURE 6.2: Comparison of the adjusted fragmentation model against the observed debris fragments for collision events.

For both the explosion scenarios and the collision scenarios the adapted equations generated fewer larger fragments, resulting in a closer fit to the observed number of medium fragments (> 0.425 m). The decrease in larger fragments was accompanied by an increase in the number of small fragments. The amount of fragments larger than 10 cm increased from around $10,000$ to more than $500,000$ for the explosion scenarios and from less than $50,000$ to more than $1,000,000$ for the collision scenarios.

6.2.2 Correcting Collision Probability

In Chapter 5 a relationship was observed between the collision probabilities and the spatial structure of space systems, quantified through the distribution of the normalised spatial density of the population. An empirical adaptation of the Orbit Trace and Cube collision algorithms was developed to remove this effect. As there is currently insufficient information to determine what the correct collision probabilities were for the scenarios modelled in Chapter 5 the corrections applied may not be optimal but the adjustment allowed the identified NewSpace bias to be removed.

A correction factor was developed empirically for each of the Orbit Trace and Cube models based on the results generated in Chapter 5 which would remove the observed correlation between the SSDM and the log of the probability proportion relative to SOCRATES. The adjustment was applied to the collision models by multiplying the individual collision probabilities calculated at each time-step for the primary populations by the correction factor calculated for that scenario:

$$P_{Corrected} = CP_{Original} \tag{6.3}$$

where C is the correction factor and P is the probability proportion relative to SOCRATES.

The first step in forming an equation for the correction factor was to identify the coefficients of the trend lines fitted to the data points in Figure 5.26. These trends are described by Equations 6.4 and 6.5 for Orbit Trace and Cube respectively:

$$log(P) = -4634.4(S) + 0.0793 \tag{6.4}$$

$$log(P) = -4025.2(S) - 0.249 \tag{6.5}$$

where S is the value of the sum squared deviation from the mean (SSDM) of the spatial density.

The correction terms were scaled towards a fixed probability proportion of 15% of the SOCRATES maximum collision probability which was the average probability proportion of the TradSpace scenarios. Using this and rearranging Equations 6.4 and 6.5 resulted in Equations 6.6 and 6.7 for the Orbit Trace and Cube correction factors:

$$C = 0.15 \times \frac{1}{10^{-4634.4(S)+0.0793}} \tag{6.6}$$

$$C = 0.15 \times \frac{1}{10^{-4025.2(S)-0.2497}} \tag{6.7}$$

where S is the value of the SSDM for the scenario.

This adaptation to the models was then tested by applying the correction factors to the output of the simulations run for the eight scenarios in Chapter 5. Using the full Iridium Next scenario as an example the correction factor was calculated to be 2.6039 for Orbit Trace and 3.7262 for Cube based on an SSDM of 0.00028457. Figure 6.3 compares the per object collision probabilities with and without the application of the correction factor.

Figure 6.4 shows how the results in Figure 5.26 change after using the correction factors to scale the collision probability of each identified conjunction event for the primary population.

The results of the figure and the lines fitted showed that the trend had been eliminated from the data. To quantify the new relationship the individual data points were again used to calculate the Pearson Correlation Coefficients for the two data sets giving value of -0.0001399 for the Orbit Trace data, and -0.0015430 for the Cube data. This indicates that the adaptation has successfully removed the correlation.

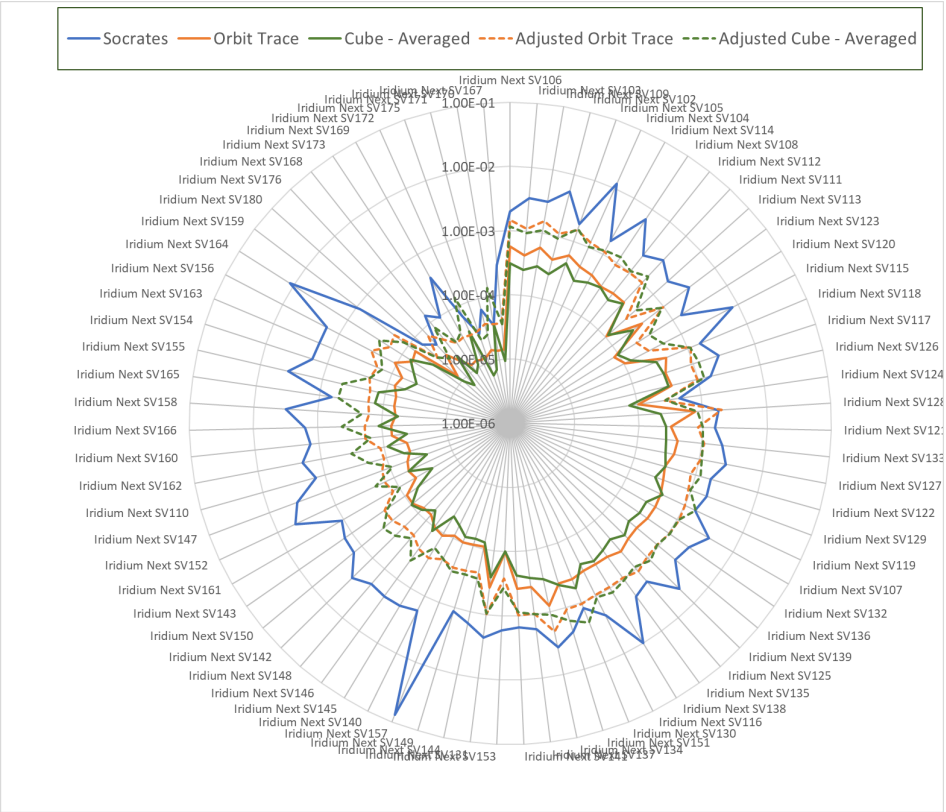

FIGURE 6.3: Comparison of collision probabilities from different methods before and after applying the correction factor for primary objects in the full Iridium Next scenario

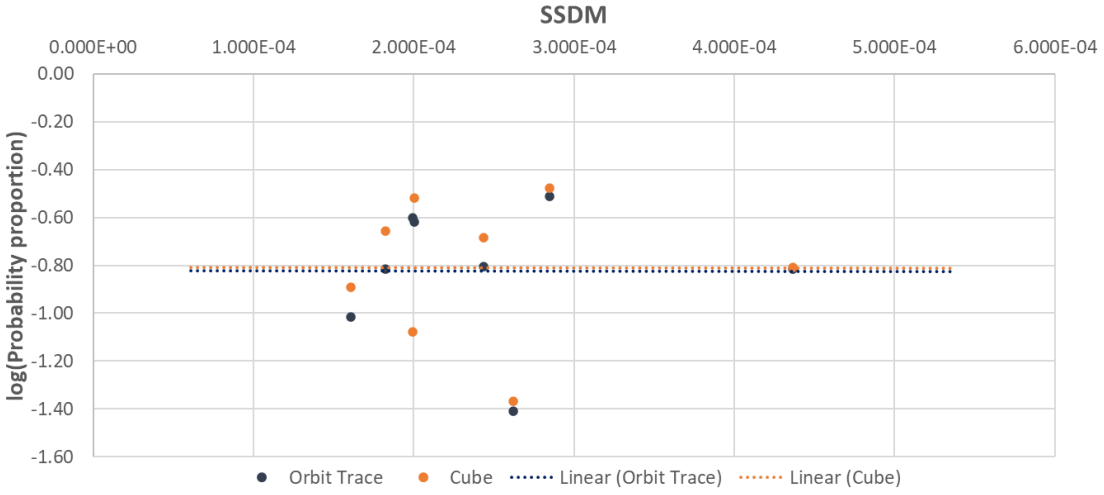

FIGURE 6.4: Trend in corrected collision probability as a proportion relative to SOCRATES as a function of the SSDM of the spatial density.

6.3 Simulating a NewSpace Environment

Simulations of a NewSpace debris environment were performed using both state-of-the-art component models and modified versions of the models which attempt to represent how the results might change when NewSpace is accounted for.

This provided a means of quantifying the severity of the identified model limitations on the assessment of constellations.

6.3.1 A NewSpace Environment

It was first necessary to define a spacecraft population which represented a NewSpace environment. As the introduction of large LEO constellations had been identified as one of the key areas of current research into NewSpace, it was determined that the core of this population should be a fully deployed large satellite constellation in LEO.

The two constellations most commonly referenced in the research were OneWeb and SpaceX's Starlink. The Starlink constellation was selected as the most relevant as this had reached a more advanced stage of deployment, with more than one thousand operational satellites at the time of writing. The version of the Starlink constellation implemented for these simulations was based on SpaceX's filing with the FCC in April 2020 (Space Exploration Holdings LLC, 2020) for 4408 spacecraft orbiting at altitudes from 540-570 km.

These 4,408 satellites were distributed across five different orbital shells, described in Table 6.3. When generating the initial orbital elements for this population the spacecraft in each orbital plane were distributed across each orbit by equally spacing their mean anomalies between zero and τ. For the first four components of the constellation the different orbital planes were separated by assigning each plane a defined RAAN and distributing the RAAN of the planes between zero and τ. However, the fifth component of the constellation is intended to provide additional capacity to highly populated regions rather than global coverage. As such, rather than the four planes being evenly distributed in RAAN they are grouped as four neighbouring planes out of 30 virtual planes, offset, so that the first plane starts with a RAAN of 1.32 radians (75.7°).

TABLE 6.3: Components of the Starlink constellation.

Component	**Altitude**	# Orbital Planes	# Satellites per Plane	Inclination
1	540	72	22	53°
2	550	72	22	53°
3	570	36	20	70°
4	560	6	58	97.6°
5	560	4	43	97.6°

The simulation scenario developed based on these parameters consisted of the evolution of the planned 4,408 Starlink spacecraft over a 25 year period with each starting the simulation active and deployed into the described target orbits. The Starlink satellites are modelled in these simulations as having a mass of 260 kg, diameter of 3.35 m and average cross section of 8.84 m^2. These parameters are based

on the assumption of a flat-body design roughly 3 x 1.5 m (McDowell, 2020) where the diameter is calculated as the diagonal ($D = \sqrt{3^2 + 1.5^2}$) and the cross section is calculated as the area of a circle with this diameter ($A = \pi D^2/4$). In addition to the defined constellation population, a background population was initialised consisting of the spacecraft, rocket bodies and debris objects known to be in orbits in the vicinity of the constellation

Background Population

The background population was derived from a reference population of objects provided by ESA which, as of 1st February 2018, were in LEO-crossing orbits and had diameter greater than or equal to 10 cm. This population was then filtered to include only objects with mass $\geq$ 1 kg and either perigee altitude $\leq$ 580 km (i.e. approaches within 10 km of constellation altitude), or, perigee altitude $\leq$ 700 km and apogee altitude $\leq$ 2000 km (i.e. LEO resident with a chance of decaying through the constellation).

The resulting population of 4183 objects consisted of 1263 payload spacecraft, 660 rocket bodies, and 2260 mission related objects and debris fragments.

Launch Rate Model

The ESA reference population also included launch dates for objects deployed between the start of 2010 and the end of 2017 allowing the use of a repeating eight year launch cycle. However, for the sake of simplicity launch traffic was omitted from the simulations conducted in this investigation. This avoided the added complexity of considering the operational life of spacecraft and any end-of-life manoeuvres required to vacate target orbits. While the use of a launch traffic model might be more representative of the real world environment this was deemed unnecessary for this study where the aim was to make comparisons between simulations run under the same set of assumptions.

6.3.2 An Integrated Debris Model

Running simulations of this environment required the use of a debris model capable of projecting the future evolution of the environment. The major components of this model were identified in Chapter 2 as the models of fragmentation, collision prediction and propagation. As a result the individual component models implemented in Chapters 4 and 5 could be used for this new debris model.

This allowed the debris model to be developed as a configurable framework where different versions of the component models could be selected and configured as

required for a specific simulation. When running a simulation, the framework would load a simulation population from specified environment and background population files and evolve the population over the defined projection period using a specified time-step. Figure 6.5 outlines the logical flow of the evolution of the environment and where the different components are utilised.

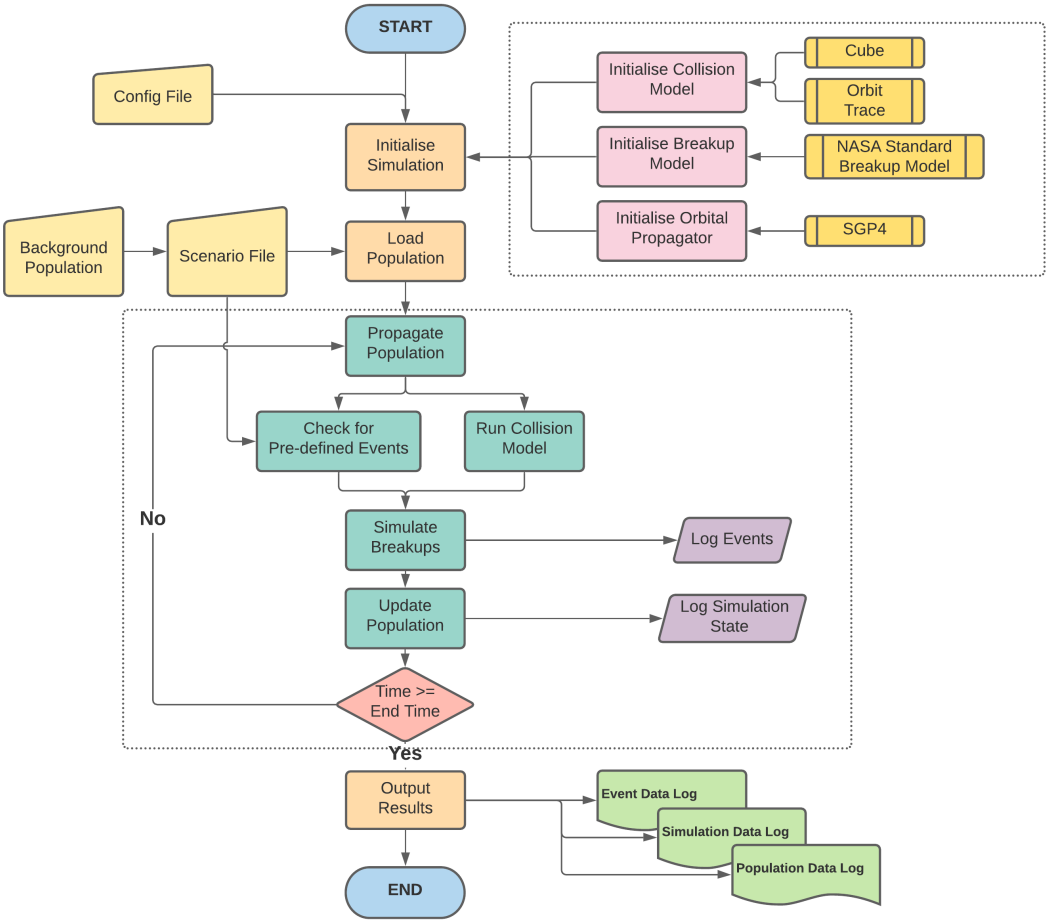

FIGURE 6.5: Logical steps of environmental evolution.

Three different output files were created to log the results of the simulations. A simulation data log recorded the state of the environment at each of the time-steps across the projection period, including information on the current number of objects of each type (upper stages, spacecraft, or debris) and the cumulative number of events (explosion, collision, and collision avoidance manoeuvres). Each of these events was then recorded in an event log with specific information on the specific event, e.g. the event epoch, the type of event, which objects were involved and the relative velocity. At the end of the simulation population data was recorded about all of the objects, both original and generated by fragmentations, including those which had been removed from orbit. This log included information on each of the objects, such as the object type, mass, and lifetime collision probability, as well as any information on the events related to the production or destruction of the object (e.g. the parent fragmentation event or the time of decay).

One of the key features of this framework was the ability to introduce defined fragmentation events to the environment. These events could be configured within the environment population files and allowed the collision between two objects, or the explosion of a specific object, to be triggered at a pre-determined point after the start of the simulation. This was implemented to enable the investigation of the impact of an event on the environment using different model configurations.

The Fragmentation Model

The fragmentation component model used was the implementation of the NASA Standard breakup Model created in Chapter 4. For these simulations the model was configured to use a minimum fragment length of 0.01 m, a threshold for catastrophic collisions of 40 J/g, a scaling factor of one, and the weighted bridging function described in Chapter 4 for the intermediate size region. Representative fragments, where multiple generated fragments are represented by a single object in the simulation, were used for fragment sizes below 0.05 to reduce the computational load from large numbers of small fragments. This reduced the number of individual objects which were handled by the processing steps in the model (with the number of representative fragments scaling dynamically with the number of fragments predicted at that size).

In addition, after simulating the fragmentation, only objects with a mass of greater than ten grams were added to the debris population. This mass limit helped to provide a more meaningful estimate of the overall collision probability by removing the contribution of the smallest debris objects which result in less severe impacts. An added benefit was the preservation of computational memory and the limiting of the number of objects to be considered in propagation and collision prediction.

The Collision Models

Both the Cube and Orbit Trace collision algorithms implemented in Chapter 5 were integrated for use as the collision module within the debris framework. In terms of configuration it was found that an enhanced collision radius was not required when using the Orbit Trace algorithm, while simulations conducted using the Cube method were made using a cube size of 10 km, in-line with most previous studies of the debris environment.

For the 25 year period of the Starlink simulation scenario a five day time-step was used for the simulations made with Orbit Trace, corresponding to 1862 samples. However, it was determined that this was an insufficient number of samples to use with the Cube method when attempting to understand the specific collision risk to an individual constellation spacecraft. A one day time-step was used to increase the

number of samples in time to 9131 and this was further increased by using the artificial enhancement of cube samples of taking one hundred evaluations of the cube at each step.

The Orbital Propagator

As in the collision environment simulation conducted in Chapter 5 the orbital propagator used within the debris framework was the analytical SGP4 propagator. Simulations were run with the propagator configured to use the improved ops mode and the 'wgs72' gravitational model.

The SGP4 propagator utilises a value known as B^* when modelling the effect of atmospheric drag to the debris objects. For these simulations it was necessary to calculate this value for the different objects using the following equation:

$$B^* = \frac{\rho_0 C_d A}{2m} \tag{6.8}$$

where ρ_0 is the reference air density, C_d is the drag coefficient of the spacecraft, and A and m are the cross sectional area and mass of the spacecraft respectively.

Within the integration of the propagator used in the debris framework a value of 2.2 was used as the drag coefficient for all spacecraft and the reference air density is taken to be 0.1570 $\mathrm{kg}/(\mathrm{m}^2\mathrm{R}_E)$ where R_E is the Earth's radius.

6.3.3 Assumptions and Expectations

The first assumption, as described above, was to assume no new launches occurred over the projection period. This assumption served to limit the total number of objects being processed by the model. Direct de-orbit at end of life and a like for like replacement of active spacecraft was assumed which was modelled as all intact payload spacecraft remaining active and in their target orbit for the duration of the simulation. This was achieved by setting the B^* value of every active spacecraft to be zero in order to remove the effect of atmospheric drag and solar radiation perturbations from the propagation of their orbits. All rocket bodies and debris objects were considered to be inactive and incapable of manoeuvring.

While all active payload spacecraft were assumed capable of manoeuvring to maintain their orbits and avoid collisions, this is not a realistic representation of the real orbital population. Many spacecraft at the low altitudes of the simulation, such as CubeSats, lack the propulsion system required to manoeuvre. The data for the background population does not provide enough detail to uniquely identify which of the payload spacecraft fall into this category, however, of the 1263 spacecraft 512 have a mass of less than or equal to 8kg which is consistent with a 6U or less CubeSat (Lee

et al., 2014). Although unrealistic this assumption simplified the simulations and will not have impacted the ability to compare between simulations.

It was also assumed that no spontaneous explosions or spacecraft failures would occur and so the only ways for a spacecraft to become inactive, or for new debris to be produced, were through defined breakup events or through a collision predicted by the model. These choices may result in a lower population of debris and spacecraft in the vicinity of the constellation when compared to a real world environment. However, it provided a consistent population of objects between the different simulations which allowed them to be compared effectively.

The one element of concept of operations which was partially implemented for these simulations was collision avoidance manoeuvres, which were deemed a requirement for simulating a constellation environment. Within this debris framework a collision probability threshold of 1×10^{-4} has been implemented as the minimum probability required to trigger a collision avoidance manoeuvre in line with current NASA recommendations (NASA, 2020). A manoeuvre is then considered possible only if both objects are greater than or equal to ten centimetres in length (i.e. both are considered to be trackable objects) and if at least one of the objects is active.

If all of these conditions are met then a collision avoidance manoeuvre is considered to have occurred with a 100% success rate and is logged as a distinct event. However, the manoeuvre itself is not actually simulated, instead the collision is determined not to have occurred and it is assumed that the spacecraft is returned to its original orbit and the orbital elements remain unchanged. The collision probability of the predicted conjunction is still included when calculating the lifetime collision probability of the two objects. No upper bound was placed on the number of manoeuvres which could be made by an active spacecraft based on the assumption of a direct de-orbit and like for like replenishment as required.

Including manoeuvres was expected to reduce the total number of collisions which occurred over the simulation by removing the majority of events which involved two intact spacecraft (i.e. the payload-payload and payload-rocket body cases) as the Starlink spacecraft make up more than half of the initial population. However, by the law of very large numbers collisions were still possible for events with low probabilities and, when considering a large number of low probability events, the cumulative probability can still be relatively high.

Identifying Invalid Collision Events

One issue that was identified with predicting collisions for the large constellation scenario was that a certain number of the potential collisions identified by the models would be invalid. This can occur as the Cube and Orbit Trace collision models are agnostic to the relative positions of the objects and are concerned only with the

orientation of the orbits and a random sampling of position along the orbit. As a result it was possible for the models to predict collisions between two spacecraft even when they were in the same plane of the constellation and effectively flying in formation resulting in a fixed mean anomaly separation. In the first component of the modelled Starlink constellation, for example, the separation between neighbouring spacecraft was 0.2856 radians.

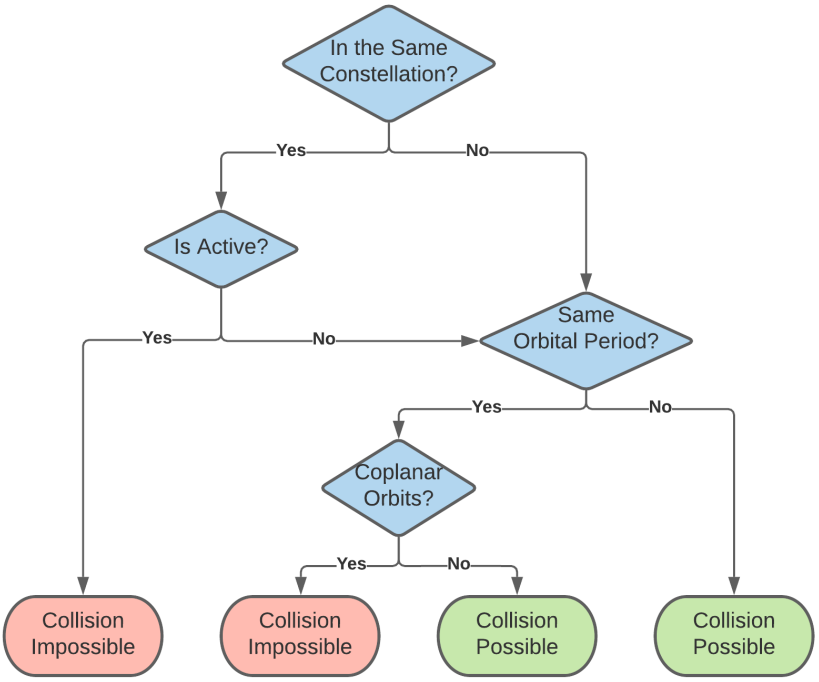

FIGURE 6.6: Diagram of the decision tree for identifying invalid collision events.

A decision tree (Figure 6.6) was implemented to distinguish between collisions which could be considered valid and those which were invalid. Invalid collision events were discarded and not included in the calculation of the lifetime collision probability of the objects. The primary decisions are made on whether the objects are active and part of the same constellation, in which case a collision is considered impossible. If the objects are not in the same constellation, or at least one is inactive, then a collision is considered possible as long as the two objects are not in the same plane with the same orbital period to within 1%. The Orbit Trace coplanar filter (Equation 5.6) is used to determine whether two orbits are coplanar. This includes reciprocal orbits, i.e. a prograde orbit with inclination 82° and a retrograde orbit with inclination 98° and a difference in Right Ascension of 180°. One consequence of this is that some possible head-on collisions may be incorrectly filtered out, however, situations where two objects are in reciprocal orbits and have the same orbital period are likely to be rare.

6.4 Defining the Simulations

The new debris modelling framework was used to simulate the evolution of the Starlink constellation scenario over a 25 year (9131 day) projection period from the 1st January 2018. Different configurations were chosen to cover the different possible events. This included multiple versions of the constellation scenario as well as different variations of the component models.

6.4.1 Simulation Scenarios

Three different scenarios were selected for this experiment using defined breakup events to allow the controlled study of the evolution of the environment using the different component model combinations. These scenarios consisted of:

1. The base scenario of the Starlink constellation
2. The constellation + a defined explosion event
3. The constellation + a defined collision event

Defined Explosion Event

The first of the modified scenarios involved the introduction of a defined explosion event. The explosion occurred 5 years (1826 days) from the beginning of the projection period.

Of particular interest was the consequence of an explosion on the spacecraft of the Starlink constellation, and so the exploding object for this scenario was one of the Starlink spacecraft in the second orbital shell of the constellation at 550 km (see Table 6.3).

Defined Collision Event

The second modified scenario included a defined collision event which again occurred 5 years from the beginning of the projection period. The motivation for this event was the close approach between ESA's Aeolus satellite with Starlink-44 on Monday 2nd September 2019 and the resulting collision avoidance manoeuvre (ESA, 2019).

As the original event occurred at a much lower altitude than the operational altitude of the Starlink constellation (Aeolus orbits at $\sim$320 km) an analogous spacecraft was created for this simulation. This Aeolus analogue had the same physical characteristics and orbital orientation as the Aeolus satellite (mass: 1366 kg; length: 2.828 m; inclination: 97°), but orbited at an altitude of 555 km where it would

potentially interact with spacecraft in the second and third components of the constellation. The second object in the collision was, again, one of the Starlink spacecraft in the second component of the constellation at 550 km (see Table 6.3). The collision was defined as taking place with a relative velocity of 10 km/s.

Modelling the Events

The specified explosion and collision events were modelled using both the original NASA Standard Breakup Model and the adjusted version. A comparison of the resulting fragment distributions provided some initial expectations about the consequences of the changed model on simulations of the environment. Figure 6.7

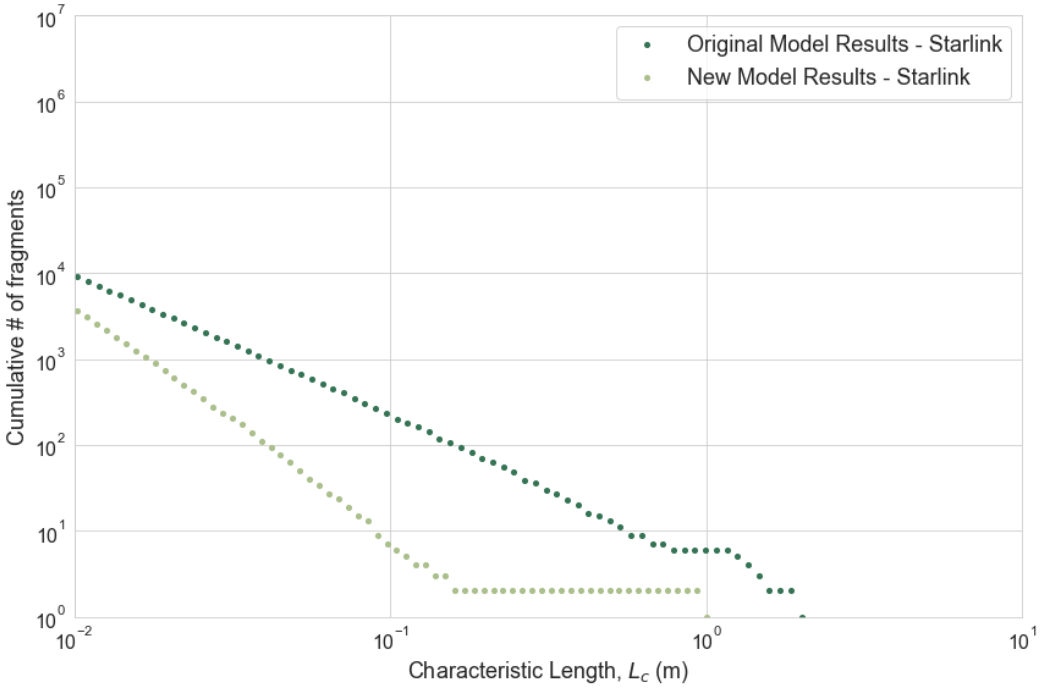

FIGURE 6.7: Comparison of the outputs from the adjusted fragmentation model against the NASA Standard Breakup Model for the defined explosion event.

shows the distributions that were generated for the explosion of a 260 kg Starlink spacecraft. The new version of the model resulted in fewer fragments at all sizes, including around ∼30 times fewer fragments at the 10 cm threshold. Above characteristic lengths of 20 cm only two large fragments were generated at around 1 m in size (hence the horizontal line for cumulative number of fragments). This reduction in fragments is consistent with the lower mass of the spacecraft compared to the historical assumption of a $600 - 1,000$ kg mass. Based on the lower number of larger fragments produced it was expected that the updated model would result in a lower collision probability across the constellation.

The results of the collision of the Aeolus analogue with a Starlink spacecraft are shown in Figure 6.8. For both of the objects involved in the collision the adapted

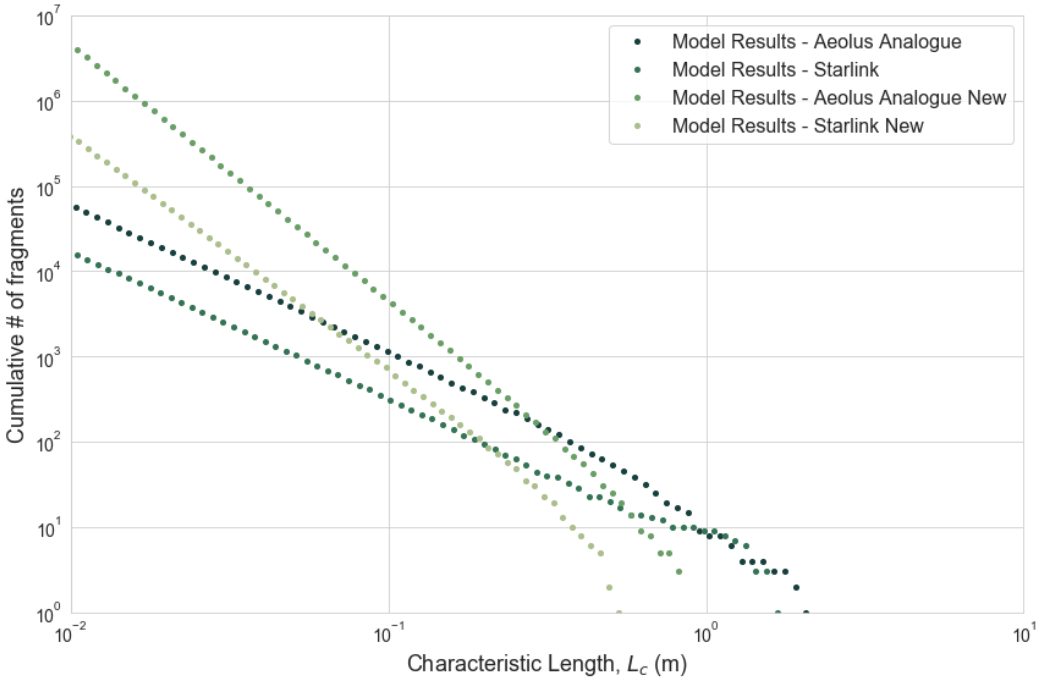

FIGURE 6.8: Comparison of the outputs from the adjusted fragmentation model against the NASA Standard Breakup Model for the defined collision event.

version of the breakup model predicted five to ten times fewer fragments larger than 50 cm and substantially more smaller fragments (∼20 to 100 times more fragments larger than 1 cm).

Applying a Collision Probability Correction

Equations 6.6 and 6.7 were then used to generate correction terms for the specific Starlink constellation scenario. The SSDM of the scenario was calculated to be 3.085×10^{-04} resulting in correction terms of 3.362 and 4.652 for Orbit Trace and Cube respectively. These terms were then used to multiply the collision probability of any conjunction event involving a constellation spacecraft in simulations run with the adjusted collision models.

6.4.2 Model Configurations

Each of these scenarios was simulated using each of the original and adjusted versions of the NASA Standard Breakup Model and the Cube collision algorithm in a series of combinations outlined in Table 6.4. This allowed a comparison to be made of the impact on the results of varying each of the models individually as well as in combination.

When using the Cube algorithm ten different runs were made of each scenario. While not a sufficient number of runs to get a good estimate of the variance of the results this

TABLE 6.4: Table of different model and scenario combinations.

#	Scenario	Breakup Model	Collision Model
1	Base Scenario	Original NSBM	Original Cube
2	Base Scenario	Adjusted NSBM	Original Cube
3	Base Scenario	Original NSBM	Adjusted Cube
4	Base Scenario	Adjusted NSBM	Adjusted Cube
5	Explosion Scenario	Original NSBM	Original Cube
6	Explosion Scenario	Adjusted NSBM	Original Cube
7	Explosion Scenario	Original NSBM	Adjusted Cube
8	Explosion Scenario	Adjusted NSBM	Adjusted Cube
9	Collision Scenario	Original NSBM	Original Cube
10	Collision Scenario	Adjusted NSBM	Original Cube
11	Collision Scenario	Original NSBM	Adjusted Cube
12	Collision Scenario	Adjusted NSBM	Adjusted Cube

helped to calculate average values for the results and identify any extreme outliers. A single simulation run of the baseline simulation using the Orbit Trace method was also performed for comparison. However, the greater run-time of this configuration prevented the more complex scenarios or multiple iterations from being run. In the simulations the adapted versions of these equations were applied only when modelling the breakups of any intact spacecraft. It was assumed that the original version of the model would be suitable for representing the breakups of any debris objects which tend not to fit the identified NewSpace criteria.

6.5 Simulation Results

A comparison was made by studying the trends across each of the simulations for three different environmental metrics[1]: the total number of objects in orbit ($>$ 10 cm and $>$ 10 g); the cumulative number of collision events; and the number of catastrophic breakups resulting from collisions (where each intact object where the energy to mass ratio was $> 40J/g$ was counted as a distinct breakup). Two additional metrics related to operational concerns were also investigated: the expected daily number of collision avoidance manoeuvres (averaged over consecutive 28 day periods) and the cumulative lifetime collision probabilities of the Starlink Spacecraft at the end of each simulation.

6.5.1 Results with the Original Models

The initial simulations of the three scenarios, using the original versions of the NASA Standard Breakup model and the Cube collision model, provided a baseline which could be used to assess the impact of the changes to the models. Collision events were

[1]For the cube simulations the mean average values of the metrics were taken across the ten runs.

found to be very rare within the simulation as initially defined. In the absence of any new spacecraft being launched or any pre-defined breakup events this led to a monotonically decreasing population count (shown in Figure 6.9) as rocket bodies and debris objects decayed from 8591 objects, at the start of the simulation, to 6280 at the end.

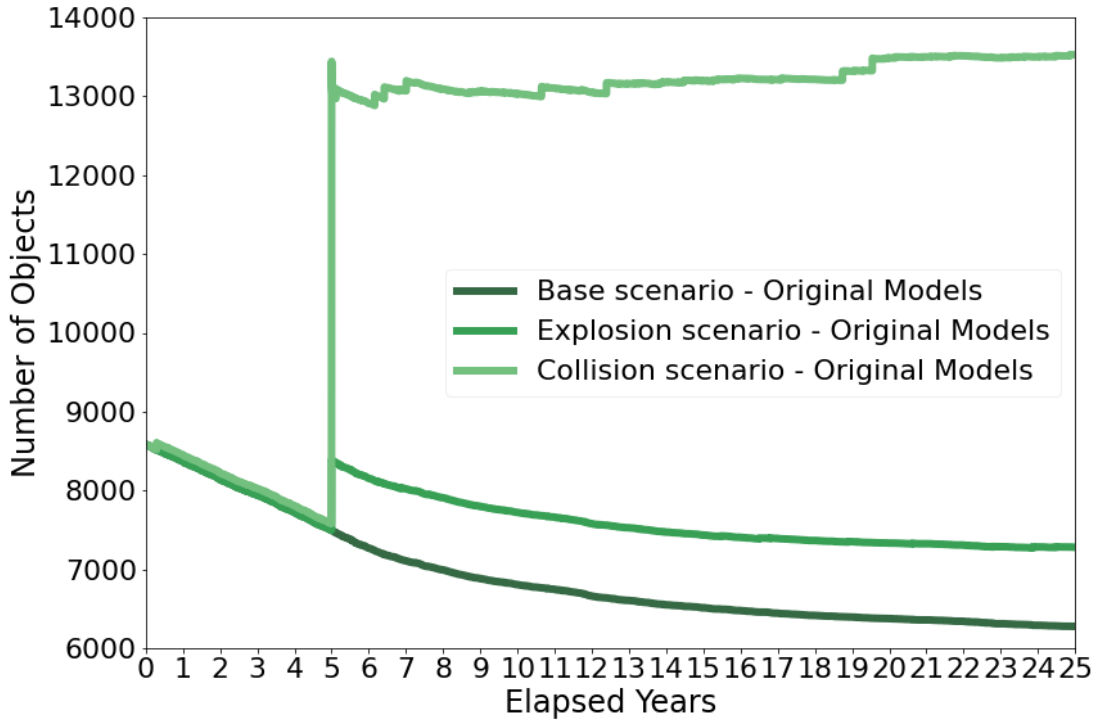

FIGURE 6.9: Evolution of the mean total object count (with length $>$ 1 cm and mass $>$ 10 grams) across ten simulations of each scenario using the original collision and breakup models.

The introduction of the defined breakup events at the five year point in the simulation caused an increase in the collision rate for both the explosion and collision scenarios. Due to the relatively small number of fragments generated for the explosion scenario (an average of 893.5), the increase in the collision rate, illustrated in Figure 6.10, was small (an average of 2.5 events over the following 20 years of the simulation, or 0.125 collisions per year). This resulted in only a small difference in the rate of change of the population, with the exception of the initial release of new fragments. The average final population of the explosion simulations was 7283, only one thousand more than the base scenario.

In the collision scenario, where an average of 5857.1 fragments were generated in the initial event, the total number of collisions reached 20 events on average over the 20 year period (0.825 collisions per year). However, of the 38 objects involved (excluding the two objects which experienced catastrophic breakups as a result of the defined collision event) only 0.9 of the resulting breakups met the conditions for a catastrophic collision breakup (see Figure 6.11).

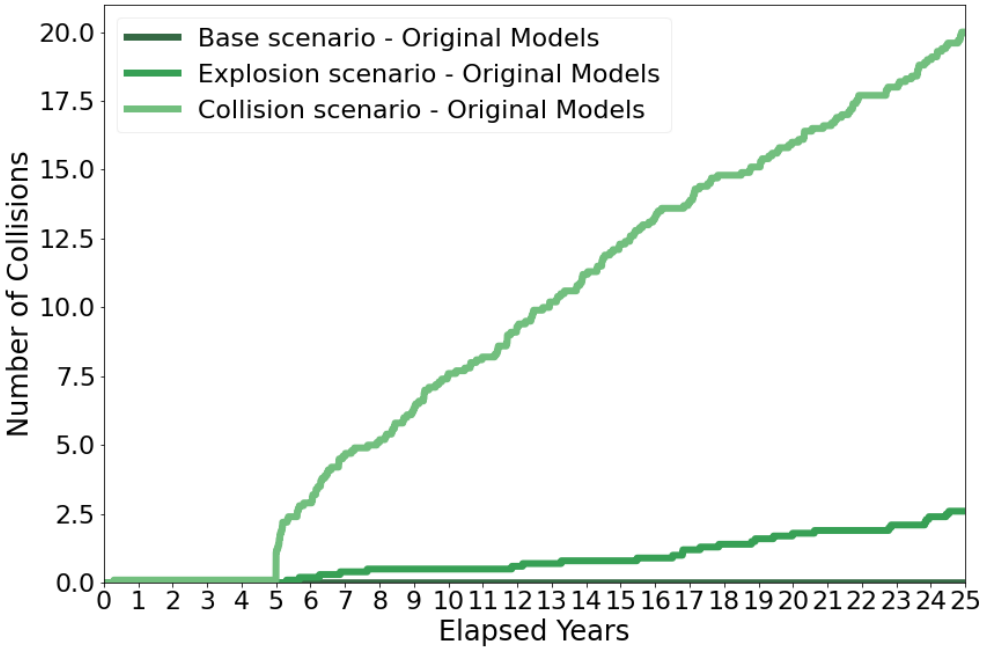

FIGURE 6.10: Evolution of the mean number of collision events across ten simulations of each scenario using the original collision and breakup models.

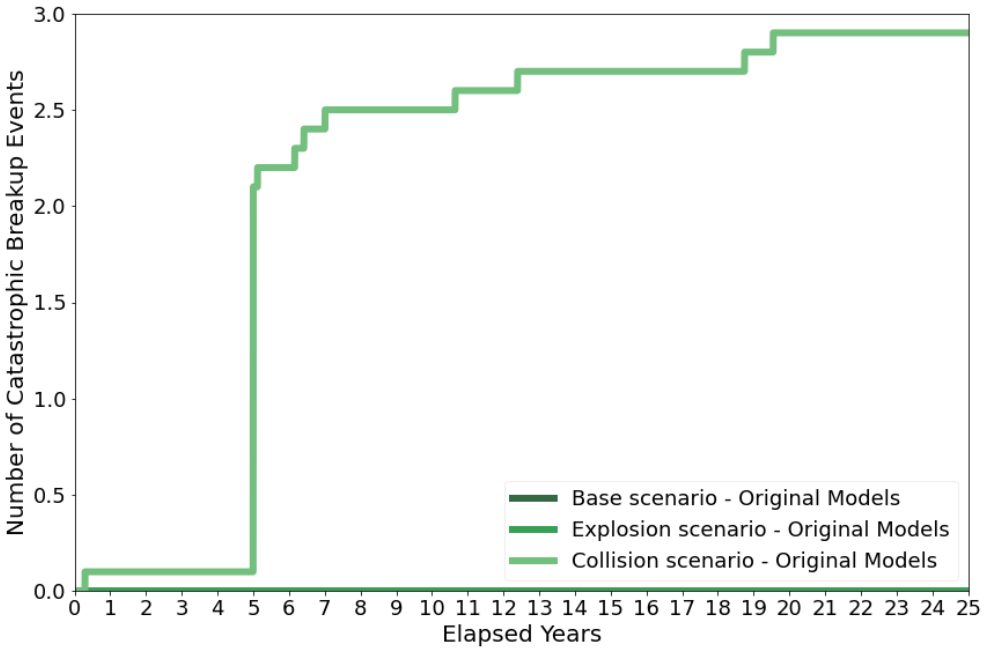

FIGURE 6.11: Evolution of the mean number of catastrophic breakups across ten simulations of each scenario using the original collision and breakup models.

As a result of the lack of catastrophic breakups there was no further growth in the debris population following the defined collision event. However, a significant change from the first two scenarios was that the resulting population was in a form of equilibrium. Due to the larger number of secondary collisions the expected decrease in the population due to atmospheric decay was balanced by the generation of new debris fragments. The average population at the end of the simulation increased by

0.62% to 13,522.7 objects from 13,439.3 immediately after the original event, compared to a reduction of 16.22% for the base scenario and 13.22% in the explosion scenario.

6.5.2 Environmental Impact of Model Variation

The results of the simulations with the different adaptations to the models were then compared to these baseline results for each of the three scenarios.

Base Scenario

Figures 6.12 and 6.13 show the evolution of the average number of objects and collisions across the 25 years of the simulation. In the absence of any defined breakup events, analysis of any systemic impact from the changes to the NASA Standard Breakup model was dependent on spontaneous collision events being identified. However, these collisions only occurred in 4 out of the 40 simulations conducted, all of which took place in simulations running with the adjusted breakup model. As such it was not possible to form any meaningful conclusions regarding the breakup model from the results of the base scenario.

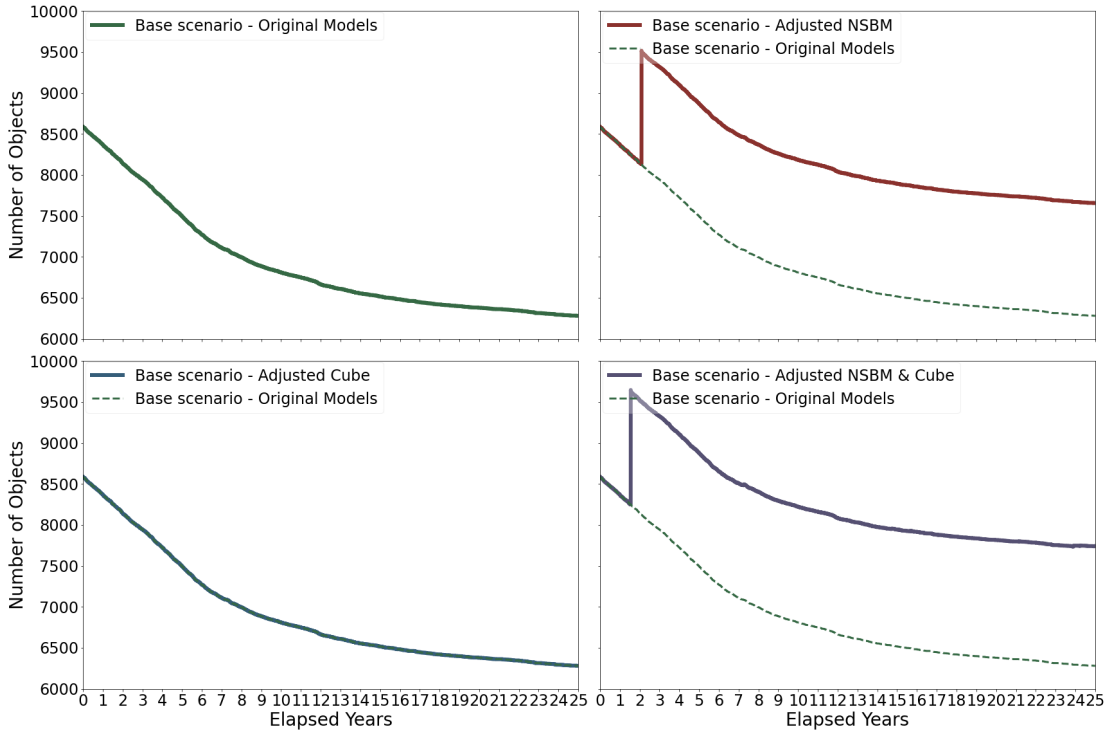

FIGURE 6.12: Mean number of objects over ten simulations for the base scenario.

No spontaneous collisions were identified in the simulations run using just the adjusted Cube model and so the results were the same as when using the original models. However, due to the presence of collisions there was a difference between the evolution of the environment in the simulations with the adjusted NASA Standard

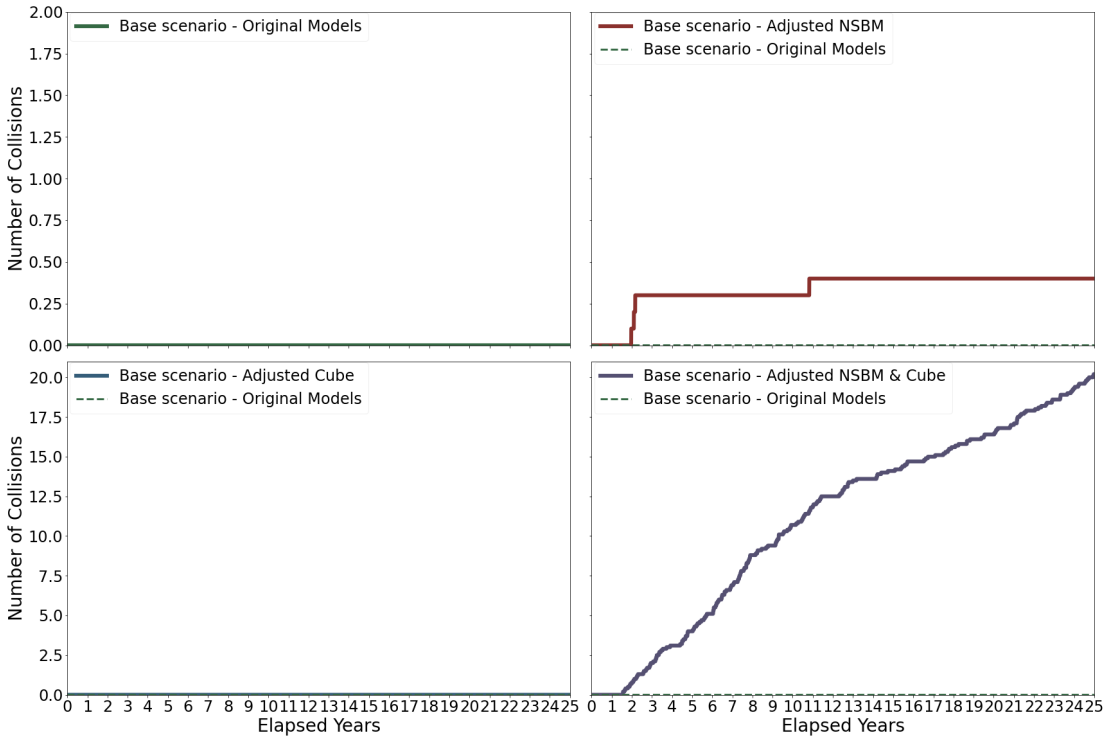

FIGURE 6.13: Mean number of collision events over ten simulations for the base scenario.

Breakup model with and without the adjusted Cube model despite the spontaneous collision occurring early in the simulation in both cases. The results showed that the adapted Cube model increased the number of secondary collisions. Using the original Cube model there were an average of 0.4 collisions across the simulation while using the adjusted Cube model the average was 20.2 collisions.

Explosion Scenario

For the explosion scenario Figure 6.14 showing the evolution of the object count and Figure 6.15 showing the collision count, illustrate how the adaptations to the breakup and collision models have competing effects. The changes to the breakup model resulted in fewer collisions and reduced population growth while the changes to the collision model stimulated a higher collision rate and so increased population growth.

When the adjusted NASA Standard Breakup Model was used in simulations of the explosion scenario, the defined explosion event had much less influence on the future of the environment. Only an additional 125.9 objects were added to the environment, compared to 893.5 using the original model. As a consequence no further collisions occurred in six of the ten simulations and the following evolution of the population was similar to the base scenario, decreasing by 15.78% over the following 20 years (compared to 13.22% using the original model). The implication is that the original

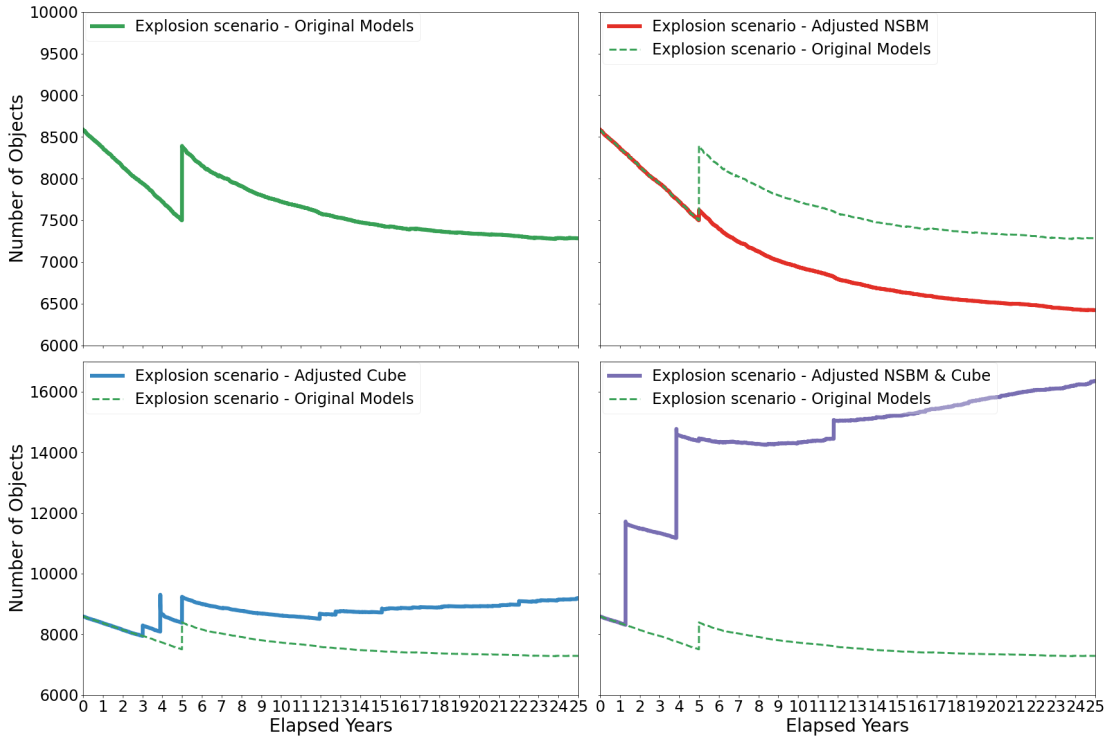

FIGURE 6.14: Mean number of objects over ten simulations for the explosion scenario.

models may exaggerate the impact of explosions on the future evolution of the environment.

The inclusion of the correction term in the collision model increased the rate at which secondary collisions occurred after the explosion from 0.13 to 0.93 collisions per year. These secondary collisions caused the release of additional debris fragments, slowing the decline of the object population with the final population averaging as 9189, an additional 1905.8 debris objects compared to simulations using the original model. There is an initial spike after 4 years in the average number of fragments which is not sustained. This spike is due to a catastrophic collision which occurred in a single simulation run which generated 6917 fragments but occurred at an altitude of 54 km[2] resulting in the fragments rapidly decaying.

When both the adjusted breakup and collision models were used, the dominant change was due to the adjusted collision model. The collision rate over the remaining 20 years of the simulation was 7.75 collisions per year. However, this increase in the average was skewed by 2 of the 10 simulations having over 750 collisions as a result of initial spontaneous collisions involving large objects. The remaining simulations averaged a rate of only 0.043 collisions per year. The deviation between these results shows how the simulated scenario is very sensitive to small differences which could indicate that the population is close to a critical point of stability.

[2]The altitude of 54 km is below the altitude where an object would normally be expected to breakup due to aero-dynamic forces but the SGP4 propagator models an object as having decayed only once it's orbit intersects the Earth's surface.

At the end of the 8 remaining simulations the mean number of objects was 6403.25, a 15.70% decrease, comparable to simulations using the adjusted breakup model alone. However, overall the average number of objects increased from 14462.6 after the explosion at 5 years to 16353.5 at the end of the simulation, a 13.07% increase. This indicates that while the adjusted breakup model reduces the impact of explosions, due to the smaller number of fragments produced in the explosion, this can be outweighed by the increased collision probabilities generated by the adjusted Cube model.

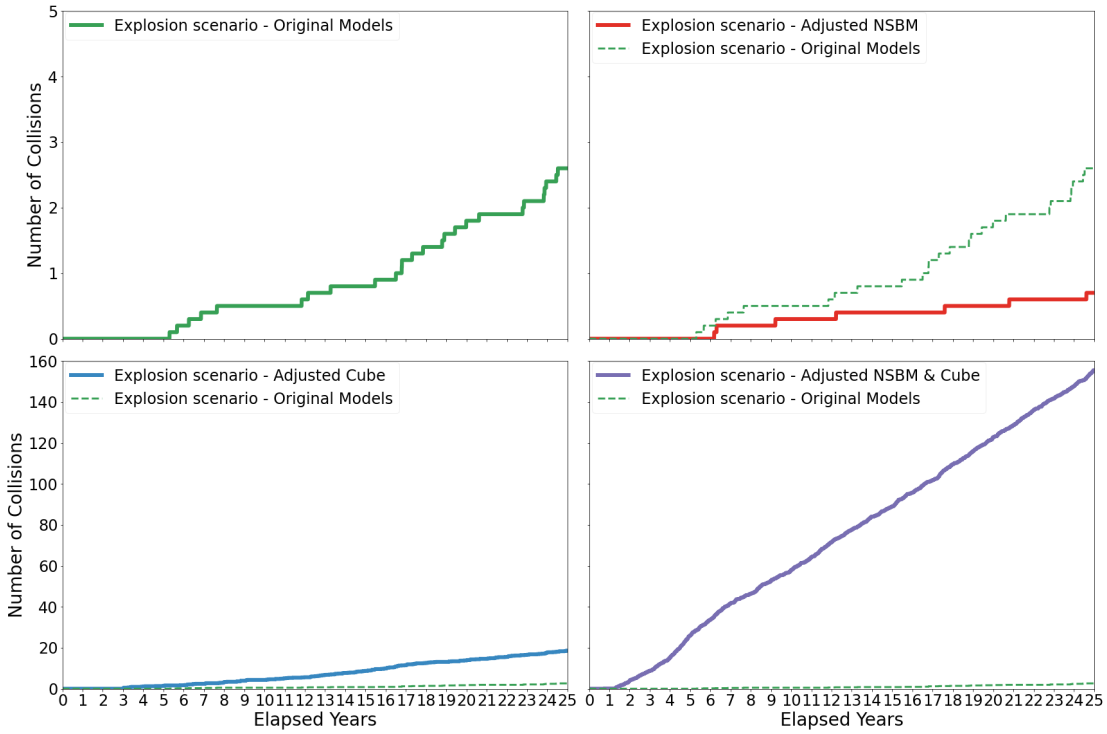

FIGURE 6.15: Mean number of collision events over ten simulations for the explosion scenario.

Across all of the simulations of the explosion scenario 7096 objects were involved in collisions. However, over 99% of the resulting breakups were non-catastrophic. Only 45 exceptions to this were seen, all in simulations using the adjusted collision model.

Collision Scenario

The impact of the different model adaptations on the collision scenario can be seen by looking at the evolution of the count of the object population (Figure 6.16)). Supporting evidence from the number of collision events and catastrophic collision breakups is provided in Figures 6.17 and 6.18 respectively.

The introduction of the adjusted breakup model (Figure 6.16 - top right) resulted in four times more debris fragments (greater than 10 cm and 10 g) being produced by the defined collision event. This increased the mean overall population to 29,926.2 objects after the defined collision event at 5 years. The greater number of debris fragments

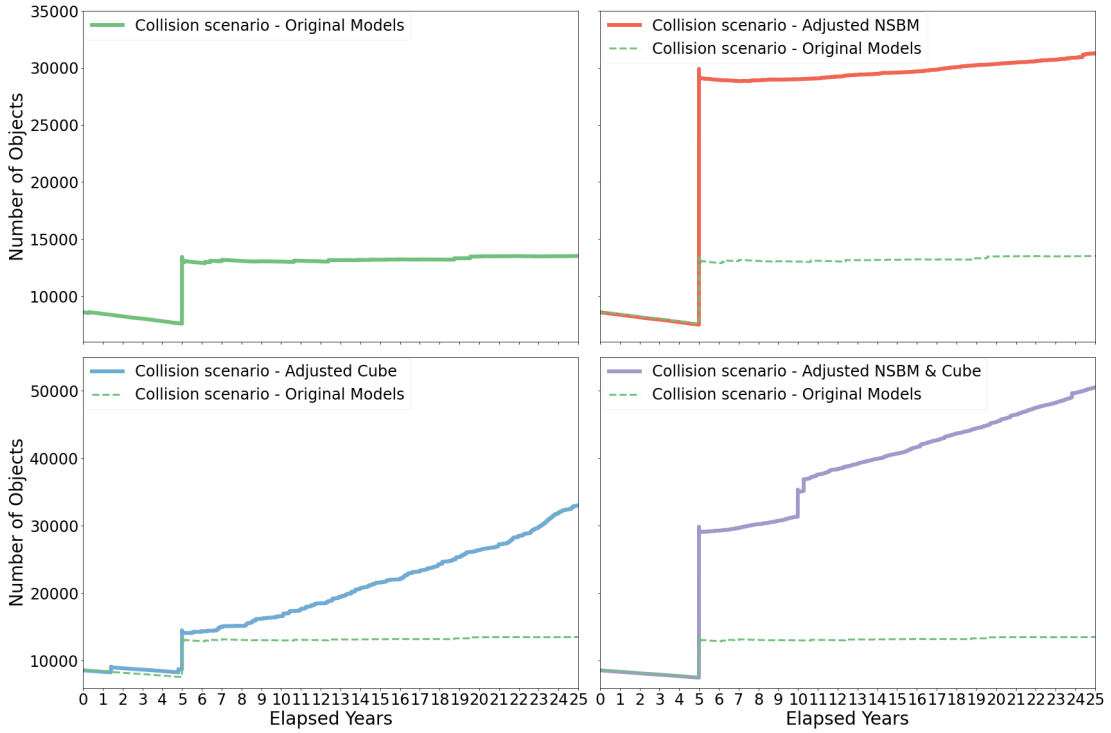

FIGURE 6.16: Mean number of objects over ten simulations for the collision scenario.

released by this initial event was accompanied by an increase in the number of secondary collisions to 7.2 collisions per year, altering the balance of the population count from net decreasing to net increasing.

Following the initial event, the debris population increased by a further 4.56% over the remaining 20 years of the simulation to 31,290 objects. The low rate of generation of new debris objects is due to the adjustment to the breakup model resulting in many more of the additional debris being small fragments. As a result there was not a large change in the number of catastrophic breakups. The mean result was for only 1.9 additional objects to be undergo a catastrophic breakup over the remaining 20 years of the simulation.

In comparison, the results from the use of the adjusted Cube model (Figure 6.17 - bottom left) reported 216.4 additional collisions, a rate of 10.87 per year, including 10.5 further objects being involved in catastrophic collisions. This corresponds to 2.43% of the objects involved in a collision undergoing a catastrophic breakup, compared to 0.66% in the adjusted breakup model simulations. Due to the increase in collisions, and the catastrophic collisions in particular, the initial event was followed by sustained growth in the total debris population over the following 20 years. As a result, the mean debris population at the end of simulations had increased by 127.69% to 33,049.1. This was 1,759.1 more objects than in the simulations with the adjusted breakup model despite the smaller number of fragments released by the initial event.

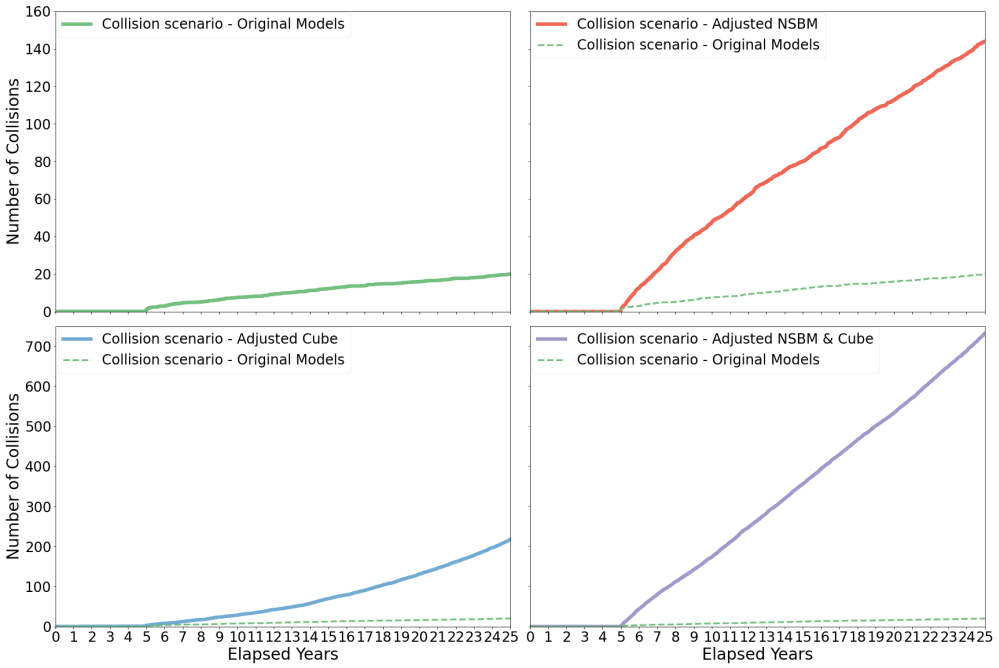

FIGURE 6.17: Mean number of collision events over ten simulations for the collision scenario.

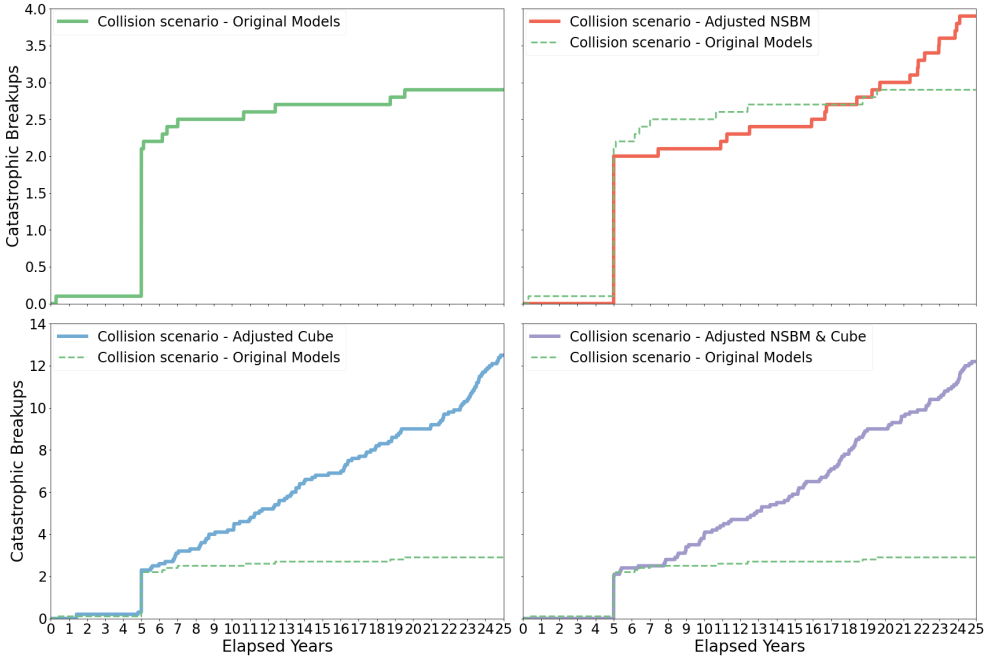

FIGURE 6.18: Mean number of objects involved in catastrophic collisions over ten simulations for the collision scenario.

In the final set of simulations, using the adjusted versions of both models (Figure 6.18 - bottom right), there was a combination of the large initial increase in population from the defined collision, followed by sustained population growth due to a high number of secondary collisions. This resulted in a total final population of 50,509.2, 273.51% greater than with the original models and $50-60\%$ greater than with either of the adjusted models individually.

However, while collision rate increased by 250% relative to the simulations with the adjusted Cube model to 36.59 collision per year, an average of only 10.2 of the objects involved in the 731.37 collisions (1.39%) experienced catastrophic breakups. Another difference was that the increase in the debris population was smaller compared to the adjusted Cube simulations as a percentage of the population (69.10% compared to 127.69%) although not in terms of the absolute number of new objects (20,639.2 compared to 18,533.9).

These two differences with respect to the adjusted Cube results are both being driven by the shift in the size distribution of the fragments generated using the adjusted breakup model. While many more fragments were created, fewer were large, high mass, fragments and many more were smaller, low mass, fragments. As a result the average mass of the object involved in a secondary collision was lower and consequentially fewer secondary fragments were released in each following collision.

Summary

The results of the 12 model and scenario combinations are summarised in Table 6.5 and Figures 6.19 to 6.21 for the average of the total number of objects, the cumulative number of collisions and the number of catastrophic breakups respectively at the end of the simulation period.

The relative difference between Figures 6.20 and 6.21 for the collision scenario highlights the impact of the adjusted breakup model on the ratio of catastrophic to

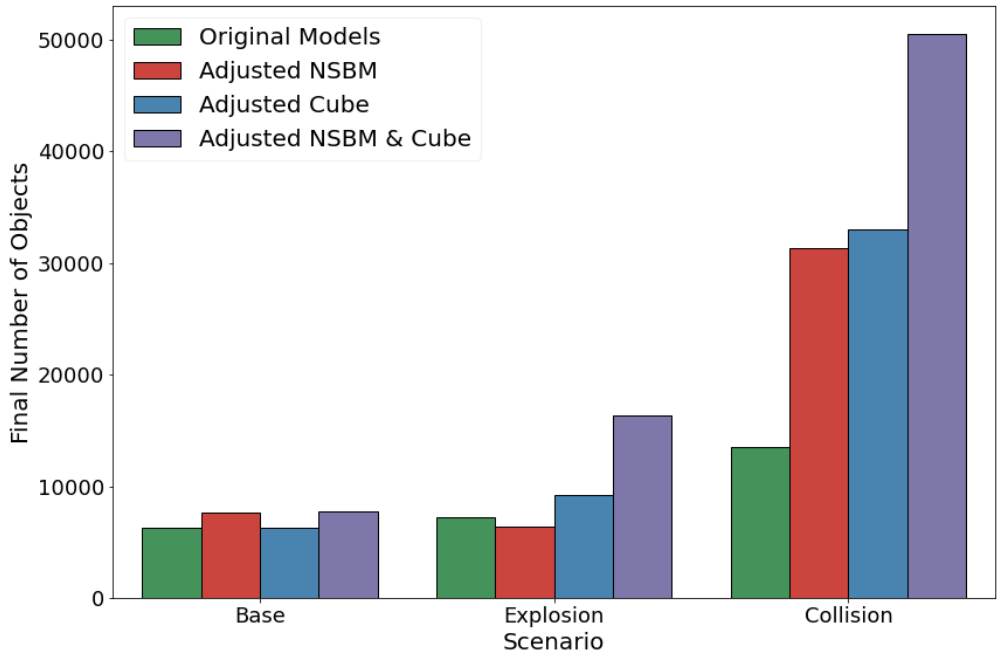

FIGURE 6.19: Summary of the average final object count for different model configurations and scenarios.

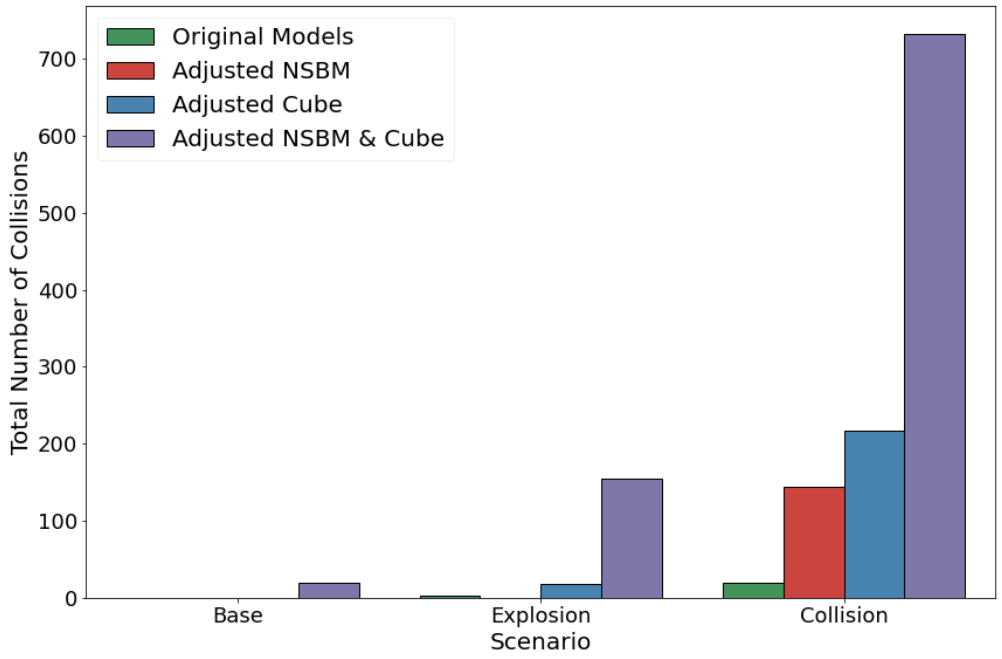

FIGURE 6.20: Summary of the average total collision count for different model configurations and scenarios.

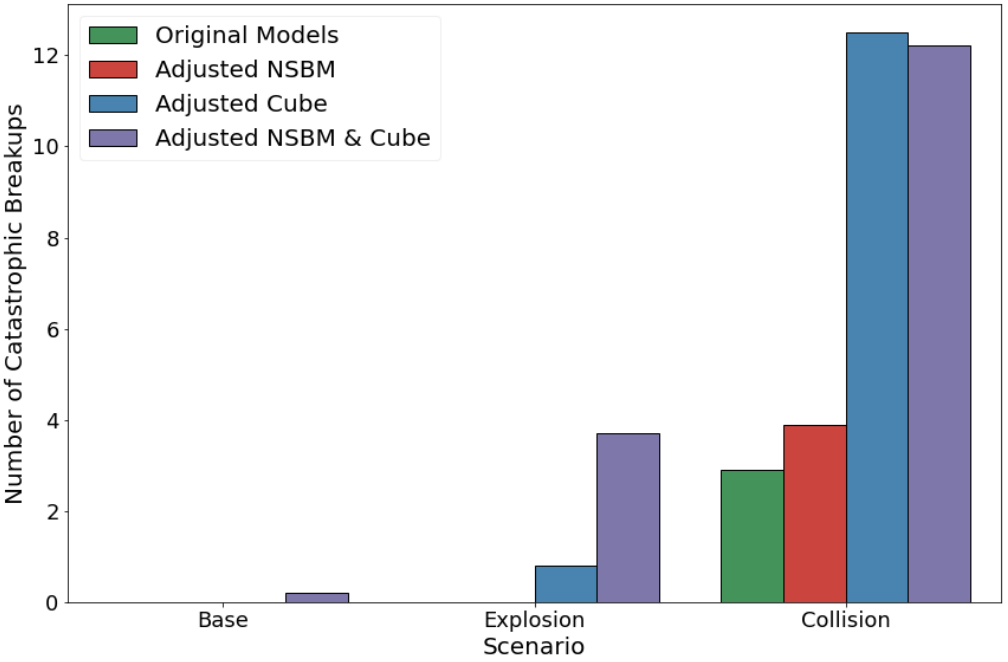

FIGURE 6.21: Summary of the average number of catastrophic breakups for different model configurations and scenarios.

non-catastrophic collisions. There were 3.5 times more collisions using both adjusted models than using only the adjusted Cube model, however the number of catastrophic breakups remained the same because the probability of a collision involving a high mass object decreased due to the greater number of small fragments relative to the number of large fragments released when using the adjusted breakup model.

TABLE 6.5: Table summarising the results of different model and scenario combinations.

#	Scenario	Breakup Model	Collision Model	Final # Objects	Total # Collisions	Catastrophic Breakups
1	Base	Original	Original	6280	0	0
2	Base	Adjusted	Original	7656.1	0.4	0
3	Base	Original	Adjusted	6280	0	0
4	Base	Adjusted	Adjusted	7741.9	20.2	0.2
5	Explosion	Original	Original	7283.2	2.6	0
6	Explosion	Adjusted	Original	6421.4	0.7	0
7	Explosion	Original	Adjusted	9189	18.6	0.8
8	Explosion	Adjusted	Adjusted	16353.5	155.5	3.7
9	Collision	Original	Original	13522.7	20	2.9
10	Collision	Adjusted	Original	31290	144	3.9
11	Collision	Original	Adjusted	33049.1	217.4	12.5
12	Collision	Adjusted	Adjusted	50509.2	731.7	12.2

6.5.3 Operational Consequences

One of the key ways in which current debris models are used, is to assess the risk the debris environment poses to spacecraft operations. Studying these impacts helped to identify some of the risks which exist if current debris models are not suitable for modelling the future evolution of the environment. One way of quantifying the impact on operations of errors within debris models was to investigate how the use of different models changed the prediction of the number and rate of collision avoidance manoeuvres required (based on conjunctions with trackable objects).

Figure 6.22 shows how the different model configurations resulted in higher or lower numbers of predicted daily collision avoidance manoeuvres for each of the three scenarios. For the base scenario the impact of the adjusted models was small. The predicted daily manoeuvre rates at the end of the simulations were 1.79 and 1.66 respectively when using just the adjusted breakup model and adjusted Cube models compared to 1.63 for the original models. A small increase was seen in the simulations using the combination of both adjusted models, where the average final manoeuvre rate was 2.41.

There was a greater divergence in the results of the different models for the explosion scenario. A consistent rate around 6 manoeuvres per day was predicted from after the explosion until the end of the simulation period when using the original models. In

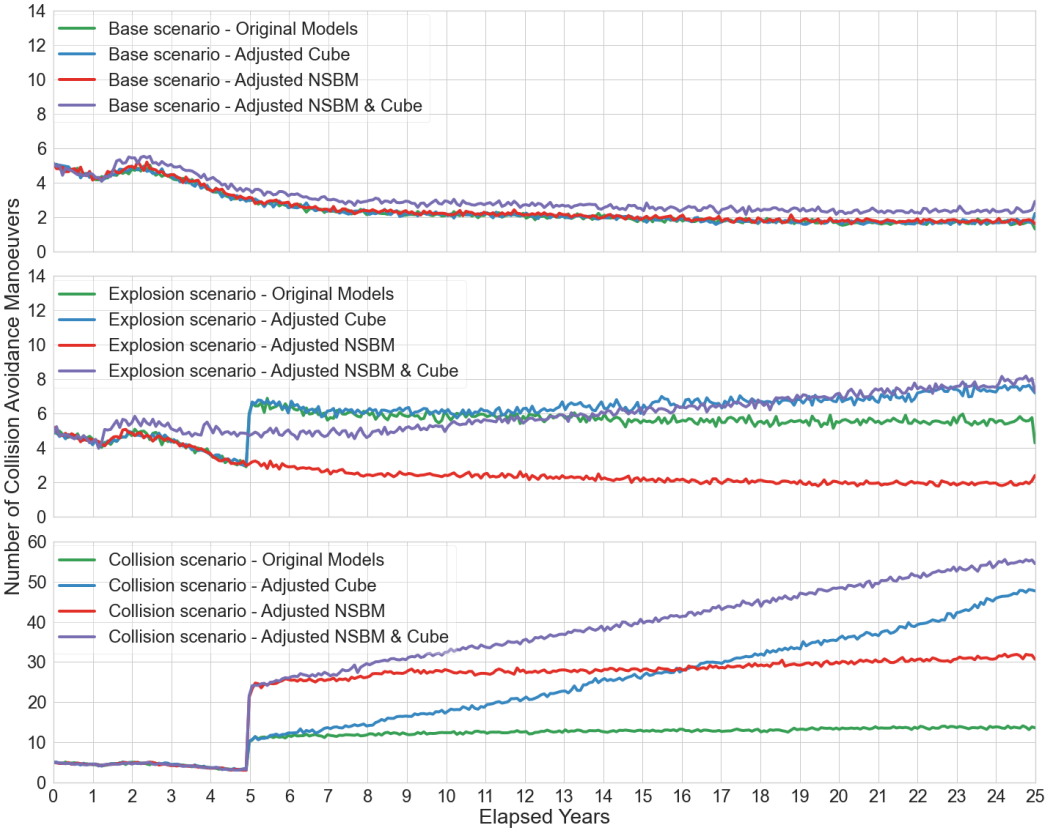

FIGURE 6.22: Average daily collision avoidance manoeuvre count over 28 days for each of the base, explosion and collision scenarios (mean result across 10 simulations).

comparison, for the simulations where the adjusted breakup model was used there was no material increase in the rate of manoeuvres following the explosion and the rate decreased from three per day immediately following the explosion to 2.08 per day at the end of the simulation. The resulting final manoeuvre rate was consistent with the results of the base scenario due to the much lower number of large fragments produced for the explosion of a Starlink spacecraft using the adjusted model (see Figure 6.7). This result suggests that simulations of NewSpace environments using the NASA Standard Breakup model are over emphasising the impact of potential explosion events on the safe operation of spacecraft.

For the simulations using the adjusted Cube model the final manoeuvre rates increased relative to the original models to 7.44 and 7.90 respectively for the original and adjusted breakup models. The results indicate that the increased collision probability as a result of the adjustment to the Cube model outweighs the impact of fewer fragments being produced by the adjusted NASA Standard Breakup model for the explosion.

More substantial impacts were observed for the collision scenario simulations run using the changes made to the collision and breakup models. In the simulations run with the original models the mean daily manoeuvre count following the collision event was 11.62 manoeuvres per day. There was a slight increase in the daily rate over

the remaining 20 years of the simulation to 13.99 despite a decrease in the overall population. This indicated that while total object count was falling due to atmospheric drag this was not reducing the encounter rate of objects in the most congested regions. The increase in the manoeuvre rate was slow, growing by 20% over 20 years.

The introduction of the adjusted breakup model doubled the expected number of manoeuvres per day to 25 manoeuvres per day immediately after the collision event. Following the defined collision the final daily manoeuvre rates underwent continued growth in the simulations using the adjusted breakup model, adjusted Cube model and both combined. The introduction of the adjusted Cube model resulted in a substantially higher rate of growth and so higher final rates than for the adjusted breakup alone. The average final manoeuvre rates for the different simulations are summarised in Figure 6.23.

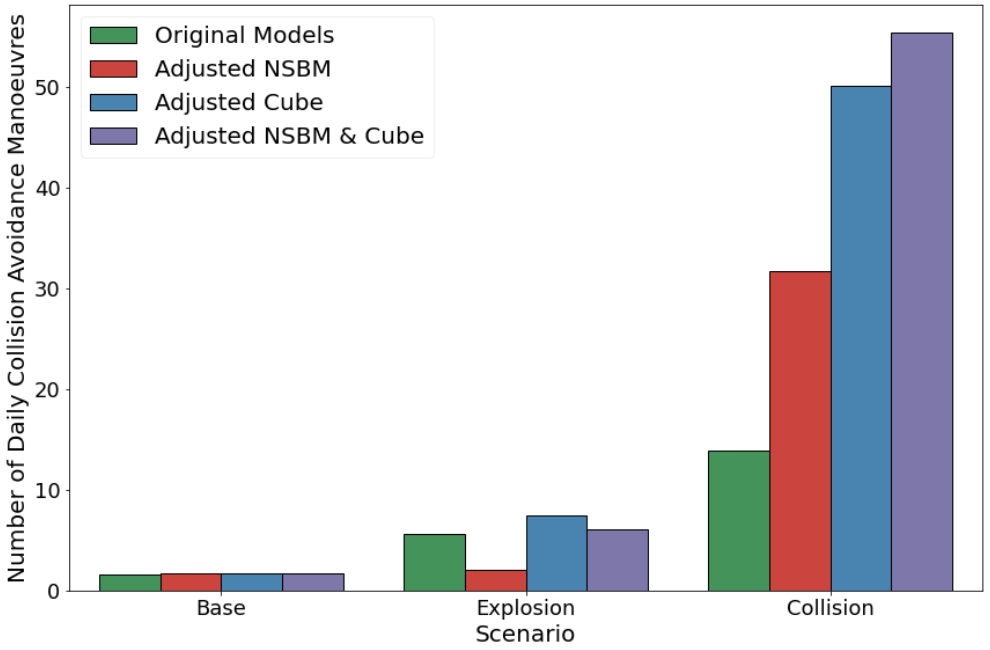

FIGURE 6.23: Summary of the average number of collision avoidance manoeuvres for different model configurations and scenarios.

The three different alternate configurations for the collisions scenario reached 31.66, 48.03, and 55.38 manoeuvres per day respectively. These results show that each of the proposed adjustments to the models indicate that a higher manoeuvre rate for a growing debris population compared to that predicted by the original models. This suggests that using current debris models to assess the impact of breakup events will result in an under-estimation of the ongoing operational burden.

Impact on Lifetime Collision Probability

Another metric used to measure the impact of NewSpace changes on spacecraft operations is the cumulative collision probability associated with a spacecraft or space

system over its orbital life. This investigation chose to focus specifically on the collision probabilities of the primary population of 4,408 Starlink spacecraft. Due to stochastic elements within the collision models there was significant variation between simulation runs in the collision probabilities accumulated for any specific spacecraft. Rather than concentrate on individual spacecraft, the distribution of collision probabilities over the constellation as a whole was analysed. By comparing these values across the whole population it is possible to understand how the expected risk varies between the different scenarios and model configurations. This metric is highly correlated with the metrics of collision and manoeuvre rate but provides a different perspective on the impacts.

The data are displayed in Figure 6.24 using a box and whisker diagram to show the median value and the spread of the different quartiles. The results using the original models provide a baseline for comparison with the adjusted versions of the models. In the base scenario the median cumulative collision probability of the Starlink spacecraft was 0.00066, a 1 in 1515 chance of collision over the 25 year period for each spacecraft. In the scenario where a defined explosion event was introduced the probability doubled to 0.001287. The inclusion of the defined collision event resulted in an almost eight-fold increase to 0.005135.

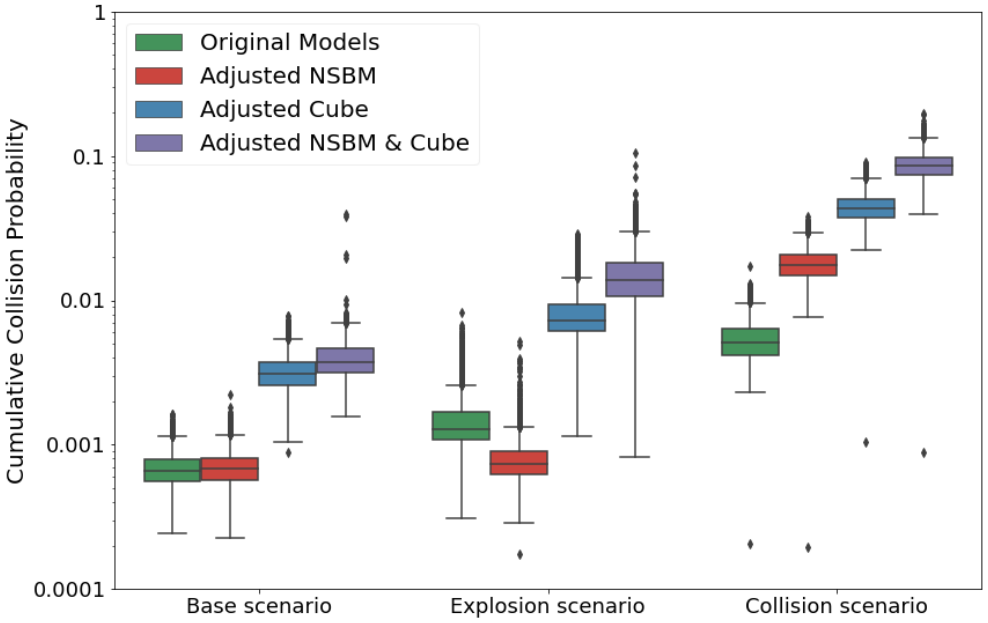

FIGURE 6.24: Distribution of collision probabilities for different model configurations and scenarios.

The use of the adjusted version of the breakup model had little impact on the base scenario resulting in a slight increase in the median collision probability from 0.00066 to 0.000681. However, the changes to the model did have a noticeable impact when used for the explosion and collision scenarios. For the explosion scenario the median cumulative collision probability decreased by 42% to 0.000741 while for the collision

scenario the median probability increased by 240% to 0.01751. This is consistent with the observed environmental changes in number of debris objects and secondary collisions. Across all three scenarios the introduction of the collision model adaptation increased the cumulative collision probability. The collision probabilities increased by 370% to 0.003103 for the base scenario, by 565% to 0.007281 for the explosion scenario, and by 850% to 0.043623 for the collision scenario.

The collision probabilities for the combined adjustments were the highest of any configuration across all three scenarios. The final cumulative collision probabilities reached 0.00374, 0.013935, and 0.085444 respectively. The current debris models resulted in substantial errors for this NewSpace scenario.

6.5.4 Comparison to Expectations

Chapters 4 and 5 quantified some of the errors associated with the assumptions in collision and breakup models when applied to NewSpace. The purpose of the investigation was to address the question of whether NewSpace related updates made to the models would result in a substantial alteration to the output of simulations of the debris environment which might change the current understanding of the future of the debris environment. The models used to conduct the investigation incorporated the results of the fragmentation and collision investigations to reduce or remove the identified errors based on the characteristics of the objects and systems involved.

The expectations, based on the results of the previous chapters, were that adjusted models would lead to:

- A greater number of collisions, due to
  - Increase in calculated collision probabilities for systems with a high spatial structure
  - More total fragments being generated for fragmentations
- A lesser impact from secondary collisions, due to
  - An increase in the number of small, low mass fragments produced, relative to the number of large, high mass fragments
  - Hence a lower proportion of the subsequent breakups will be catastrophic

The results **confirmed the expectations** with the increased number of collisions resulting in larger debris populations and raised manoeuvre counts despite the decrease in the proportion of subsequent collisions which resulted in catastrophic breakups. While it had been thought that the adjustment to the size distribution of the breakup model towards more smaller fragments might decrease the impact of secondary collisions this was outweighed by the increased number of collisions which took place, particularly when combined with the adjusted collision model. As a result,

the highest final debris populations and lifetime collision probabilities were seen for the simulations run using both adjusted models.

In preparing the simulations a number of choices and assumptions were made which will have had consequences for the results. These assumptions were made both in constructing the debris model used and when establishing the scenarios. In addition, there were also several assumptions inherent to the adjusted models which are discussed further in Chapter 7.

One of the choices made in setting up the simulations was to limit the number of Monte Carlo runs of each of the model and scenario combinations to ten in order to conduct simulations across the range of scenarios in a practical time frame. The ten runs provided some insight into the variation of the results but was not sufficient to give a good understanding of the deviation of the possible outcomes or of the reliability of the mean values. As the changes made to the models were systemic they affected all of the Monte Carlo runs equivalently and the impact of the changes was felt consistently, in spite of the variance. However, the actual number of collisions occurring varied a lot between the runs leading to a lack of consistency in the output.

For performance reasons the fragmentation models used made a number of simplifications for small fragment sizes. These included the use of representative fragments as well as limiting fragments to those greater than 1 cm in length with masses greater than 10 g. While the fragments were excluded by this limit for each simulation run, the differences in the fragment size distribution means that a greater number of fragments are excluded from the simulations run with the adjusted model. Inclusion of these fragments would result in increased debris population and hence more opportunity for further collisions in simulations with the adjusted breakup model compared to those using the original model. Although collisions involving the smaller, less massive objects will have less severe consequences than for larger objects. However overall, the inclusion of these fragments would not change the conclusions drawn from the results as it would only result in a small exaggeration of the observed difference between the models.

The Cube algorithm was utilised with a 10 km cube size. The investigation in Chapter 5 found that variations in the cube size around 10 km did not have a large impact on calculated collision probabilities. As such this choice will not directly impact the results. However, the choice of cube size did impact the frequency with which encounters were identified and so the required sampling rate. The sampling rate used was a 1 day time-step with 100 samples taken at each step. On the basis of the results in Chapter 5 this sampling rate should have been sufficient to gain a good estimate of the encounter frequency of objects for a population of this size. Additionally, the sampling rate and cube size were applied consistently across the different simulations. As a result, the only opportunity for errors to affect the conclusions drawn would be if

differences in the evolution of the population led to the sampling rate no longer being appropriate.

The more general assumptions made in the simulation scenario included the use of a B^* value of 0 for every active spacecraft. In reality the orbits would constantly change, requiring orbit maintenance manoeuvres. As a result of these changing orbits the number of orbits of other objects with which the spacecraft could intersect would be higher. However, using a 10 km cube captures the potential for short-period perturbations and identifies the interactions of closely approaching objects which somewhat mitigates the impact of this assumption. Several further assumptions were also made:

- Perfect collision avoidance for active spacecraft when the probability of collision was greater than 0.0001
  - Might result in an underestimation of the number of collisions
  - However, might also underestimate the number of manoeuvres performed
- No spontaneous spacecraft failures or explosions
  - No failures results in fewer objects in orbit which might be involved in collisions.
  - Will result in less debris generated than might be expected in reality
- No new launches, including constellation replenishment
  - Will result in fewer objects in orbit than reality
- No end of life operations such as post-mission disposal,
  - Will result in a static population with fewer objects in orbit than if like-for-like replacement was taking place

However, the impact for each was consistent across all simulations and so will not alter the conclusions made on the basis of the differences between the models.

Overall, it is clear that the results of the simulations will have been impacted by a number of the assumptions discussed. However, on the whole the impacts will be consistent across the different simulations while the key to this investigation is the comparison of the results between the simulations where adjusted models were employed. As such, on the balance of the evidence, the findings of this investigation uphold the original hypothesis that ”Updates to models to incorporate the effect of NewSpace will change the current understanding of the future evolution of the debris environment”.

6.6 Significance for the Use of Evolutionary Debris Models

Overall the results of the simulations conducted in this investigation supported the idea that changes made to the collision and fragmentation component models to

account for NewSpace will alter current expectations around the future of the debris environment, particularly in the aftermath of a collision event. This supports the hypothesis and implies that current models might not provide a good representation of a NewSpace environment. This implies that **updates to the debris models** currently in use will result in a **re-assessment of the stability of the future of the current space environment** and the impact of NewSpace systems.

The indications were that the future evolution of the debris environment is more sensitive to future collision events, and less sensitive to explosion events, than current debris models predict. Within the simulations conducted the **adjusted versions of the breakup and collision models resulted in a 166-fold increase in the average cumulative collision probability** of spacecraft in the Starlink constellation following a collision event. As a consequence, **current debris models might be leading users to underestimate the risks associated with the debris environment and NewSpace systems** that are similar to Starlink.

The significance of this outcome is that **current assessments of NewSpace systems**, such as large constellations, **may be falsely optimistic**. This may lead to inadequate regulation of space missions, in particular NewSpace systems, and insufficient steps being taken to appropriately mitigate against future debris generating events and any consequent ramifications for the environment. For instance, the ”25-year rule” for spacecraft de-orbiting may not be appropriate, as some studies using the current models already indicate (Lewis et al., 2012), although some operators already recognise this problem and have indicated that they aim to do better than is currently required.

A failure to understand the level of risk associated with these systems and the severity of the possible impact on the debris environment could have serious consequences for both space safety and environmental sustainability. For example, if the introduction of these systems leads to faster than anticipated debris growth then it could rapidly increase the cost of operating in and avoiding the orbital regions experiencing population growth as well as increasing the mitigation and remediation required to control further growth (Mcknight, 2010).

The alteration in predicted collision probabilities might change the prioritisation of which objects should be subject to ADR missions, for instance where the calculated collision probabilities of large derelict objects intersecting constellation orbits would increase.

The higher encounter rates could lead to revision of design considerations. For example, a need for an increased capacity for the planning and execution of collision avoidance manoeuvres, and increasing on-board fuel levels or a higher replenishment rate for constellations if end-of-life is reached sooner due to greater manoeuvring requirements. A greater perceived risk to spacecraft would also impact on licensing,

insurance and investment, resulting in an increased cost and so raising the barrier for entry for new operators.

Chapter 7

Discussion

> It isn't what we don't know that gives us trouble, it's what we know that ain't so.
>
> Will Rogers

7.1 Introduction

The aim of this project was to study NewSpace changes and to understand their implications for modelling the space debris environment. A review of relevant literature around NewSpace and space debris modelling highlighted the effort directed towards understanding the impact of novel space activities, such as the operation of large satellite constellations. This review identified fragmentation and collision models as two key components of evolutionary debris models where there is a potential lack of robustness for assessing NewSpace and limited opportunities for cross-validation between models due to the use of common approaches. Consequently, it was theorised that the accuracy of debris models might be compromised when they are applied to NewSpace scenarios. The research undertaken was structured around the investigation of three key hypotheses focussed, respectively, on the nature of NewSpace, the suitability of component models, and the impact of model updates on the results of debris environment simulations.

The results described in this thesis provide useful insight into the nature of NewSpace and how debris models perform when applied to the changing space environment and whether confidence in their results is warranted. To this end various models were implemented to investigate the primary hypotheses. However, while the implementations of these models were sufficient to answer the hypotheses, they were also dependent on several assumptions, introducing limitations which should be acknowledged and discussed.

7.2 The Changing Use of Space

In Chapter 3, an investigation was conducted into the hypothesis that "NewSpace is associated with measurable changes in the physical and orbital characteristics of the spacecraft population". The different changes that are included under the banner of NewSpace were quantified to develop a better understanding of how these changes impact the ability to accurately model the evolution of the space debris environment.

Machine learning techniques, used to develop a decision tree classifier, identified object mass and object area-to-mass ratio as well as the number of objects launched together as being key to distinguishing between NewSpace and TradSpace. Analysis of the changes in these characteristics confirmed the presence of a change in the physical characteristics of spacecraft. Particular trends were identified as consistent with known NewSpace elements such as the growing popularity of small spacecraft like CubeSats. These trends are resulting in a divergence between the physical characteristics of spacecraft that are deployed to different regions. Operators have been trending towards smaller, lower mass spacecraft in Low Earth Orbit and larger, higher mass spacecraft in Geosynchronous Orbit.

Investigation of the orbital characteristics of the launched population showed an increased clustering of spacecraft into similar orbits. This clustering was consistent with new modes of operation, such as large satellite constellations and multiple satellite deployments. There has been a resulting shift in the spatial distribution of objects towards greater spatial structure. This shift constitutes a considerable change in the orbital characteristics of the spacecraft population.

A review was conducted of the prevalence of different spacecraft fragmentation events. Explosions were found to have occurred at a constant rate of $4 - 5$ events per year despite an exponential increase in the number of spacecraft in orbit. This corresponds to a reduction in the probability of explosion for an individual spacecraft from $\sim$0.3% to $\sim$0.05% and suggests that attempts to mitigate the spontaneous production of debris are having an effect. However, the decrease for recent years may be biased by the increase launch rate of spacecraft resulting in a lower average age for the spacecraft population and so fewer end-of-life failure modes being exhibited.

By contrast, the increased population of spacecraft and debris objects in orbit is expected to result in a greater conjunction rate and so a higher frequency of collisions. This, along with the fact that collisions are more energetic than explosions and therefore produce more fragments, supports the widely held belief that collisions rather than explosions will become the dominant source of new debris objects in the future.

As part of the initial development of the classification model to categorise objects as NewSpace or TradSpace a training set of examples were manually categorised by the

author. A consequence of this is that the classifier was vulnerable to any initial bias in the author's opinion of what could be considered to be NewSpace and as a result this classification may not be consistent with other approaches. Additionally, the manual selection of inputs and stopping criteria could have led to an under appreciation of the relevance of certain characteristics when NewSpace trends were examined later in Chapter 3.

Nonetheless, the limitations of the classifier do not detract from the significance of those trends identified as being correlated to an increase in NewSpace activities. In confirming the initial hypothesis the analysis showed how the current, and potentially future, spacecraft populations differ from the historical population. The fact that the spacecraft population is changing suggests that future interactions within this population and with the space debris population may also be different, with consequences for the capability of current debris models, based on observations of the historic population, to provide insight into the future debris environment.

7.3 Component Models and NewSpace

Many of the current generation of debris models were identified as having several key component models in common, limiting the value of any cross-validation between the models. Of particular note was that the models for fragmentation and collision prediction, whose processes represent the main source of new debris objects, were determined to be based on a limited set of historic data. Given that the assumptions based on historic data are no longer valid for the spacecraft population, the current generation of space debris models might be providing an inaccurate picture of the future evolution of the environment. It was hypothesised that "NewSpace changes fall outside of the scope of current assumptions, reducing the accuracy of the existing component models of debris processes". The most common shared fragmentation and collision models were investigated in Chapters 4 and 5 respectively.

7.3.1 Fragmentation models

The investigation into the use of the NASA Standard Breakup Model highlighted several areas where the changing characteristics of spacecraft may result in different behaviours than are predicted using the current assumptions in the model. The fragment size distribution generated for breakups of large upper stages, traditionally the dominant source of new fragments, showed good agreement with observed results. However, the analysis of environmental trends indicated that the future environment will depend on a more diverse set of events, including smaller upper-stages, battery based explosions, and collisions between objects.

A comparison of observed fragmentation debris against the results of the model for satellite explosions and collisions revealed a consistent over-prediction of large fragments above 50 cm in length and suggested an under-prediction of smaller fragments. With regard to more general simulations of the environment, the divergence in physical characteristics between the LEO and GEO regions means that the 'average spacecraft' for the environment as a whole is not representative of that found in any particular region. This could result in an unrealistic distribution of fragments by altitude. For example, models may predict too many fragments being produced in LEO and too few being produced in GEO. A consequence is for a potential bias in the perceived risk of operating in different regions, with potentially greater risk to GEO spacecraft and less to LEO spacecraft than currently expected.

When investigating the NASA Standard Breakup model a comparison was made with observational data, using a trend-line fitted to the number of fragments of different size for comparison against the power-law described by the model. A limitation of this was that the publicly available data relating to the size of objects was restricted to three size categories. This lack of fidelity leads to some uncertainty in the analysis - and in the model adjustments made in Chapter 6 - although this has been done using the best available knowledge.

Due to tracking limitations there was some uncertainty around the number and size distribution of the fragments in each size category which results in a range of possible values for the fitted line. For many of the scenarios modelled (such as the breakups of Cosmos-2251, Fengyun-1C, NOAA-16 and Cosmos-2241) the number of small but still trackable objects were underestimated resulting in a steeper fitted line. This led to the conclusion that the model was under-predicting the number of small fragments generated in breakups.

To alter the significance of the result and agree with the original breakup model this uncertainty would have to result in a greater number of large fragments and fewer small fragments. However, the uncertainty is likely to be least for the largest fragments which are easiest to track, while the smaller fragments are harder to track consistently. Therefore it is reasonable to expect that, if anything, the size distribution would be even more skewed towards more smaller fragments which would be an even greater deviation from the current model. As such, the uncertainty is not considered to diminish the usefulness of this investigation in showing the limitations of the currently most commonly used breakup model and assessing the possible implications.

In addition to the flawed assumptions identified in the NASA Standard Breakup Model the lack of empirical data to create better models is a problem that needs to be addressed. Better data for the next generation of fragmentation models will come from a variety of sources. The ongoing work to characterise the DebrisSat and DebrisLV fragments is providing insight into the breakup of modern spacecraft and

the size and shape of fragments. However, these are just two specific breakup examples, and more will be needed. Improvements to the space surveillance and tracking capability, including the ability to track and catalogue smaller objects (down to sizes of 1 - 2 cm), will provide additional data on the distribution of fragment sizes but this does not provide detail on the other characteristics of the fragments. Improvements to models might also include a better understanding of fragment material and density or the effects of different shapes on hyper-velocity impact outcomes. These would represent additional improvements to our understanding of high-velocity impacts and breakups and would complement improvements made to reflect the physical changes in NewSpace spacecraft and upper stages.

7.3.2 Collision Prediction Models

An increased clustering of spacecraft as a result of changes to spacecraft deployment and operation was identified as potentially conflicting with the assumptions made in the current generation of collision models. The increase in spatial structure that this clustering represents was theorised to invalidate the assumption of molecular chaos that underpins the use of the kinetic theory of gases utilised in the Cube and Orbit Trace algorithms, the two most common models used in evolutionary debris models for collision prediction.

Preliminary validations of the Cube algorithm, focussed on a scenario consisting of several Jovian moons, indicated that the Cube method was not suitable for estimating the collision probability of a specific pair of objects as there was still substantial variation in the average collision rates after 7 billion applications (although this scenario involved the randomisation of three orbital elements rather than just the mean anomaly which will have increased the number of sample required). The collision rate was also found to be sensitive to the size of cube used in the algorithm. A linear relationship was indicated: decreasing collision rate with decreasing cube size and a greater number of samples was required for convergence of the collision rate.

A limitation which was identified for the Cube algorithm was that the method of discretising space could introduce a bias. When using a hashing function as implemented the location of every cube in Cartesian space is fixed at every time step. The length of orbit arcs intersecting these cubes is fixed within a time-step and can be very short - leading to a very low probability that the sampling will place the object in those particular cubes. If these are the cubes where the conjunctions occur then many more samples might be needed, compared with the case where the orbit arc intersecting a cube is longer. Even for circular orbits, the probability of putting the object into a particular cube is not uniform around the orbit. This then introduces a bias against the models predicting conjunctions occurring in specific locations as these events are no less likely to occur but are less likely to be identified by the model.

There is then the question of whether there are sufficient samples. Given an orbit with a radius of 7000 km, with a circumference of 44,000 km, there would be thousands of cubes that would intersect this orbit, so 100 samples per time-step might not be sufficient. What's interesting is the sampling through time, however, because if the orbits remain unperturbed then this might still enable good sampling of the whole orbit. This suggests that the impact of this bias might be worse for objects in rapidly changing orbits.

The Orbit Trace algorithm was investigated as an alternative method without the sampling limitations of the Cube method. However, it exhibited poor scaling with increasing population sizes. While GPU methods were attempted to improve speed these were not sufficient when utilising the available hardware. As such use of this method required compromises be made to reduce the compute time such as the use of longer time-steps for evaluating the collision probability to reduce the total number of calculations necessary. The cost of having a longer time-step is that errors are introduced if the orbits of the objects are perturbed over the time-step, resulting in loss of fidelity. Consequently, while the Orbit Trace model might be a better option for investigations of small populations (hundreds rather than thousands of objects) or short projection periods, the poor scaling leaves the Cube as the most viable option for simulations of large space debris populations.

Comparative testing of the two models for debris collision scenarios was achieved by using the maximum collision probabilities predicted by the SOCRATES system as a ground truth. By comparing the differences between SOCRATES with the outputs of the models for a range of scenarios, a relative decrease in the predicted collision probabilities was identified for scenarios consisting of space systems with greater spatial structure.

One uncertainty in the interpretation of the results of the collision investigations is that there could be systematic and competing issues with the Cube and Orbit Trace methods, which are exacerbated by the differences between TradSpace and NewSpace. It was difficult to pin down the root cause as the analysis was based on relative differences with respect to SOCRATES. An alternative perspective on the results was that NewSpace collision probabilities were being predicted correctly by the current models and an over-estimation was taking place for the TradSpace scenarios. Taking this interpretation would lead to the argument that the Cube and Orbit Trace methods need to be modified to reduce collision probabilities for TradSpace whilst remaining unmodified for NewSpace systems - the inverse of what was done in Chapter 6. The difference in the modification of the collision models would still have a substantial effect on long term simulations, albeit in a different direction, and so it would remain important to update models to properly account for the observed deviation.

A weakness of the investigation that identified these trends was that it was only possible to conduct simulations of eight scenarios. As a result, the analysis that lead to

the conclusion of an under-prediction was more sensitive to the influence of individual cases than if a larger set of results had been available. A correlation was found between the probabilities and the spatial structure, as measured by the SSDM, but the correlation was not hugely robust due to the relatively low number of data points. In particular the trends shown in Figure 5.26 were heavily influenced by the partial Iridium Next scenario and the PSLV C-37 scenario which both had much lower probability proportions than the other scenarios. Without these two scenarios the relationship between the probability and the SSDM of the population would be much weaker. However, the purpose of the investigation was to determine whether the collision algorithms were appropriate for NewSpace systems which both of these scenarios represent and a clear difference was visible in the relative probabilities compared to the TradSpace scenarios.

7.4 Environmental Simulations

In validating the first two hypotheses it was identified that a number of ongoing changes are taking place to the make-up of the spacecraft population with resultant impacts on several models of different debris processes which are not robust to the changes. The third hypothesis of this work asserts that ”Updates to models to incorporate the effect of NewSpace will change the current understanding of the future evolution of the debris environment”.

To investigate the third hypothesis an integrated debris model was developed using the component collision and fragmentation models previously studied. This was used to study a NewSpace scenario consisting of an idealised Starlink-like constellation with a background population of spacecraft and debris. Simulations were run of the evolution of the projected environment with defined explosion and collision events being introduced in some of the scenarios. Variations on the collision and fragmentation models were used to represent how component model results may change when corrections to address the assumptions related to NewSpace are introduced. The results of these simulations were then compared to quantify the severity of the impact of changing the models and understand what the implications of updating the models might be.

One of the problems to be overcome in performing this testing was identifying how next generation debris models might realistically differ from current models. In the absence of sufficient data to develop viable alternative component models the alternative was to make adjustments to the existing models which reflected the changes predicted by the earlier analysis. The resultant breakup model had an altered fragment size distribution which generated fewer larger fragments and an increased number of small fragments in accordance with the results of Chapter 4. The adapted collision models applied a correction factor, extrapolated from a regression model of

the relationship between the model results and SOCRATES data, which increased the collision probabilities generated for constellation spacecraft.

The development of the adjusted models was achieved by incorporating some of the key characteristics of objects classified as NewSpace, such as the area-to-mass ratio of spacecraft and measures of orbital clustering of the population, and then tuning the models so that their results better fit the limited observational data available. An assumption inherent to the adjusted models was that it was possible to extrapolate from the deviations identified in the specific cases examined in Chapters 4 and 5. However, a valid concern is that the generalisation from a low number of scenarios could lead to these adjusted models being overfitted and as such they may not be appropriate for the Starlink constellation and the Aeolus and Starlink breakups being simulated.

In developing an adjusted form of the breakup model for the simulations conducted in Chapter 6 the assumption was made that the observed trends continued for fragment sizes below the limit of the observations. This assumption is consistent with the assumptions made in the original model but resulted in a greater than 20-fold increase in the number of fragments larger than 1 cm for the simulated collision between Starlink and Aeolus. This increase in the smallest fragments modelled was responsible for a large amount of the increase in final debris population when using this model and hence the subsequent collisions. As a result, the adjusted model could be resulting in the over-estimation of both the final debris population and number of collisions. However, the adjustments made are consistent given the limitations on the available data and provide important insight into the effect of changing the model. Improved knowledge of hyper-velocity impacts - e.g. through experiments like DebriSat - would also add to the data available, and possibly improve the adjustment.

The significance of using a properly representative collision model was highlighted in the changes to the output of the environmental simulations in Chapter 6 when the adjusted version of the Cube model was used. However in the absence of a well understood physical justification for the under-prediction, the correction factor used in the adjusted model was developed empirically on the basis of the results of the simulations from Chapter 5. The assumption was that the relationship between probability and SSDM was linear in the absence of any contrasting evidence.

A key assumption in the adjusted collision models was that spatial structure of space systems is a valid source of error in collision probability estimation when using the Cube and Orbit Trace methods. The results of the collision investigation were highly suggestive of this link but not conclusive, in part because of limitations on available data - SOCRATES was the only public source of data but it predicts a different type of collision probability and so the analysis was restricted to the correlation between SOCRATES and the Cube and Orbit Trace results. It is possible that the source of the observed differences are not a result of the spatial structure but of other differences

between the NewSpace and TradSpace scenarios. If this is the case then the required adjustment may be different to that developed. This results in some uncertainty in the magnitude of the adjustment applied to the Starlink-like scenario simulated in Chapter 6. Ultimately, the adjustments to the models were made empirically using the data available in the public domain and are consistent with the results of the previous investigations.

The impact of the changes to the models became visible once an initial collision event was introduced to the environment. In simulations run using this scenario the final object population was larger; reaching 250% of the result using baseline models when using the adjustments to the collision and breakup models individually and 350% when they were used together. This increase was accompanied by a rise in the collision rates and represents a considerable impact on the environment, highlighting the potential for updates to debris models to substantially change expectations around the future evolution of the environment. Given the acknowledged limitations of the models there is uncertainty around the magnitude of the difference, however the results provide good evidence that updating the models substantially alters the outcome of the simulations.

Analysis of the expected daily number of collision manoeuvres and lifetime collision probability also revealed the impact of updates to the models. The adapted models resulted in substantial increases to the median cumulative collision probability of the Starlink spacecraft - around 250%, 850% and 1500% for the breakup, collision and combined model changes respectively. This raised probability manifested in an increased number of expected daily collision avoidance manoeuvres, with between 3 and 5.5 times more manoeuvres expected for different combinations of the models. The presence of these differences underscored the importance of updating current debris models in order to properly understand the risks and potential costs of these constellations, both to the environment and the individual operators.

While the limitations of the adjusted models introduce uncertainty around the magnitude of these changes there are also limitations in the predictions made by the Cube method due to the impact on probability of the distribution of the Cubes in Cartesian space and the potential for under-sampling. As a result, if the Cube method is not giving the right answers then NewSpace systems could exacerbate these errors and therefore the correlation established with the SOCRATES results. This leads to the conclusion that fundamental limitations in the Cube and Orbit Trace methods combined with NewSpace characteristics are problematic, highlighting the need to update the models.

The results accentuate the sensitivity of the simulations to prospective changes in the breakup model and so confirm the importance of updating the model to ensure a proper understanding of the future environment. Even given the potential impact of the limitations and the required assumptions, the results of the different scenarios and

model combinations provided valuable insight into the sensitivity of simulations to changes in the component models.

7.5 Implications of the Results

It has been shown through this work that updates are required to state of the art debris models to provide accurate insights into NewSpace scenarios. The results of both Chapter 6 and previous studies (Beck, 2013) highlighted how different models can have a substantial effect on the outcome of simulations of the debris environment. As a result, these updates are likely to lead to changes in the understanding of the environment with implications for future space operations. There is an associated risk of thinking that the future of the environment is better understood than it is. This may result in regulation being either inadequate leading to the uncontrolled debris growth or overly strict, stifling future development.

The differences implied by the results of the investigation into the NASA Standard Breakup Model indicate the potential for a significant divergence between the future environment and the results of current models including an increase in the number of small fragments below the trackable size. Simulations incorporating the predicted increase in the number of small fragments resulted in more overall fragments being generated in an initial collision event, which resulted in more collisions but a smaller proportion of catastrophic breakups.

However, there is a population of lethal-non-trackable objects, i.e. one centimetre objects which are too small to reliably track but can still be fatal to a spacecraft involved in a collision. As such there might be a higher than expected risk to individual spacecraft missions resulting in a higher number of anomalous events and disruption to spacecraft services following a major fragmentation event. As tracking capabilities are expanded to include lethal-non-trackable objects there may be many more objects to screen for conjunctions than expected. This would represent a significant alteration of the current understanding of the space environment with implications for the safety of space operations resulting in much greater overhead for spacecraft operators and their regulators. For example, the increased requirements for collision prediction and the management of collision avoidance manoeuvres once these objects are tracked.

The identified under-prediction of the collision probabilities associated with NewSpace implies that conjunctions will be more frequent within large constellations and other highly structured NewSpace systems than is currently expected. A consequence of this will be a greater emphasis on collision avoidance (and the associated tracking) and the likelihood of needing more manoeuvres than expected. There is also the potential for an increased collision rate due to: a failure to manoeuvre

the spacecraft involved; or the objects involved are non-manoeuvrable spacecraft; or the collision involves lethal-non-trackable debris. This higher collision frequency could lead to a negative impact on the stability and sustainability of these regions of the space environment. As a result, mitigation of this risk to environmental sustainability will require a greater emphasis on high reliability of spacecraft, good tracking and conjunction screening capabilities, and a conservative approach to collision avoidance.

A higher frequency of collisions would result in more debris objects being released into the environment, further increasing the collision risk for spacecraft and potentially the collision rate. However, the impact on the sustainability of the environment will depend on the altitude of the constellation and the residual lifetime of the produced debris fragments. When the altitude is low (e.g. for Starlink) the residual lifetime of the majority of debris fragments will be measured in months and so while there will be a short term impact on space safety there will be limited impact on sustainability.

Two key areas of research in the literature have been to study the impact of large constellations and to estimate the effectiveness of different levels of debris mitigation and remediation on the overall environment. The first scenario, large constellations, is a prime example of a NewSpace system and, as the large numbers of constellation spacecraft result in NewSpace spacecraft being a high proportion of the total population, the scenario is one where impacts of model deviations are expected to be most substantial. The higher expected collision probabilities and the increased number of objects released from collisions indicate that current models lead to an underestimation of the impact of these systems. As a result appropriate measures may not be being taken to mitigate the risk that they pose to the sustainability of the environment.

In the case of research into debris mitigation and remediation, which are less focussed on NewSpace specifically, there are also implications of the model deviations. NewSpace spacecraft are becoming increasingly prevalent and with the long term nature of the simulations conducted the compound risk of breakups from collisions resulting in an increased probability of future collisions is likely to be considerable. As a result, the research conducted using current debris models may be underestimating the actions required to maintain a stable environment, such as the required success rate for post mission disposal or the removal rate for ADR.

Additionally, which objects are considered the greatest risk to the environment would potentially change based on updates to the collision models. A large derelict object which intersects a constellation, for example, would have a higher estimated collision probability using updated models. Methods of ranking the criticality of debris objects - for instance those used in McKnight et al. (2021) - tend to focus on risk as a product of the collision probability and the mass (where mass is used as a proxy for the

severity of the collision). Consequently, the increased collision probability would raise the perceived risk from the object compared to an object encountering a more traditional population. As a result, significantly different conclusions might be drawn as to how many and which objects should be prioritised for ADR missions.

Conversely, the results of this investigation suggest that, if models were to be updated, then the different perception of the future of the environment may motivate changes in behaviour for both regulators and spacecraft operators. For instance, NASA's current guidance on collision avoidance manoeuvres is that manoeuvres should be performed for any collision probability in excess of 1 in 10,000 (NASA, 2020) to mitigate the risk to the debris environment. However, if the consequences of a collision are more severe than currently understood then the risk increases. As such, are the collision probability thresholds used for triggering avoidance manoeuvres low enough? SpaceX have recently affirmed the use of a 1-in-100,000 threshold for manoeuvres (Selding, 2021). This choice of a more exacting threshold could be another sign that NewSpace introduces exactly the change proposed here.

Collisions are most likely to be between debris fragments or failed spacecraft which cannot manoeuvre. As a result each spacecraft failure increases the number of objects to potentially be involved in a collision. Due to the greater number of spacecraft involved and the potentially higher than expected collision probability should spacecraft in (or in the vicinity of) constellations be subject to higher standards to reduce the failure probability? Tools used in the licensing process (such as DRAMA and ORDEM) need to reflect the current environment, not an outdated historical or poorly projected future environment. Updates to these tools to enable the proper consideration of recently launched space systems that might be in proximity to the licensee's system could result in stricter approaches being applied to the licensing of new missions and operators might find that the cost of liability insurance increases if the perceived risk is higher.

7.6 Improvements and Recommendations for Future Research

In the process of completing this research there were several limitations identified which future work could refine and expand upon to develop additional knowledge in this field. This section aims to explore several of the most conspicuous of these avenues. In addition, a number of interesting topics for future research were identified. Often these areas were not suitable for inclusion within this project, either due to lack of publicly available data or due to computational limitations.

When looking at the investigation into fragmentation models, the single greatest limitation to the work was the lack of resolution on fragment size. Additional data on the relative RCS of observed fragments would improve estimates made of the size

distribution of fragments. This could then be compared against the results of the model and used to inform the development of new, more refined, models. An alternative option would be to analyse the recorded orbital data for different tracked fragments to calculate the rate of atmospheric decay each experienced. From this it would be possible to extrapolate an estimate of the area to mass ratio of the fragments, providing a different reference characteristic which could be used to train models.

A major advancement would be to gain a physical understanding of why the spatial structure associated with NewSpace is leading to the deviations observed for the Cube and Orbit Trace algorithms. Understanding the root cause of this deviation will be essential to developing the next generation of collision models from a theoretical basis as opposed to the empirical correction performed in this work.

Future investigations of NewSpace collision probabilities could also look at expanding the number and variety of scenarios being simulated. Extracting and processing SOCRATES and TLE data to create new scenarios was a time intensive process. However, a greater number of data points with a broader range of cases would improve understanding of the relationship identified between clustering and relative probability. This would also enable the exploration and testing of different theories about the physical behaviour driving the underestimation of the collision probabilities.

One possible extension of the implementation of the Cube algorithm would be to alter the model to mitigate any biases introduced by the static arrangement of the cubes in Cartesian space. A possible fix would be to remove biases due to the fixed location of cubes either by introducing some randomness to the origin of the frame of reference or by averaging across two or more offset grids of cubes. An alternative method would be to also identify objects in surrounding cubes and then filter for separations less than the cube length - effectively finding all secondary objects within a sphere centred on the first object, a method which is currently employed by DAMAGE and SOLEM (Wang and Liu, 2019).

Another area for investigation would be the identification of an ideal cube size to achieve the minimum simulation error where:

$$overall\_error = sampling\_error + colocation\_error$$

An approach to this would be to treat it as an optimisation problem on the combined error which could be solved to find the optimal cube volume, V. If the co-location error is proportional to V and an asymptotic estimate for the sampling error can be found, then this function can be minimised for one variable, V. This approach may also enable the calculation of the optimal number of samples, N, for a given error bound.

Two of the identified limitations of the environmental simulations were the relatively small number of simulation runs conducted for each scenario; and the extrapolation of

the adjusted models from the small number of observed results in the previous chapters. Future work could include a simulation campaign to alleviate these issues. Ideally increased computational resource would allow these simulations to focus on running at least 100 simulation runs of a smaller set of scenarios in order to gain a robust understanding of the variance in the different metrics and how this changes when the models are adjusted. A potential new scenario would be to use the example of an observed breakup for the defined event, for example the collision of Iridium-33 and Cosmos-2251. In this proposed scenario the investigation could focus on the changed outcomes with less concern about over fitting as the adjusted model would be known to provide an accurate representation of the breakup.

With regard to the analysis of NewSpace and the changes to spacecraft some additional analysis is suggested of a wider range of distinguishing characteristics to help to distinguish between NewSpace and TradSpace. One key consideration which would improve on the current understanding, if the data were made available, is a study of changes in the material composition of spacecraft and what the resulting impact is on the density as these changes might impact the mechanics of fragmentation. Another area which could provide benefits is an analysis of the features of different spacecraft, for instance the number, size, and configuration of deployable solar panels.

One extension to the work would be to repeat the collision and environmental simulations using alternative propagation methods which better capture the range of expected perturbations and the additional uncertainty this introduces to the systems. The use of more advanced orbital propagators would also augment the research into the environmental impact of changes to the component models. Further complexity could also be introduced by incorporating operational behaviours such as constellation replenishment, new background launches, and end-of-life (including post mission disposal). These additions would align the simulation scenarios more closely with existing studies and expected real world behaviour.

The research could also be expanded to study the impact of changing the models on different areas of debris research. By replicating long term simulations (100-200 years) of the stability of the debris environment it would be possible to investigate how NewSpace updates to models might alter predictions around the levels of mitigation and ADR required to achieve a stable environment.

Chapter 8

Conclusions

> I think and think for months and years. Ninety-nine times, the conclusion is false. The hundredth time I am right.
>
> Albert Einstein

The goal of this thesis was to investigate the impact of NewSpace on the future modelling of the space debris environment. This goal arose from the understanding that the next generation of space debris models would need to incorporate more than just more efficient algorithms or increased computational power. These models would also need to take into account how the changes taking place across the space industry are changing the spacecraft population and the expected behaviour of the debris environment.

To provide internal consistency a **novel** definition which quantified the **classification of 'NewSpace' spacecraft** was derived from an initial subjective review. Analysis of characteristics of spacecraft and the space environment concluded that a divergence from historic norms existed for:

- Physical characteristics
- Relative orbital distribution
- Probability of spontaneous breakups

This led to the hypothesis that the assumptions currently used in debris modelling have become less representative of the spacecraft population as NewSpace has become more established. This would result in models failing to adequately capture the behaviour of the processes governing the space debris environment, hampering the utility of the models as tools for research and evaluation.

The results of the investigation conducted into the NASA Standard Breakup Model and the Cube and Orbit Trace collision models, as well as the analysis of the potential significance, demonstrate that it is important for the models to be re-evaluated in response to the changing spacecraft population associated with NewSpace. The inconsistencies identified in both the key fragmentation model and the common collision models will prevent current models from accurately modelling a NewSpace environment, causing the results of the simulations to diverge from reality. This effect is likely to become more pronounced with the continued growth of NewSpace as a segment of the spacecraft population, a process which is accelerated by the deployment of large constellations such as Starlink.

A good understanding of the expected breakup behaviour is essential for understanding the future evolution of the debris environment and the potential risk profile of spacecraft operating in different regions. The issues identified with the current fragmentation model in Chapter 4 provided novel insights into how changes to debris models might alter the current predictions about the future debris environment:

- The increase in the released number of fragments will have a **greater impact on space safety** as secondary collision frequency is increased
    - Leading to an **increased threat to space sustainability**
- The decreased number of large fragments may **reduce the severity of subsequent secondary collisions** as fewer fragments are generated
    - Leading to a **diminished threat to space sustainability**

The conclusion drawn is that overall impact on space sustainability will be dependant on which of these shifts dominates. The need to understand this strengthened the conviction that further development of fragmentation models is essential for establishing a proper understanding of a space environment which includes a significant NewSpace component.

The inferences from the response of collision models in Chapter 5 to the deviation between NewSpace and TradSpace systems were that:

- Current studies of highly ordered space systems, such as large constellations, may be **under-estimating the risk** that the systems pose to the environment.
- **Collisions** in the future environment will be **more common**
- Resulting in **faster growth** of the **debris** population
- Consequently a greater likelihood of an **unsustainable debris environment**

As such it is essential that a better understanding of the true collision risk within these systems is developed in order to understand the potential consequences. As collisions are expected to be a major source of debris generation in the future it is apparent that more research is required to properly understand the probability of collisions in different scenarios.

Further research investigating the sensitivity of simulations of a NewSpace environment to changes in the models supported the argument that updated debris models are needed. The model variations considerably changed the results of several of the modelled scenarios. It was found that the model changes appreciably altered the importance which an initial breakup event had for the predicted evolution of the environment.

The conclusion was drawn that current debris models are likely to be underestimating the impact which NewSpace will have upon the debris environment. It is expected that the increased collision rate identified for large constellations and the potential for this to result in large releases of debris fragments will lead to higher debris growth rates in the occupied regions. This growth will have consequences for the risk profile of future space missions.

The prospect of the space debris environment deteriorating faster than predicted highlights that the threat of **unsustainable space debris growth** may be a **more immediate** and **higher severity** risk than is appreciated. The consequence is that **current approaches to controlling the debris population and mitigating the risks posed might be insufficient** because they have been based on potentially flawed model predictions and as a result there may be **less time to develop appropriate means of counteracting the problem**.

The overall conclusions of this thesis are that:

- **NewSpace could pose an under-recognised threat to the stability of the environment**
- **Continued work to update current debris models and understand their limits should be a priority for the debris modelling community**

It is hoped that a new generation of debris models will change perspectives and lead to a better understanding of space debris behaviour and risks in the current and future space environment.

8.1 Novel Contributions

This work provides a number of novel contributions to the understanding of NewSpace and its impact on debris modelling capabilities. These contributions include:

- A new classification scheme for identifying NewSpace spacecraft
- An understanding of current and historic trends in spacecraft characteristics, spatial structure and explosions
- Insight into the limitations of the NASA Standard Breakup Model
- The identification of deviations in fragment size distributions for the NASA Standard Breakup Model compared to recent observed breakups
- A comparison of the limitation and computational performance of the Cube and Orbit Trace collision algorithms
- The discovery and quantification of a relationship between spatial structure and relative collision probability for both the Cube and Orbit Trace collision algorithms
- Development of empirically adjusted versions of the Cube, Orbit Trace and NASA Standard Breakup models to account for the NewSpace deviations identified
- Evidence of the sensitivity of evolutionary debris models to justifiable adjustments to the component fragmentation and collision models
- Insight into how updates to debris models to account for NewSpace could alter the results of simulations of constellations

Appendix A

Verification of the Implementation of the NASA Standard Breakup Model

Verifying Fragment Generation Against Historic Studies

In order to verify the new implementation of the NASA Standard Breakup model test cases from an historic study were replicated and the results compared. The study used for this verification was originally conducted by the IADC WG2 in 2006 (Rossi, 2006). The study consisted of two key test cases, an exploding 1,000 kg rocket body, and the collision of a 10 kg object with a 1,000 kg spacecraft at a relative velocity of 10 km/s.

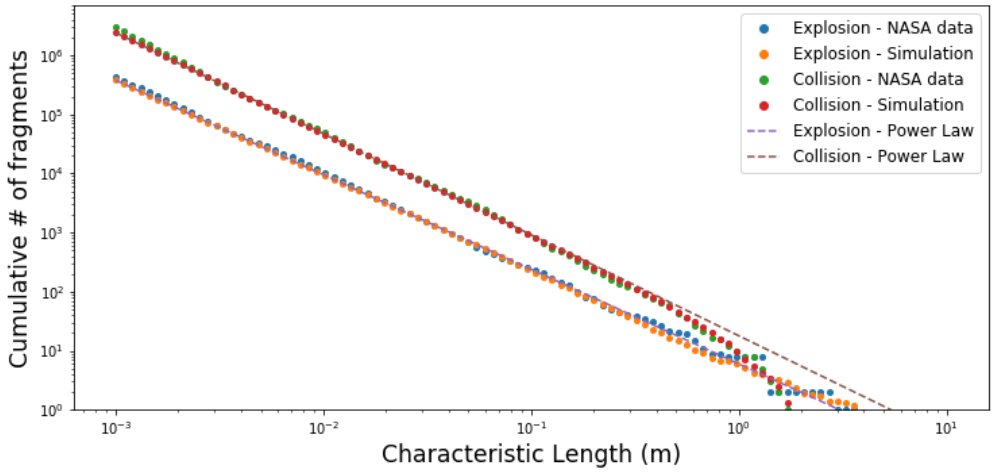

FIGURE A.1: Showing the cumulative number of debris generated by the model against characteristic length for both explosions and collisions compared to the results published by NASA (Krisko, 2011).

The new implementation was used to simulate these fragmentations and evaluate the cumulative number of fragments greater than 100 different characteristic lengths evenly distributed in log-space. Figure A.1 shows the results generated by the new implementation against those generated by NASA for the original study. The newly generated results in this figure were averaged across 10 independent simulations of each fragmentation.

A quantitative comparison of the NASA results with those of the new implementation gave values for the mean arctangent absolute percentage error (Kim and Kim, 2016) of 0.2715 for the explosion scenario (0.1286 if bins with zero fragments are excluded) and 0.0739 for the collision scenario[1]. These results suggest a strong agreement between the results of the NASA model and those generated by the new implementation.

Verifying Distributions of Fragment Characteristics

In addition to testing the total number of fragments generated a comparison was made against the IADC study across a wider range of fragment characteristics to complete the verification of the results from the new implementation. The generated distributions for characteristic length, mass, cross sectional area and velocity were compared against the results published in the IADC report (Rossi, 2006) for the outputs generated by each of NASA, ESA, German Aerospace Center (DLR), China National Space Administration (CNSA) and Agenzia Spaziale Italiana (ASI).

TABLE A.1: A table comparing the characteristics of explosion fragments generated by the newly implemented model and those reported by IADC WG2 (Rossi, 2006).

Model	**Number of Fragments**						
	Length				Mass	Area	Velocity
	> 1 mm	> 1 cm	> 10 cm	> 1 m	> 1 g	$> 1\,cm^2$	$> 100\,ms^{-1}$
ASI	378,581	9,403	234	7	2,472	5,878	112,932
CNSA	37,865	960	32	9	254	-	11,380
DLR	1,217,054	11,724	230	0	25,844	31,124	31,124
ESA	324,886	8,159	206	6	2,093	5,024	98,717
NASA	434,928	10,731	248	8	2,525	6,416	132,032
New Model	473,218	11,857	288	7	3,299	7,279	142,829
Deviation[2](σ)	1.70	1.89	2.74	0.00	3.97	2.15	1.69

In the first instance the number of fragments generated with characteristic values above defined thresholds are examined for the explosion case. This data can be seen in table A.1. The results for DLR and CNSA deviate noticeably from these values suggesting differences in implementation. While the effect of these models combine to have relatively little effect on the mean, including them significantly increases the

[1] This error calculation returns a value between 0 and $\pi/2$ and was adopted due to the combination of logarithmic scaling and zeros.

[2] Number of standard deviations from the mean (excluding results as noted)

variance of the results. Consequently the results of the new implementation have been primarily compared against the models from NASA, ASI and ESA, which show similar results to each other.

TABLE A.2: A table comparing the characteristics of collision fragments generated by the newly implemented model and those reported by IADC WG2 (Rossi, 2006).

Model	**Number of Fragments**				
	Length		Mass	Area	Velocity
	> 1 mm	> 10 cm	> 1 g	$> 1\, cm^2$	$> 1\, kms^{-1}$
ASI	2,416,795	850	11,330	27,450	528,301
CNSA	2,416,790	935	11,125	-	523,120
ESA	4,723,391	1,539	13,467	30,366	822,539
NASA	2,957,159	862	12,600	28,892	638,537
New Model	2,416,788	915	12,096	28,059	533,979
Deviation^2 (σ)	-0.58	0.71	0.51	-0.01	-0.45

Similar data was generated for the described collision scenario, as shown in table A.2. In this data set the numbers reported by ESA are significantly greater than the remainder - as before, these have been excluded from the statistical analysis.

Fragment Length

The first characteristic to be compared was the fragment length. Histogram plots showing the number of fragments generated at each characteristic length are shown below with the results of the new model visible in figures A.2(a) & A.2(c) and the results of the IADC investigation in figures A.2(b) & A.2(d). The scale of the axes have been matched across all the graphs for ease of visual comparison.

Looking first at the behaviour of the explosion scenario in figures A.2(a) & A.2(b) it is possible to see, graphically, the trend visible in table A.1 for the relationship between number of fragments and characteristic length. The results from the new implementation have a slightly higher starting point than the results from the IADC study but follow the same exponential curve downwards.

Next, comparing between figures A.2(c) & A.2(d) showing the collision scenario, a similar relationship can be seen. The curve generated by the new implementation fits between those generated by the NASA and ASI models. These graphs confirm the concurrence already observed between the models for the characteristic length.

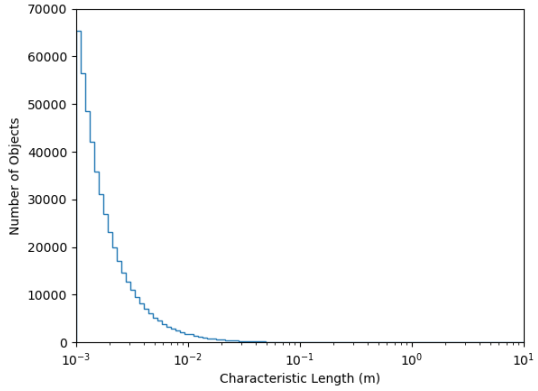

(A) Distribution of generated fragment lengths for the explosion scenarios.

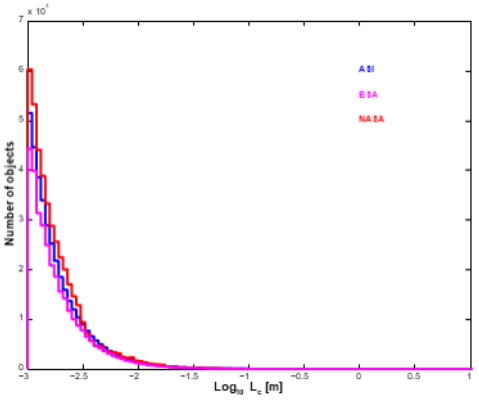

(B) Distribution of IADC fragment lengths for the explosion scenario.

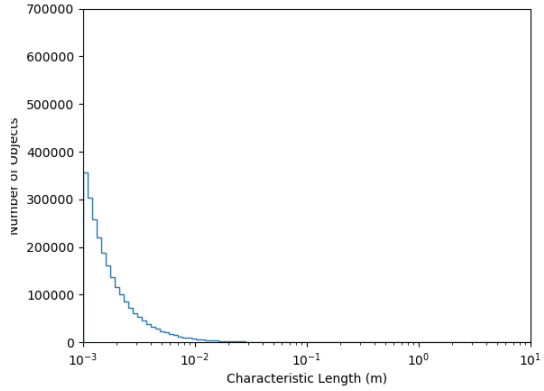

(C) Distribution of generated fragment lengths for the collision scenarios.

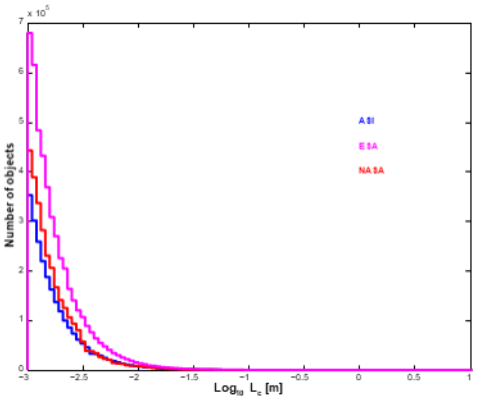

(D) Distribution of IADC fragment lengths for the collision scenario.

FIGURE A.2: Graphs showing the distribution of fragment lengths compared to the results of the IADC WG2 (Rossi, 2006).

Fragment Mass

Next to be investigated was the distribution of the mass assigned to each fragment by the different models. The results of this are observable in figure A.3. As previously the graphs used have been scale matched to enable visual inspection. In the explosion scenario the distribution generated by the new implementation has a comparable shape to that reported by the IADC models. In all cases the distribution tends sharply upwards from 10^{-7}kg to a peak at around $10^{-5.5}$kg beyond which there is a shallower exponential curve on both graphs to about 2,500 objects at 0.0001kg. The distribution shown for the new model seems to match that of the NASA model closest, peaking between 45,000 and 50,000 objects in the bins at this mass.

For the collision case there is also a good fit observed, with the limits and peaks of the distribution occurring at the same points as in the explosion scenario. Here the closest fit appears to be to the ASI model, with both peaking around 250,000 objects per bin. However, there is also a close match with the NASA model which peaks at 300,000. These results indicate that there is a strong agreement between the new

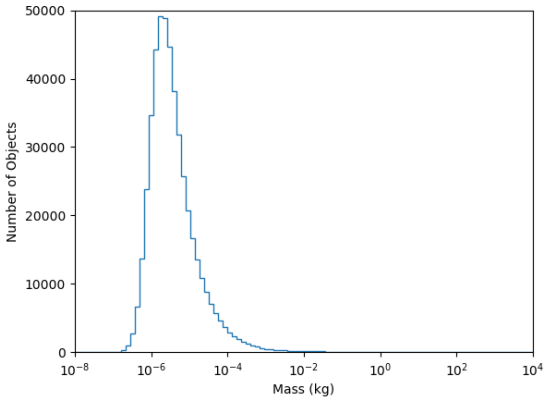

(A) Distribution of generated fragment masses for the explosion scenarios.

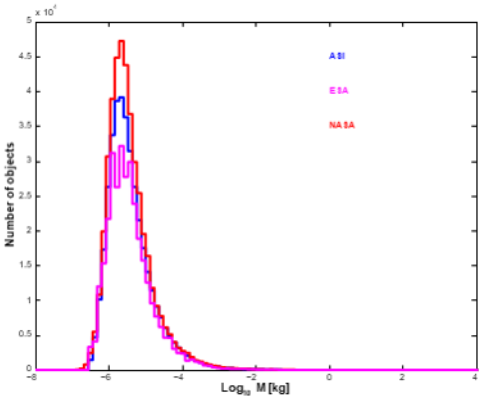

(B) Distribution of IADC fragment masses for the explosion scenario.

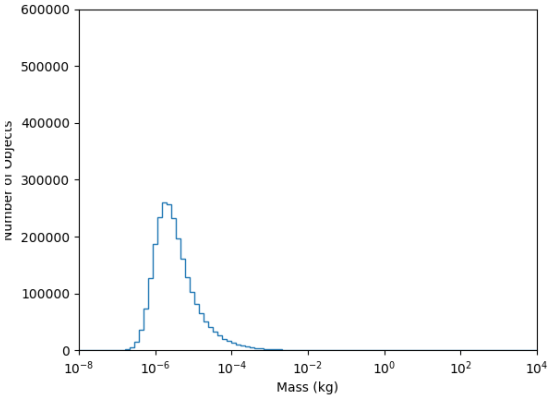

(C) Distribution of generated fragment masses for the collision scenarios.

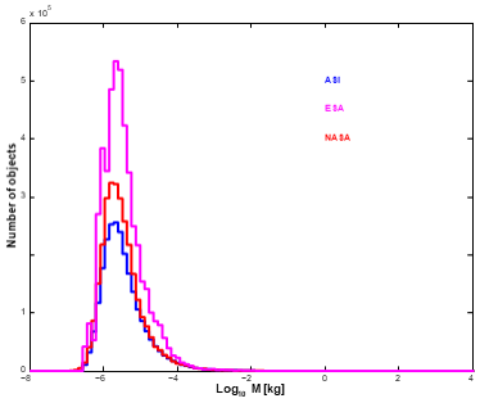

(D) Distribution of IADC fragment masses for the collision scenario.

FIGURE A.3: Graphs showing the distribution of fragment masses compared to the results of the IADC WG2 (Rossi, 2006).

implementation of the NASA Standard Breakup Model and those used in the IADC study when it comes to distributing mass across a population of fragments.

Fragment Area

Figure A.4 shows the distribution of the cross sectional areas of the fragments for both scenarios. For this characteristic the axes could not be completely matched as, for figure A.4(b), the maximum of the scale for number of objects is 60,000 while for each of the other graphs it has been set to 70,000 to accommodate the peak values.

Comparing the model results against those published by the IADC, for both the explosion and collision scenarios, there is again a good fit. The results for the areas of the fragments follow a similar distribution to that of the characteristic length, as might be expected due to the direct relationship between the two features. As with the other characteristics the peak for the explosion test case is highest for the new

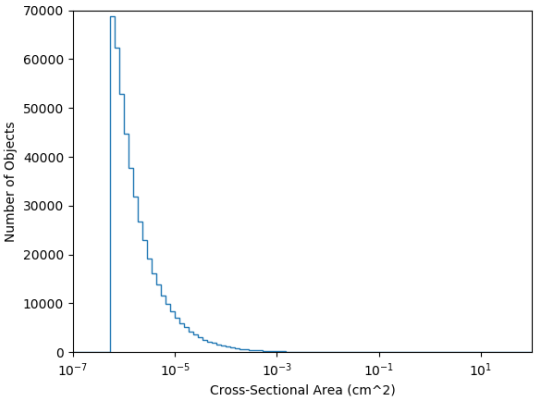

(A) Distribution of generated fragment areas for the explosion scenarios.

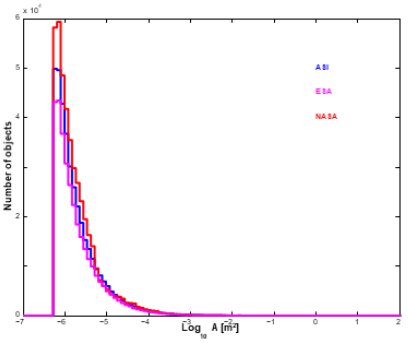

(B) Distribution of IADC fragment areas for the explosion scenario.

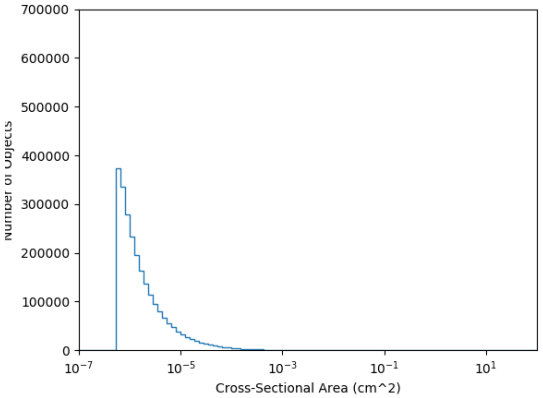

(C) Distribution of generated fragment areas for the collision scenarios.

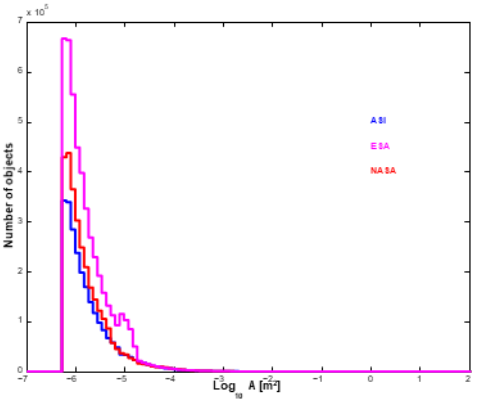

(D) Distribution of IADC fragment areas for the collision scenario.

FIGURE A.4: Graphs showing the distribution of fragment areas compared to the results of the IADC WG2 (Rossi, 2006).

implementation, at almost 70,000 objects per bin, but this is also close to the NASA model at 60,000. For the collision test case the peak value at 37,000 falls between those of the ASI and NASA models at 35,000 and 45,000 respectively.

The comparison of these distributions serves to reinforce the confidence in the convergence of the new implementation to existing models.

Fragment Velocity

The final characteristic to be compared is the distribution of the velocity of the generated fragments. This has been plotted below in figure A.5 for the new implementation and the IADC study. As above the graphs have been plotted on matched axes for visual comparison.

When compared against the reported results the new model for the explosion case demonstrated a convincing fit. The plotted data shows a peak of 19,000 objects

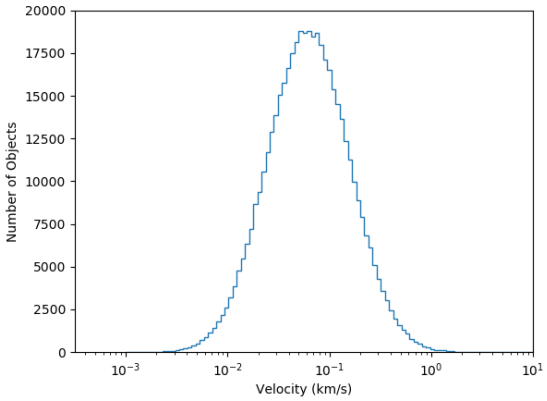

(A) Distribution of generated fragment velocities for the explosion scenarios.

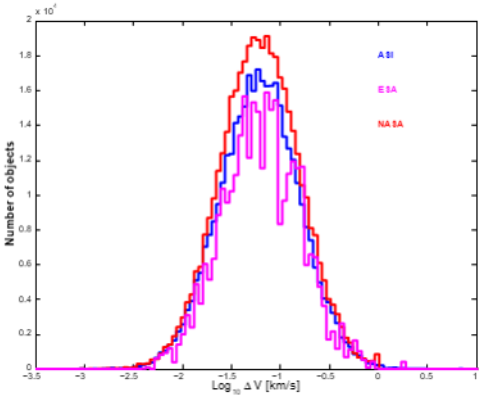

(B) Distribution of IADC fragment velocities for the explosion scenario.

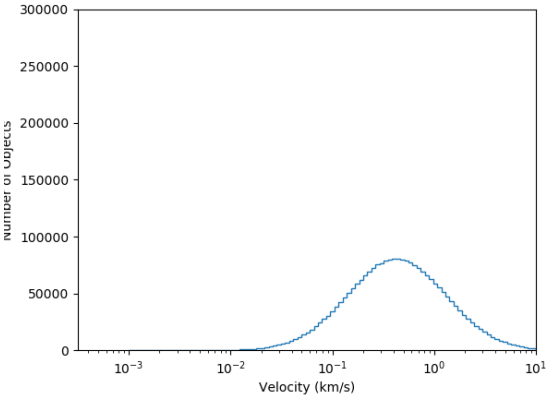

(C) Distribution of generated fragment velocities for the collision scenarios.

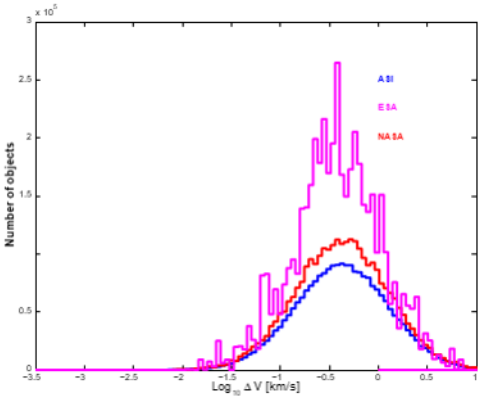

(D) Distribution of IADC fragment velocities for the collision scenario.

FIGURE A.5: Graphs showing the distribution of fragment velocities for collisions compared to the results of the IADC WG2 (Rossi, 2006).

occurring at approximately 70m/s while the reported data shows peaks of 16,000, 17,000 and 19,000 for ESA, ASI and NASA respectively. In both graphs the distribution falls away evenly to either side in log-space.

For the collision scenario the results are slightly less clear due to the magnitude of the distribution generated by the ESA model. However, each model peaks at 400m/s and the peak of the results compares favourably to the NASA and ASI results at 800,000 objects per bin.

This comparison suggests that the new implementation agrees strongly with the ASI, NASA and ESA models when assigning velocity to the fragments. A notable exception is the ESA model for collision fragmentations, which appears to generate significantly more energetic fragments than the new implementation or either of the other models.

Summary of Verification

Over the course of this verification process, simulations were run for two different scenarios, representing an explosion and a catastrophic collisions. The results from each of these were visually and numerically compared against published sets of results generated by alternative implementations of the NASA Standard Breakup model. A comparison was made of the number of fragments generated by the model as well as the distributions of the length, mass, area and velocity characteristics of the fragments.

Comparing the numbers for the different model implemented it can be seen that the results of three agencies (ASI, ESA and NASA) produce comparable results. An examination of the results generated by the new implementation shows that the number of fragments generated at each threshold value are of the same order as those generated by the NASA, ESA and ASI models. A measure of the deviation can also be seen in table A.1, reported as a number of standard deviations (σ) away from the mean value.

Ignoring fragments greater than 1 m in length, which are statistically small and generated using conservation of mass, the deviation varies from 1.69σ to 3.79σ. The deviation is noticeably larger with the smaller statistical populations that exist for the larger fragment sizes. These results indicate agreement between the new implementation and existing models for an explosion fragmentation event. The results generated by the new implementation were shown to be consistent with those reported by NASA, ASI and ESA for each of the key characteristics examined. The main difference observed was that the new implementation generated slightly more fragments for explosions, particularly of smaller size, than was reported in the existing studies.

There were a few cases where there was some level of deviation, including the comparison of cumulative number of fragments at different characteristic lengths for the NASA explosion scenario where the new implementation reports a larger number of fragments between 10cm and 1m. The deviation in this case does not appear to be significant. Another difference was that the magnitude of the velocity distribution reported by ESA for the collision scenario is significantly higher, however, the results of the new implementation compare well with those reported by NASA and ASI, making the ESA model the outlier.

Taking the combination of the results of each of these test cases provides a high level of confidence in the implementation of the model. While some deviations exist these are expected, to a small degree, due to differences in implementation. The results generated by the new implementation are of a consistent order of magnitude with those reported by the existing models. This suggests that no significant issues exist in

this implementation of the NASA Standard Breakup Model and as such it is suitable for use in validating the mathematics underlying the model.

Appendix B

Verification of the Implementation of Collision Algorithms

Verifying Against Historic Test Cases

Two historic studies were replicated in order to verify the new implementations of the Cube approach and the Orbit Trace collision algorithm for this investigation. The two studies described by Liou et al. (2003) for the original Cube implementation were replicated and the results compared against the published values. The studies described were themselves repetitions of earlier studies conducted using Orbit Trace techniques.

The first scenario was a study of calculated collision rates for different combinations of four pro-grade Jovian moons (Kessler, 1981) and the second of calculated intrinsic collision rates between six known asteroids and a hypothetical asteroid 'Astrid' (Wetherill, 1967). The new implementations were used to generate collision probabilities across a large number of potential orbital configurations of each scenario using one day time-steps.

The test objects were initialised using the values defined for their orbital elements in the original literature, with fixed values for the semi-major axis, eccentricity, and inclination and random sampling of the mean anomaly, the RAAN, Ω, and argument of perigee, ω. Varying these angular orbital elements accounted for the expected long term effects of perturbations on the orbits and so avoided the need for a more involved propagation process.

B.1 Cube Results

For both of the scenarios the test objects were initialised using the orbital elements from the original literature. When replicating the two studies an initial value of 1% of the average semi-major axis of the respective systems was chosen for the dimension for the cubes. This gave side length of 115,075 km and 3,306,374 km for the Jovian moons and asteroid scenarios respectively. The Cube algorithm was applied repeatedly to each system over 3.65×10^{10} samples to calculate the average collision rates for each collision pair in the system. This was considered to provide a sufficient number of evaluations to ensure that the total average collision rate had converged for each collision pair.

Table B.1 shows how the results calculated using the new implementation compared against the previously published results for both the Cube approach and an earlier method. This earlier approach was formulated by Kessler (1981) and was repeated around the original release of the Cube Approach algorithm for comparison.

TABLE B.1: Collision rates ($10^{-10}/year$) between different combinations of fours Jovian moons (Liou et al., 2003).

Collision Pair	**Kessler (1981)**	**2003 - Kessler**	**Liou et al. (2003) - Cube**	***New - Cube***	Deviation from Cube (%)
Himalia-Elara	4.3	4.1	4.2	*4.2227*	*0.54*
Himalia-Lysithea	2.8	3.4	3.5	*3.5756*	*2.16*
Himalia-Leda	3.1	3.0	3.2	*3.2239*	*0.75*
Elara-Lysithea	0.52	0.51	0.52	*0.5280*	*1.54*
Elara-Leda	0.57	0.57	0.56	*0.5917*	*5.66*
Lysithea-Leda	0.039	0.038	0.038	*0.0386*	*1.58*

The new results are consistently higher than the previous results with errors of only a few percent relative to the published Cube results. Each is of the same order of magnitude as the published results and have the same scale relative to one another. This deviation is expected to be due to minor differences in implementation and computing platform. The results generated by the new implementation are consistent with the original Cube results to the same degree that the Cube results were with the preceding results.

TABLE B.2: Intrinsic collision rates ($10^{-18}/year$) between six different asteroids and the hypothetical asteroid 'Astrid' (Liou et al., 2003).

Asteroid	**Wetherill (1967)**	**Greenberg (1982)**	**Bottke and Greenberg (1993)**	**Liou et al. (2003) - Cube**	***New - Cube***	Deviation from Cube (%)
1948EA	3.10	2.49	3.20	3.23	*3.3003*	*2.18*
Apollo	4.22	3.24	3.60	3.77	*3.7758*	*0.15*
Adonis	4.13	3.92	4.53	4.79	*5.1734*	*8.00*
1950DA	3.90	3.13	3.76	3.65	*3.9003*	*6.86*
Encke	3.49	2.91	3.43	3.64	*3.447*	*-5.30*
Brorsen	0.94	0.81	0.95	1.01	*1.0378*	*2.75*

The converged collision rates for the asteroids scenario are shown in table B.2 against the results published in several earlier studies using both the Cube approach and its predecessors. In this scenario, intrinsic collision rates are calculated using an assumed combined radius for two asteroids of 1 km. As with the Jovian moons case there are

differences between the results reported by the new implementation and those published. However, as before the results as a whole are consistent with both the published Cube results and the historic results, with errors of less than 10%.

While the agreement between the new results and the original Cube study for this scenario is worse than for the Jovian moons, there is still good agreement with the previous results. When taken together the results from these two scenarios indicates that this implementation is behaving as expected and overall this provides a high level of confidence in the new implementation of the Cube algorithm.

B.2 Orbit Trace Results

When testing the Orbit Trace algorithm an enhanced collision threshold and correction factor was used to artificially increase the number of conjunctions and so improve the rate of convergence of the collision probabilities due to the small number of objects used for each scenario. A value of 0.1% of the average semi-major axis of the systems was used, giving thresholds of 11,507.5 km and 330,637.4 km for the Jovian moons and asteroid cases respectively. This allowed a reduction in the number of evaluations needed for the Cube verification to give collision rates based on only 3.65×10^6 samples.

Table B.3 shows the results of the replication of the Jovian moons case and the percentage deviation of the results from the historically computed values Kessler (1981); Liou et al. (2003). The collision rates generated by the new implementation are in good agreement with previous results, with each of the results falling within the range of the previous values and an average deviation from the previous results of only 1.37%.

TABLE B.3: Collision rates ($10^{-10}/year$) between different combinations of fours Jovian moons (Liou et al., 2003).

Collision Pair	**Kessler (1981)**	**2003 - Kessler**	**Liou et al. (2003) - Cube**	***New - Orbit Trace***	Deviation from Orbit Trace (%)
Himalia-Elara	4.3	4.1	4.2	*4.1793*	*0.49*
Himalia-Lysithea	2.8	3.4	3.5	*3.4067*	*5.36*
Himalia-Leda	3.1	3.0	3.2	*3.0628*	*1.20*
Elara-Lysithea	0.52	0.51	0.52	*0.5149*	*0.34*
Elara-Leda	0.57	0.57	0.56	*0.5702*	*0.62*
Lysithea-Leda	0.039	0.038	0.038	*0.0384*	*0.17*

The majority of this deviation is caused by the results for one of the historic results for Himalia-Lysithea while the more recent calculations of the collision rate agree with the new implementation. Excluding the value of 2.8 as an outlier reduces the average deviation of the new results to 0.68%.

Table B.4 shows the results of the new implementation when it was applied to the asteroids scenario. As with the Jovian moons test case all of the results fall within the range of previous values generated for each object pair indicating good agreement

with these historic results. For this scenario the average deviation from the historic results is slightly higher, at 5.66%, however this is largely due to the larger variance between the different historic results. A direct comparison against the most recent historical results published by Bottke and Greenberg (1993) gives an average deviation of only 0.49%.

TABLE B.4: Intrinsic collision rates ($10^{-18}/year$) between six different asteroids and the hypothetical asteroid 'Astrid' (Liou et al., 2003).

Asteroid	**Wetherill (1967)**	**Greenberg (1982)**	**Bottke and Greenberg (1993)**	**Liou et al. (2003) - Cube**	***New - Cube***	Deviation from Orbit Trace (%)
1948EA	3.10	2.49	3.20	3.23	*3.1676*	*8.11*
Apollo	4.22	3.24	3.60	3.77	*3.5920*	*2.57*
Adonis	4.13	3.92	4.53	4.79	*4.5126*	*7.61*
1950DA	3.90	3.13	3.76	3.65	*3.7510*	*4.29*
Encke	3.49	2.91	3.43	3.64	*3.4522*	*5.36*
Brorsen	0.94	0.81	0.95	1.01	*0.9543*	*6.03*

In conjunction these two sets of results show that this implementation of the Orbit Trace algorithm is performing to expectations. This provides a high level of confidence in the further use of the implementation to study the impacts of NewSpace on its performance.

Summary of Verification

In this verification processes two historic simulations have been replicated and the results for the new implementation compared against published results. The generated collision rates using the Cube method were of the same order of magnitude and had the same size relative to one another. The average error was 2.04% for the Jovian moons scenario and 2.44% for the Asteroids scenario relative to the published results from the Cube. For both of the two verification test sets the results using the new model were seen to be in good agreement with the published results.

The same two scenarios were then replicated using an implementation of the Orbit Trace algorithm. Again, good results were generated which favourably compared to the results of historic investigations. An average deviation was achieved of 1.37% for the Jovian moons scenario and 5.66% for the Asteroids scenario, which dropped to 0.68% and 0.49% respectively when comparing against only the most recent results.

These results were deemed to be within the limits of acceptable deviation from the published results providing a high level of confidence in the new implementations of both the Cube and Orbit Trace algorithms. This indicated that they were suitable for further use in testing the performance of the models in simulations of the NewSpace environment. However, it was noted that for these test cases the Cube model was sensitive to the choice of cube size and this should be considered in further investigations.

Appendix C

Verification of the Implementation of the SGP4 Propagator

Verifying Against Recorded Test Cases

A pre-existing implementation of the SGP4 propagator created in C++ by Vallado et al. (2006) was used for this project. However, it was still necessary to perform verification testing of the integration of this model within the debris simulation framework created for this project. A defined set of verification test cases exist for this implementation of the SGP4 model and these were replicated using the new integration for comparison.

The verification test set consists of the TLEs of 33 different objects which span the different modes of operation and different error states of the propagator. For each scenario a set of position and velocity vectors are defined as the expected state at a set of given points in time around the defined epoch for the object. Using the new integration these position and velocity vectors were regenerated for each scenario. The magnitude of the error between the new output and the historic result was calculated for each of the position and velocity vectors and the mean and standard deviations of these errors were calculated across the different points for each scenario.

The results of this testing are shown in table C.1. Good results were generated for 32 of the 33 scenarios, with the exception being the test case 33334 xx. This test case is intended to test the handling of error code 4 within the implementation, which indicates that the semi-latus rectum of the described ellipse is less than zero. No results are generated for comparison in this instance as the error is thrown on the first propagation step and this integration handles reported errors by removing the objects from the orbital population. As such an absence of results is treated as the correct behaviour for this scenario.

For the remaining 32 scenarios the magnitude of the position error varied between 1.502×10^{-6} and 0.00227 km, with an average error of 3.521×10^{-5} km, or 35.21 mm

TABLE C.1: Results of the comparison of regenerated position and velocity vectors against historic values.

Test Case	**Mean Error**		**Standard Deviation (error)**	
	Position (km)	Velocity (km/s)	Position (km)	Velocity (km/s)
00005 xx	2.6713E-06	4.6594E-07	6.0053E-07	1.6586E-07
04632 xx	1.1313E-05	4.1942E-07	1.0421E-06	1.0678E-07
06251 xx	1.0055E-05	5.0995E-07	5.4021E-06	1.3599E-07
08195 xx	1.1074E-05	4.6605E-07	3.4115E-06	1.2474E-07
09880 xx	1.1097E-05	4.8745E-07	3.5296E-06	1.1060E-07
09998 xx	1.1604E-05	4.5184E-07	6.1944E-07	1.3145E-07
11801 xx	7.0501E-05	5.6855E-07	5.8211E-05	9.8564E-08
14128 xx	1.3392E-05	4.7082E-07	6.1610E-07	1.5720E-07
16925 xx	8.7473E-05	4.2717E-07	1.0297E-04	1.1586E-07
20413 xx	5.1123E-05	4.7032E-07	9.2194E-06	1.3469E-07
21897 xx	1.1159E-05	5.1313E-07	3.4989E-06	1.2043E-07
22312 xx	2.1609E-04	5.7499E-07	1.7743E-04	2.0280E-07
22674 xx	1.2031E-05	4.6843E-07	4.1546E-06	1.4397E-07
23177 xx	9.4670E-06	4.5233E-07	3.4008E-06	1.3160E-07
23333 xx	4.0916E-05	4.9634E-07	1.8646E-05	1.7761E-07
23599 xx	1.4591E-05	4.5823E-07	9.1787E-06	1.3810E-07
24208 xx	1.2640E-05	4.2420E-07	4.2925E-07	1.5568E-07
25954 xx	1.3290E-05	4.9405E-07	6.8184E-07	1.3132E-07
26900 xx	1.2650E-05	5.7161E-07	2.2675E-07	5.9871E-08
26975 xx	1.0440E-05	4.5252E-07	2.6111E-06	1.4826E-07
28057 xx	1.0081E-05	4.5297E-07	5.3523E-06	1.6567E-07
28129 xx	8.4999E-06	4.2337E-07	4.6512E-07	1.2411E-07
28350 xx	2.4392E-04	6.3716E-07	2.2779E-04	2.1124E-07
28623 xx	2.5668E-05	5.2177E-07	2.2753E-05	9.3935E-08
28626 xx	1.2668E-05	5.1271E-07	3.4728E-07	1.0603E-07
28872 xx	1.9830E-06	4.0861E-07	2.3152E-07	1.2066E-07
29141 xx	9.3003E-05	4.4826E-07	1.0564E-04	1.5369E-07
29238 xx	3.2846E-06	5.4221E-07	1.3645E-06	1.2952E-07
88888 xx	3.9163E-06	4.0603E-07	1.7103E-06	1.0009E-07
33333 xx	4.9134E-04	4.8874E-07	8.9113E-04	1.0133E-07
33334 xx	-	-	-	-
33335 xx	2.0925E-05	5.0376E-07	6.4457E-06	1.2503E-07
20413 xx	2.0146E-05	4.6315E-07	2.5862E-06	1.3879E-07

across every time point for every scenario. When compared against the average magnitude of the position vectors (36,946 km) this corresponds to an error of 9.53×10^{-8}%. For the velocity errors these values were 5.647×10^{-8} and 1.116×10^{-6} km/s with an average error of 4.810×10^{-7} km/s, or 0.481 mm/s. Compared against the average magnitude of the velocity (4.387 km/s) this is an error of around 1.10×10^{-5}%.

Summary of Verification

A verification of this integration of the SGP4 propagator was performed against a historic set of defined test cases for the propagator. Across the 33 test cases the average across all scenarios of the mean errors for position and velocity was found to be 4.9×10^{-5} km and 4.8×10^{-7} km/s with standard deviations of 5.2×10^{-5} and 1.3×10^{-7} respectively. These results show a strong agreement with the historic results as the errors were considered sufficiently small relative to the scale of the vectors. This gives a high level of confidence to the use of this integration of the model.

References

Nodir Adilov, Peter J. Alexander, and Brendan M. Cunningham. An Economic Analysis of Earth Orbit Pollution. *Environmental and Resource Economics*, 60(1):81–98, jan 2015. ISSN 15731502. . URL http://www.orbitaldebris.jsc.nasa.gov/newsletter/pdfs/ODQNv13i2.

Salvatore Alfano. Relating position uncertainty to maximum conjunction probability. *Journal of the Astronautical Sciences*, 53, 01 2004.

Kyle T Alfriend, Maruthi R Akella, Joseph Frisbee, James L Foster, Deok-Jin Lee, and Matthew Wilkins. Probability of collision error analysis. *Space Debris*, 1(1):21–35, 1999.

M. R. Ananthasayanam, A. K. Anilkumar, and P. V. Subba Rao. A new stochastic impressionistic low Earth model of the space debris scenario. *Acta Astronautica*, 59 (7):547–559, oct 2006. ISSN 0094-5765. . URL https://www.sciencedirect.com/science/article/pii/S0094576506001676.

Roxana Larisa Andrișan, Alina Georgia Ioniță, Raúl Domínguez González, Noelia Sánchez Ortiz, Fernando Pina Caballero, and Holger Krag. Fragmentation Event Model and Assessment Tool (Fremat) Supporting on-Orbit Fragmentation Analysis. In *7th European Conference on Space Debris, Darmstadt, Germany*, 2017.

L. Anselmo. The long-term evolution of the space debris environment. In Huguette Sawaya-Lacoste, editor, *Space Debris*, volume 1 of *ESA Special Publication*, pages 333–340, October 2001.

L. Anselmo and C. Pardini. An Index for Ranking Active Debris Removal Targets in LEO. In *Proc. 7th European Conference on Space Debris, Darmstadt, Germany, 18–21 April 2017*, number 1, pages 18–21, 2017.

L. Anselmo and C. Pardini. Dimensional and scale analysis applied to the preliminary assessment of the environment criticality of large constellations in LEO. *Acta Astronautica*, 158:121–128, may 2019. ISSN 00945765. .

P. Anz-Meador. Top Ten Satellite Breakups Reevaluated. *Orbital Debris Quarterly News*, 20(1&2), 2016. URL https://www.orbitaldebris.jsc.nasa.gov/quarterly-news/pdfs/

odqnv20i1-2.pdf.

Phillip D. Anz-Meador, John N. Opiela, Debra Shoots, and J.-C. Liou. History of On-Orbit Satellite Fragmentations, 15th Edition. Technical report, NASA, jul 2018. URL https://ntrs.nasa.gov/search.jsp?R=20180008451.

R. Arlt. The sunspot observations by Samuel Heinrich Schwabe. *Astronomische Nachrichten*, 332(8):805–814, oct 2011. ISSN 00046337. . URL http://doi.wiley.com/10.1002/asna.201111601.

E Ausay, A Cornejo, A Horn, K Palma, T Sato, B Blake, F Pistella, C Boyle, N Todd, J Zimmerman, N Fitz-Coy, J.-C Liou, M Sorge, T Huynh, J Opiela, P Krisko, and H Cowardin. A Comparison of the SOCIT and DebriSat Experiments. In *7th European Conference on Space Debris*, 2017. URL https://conference.sdo.esoc.esa.int/proceedings/sdc7/paper/729/SDC7-paper729.pdf.

R. V. Baluev and D. V. Mikryukov. Fast error-controlling MOID computation for confocal elliptic orbits. *Astronomy and Computing*, 27:11–22, apr 2019. ISSN 22131337. .

Roman V. Baluev and Denis V. Mikryukov. distlink: Minimum orbital intersection distance (MOID) computation library, December 2018.

Pang Baojun, Xiao Weike, Peng Keke, and Wang Dongfang. The Space Debris Environment Engineering Model SDEEM 2015. In *7th European Conference on Space Debris, Darmstadt, Germany*, number April, pages 18–21, 2015.

B. Bastida Virgili, J. C. Dolado, H. G. Lewis, J. Radtke, H. Krag, B. Revelin, C. Cazaux, C. Colombo, R. Crowther, and M. Metz. Risk to space sustainability from large constellations of satellites. *Acta Astronautica*, 126(2016):154–162, 2016a. ISSN 00945765. . URL http://dx.doi.org/10.1016/j.actaastro.2016.03.034.

B Bastida Virgili, H Krag, H Lewis, J Radtke, and A Rossi. Mega-constellations, small satellites and their impact on the space debris environment. In *Proc. of the 67th International Astronautical Congress (IAC), Guadalajara, Mexico, 26-30 September 2016*, 2016b.

J Beck. Review of Space Debris Population Prediction. Technical Report November, Belstead Research Ltd., 2013.

G. Bianchi, G. S. Aglietti, and G. Richardson. Development of efficient and cost-effective spacecraft structures based on honeycomb panel assemblies. In *2010 IEEE Aerospace Conference*, pages 1–10, 2010. .

Lars Blackmore. Autonomous precision landing of space rockets. *The Bridge*, 46:15–20, 01 2016.

Byron Blakey-Milner, Paul Gradl, Glen Snedden, Michael Brooks, Jean Pitot, Elena Lopez, Martin Leary, Filippo Berto, and Anton du Plessis. Metal additive manufacturing in aerospace: A review. *Materials & Design*, 209:110008, 2021. ISSN 0264-1275. . URL https://www.sciencedirect.com/science/article/pii/S0264127521005633.

William F. Bottke and Richard Greenberg. Asteroidal collision probabilities. *Geophysical Research Letters*, 20(10):879–881, may 1993. ISSN 00948276. . URL http://doi.wiley.com/10.1029/92GL02713.

Stanley A Bouslog, Brian P Ross, and Christopher B Madden. Space debris- reentry risk analysis. In *AIAA, Aerospace Sciences Meeting and Exhibit, 32 nd, Reno, NV*, pages 89–103, 1994.

Bleddyn E. Bowen. Cascading Crises: Orbital Debris and the Widening of Space Security. *Astropolitics*, 12(1):46–68, jan 2014. ISSN 1477-7622. . URL http://www.tandfonline.com/doi/abs/10.1080/14777622.2014.890489.

V Braun, S Lemmens, B Reihs, H Krag, A Horstmann, and Space Debris Office. Analysis of breakup events. In *7th European Conference on Space Debris*, number April, pages 18–21, 2017.

L Breiman, JH Friedman, R Olshen, and CJ Stone. *Classification and Regression Trees*. Wadsworth, 1984.

Leo Breiman. Some properties of splitting criteria. *Machine Learning*, 24(1):41–47, 1996.

Leo Breiman. Random forests. *Machine Learning*, 45(1):5–32, oct 2001. ISSN 08856125. . URL https://link.springer.com/article/10.1023/A:1010933404324.

Dirk Brouwer. Solution of the problem of artificial satellite theory without drag. *The Astronomical Journal*, 64:378, nov 1959a. ISSN 00046256. . URL https://ui.adsabs.harvard.edu/abs/1959AJ.....64..378B/abstract.

Dirk Brouwer. Solution of the problem of artificial satellite theory without drag. *The Astronomical Journal*, 64:378, 1959b.

Matthew K Brown, Hugh G Lewis, Andrew J Kavanagh, and Ingrid Cnossen. Future Secular Neutral Density Trends at LEO Altitudes and Their Implications for the Debris Population. In *First Int'l. Orbital Debris Conf.*, 2019.

Bryce Space and Technology. Start-Up Space Update on Investment in Commercial Space Ventures 2018. Technical report, Bryce Space and Technology, 2018. URL https://www.brycetech.com/downloads/Bryce{_}Start{_}Up{_}Space{_}2018.pdf.

Leonie Buckley, Jonathan Byrne, and David Moloney. Investigating the Impact of Suboptimal Hashing Functions. In *2018 IEEE Games, Entertainment, Media Conference*

(GEM), pages 324–331. IEEE, aug 2018. ISBN 978-1-5386-6304-2. . URL https://ieeexplore.ieee.org/document/8516265/.

J. W. Campbell and C. R. Taylor. Power beaming for orbital debris removal. In Claude R. Phipps, editor, *SPIE PROCEEDINGS*, volume 3343, pages 583–589. International Society for Optics and Photonics, sep 1998. . URL http://proceedings.spiedigitallibrary.org/proceeding.aspx?articleid=943553.

NASA Community Coordinated Modeling Center CCMC. Nrlmsise-00 atmosphere model, 2021. URL https://ccmc.gsfc.nasa.gov/modelweb/models/nrlmsise00.php.

Paul Charbonneau. Dynamo models of the solar cycle. *Living Reviews in Solar Physics*, 17(1):4, dec 2020. ISSN 16144961. . URL https://doi.org/10.12942/lrsp-2010-3.

Stephen Clark. Nasa takes a chance on virgin orbit with company's second test launch – spaceflight now, 2021. URL https://spaceflightnow.com/2021/01/16/nasa-takes-a-chance-on-virgin-orbit-with-companys-second-orbital-test-launch/.

Camilla Colombo, Alessandro Rossi, FD Vedova, Vitali Braun, Benjamin Bastida Virgili, Holger Krag, et al. Drag and solar sail deorbiting: re-entry time versus cumulative collision probability. In *68th International Astronautical Congress (IAC 2017)*, pages 3535–3553. International Astronautical Federation, IAF, 2017.

Heather Cowardin, J Liou, Phillip Anz-meador, Marlon Sorge, and John Opiela. Characterization of Orbital Debris Via Hyper-Velocity Laboratory-Based Tests. In *7th European Conference on Space Debris, Darmstadt, Germany*, number April, pages 18–21, 2017.

Howard D. Curtis. Chapter 12 - introduction to orbital perturbations. In Howard D. Curtis, editor, *Orbital Mechanics for Engineering Students (Third Edition)*, pages 651–720. Butterworth-Heinemann, Boston, third edition edition, 2014. ISBN 978-0-08-097747-8. . URL https://www.sciencedirect.com/science/article/pii/B9780080977478000128.

Gil Denis, Didier Alary, Xavier Pasco, Nathalie Pisot, Delphine Texier, and Sandrine Toulza. From new space to big space: How commercial space dream is becoming a reality. *Acta Astronautica*, 166:431–443, jan 2020. ISSN 00945765. .

A Deprit. Ideal elements for perturbed Keplerian motions. *J. Res. Natl. Bur Standards B*, 79:1–2, 1975.

André Deprit and Arnold Rom. The main problem of artificial satellite theory for small and moderate eccentricities. *Celestial Mechanics and Dynamical Astronomy*, 2(2): 166–206, 1970.

Samuel Diserens, Hugh G. Lewis, and Joerg Fliege. Assessing collision algorithms for the newspace era. *Journal of Space Safety Engineering*, jul 2020a. ISSN 24688967. .

Samuel Diserens, Hugh G. Lewis, and Jörg Fliege. NewSpace and its implications for space debris models. *Journal of Space Safety Engineering*, jul 2020b. ISSN 24688967. . URL https://linkinghub.elsevier.com/retrieve/pii/S2468896720300914.

J. C. Dolado-Perez, Carmen Pardini, and Luciano Anselmo. Review of uncertainty sources affecting the long-term predictions of space debris evolutionary models. *Acta Astronautica*, 113:51–65, 2015. ISSN 00945765. . URL http://dx.doi.org/10.1016/j.actaastro.2015.03.033.

JC Dolado-Perez, Di COSTANZO Romain, and Revelin Bruno. Introducing MEDEE – A New Orbital Debris Evolutionary Model. In *6th European Conference on Space Debris*, Darmstadt, 2013. URL https://conference.sdo.esoc.esa.int/proceedings/sdc6/paper/168/SDC6-paper168.pdf.

Adrian Dumitrescu, Scott J. I. Walker, Federico Romei, and Atul Bhaskar. Structural assessment and material validation of 3d printed corrugated spacecraft debris shields. In *8th European Conference on Space Debris*, 2021. URL https://conference.sdo.esoc.esa.int/proceedings/sdc8/paper/32.

P Eichler and A Bade. Removal of debris from orbit. In *Orbital Debris Conference: Technical Issues andFuture Directions*, page 1366, 1990.

P. Eichler and A. Bade. Strategy for the economical removal of numerous larger debris objects from Earth orbits. *Acta Astronautica*, 29(1):29–36, jan 1993. ISSN 0094-5765. . URL https://www.sciencedirect.com/science/article/pii/0094576593900666.

ESA. Space in Images - 2016 - 05 - Impact chip, 2016. URL https://www.esa.int/spaceinimages/Images/2016/05/Impact{_}chip.

European Space Agency ESA. DISCOSWeb, 2018a. URL https://discosweb.esoc.esa.int/group/guest/data-browser.

European Space Agency ESA. FAQ: Frequently asked questions / Space Debris / Operations / Our Activities / ESA, 2018b. URL http://www.esa.int/Our_Activities/Operations/Space_Debris/FAQ_Frequently_asked_questions.

European Space Agency ESA. ESA - ESA spacecraft dodges large constellation, 2019. URL https://www.esa.int/Safety{_}Security/ESA{_}spacecraft{_}dodges{_}large{_}constellation.

European Space Agency ESA. ESA - Space debris by the numbers, 2020a. URL https://www.esa.int/Safety{_}Security/Space{_}Debris/Space{_}debris{_}by{_}the{_}numbers.

European Space Agency ESA. Space Environment Statistics · Space Debris User Portal, 2020b. URL https://sdup.esoc.esa.int/discosweb/statistics/.

European Space Agency ESA. Esa - esa space debris office, 2021. URL https://www.esa.int/Enabling_Support/Operations/Ground_Systems_Engineering/ESA_Space_Debris_Office.

Space Debris Mitigation WG ESA. ESA Space Debris Mitigation Compliance Verification Guidelines. Technical report, ESA, 2015. URL https://www.iadc-online.org/References/Docu/ESSB-HB-U-002-Issue1(19February2015).pdf.

ESA Safety & Security. "the history of space debris creation", 2021. URL https://www.esa.int/ESA_Multimedia/Images/2021/03/The_history_of_space_debris_creation.

ESA Space Debris Office. ESA's Annual Space Environment Report. Technical report, ESA, 2020. URL https://www.sdo.esoc.esa.int/environment_report/Space_Environment_Report_latest.pdf.

Jeff Foust. NOAA Weather Satellite Breaks Up in Orbit - SpaceNews.com. *Space News*, 2015. URL http://spacenews.com/noaa-weather-satellite-suffers-in-orbit-breakup/.

Jeff Foust. Spacex launches record-setting cluster of smallsats - spacenews, 2021. URL https://spacenews.com/spacex-launches-record-setting-cluster-of-smallsats/.

H Fraysse, V Morand, C Le Fevre, A Cauhert, A Lamy, P Mercier, C Dental, and F Deleflie. Stela, a tool for long term orbit propagation. In *Proceedings of the 5th International Conference on Astrodynamics Tools and Techniques*, volume 29, 2012.

S Frey and S Lemmens. Status of the Space Environment : Current Level of Adherence To the Space Debris Mitigation Policy. In *Proc. 7th European Conference on Space Debris, Darmstadt, Germany, 18-21 April 2017*, volume 18500, pages 18–21, April 2017.

Eleftherios Gdoutos, Christophe Leclerc, Fabien Royer, Daniel A. Türk, and Sergio Pellegrino. Ultralight spacecraft structure prototype. In *AIAA Scitech 2019 Forum*. . URL https://arc.aiaa.org/doi/abs/10.2514/6.2019-1749.

Bill Gray. lunar/moid.cpp, 2018. URL https://github.com/Bill-Gray/lunar/blob/master/moid.cpp.

R. Greenberg. Orbital interactions - A new geometrical formalism. *The Astronomical Journal*, 87:184, jan 1982. ISSN 00046256. . URL http://adsabs.harvard.edu/cgi-bin/bib{_}query?1982AJ.....87..184G.

IADC Steering Group. Iadc statement on large constellations of satellites in low earth orbit (rev 3), 2017. URL https://www.iadc-home.org/documents_public/file_down/id/4129.

IADC Steering Group and Working Group 4. Iadc space debris mitigation guidelines - revision 2, 2020. URL https://orbitaldebris.jsc.nasa.gov/library/iadc-space-debris-guidelines-revision-2.pdf.

T. Hanada. Orbital debris modeling and applications at Kyushu University. In *Procedia Engineering*, volume 67, pages 404–411. Elsevier Ltd, jan 2013. .

T. Hanada and J. C. Liou. Theoretical and empirical analysis of the average cross-sectional areas of breakup fragments. *Advances in Space Research*, 47(9): 1480–1489, 2011. ISSN 02731177. .

T. Hanada, J. C. Liou, T. Nakajima, and E. Stansbery. Outcome of recent satellite impact experiments. *Advances in Space Research*, 44(5):558–567, 2009. ISSN 02731177. .

Shin Harase. On the F 2-linear relations of Mersenne Twister pseudorandom number generators. *Mathematics and Computers in Simulation*, 100:103–113, 2014. ISSN 03784754. . URL https://arxiv.org/pdf/1301.5435.pdf.

José M. Hedo, Manuel Ruíz, and Jesús Peláez. On the minimum orbital intersection distance computation: A new effective method. *Monthly Notices of the Royal Astronomical Society*, 479(3):3288–3299, sep 2018. ISSN 13652966. . URL https://academic.oup.com/mnras/article/479/3/3288/5039662.

Felix R Hoots and Richard G France. An analytic satellite theory using gravity and a dynamic atmosphere. *Celestial Mechanics*, 40(1):1–18, 1987.

Felix R. Hoots and Ronald L. Roehrich. Spacetrack Report No. 3–Models for Propagation of NORAD Elements Sets. *Spacetrack Report*, 3(3):1–91, 1980a.

Felix R Hoots and Ronald L Roehrich. Spacetrack report number 3: Models for propagation of norad element sets, 1980b.

Felix R. Hoots, Linda L. Crawford, and Ronald L. Roehrich. An analytic method to determine future close approaches between satellites. *Celestial Mechanics*, 33(2): 143–158, jun 1984. ISSN 0008-8714. . URL http://link.springer.com/10.1007/BF01234152.

S. Hughes. Satellite orbits perturbed by direct solar radiation pressure: General expansion of the disturbing function. *Planetary and Space Science*, 25(9):809–815, 1977. ISSN 0032-0633. . URL https://www.sciencedirect.com/science/article/pii/0032063377900344.

Inter-Agency Space Debris Coordination Committee IADC. Terms of Reference of the Inter-Agency Space Debris Coordination Committee. Technical report, Inter-Agency Space Debris Coordination Committee, 2016.

Albert Jackson, Paula Krisko, and Phillip Anz-meador. Breakup model update at nasa / jsc. Technical Report January, NASA JSC, 2000.

R. Jastrow and C. A. Pearse. Atmospheric drag on the satellite. *Journal of Geophysical Research*, 62(3):413–423, sep 1957. ISSN 01480227. . URL http://doi.wiley.com/10.1029/JZ062i003p00413.

Alan B Jenkin, Marlon Sorge, Glenn Peterson, John McVey, and Bernard Yoo. Recent Enhancements to ADEPT and Sample Debris Environment Projections. In *International Astronautical Congress*, 2015. URL https://iafastro.directory/iac/archive/tree/IAC-15/A6/2/IAC-15,A6,2,2,x28103.brief.pdf.

Alan B. Jenkin, John P. McVey, and Marlon E. Sorge. Orbital lifetime and collision risk reduction for inclined geosynchronous disposal orbits. *Acta Astronautica*, 161: 153–165, aug 2019. ISSN 00945765. .

Youngmin JeongAhn and Renu Malhotra. The current impact flux on Mars and its seasonal variation. *Icarus*, 262:140–153, dec 2015. ISSN 10902643. .

Youngmin JeongAhn and Renu Malhotra. Simplified Derivation of the Collision Probability of Two Objects in Independent Keplerian Orbits. *The Astronomical Journal*, 153(5):235, 2017. ISSN 0004-6256. . URL http://arxiv.org/abs/1701.03096http://dx.doi.org/10.3847/1538-3881/aa6aa7.

N. L. Johnson, P. H. Krisko, J. C. Liou, and P. D. Anz-Meador. NASA's new breakup model of EVOLVE 4.0. *Advances in Space Research*, 28(9):1377–1384, 2001. ISSN 02731177. .

Rumiya N. Kamalieva and Ramaz V. Charkviani. Creation of ultra-light spacecraft constructions made of composite materials. *Procedia Engineering*, 185:190–197, 2017. ISSN 1877-7058. . URL https://www.sciencedirect.com/science/article/pii/S1877705817314911. Electric Propulsions and Their Application.

Karanpreet Kaur. China's Anti-Satellite Warfare Programme: Implications and Lessons. *Scholar Warior*, (Spring):112–115, 2014. URL http://www.claws.in/images/journals_doc/1541462064_KaranpreetKaur.pdf.

Satomi Kawamoto, Takayuki Hirai, Shiki Kitajima, Shuji Abe, and Toshiya Hanada. Evaluation of Space Debris Mitigation Measures Using a Debris Evolutionary Model. *Transactions of the Japan Society for Aeronautical and Space Sciences, Aerospace Technology Japan*, 16(7):599–603, 2018. ISSN 1884-0485. . URL https://www.jstage.jst.go.jp/article/tastj/16/7/16{_}599/{_}article.

Satomi Kawamoto, Nobuaki Nagaoka, Toshiya Hanada, and Shuji Abe. Evaluation of active debris removal strategy using a debris evolutionary model. In *Proceedings of the International Astronautical Congress, IAC*, volume 2019-October. International Astronautical Federation, IAF, 2019.

T. S. Kelso and S. Alfano. Satellite orbital conjunction reports assessing threatening encounters in space (SOCRATES). In Pejmun Motaghedi, editor, *Modeling, Simulation, and Verification of Space-based Systems III*, volume 6221, pages 1 – 9. International Society for Optics and Photonics, SPIE, 2006. . URL https://doi.org/10.1117/12.665612.

T.S. Kelso. CelesTrak: SOCRATES, 2020. URL https://www.celestrak.com/SOCRATES/.

Mclee Kerolle. NewSpace - Is this the Advent of the Second Space Age? — Space Out — SpaceBoard, nov 2015. URL https://www.spaceboard.eu/articles/space-out/newspace-is-this-the-advent-of-the-second-space-age-.

Donald J. Kessler. Derivation of the collision probability between orbiting objects: the lifetimes of jupiter's outer moons. *Icarus*, 48(1):39–48, 1981. ISSN 10902643. .

Donald J. Kessler. Collisional cascading: The limits of population growth in low earth orbit. *Advances in Space Research*, 11(12):63–66, jan 1991. ISSN 02731177. .

Donald J. Kessler and Phillip D. Anz-Meador. Critical number of spacecraft in low Earth orbit: using satellite fragmentation data to evaluate the stability of the orbital debris environment. In *Proceedings of the Third European Conference on Space Debris, 19 - 21 March 2001*, 2001.

Donald J Kessler and Burton G Cour-palais. Collision Frequency of Artificial Satellites: The Creation of a Debris Belt. *Journal of geophysical research. Space physics*, 83(8): 918–924, 1978.

Sungil Kim and Heeyoung Kim. A new metric of absolute percentage error for intermittent demand forecasts. *International Journal of Forecasting*, 32(3):669–679, jul 2016. ISSN 01692070. .

D King-Hele. *Satellite orbits in an atmosphere. Theory and applications.* Blackie and Son Ltd., Glasgow, UK., 1987. ISBN 0-216-92252-6.

H. Klinkrad, H. Sdunnus, and J. Bendisch. Development status of the ESA space debris reference model. *Advances in Space Research*, 16(11):93–102, jan 1995. ISSN 0273-1177. . URL https://www.sciencedirect.com/science/article/pii/027311779598757F.

H. Klinkrad, J. Bendisch, H. Sdunnus, P. Wegener, and R. Westerkamp. An introduction to the 1997 ESA MASTER model. *European Space Agency, (Special Publication) ESA SP*, (393):217–221, 1997. ISSN 03796566.

Heiner Klinkrad. *Space Debris: Models and Risk Analysis*. Springer Science & Business Media, 2006.

D.J. Knipp, T. Welliver, M.G. McHarg, F.K. Chun, W.K. Tobiska, and D. Evans. Climatology of extreme upper atmospheric heating events. *Advances in Space Research*, 36(12):2506–2510, jan 2005. ISSN 0273-1177. . URL https://www.sciencedirect.com/science/article/pii/S0273117705002103.

Gottfried Konecny. Small Satellites-A Tool for Earth Observation? In *ISPRS Congress Istanbul*, pages 580–582, 2004. URL http://centaur.sstl.co.uk.

Holger Krag, Tim Flohrer, Klaus Merz, Stijn Lemmens, Benjamin Bastida Virgili, Quirin Funke, and Vitali Braun. Esa's modernised collision avoidance service. In *14th International Conference on Space Operations*, page 2449, 2016.

Herbert J. Kramer. RemoveDebris - Satellite Missions - eoPortal Directory, 2018. URL https://directory.eoportal.org/web/eoportal/satellite-missions/r/removedebris.

P. H. Krisko. Proper Implementation of the 1998 NASA Breakup Model. *Orbital Debris Quarterly News*, 15(4):4–5, 2011. ISSN 1364-503X. .

P.H. Krisko, M. Horstman, and M.L. Fudge. Socit4 collisional-breakup test data analysis: With shape and materials characterization. *Advances in Space Research*, 41 (7):1138–1146, 2008. ISSN 0273-1177. . URL https://www.sciencedirect.com/science/article/pii/S0273117707010423.

P.H. Krisko, S. Flegel, M.J. Matney, D.R. Jarkey, and V. Braun. ORDEM 3.0 and MASTER-2009 modeled debris population comparison. *Acta Astronautica*, 113: 204–211, aug 2015. ISSN 0094-5765. . URL https://www.sciencedirect.com/science/article/pii/S0094576515001241.

Ed Kyle. Space Launch Report, 2021. URL http://www.spacelaunchreport.com/logyear.html.

Patrik Kärräng, Tobias Lips, and Tiago Soares. Demisability of critical spacecraft components during atmospheric re-entry. *Journal of Space Safety Engineering*, 6(3): 181–187, 2019. ISSN 2468-8967. . URL https://www.sciencedirect.com/science/article/pii/S2468896719300874.

Robert Lafranco. Allen and Branson Best Musk as the Billionaire Space Race Takes Off - Bloomberg. *Bloomberg*, apr 2015. URL https://www.bloomberg.com/news/articles/2015-04-13/allen-and-branson-best-musk-as-the-billionaire-space-race-takes-off.

Sheng Wei Lan, Sen Liu, Yi Li, Fa Wei Ke, and Jie Huang. Debris area distribution of spacecraft under hypervelocity impact. *Acta Astronautica*, 105(1):75–81, 2014. ISSN 00945765. .

J. Laštovička. Global pattern of trends in the upper atmosphere and ionosphere: Recent progress. *Journal of Atmospheric and Solar-Terrestrial Physics*, 71(14-15):

1514–1528, oct 2009. ISSN 1364-6826. . URL https://www.sciencedirect.com/science/article/pii/S1364682609000066.

J Laštovička, R A Akmaev, G Beig, J Bremer, and J T Emmert. Global Change in the Upper Atmosphere. *Science*, 314(5803):1253 LP – 1254, nov 2006. . URL http://science.sciencemag.org/content/314/5803/1253.abstract.

S. Le May, S. Gehly, B. A. Carter, and S. Flegel. Space debris collision probability analysis for proposed global broadband constellations. *Acta Astronautica*, 151: 445–455, oct 2018. ISSN 00945765. .

D Lear, J Hyde, E Christiansen, J Herrin, and F Lyons. STS-118 Radiator Impact Damage. Technical report, NASA, 2008. URL https://ntrs.nasa.gov/archive/nasa/casi.ntrs.nasa.gov/20080010742.pdf.

Simon Lee, Amy Hutputanasin, Armen Toorian, Wenschel Lan, Riki Munakata, Justin Carnahan, David Pignatelli, and Arash Mehrparvar. CubeSat Design Specification Rev. 13 The CubeSat Program, Cal Poly SLO CubeSat Design Specification (CDS) REV 13 Document Classification X Public Domain ITAR Controlled Internal Only. Technical report, California Polytechnic State University, 2014. URL https://static1.squarespace.com/static/5418c831e4b0fa4ecac1bacd/t/56e9b62337013b6c063a655a/1458157095454/cds{_}rev13{_}final2.pdf.

Francesca Letizia, Stijn Lemmens, Benjamin Bastida Virgili, and Holger Krag. Application of a debris index for global evaluation of mitigation strategies. *Acta Astronautica*, 161:348–362, aug 2019. ISSN 00945765. .

Dan R. Lev, Gregory D. Emsellem, and Ashley K. Hallock. The rise of the electric age for satellite propulsion. *New Space*, 5(1):4–14, 2017. .

H G Lewis, J Radtke, J Beck, B Bastida Virgili, H Krag, United Kingdom, Technische Universitaet Braunschweig, and United Kingdom. Self-Induced Collision Risk Analysis for Large Constellations. In *Proc. 7th European Conference on Space Debris, Darmstadt, Germany, 18-21 April 2017*, number April, pages 18–21, 2017a.

H G Lewis, J Radtke, A Rossi, J Beck, M Oswald, P Anderson, B Bastida Virgili, H Krag, United Kingdom, Technische Universitaet Braunschweig, United Kingdom, Airbus Defence, Space Gmbh, Clyde Space Limited, and United Kingdom. Sensitivity of the Space Debris Environment To Large Constellations and Small Satellites. In *Proc. 7th European Conference on Space Debris, Darmstadt, Germany, 18-21 April 2017*, number April, pages 18–21, 2017b.

H.G. Lewis, G.G. Swinerd, R.J. Newland, and A. Saunders. The fast debris evolution model. *Advances in Space Research*, 44(5):568–578, sep 2009. ISSN 0273-1177. . URL https://www.sciencedirect.com/science/article/pii/S0273117709003718.

H.G. Lewis, B. Schwarz, S. George, and H. Stokes. An assessment of cubesat collision risk. In *65th International Astronautical Congress (03/10/14)*, September 2014. URL https://eprints.soton.ac.uk/369583/.

Hugh G Lewis. [twitter], February 2021. URL https://twitter.com/ProfHughLewis/status/1356549794601324545.

Hugh G Lewis, Graham Swinerd, Neil Williams, and Gavin Gittins. DAMAGE: a dedicated GEO debris model framework. In *Third European Conference on Space Debris*, Darmstadt, 2001. URL https://www.researchgate.net/publication/241304490.

Hugh G. Lewis, Adam E. White, Richard Crowther, and Hedley Stokesc. Synergy of debris mitigation and removal. *Acta Astronautica*, 81(1):62–68, 2012. ISSN 00945765. . URL http://dx.doi.org/10.1016/j.actaastro.2012.06.012.

Hugh G Lewis, Samuel Diserens, Timothy Maclay, and J P Sheehan. Limitations of the cube method for assessing large constellations. In *First Int'l. Orbital Debris Conf.*, 2019.

J. C. Liou. Collision activities in the future orbital debris environment. *Advances in Space Research*, 38(9):2102–2106, 2006. ISSN 02731177. .

J. C. Liou. An active debris removal parametric study for LEO environment remediation. *Advances in Space Research*, 47(11):1865–1876, 2011. ISSN 02731177. . URL http://dx.doi.org/10.1016/j.asr.2011.02.003.

J. C. Liou and Nicholas L. Johnson. A sensitivity study of the effectiveness of active debris removal in LEO. *Acta Astronautica*, 64(2-3):236–243, 2009. ISSN 00945765. .

J.-C. Liou, Donald J. Kessler, M.J. Matney, and E.G. Stansbery. A New Approach To Evaluate Collision Probabilities Among Asteroids, Comets. *Lunar and Planetary Science*, XXXIV:2–3, 2003. URL https://www.lpi.usra.edu/meetings/lpsc2003/pdf/1828.pdf.

J. C. Liou, D. T. Hall, P. H. Krisko, and J. N. Opiela. LEGEND - A three-dimensional LEO-to-GEO debris evolutionary model. *Advances in Space Research*, 34(5):981–986, 2004. ISSN 02731177. .

J. C. Liou, N. L. Johnson, and N. M. Hill. Controlling the growth of future LEO debris populations with active debris removal. *Acta Astronautica*, 66(5-6):648–653, 2010. ISSN 00945765. . URL http://dx.doi.org/10.1016/j.actaastro.2009.08.005.

J J F Liu and R L Alford. Semianalytic theory for a close-Earth artificial satellite. *J. Guidance and Control*, 3(4):304–311, 1980.

Lockheed Martin. Space fence, 2021. URL https://www.lockheedmartin.com/en-us/products/space-fence.html.

Anne C Long, J O Cappellari Jr, C E Velez, and A J Fuchs. Goddard trajectory determination system (gtds) mathematical theory (revision 1). *National Aeronautics and Space Administration/Goddard Space Flight Center, FDD/552-89/001 and CSC/TR-89/6001*, 1989.

R H Lyddane. Small eccentricities or inclinations in the Brouwer theory of the artificial satellite. *The Astronomical Journal*, 68:555, 1963.

Molly K. Macauley. The economics of space debris: Estimating the costs and benefits of debris mitigation. *Acta Astronautica*, 115:160–164, 2015. ISSN 00945765. . URL http://dx.doi.org/10.1016/j.actaastro.2015.05.006.

Mark J Matney. Algorithms for the computation of debris risk. In *Proc. 7th European Conference on Space Debris, Darmstadt, Germany, 18-21 April 2017*, number April, pages 18–21, 2017.

Jonathan C. McDowell. The low earth orbit satellite population and impacts of the SpaceX starlink constellation. *The Astrophysical Journal*, 892(2):L36, apr 2020. . URL https://doi.org/10.3847/2041-8213/ab8016.

D. Mcknight. Pay Me Now or Pay Me More Later : Start the Development of Active Orbital Debris Removal Now. *Proceedings of the 2010 AMOS Conference*, pages 1–21, 2010.

Darren McKnight, Robert Maher, and Larry Nagl. Refined algorithms for structural breakup due to hypervelocity impact. *International Journal of Impact Engineering*, 17 (4-6):547–558, 1995. ISSN 0734743X. .

Darren McKnight, Rachel Witner, Francesca Letizia, Stijn Lemmens, Luciano Anselmo, Carmen Pardini, Alessandro Rossi, Chris Kunstadter, Satomi Kawamoto, Vladimir Aslanov, Juan Carlos Dolado Perez, Vincent Ruch, Hugh Lewis, Mike Nicolls, Liu Jing, Shen Dan, Wang Dongfang, Andrey Baranov, and Dmitriy Grishko. Identifying the 50 statistically-most-concerning derelict objects in leo. *Acta Astronautica*, 181:282–291, 4 2021. ISSN 00945765. .

G Métris and P Exertier. Semi-analytical theory of the mean orbital motion. *Astronomy and Astrophysics*, 294:278–286, 1995.

Shahir Mohd Yusuf, Samuel Cutler, and Nong Gao. Review: The impact of metal additive manufacturing on the aerospace industry. *Metals*, 9(12), 2019. ISSN 2075-4701. . URL https://www.mdpi.com/2075-4701/9/12/1286.

David Monroe. Space debris removal using a high-power ground-based laser. In *Space Programs and Technologies Conference and Exhibit*, Reston, Virigina, sep 1993. American Institute of Aeronautics and Astronautics. . URL http://arc.aiaa.org/doi/10.2514/6.1993-4238.

Morgan Stanley. Space: Investing in the Final Frontier — Morgan Stanley, 2018. URL https://www.morganstanley.com/ideas/investing-in-space.

Theodore J. Muelhaupt, Marlon E. Sorge, J. Morin, and Robert S. Wilson. Space traffic management in the new space era. *Journal of Space Safety Engineering*, 6(2):80–87, jun 2019. ISSN 24688967. .

NASA. *History of On-Orbit Satellite Fragmentations*. NASA Orbital Debris Program Office, 14th edition, 2008. URL https://orbitaldebris.jsc.nasa.gov/library/satellitefraghistory/tm-2008-214779.pdf.

NASA. Vanguard 1, 2018. URL https://nssdc.gsfc.nasa.gov/nmc/spacecraftDisplay.do?id=1958-002B.

Nasa. Nasa safety standard: Guidelines and assessment procedures for limiting orbital debris. Technical report, NASA, 2019.

Office of Safety and Mission Assurance NASA. NASA Procedural Requirements Subject: NPR 8715.6B, NASA Procedural Requirements for Limiting Orbital Debris and Evaluating the Meteoroid and Orbital Debris Environments. Technical report, NASA, 2017. URL https://www.orbitaldebris.jsc.nasa.gov/library/npr{_}8715{_}006b{_}.pdf.

Office of the Chief Engineer NASA. Nasa interim directive subject: Collision avoidance for space environment protection. Technical report, NASA, 2020. URL https://public.ccsds.org/pubs/502x0b2c1.pdf.

National Research Council. *Orbital Debris*. National Academies Press, Washington, D.C., jun 1995. ISBN 978-0-309-05125-5. . URL http://www.nap.edu/catalog/4765.

Jonathan O'Callaghan. 'Historic Accomplishment' As Two Private Spacecraft Dock In Space For The First Time. *Forbes*, 2020. URL https://www.forbes.com/sites/jonathanocallaghan/2020/02/27/historic-accomplishment-as-two-private-spacecraft-dock-in-space-for-the-first-time-in-his{#}66f141a3223a.

NASA ODPO. Ares — orbital debris program office, 2021. URL https://www.orbitaldebris.jsc.nasa.gov/.

NASA Orbital Debris Program Office. Satellite collision leaves significant debris clouds. *Orbital Debris Quarterly News*, 13, 2009. URL https://orbitaldebris.jsc.nasa.gov/quarterly-news/pdfs/odqnv13i2.pdf.

Lorenzo Olivieri, Cinzia Giacomuzzo, Alessandro Francesconi, Hedley Stokes, and Alessandro Rossi. Experimental characterization of multi-layer 3D-printed shields for microsatellites. *Journal of Space Safety Engineering*, 7(2):125–136, jun 2020. ISSN 24688967. .

E. J. Öpik. Collision Probabilities with the Planets and the Distribution of Interplanetary Matter. *Proceedings of the Royal Irish Academy. Section A: Mathematical and Physical Sciences*, 54:165–199, 1951. . URL http://www.jstor.org/stable/20488532.

Orbex. Orbex Unveils Prime Rocket at New Facility in Scotland — Orbex, 2019. URL https://orbex.space/news/orbex-unveils-prime-rocket-at-new-facility-in-scotland.

Brian R. Overholser and Kevin M. Sowinski. Biostatistics primer: Part 2. *Nutrition in Clinical Practice*, 23(1):76–84, 2008. . URL https://onlinelibrary.wiley.com/doi/abs/10.1177/011542650802300176.

Mathew J Owens, Ken G Mccracken, Mike Lockwood, and Luke Barnard. The heliospheric Hale cycle over the last 300 years and its implications for a "lost" late 18th century solar cycle. *Journal of Space Weather and Space Climate*, 5, 2015. . URL https://www.swsc-journal.org/articles/swsc/pdf/2015/01/swsc150038.pdf.

Deganit Paikowsky. What Is New Space? The Changing Ecosystem of Global Space Activity. *New Space*, 5(2), 2017. . URL www.liebertpub.com.

C. Pardini and L. Anselmo. Assessment of the consequences of the Fengyun-1C breakup in low Earth orbit. *Advances in Space Research*, 44(5):545–557, sep 2009. ISSN 0273-1177. . URL https://www.sciencedirect.com/science/article/pii/S0273117709002531.

C. Pardini and L. Anselmo. Environmental sustainability of large satellite constellations in low earth orbit. *Acta Astronautica*, 170:27–36, may 2020. ISSN 00945765. .

Carmen Pardini and Luciano Anselmo. Review of past on-orbit collisions among cataloged objects and examination of the catastrophic fragmentation concept. *Acta Astronautica*, 100(1):30–39, 2014. ISSN 00945765. . URL http://dx.doi.org/10.1016/j.actaastro.2014.03.013.

Carmen Pardini and Luciano Anselmo. Uncontrolled re-entries of spacecraft and rocket bodies: A statistical overview over the last decade. *Journal of Space Safety Engineering*, 6(1):30–47, 2019. ISSN 2468-8967. . URL https://www.sciencedirect.com/science/article/pii/S2468896718300788.

Seong-Hyeon Park, Hae-Dong Kim, and Gisu Park. Orbit, orbital lifetime, and reentry survivability estimation for orbiting objects. *Advances in Space Research*, 62(11): 3012–3032, dec 2018. ISSN 02731177. . URL https://linkinghub.elsevier.com/retrieve/pii/S0273117718306252.

Seong-Hyeon Park, Stefano Mischler, and Pénélope Leyland. Re-entry analysis of critical components and materials for design-for-demise techniques. *Advances in*

Space Research, 68(1):1–24, 2021. ISSN 0273-1177. . URL https://www.sciencedirect.com/science/article/pii/S0273117721002428.

Jesús Peláez, José Manuel Hedo, and Pedro Rodr\'\iguez de Andrés. A special perturbation method in orbital dynamics. *Celestial Mechanics and Dynamical Astronomy*, 97(2):131–150, 2007.

Joseph N. Pelton and Scott Madry. Global Launch Vehicle Systems for Potential Small Satellite Deployment. In *Handbook of Small Satellites*, pages 1–47. Springer International Publishing, 2019. . URL https://doi.org/10.1007/978-3-030-20707-6{_}82-1.

Iván Pérez, Juan Félix San-Juan, Montserrat San-Mart\'\in, and Luis Mar\'\ia López-Ochoa. Application of computational intelligence in order to develop hybrid orbit propagation methods. *Mathematical Problems in Engineering*, 2013, 2013.

G E Peterson, A B Jenkin, M E Sorge, and J P McVey. Implications of proposed small satellite constellations on space traffic management and long-term growth in near-earth environment. In *Proc. of the 67th International Astronautical Congress (IAC), Guadalajara, Mexico, 26-30 September 2016*, 2016.

J. M. Picone, A. E. Hedin, D. P. Drob, and A. C. Aikin. NRLMSISE-00 empirical model of the atmosphere: Statistical comparisons and scientific issues. *Journal of Geophysical Research: Space Physics*, 107(A12):SIA 15–1, dec 2002. ISSN 21699402. . URL https://agupubs.onlinelibrary.wiley.com/doi/full/10.1029/2002JA009430.

E Marshall Polk and Brian E Roebuck. DebriSat Hypervelocity Impact Test ARNOLD ENGINEERING DEVELOPMENT COMPLEX. Technical Report April 2014, USAF / Aerospace Corporation, 2015.

Goparaju Purna Sudhakar. ISRO: 104 Satellites in 1 go. *Vidyaniketan Journal of Management Research*, pages 74–94, 2018. URL https://ssrn.com/abstract=3245559Sudhakar,G.P.

J Radtke, S Flegel, J Gelhaus, M Moeckel, V Braun, C Kebschull, C Wiedemann, H Krag, K Merz, and P Voersmann. Revision of statistical collision analysis for objects inside of satellite constellations. In *Proceedings of the 64th International Astronautical Congress, Beijing, China, IAC-13 A*, volume 6, page 8, 2013.

Jonas Radtke, Christopher Kebschull, and Enrico Stoll. Interactions of the space debris environment with mega constellations: Using the example of the OneWeb constellation. *Acta Astronautica*, 131(November 2016):55–68, 2017a. ISSN 00945765. . URL http://dx.doi.org/10.1016/j.actaastro.2016.11.021.

Jonas Radtke, Sven Mueller, Volker Schaus, and Enrico Stoll. LUCA2 -An Enhanced Long-Term Utility for Collision Analysis. In *7th European Conference on Space Debris*, Darmstadt, 2017b. URL https://conference.sdo.esoc.esa.int/proceedings/sdc7/paper/354/SDC7-paper354.pdf.

Jonas Radtke, Enrico Stoll, Hugh Lewis, and Benjamin Bastida Virgili. the Impact of the Increase in Small Satellite Launch Traffic on the Long-Term Evolution of the Space Debris Environment. In *Proc. 7th European Conference on Space Debris, Darmstadt, Germany, 18-21 April 2017*, number April, pages 18–21, 2017c.

Jonas Radtke, Enrico Stoll, Hugh Lewis, and Benjamin Bastida Virgili. The impact of the increase in small satellite launch traffic on the long-term evolution of the space debris environment. In *Proc. 7th European Conference on Space Debris, Darmstadt, Germany, 18-21 April 2017*, 2017d.

Robert C Reynolds, Norman H Fischer, and Eric E Ricej. Man-Made Debris in Low Earth Orbit- A Threat to Future Space Operations. *Journal of Spacecraft and Rockets*, 20(3), 1983. . URL https://arc.aiaa.org/doi/pdf/10.2514/3.25593.

Robert C Reynolds, Anette Bade, Peter Eichler, Albert A Jackson, Paula H Krisko, Mark Matney, Donald J Kessler, and Phillip D Anz-Meador. Nasa standard breakup model 1998 revision. Technical Report LMSMSS-32532, Lockheed Martin Space Operations, Houston, TX, 1998.

A. Rossi and P. Farinella. Collision rates and impact velocities for bodies in low earth orbit. *ESA Journal*, 16(3):339–348, January 1992.

A Rossi, A Cordelli, C Pardini, L Anselmo, and P Farinella. Modelling the space debris evolution: Two new computer codes. *Advances in the Astronautical Sciences*, 89:1217–1217, 1995.

A Rossi, L Anselmo, C Pardini, R Jehn, and G B Valsecchi. The New Space Debris Mitigation (SDM 4.0) Long Term Evolution Code. In *Fifth European Conference on Space Debris*, 2009. URL http://articles.adsabs.harvard.edu/cgi-bin/nph-iarticle{_}query?2009ESASP.672E..90R{&}data{_}type=PDF{_}HIGH{&}whole{_}paper=YES{&}type=PRINTER{&}filetype=.pdf.

A Rossi, H Krag, M Xavier James Raj, A K Anilkumar, and H Lewis. Stability of the Future LEO Environment. Technical report, Inter-Agency Space Debris Coordination Committee, 2013. URL https://www.iadc-online.org/Documents/IADC-2012-08,Rev1,StabilityofFutureLEOEnvironment.pdf.

Alessandro Rossi. NASA Breakup Model Implementation Comparison of results. Technical report, IADC Working Group 2, 2006.

Alessandro Rossi, Camilla Colombo, Kleomenis Tsiganis, James Beck, Jonathan Rodriguez, Scott Walker, Federico Letterio, Florio Dalla Vedova, Volker Schaus, Rada Popova, Alessandro Francesconi, Hedley Stokes, Thorn Schleutker, Elisa Alessi, Giulia Schettino, Ioannis Gkolias, Despoina Skoulidou, Ian Holbrough, Franco Bernelli Zazzera, Enrico Stoll, and Youngkyu Kim. ReDSHIFT: A Global Approach to Space Debris Mitigation. *Aerospace*, 5(2):64, jun 2018. ISSN 2226-4310. . URL http://www.mdpi.com/2226-4310/5/2/64.

A E Roy. *Orbital Motion*. Adam Hilger, 3rd edition, 1988. ISBN 9780852742280.

Juan Félix San-Juan, Montserrat San-Mart\'\in, Iván Pérez, and Rosario López. Hybrid perturbation methods based on statistical time series models. *Advances in Space Research*, 57(8):1641–1651, 2016.

Montserrat San-Martin, Iván Pérez, Rosario López, and Juan Félix San-Juan. Hybrid SGP4: tools and methods. In *In Proceedings of the 6th International Conference on Astrodynamics Tools and Techniques, 14.03. - 17.03.2016, Darmstadt, Germany.*, 2016.

Noelia Sánchez-Ortiz, Raúl Domínguez-González, Holger Krag, and Tim Flohrer. Impact on mission design due to collision avoidance operations based on TLE or CSM information. *Acta Astronautica*, 116:368–381, nov 2015. ISSN 00945765. .

F Schäfer, M Lambert, E Christiansen, S Kibe, H Stokes, H-G Reimerdes, SA Meshcheryakov, F Angrilli, and Han Zengyao. The inter-agency space debris coordination committee (iadc) protection manual. In *4th European Conference on Space Debris*, volume 587, page 39, 2005.

Wolfgang O. Schall. Orbital debris removal by laser radiation. *Acta Astronautica*, 24: 343–351, jan 1991. ISSN 0094-5765. . URL https://www.sciencedirect.com/science/article/pii/0094576591901847.

Volker Schaus, Elisa Maria Alessi, Giulia Schettino, Alessandro Rossi, and Enrico Stoll. On the practical exploitation of perturbative effects in low Earth orbit for space debris mitigation. *Advances in Space Research*, 63(7):1979–1991, apr 2019. ISSN 18791948. .

Bernardo Schneiderman. The Next Wave: Low Earth Orbit Constellations — Satellite Markets & Research, 2019. URL http://satellitemarkets.com/news-analysis/next-wave-low-earth-orbit-constellations.

H. Sdunnus, P. Beltrami, H. Klinkrad, M. Matney, A. Nazarenko, and P. Wegener. Comparison of debris flux models. *Advances in Space Research*, 34(5):1000–1005, 2004. ISSN 02731177. .

Peter B. De Selding. Spacex: We performed 2,219 starlink collision-avoidance maneuvers in the six months ending may 31 - space intel report. *Space Intel Report*, 8 2021. URL https://www.spaceintelreport.com/spacex-we-performed-2219-starlink-collision-avoidance-maneuvers-in-the-six-months-ending-

Jae-Dong Seong, Hae-Dong Kim, and Ha-Yeon Choi. A study of a target identification method for an active debris removal system. *Proceedings of the Institution of Mechanical Engineers, Part G: Journal of Aerospace Engineering*, 231(1):180–189, 2017. ISSN 0954-4100. . URL http://journals.sagepub.com/doi/10.1177/0954410016662065.

18 SPCS/SSA Sharing. Re: Odr number 20-074-2c - re: Request for rcs values of debris fragments [email], 2020.

Rob Sladen. Iridium constellation status, 2020. URL http://www.rod.sladen.org.uk/iridium.htm.

Marlon E. Sorge and Deanna L. Mains. IMPACT fragmentation model developments. *Acta Astronautica*, 126:40–46, sep 2016. ISSN 0094-5765. . URL https://www.sciencedirect.com/science/article/pii/S0094576515303349.

Space Exploration Holdings LLC. SAT-MOD-20200417-00037 (Technical attachment). Technical report, FCC INTERNATIONAL BUREAU, 2020. URL https://licensing.fcc.gov/cgi-bin/ws.exe/prod/ib/forms/reports/swr031b.hts?q{_}set=V{_}SITE{_}ANTENNA{_}FREQ.file{_}numberC/File+Number/{%}3D/SATMOD2020041700037{&}prepare={&}column=V{_}SITE{_}ANTENNA{_}FREQ.file{_}numberC/File+Number.

Space-Track. Space-Track.Org, 2018. URL https://www.space-track.org/{#}/catalog.

Space-Track. Space-Track.Org, 2020. URL https://www.space-track.org/documentation{#}/tle.

Spaceflight Industries. SSO-A - Spaceflight, 2019. URL http://spaceflight.com/sso-a/.

SpaceX. Application for Fixed Satellite Service by Space Exploration Holdings, LLC [SAT-MOD-20181108-00083], 2018. URL https://fcc.report/IBFS/SAT-MOD-20181108-00083.

STK. STK Conjunction Analysis Tool, 2020. URL https://p.widencdn.net/ufgtuc/Conjunction-Analysis--Product-Specsheet.

PH Stokes and GG Swinerd. Debris protection optimisation of a realistic unmanned spacecraft using shield. In *4th European Conference on Space Debris*, volume 587, page 515, 2005.

Jinyuan Su. Active debris removal: Potential legal barriers and possible ways forward. *Journal of East Asia and International Law*, 9(2):403–426, 2016. ISSN 19769229. .

Swiss Re. Space debris: On a collision course for insurers?, 2011. URL https://www.swissre.com/dam/jcr:b359fb24-857a-412a-ae5c-72cdff0eaa94/Publ11_Space+debris.pdf.

David L. Talent. Analytic model for orbital debris environmental management. *Journal of Spacecraft and Rockets*, 29(4):508–513, jul 1992. ISSN 0022-4650. . URL http://arc.aiaa.org/doi/10.2514/3.25493.

A Tan, T X Zhang, and M Dokhanian. Analysis of the Iridium 33 and Cosmos 2251 Collision Using Velocity Perturbations of the Fragments. *Advances in Aerospace Science and Applications*, 3(1):13–25, 2013.

Matthias Teschner, Bruno Heidelberger, Matthias Müller, Danat Pomeranets, and Markus Gross. Optimized spatial hashing for collision detection of deformable objects. *VMV'03: Proceedings of the Vision, Modeling, Visualization*, 3, 12 2003.

The Week. The great billionaire space race. *The Week*, sep 2016. URL http://theweek.com/articles/648995/great-billionaire-space-race.

UN Committee on the Peaceful Uses of Outer Space UNCOPUOS. Space debris mitigation guidelines of the committee on the peaceful uses of outer space. Technical report, Office for Outer Space Affairs, United Nations, Vienna, 2010.

Union of Concerned Scientists. UCS Satellite Database, 2017. URL https://www.ucsusa.org/nuclear-weapons/space-weapons/satellite-database{#}.Wv6vDIgvyUk.

Union of Concerned Scientists. Record Number of Satellites in Orbit, 2019. URL https://allthingsnuclear.org/lgrego/2018satellitedata.

Union of Concerned Scientists. UCS Satellite Database, 2020. URL https://www.ucsusa.org/resources/satellite-database.

Stephane Valk, Anne Lema\^\itre, and Florent Deleflie. Semi-analytical theory of mean orbital motion for geosynchronous space debris under gravitational influence. *Advances in Space Research*, 43(7):1070–1082, 2009.

D. Vallado, P. Crawford, R. Hujsak, and T.S. Kelso. Revisiting Spacetrack Report #3. In *AIAA/AAS Astrodynamics Specialist Conference and Exhibit*, Reston, Virigina, aug 2006. American Institute of Aeronautics and Astronautics. ISBN 978-1-62410-048-2. . URL http://arc.aiaa.org/doi/10.2514/6.2006-6753.

David A. Vallado and David Finkleman. A critical assessment of satellite drag and atmospheric density modeling. *Acta Astronautica*, 95:141–165, feb 2014. ISSN 0094-5765. . URL https://www.sciencedirect.com/science/article/pii/S0094576513003755.

David A Vallado and Daniel L Oltrogge. Fragmentation Event Debris Field Evolution Using 3D Volumetric Risk Assessment. In *Proc. 7th European Conference on Space Debris, Darmstadt, Germany, 18-21 April 2017*, number April, pages 18–21, 2017.

A Vavrin, A Manis, D Gates, and M Matney. Risk of Increased Fragmentation Events due to Low Altitude Large Constellation Spacecraft. Technical report, NASA, dec 2019a. URL https://ntrs.nasa.gov/search.jsp?R=20190033487.

A Vavrin, A Manis, D Gates, and M Matney. Risk of increased fragmentation events due to low altitude large constellation spacecraft. In *First Int'l. Orbital Debris Conf.*, 2019b.

Andrew Vavrin, Alyssa Manis, Drake Gates, J C Liou, and Mark Matney. Summary of the NASA Large Constellations Parametric Study. Technical report, NASA, jun 2019c. URL https://ntrs.nasa.gov/search.jsp?R=20190025975.

B Bastida Virgili and Holger Krag. Small satellites and the future space debris environment. *Proceedings of the 30th ISTS, Kobe, Japan*, 2015.

Benjamin Bastida Virgili. DELTA (Debris Environment Long-Term Analysis). In *6th International Conference on Astrodynamics Tools and Techniques (ICATT)*, 2016.

SJI Walker, F Romei, J Becedas Rodríguez, F Dalla Vedova, J Beck, I Holbrough, A Francesconi, L Olivieri, A Caparrós, G Rodríguez Flores, et al. An overview of the application of 3d printed spacecraft structures within the redshift project. In *70th International Astronautical Congress (IAC 2019)*, pages 1–10, 2019.

David W Walsh. Effect of Radar Measurement Errors on Small Debris Orbit Prediction, 2011. URL https://pdfs.semanticscholar.org/1a45/b903f6a988b38fe1760f8b0bb6010875905b.pdf.

R. L. Walterscheid. Solar cycle effects on the upper atmosphere - implications for satellite drag. *Journal of Spacecraft and Rockets*, 26(6):439–444, 1989. . URL https://doi.org/10.2514/3.26089.

Xiao-wei Wang and Jing Liu. An Introduction to a New Space Debris Evolution Model: SOLEM. *Advances in Astronomy*, 2019:2738276, 2019. ISSN 1687-7969. . URL https://doi.org/10.1155/2019/2738276.

Brian Weeden. Overview of the legal and policy challenges of orbital debris removal. *Space Policy*, 27(1):38–43, feb 2011. ISSN 0265-9646. . URL https://www.sciencedirect.com/science/article/pii/S0265964610001268.

Timo Wekerle, JosÃ© Bezerra Pessoa Filho, LuÃs Eduardo Vergueiro Loures da Costa, and LuÃs Gonzaga Trabasso. Status and Trends of Smallsats and Their Launch Vehicles - An Up-to-date Review. *Journal of Aerospace Technology and Management*, 9: 269 – 286, 09 2017. ISSN 2175-9146. URL http://www.scielo.br/scielo.php?script=sci_arttext&pid=S2175-91462017000300269&nrm=iso.

G. W. Wetherill. Collisions in the asteroid belt. *Journal of Geophysical Research*, 72(9): 2429–2444, may 1967. ISSN 01480227. . URL http://doi.wiley.com/10.1029/JZ072i009p02429.

Adam E. White and Hugh G. Lewis. An adaptive strategy for active debris removal. *Advances in Space Research*, 53(8):1195–1206, 2014a. ISSN 02731177. . URL http://dx.doi.org/10.1016/j.asr.2014.01.021.

Adam E. White and Hugh G. Lewis. The many futures of active debris removal. *Acta Astronautica*, 95(1):189–197, 2014b. ISSN 00945765. . URL http://dx.doi.org/10.1016/j.actaastro.2013.11.009.

Carsten Wiedemann, Sven Flegel, Marek Möckel, Johannes Gelhaus, Vitali Braun, Christopher Kebschull, Jörg Kreisel, Manuel Metz, and Peter Vörsmann. The economics of the control of the space debris environment. In *6th European Conference on Space Debris*, 2013.

James Woodburn, Vincent Coppola, and Frank Stoner. A Description of Filters for Minimizing the Time Required for Orbital Conjunction Computations. Technical report, AGI, 2009. URL https://www.agi.com/resources/white-papers/a-description-of-filters-for-minimizing-the-time-r.

Qin Zheng and Liang YanGang. Layout optimization of satellite cabin considering space debris impact risk. *Journal of Spacecraft and Rockets*, 54(5):1178–1182, 2017.

W U Ziniu, H U Ruifeng, Q U Xi, Wang Xiang, and W U Zhe. Space Debris Reentry Analysis Methods and Tools. *Chinese Journal of Aeronautics*, 24:387–395, 2011. . URL www.elsevier.com/locate/cja.